Dirhodium(II,II) paddlewheel complexes conjugated to a polypyridyl tris-amine scaffold: synthesis and application as pre-catalysts in the hydroformylation of 1-octene

Stephen de Doncker

University of Cape Town

November 2019

Dirhodium(II,II) paddlewheel complexes conjugated to a polypyridyl tris-amine scaffold: synthesis and application as pre-catalysts in the hydroformylation of 1-octene

Dissertation presented for the degree of

Master of Science

By

Stephen de Doncker

Supervisors: **Associate Professor Gregory S. Smith (UCT)**

Doctor Siyabonga Ngubane (UCT)

Department of Chemistry
University of Cape Town
Rondebosch, 7701
Cape Town

November 2019

Plagiarism Declaration

I know the meaning of plagiarism and declare that all work contained in the document,

"**Dirhodium(II,II) paddlewheel complexes conjugated to a polypyridyl tris-amine scaffold: synthesis and application as pre-catalysts in the hydroformylation of 1-octene"**,

is my own work and, to the best of my knowledge has never been submitted for examination for any degree at any university. All sources of information contained herein are cited and fully referenced.

Signature:

Signed by candidate

Stephen de Doncker

Date: 29 November 2019

Acknowledgements

Firstly, I would like to extend my utmost gratitude to my supervisors, Assoc. Prof. Gregory Smith and Dr Siyabonga Ngubane for the continuous support, encouragement and guidance throughout the duration of the degree. The constructive criticism, input and discussion over the past few years, resulting in my general and academic growth has been invaluable, Thank you.

I would like to acknowledge Pete Roberts for his expertise and advice on NMR related topics, Dr. Hong Su for single-crystal X-ray diffraction studies, Dr. Marietjie Stander (University of Stellenbosch) for collection of ESI-MS data, and Eva Fischer-Fodor and her colleagues in Romania for hosting me for a brief, but informative, 2-week period. Special mention must be given to Deirdre Brooks for the meaningful chats and much needed laughter and smiles.

To my closest friends, Desmond, Geoffrey, Jauhar, Litha and Raihaan, thank you for the friendship, support and good times over the years. The impact you guys have had on my life is immeasurable.

To my colleagues and friends, Allan, Athi, Ana, Jasmin, Preshendren, Richard, Shepherd, Taella, Taryn and Thato, thank you for the general atmosphere you provided in and around the lab. Time could not have been spent more wisely in other company. A special thanks to Leah for her advice in the final stages of writing.

I would like to acknowledge the members of the organometallic research group for the advice, guidance and encouragement.

To my family; Edgar, Emma, Lauren and Michelle, lessons learned through and with you have helped me throughout my life, and this instance was no exception.

Funding for this project was provided by the National Research Foundation- Department of Science and Technology, c*change.

"Only those who will risk going too far can possibly find out how far one can go"

-T. S. Eliot

Abstract

The hydroformylation reaction is the addition of CO/H_2 (synthesis gas) to olefins using a transition-metal catalyst to produce linear and/or branched aldehydes. This reaction is in alignment with the Green Chemistry philosophy, applying principles such as using renewable feedstocks, atom economy, and catalysis. The use of rhodium-based catalysts for hydroformylation offers greater selectivity and catalytic activity under milder conditions compared to cobalt-based counterparts. Furthermore, the introduction of sterically demanding ligands such as phosphines are often introduced to enhance selectivity and activity of active catalysts. The conjugation of dendritic structures to transition-metal catalysts, to form metallodendrimers, may be useful in introducing functional groups that alter electronic and steric factors as well as increasing the activity through multinuclearity.

Dirhodium(II,II) complexes contain two rhodium atoms, a metal-metal bond and an oxidation state of 4+ over the bimetallic core, resulting in each rhodium atom having an oxidation state of 2+. The electronic and steric influences can be altered by variety of ligands, bearing alkyl or aryl substituents. The purpose of this investigation was to synthesize and characterize a series of dirhodium(II,II) complexes, a suitably functionalized poly-pyridyl scaffold and conjugation of the synthesized complexes to the periphery of the scaffold to form low valent metallodendrimers.

A series of diphenylformamidine ligands bearing electron-withdrawing (fluoro) and electron-donating (methyl) substituents at the *ortho*- and *para*-postions on the phenyl rings were synthesized. Two dirhodium(II,II) complexes bearing acetate bridging ligands with methyl or trifluoromethyl groups and four dirhodium(II,II) complexes, bearing synthesized diphenylformamidinate bridging ligands, were obtained. A trisamine-based pyridyl scaffold was synthesized and conjugated to each dirhodium complex to afford the corresponding low-valent metallodendrimers.

All ligands, complexes and metallodendrimers were characterized by spectroscopic (^{1}H, $^{13}C\{^{1}H\}$, ^{19}F NMR, FT-IR) and analytical (mass spectrometry) techniques where applicable. The paddlewheel structure of the complex and pseudo-planar nature of the formamidine N-C-N system was confirmed by Single crystal X-ray diffraction analyses.

The activity of the synthesized complexes and metallodendrimers were evaluated as catalyst precursors in the hydroformylation of 1-octene. Model reactions were carried out with dirhodium(II,II) tetraacetate as a precursor varying time, pressure and temperature resulting in optimized conditions for the formation of aldehydes, with negligible effects on the activity observed in the presence of mercury.

Acetate bearing complexes showed near quantitative conversion (>99.8%) of 1-octene, excellent activity and chemoselectivity toward aldehydes (>98%) with moderate regioselectivity towards linear products (40-44%). Excellent conversion (97-99%), moderate to good chemoselectivity toward aldehyde products (59-87%) and moderate to good regioselectivity (48-71%) where obtained for diphenylformamidine compounds.

Coordination of the trisamine-based scaffold leads to a general decrease (*ca.* 10%) in the chemoselectivity toward aldehydes and an anticipated general increase in the regioselectivity towards linear aldehyde of between 3-5% under optimized hydroformylation conditions. Chemoselectivity towards aldehydes was favoured by electron-donating groups over electron-withdrawing groups in the diphenylformamidinate complexes, with regioselectivity favouring linear aldehydes observed for analogous complexes containing electron-withdrawing groups.

Conference/ Symposia contributions

1. **Poster Presentation**: Stephen de Doncker, Siyabonga Ngubane and Gregory S. Smith, *Dirhodium paddlewheel complexes: synthesis and application as pre-catalysts in the hydroformylation of 1-octene*, presented at the 2nd Annual PhD Seminar, Department of Chemistry, University of Cape Town, South Africa, **2019**.

2. **Oral Presentation**: Stephen de Doncker, Siyabonga Ngubane and Gregory S. Smith, *Bimetallic dirhodium(II,II) complexes as catalyst precursors in the hydroformylation of 1-octene*, presented at the Cape Organometallic Symposium, University of Cape Town, South Africa, **2019**.

3. **Poster Presentation**: Stephen de Doncker, Siyabonga Ngubane and Gregory S. Smith, *Dirhodium paddlewheel complexes: synthesis and application as pre-catalysts in the hydroformylation of 1-octene*, presented at the University of Cape Town 12th Annual Science Postgraduate Symposium, University of Stellenbosch, South Africa, **2019**.

4. **Oral Presentation:** Stephen de Doncker, Siyabonga Ngubane and Gregory S. Smith, *Dirhodium paddlewheel complexes conjugated to dendrimers: synthesis, structure and applications in catalysis,* presented at the Catalysis Society of South Africa annual Conference, South Africa, **2019.**

Abbreviations, Symbols and Units

°	Degree(s)
δ	Chemical shift
2D	Two-dimensional
°C	Degrees Celsius
μ	Mu(bridging)
Å	Angstrom(s)
Ar	Aromatic or aryl
ATR	Attenuated total reflectance
br	Broad signal (NMR)
$^{13}C\{^{1}H\}$	Proton decoupled carbon-13
cat.	Catalyst
cm^{-1}	Wavenumbers (reciprocal centimetres)
d	Doublet
dd	Doublet of doublets
DAB	1,4-Diaminobutane
DCM	Dichloromethane
DMSO	Dimethylsulfoxide
EI	Electron impact
eq.	Equivalent(s)
ESI	Electrospray ionisation
ETOH	Ethanol
FT-IR	Fourier transform infrared spectroscopy
g	Gram(s)
GC	Gas chromatography
^{1}H	Proton
HAM	Hydroaminomethylation
HETCOR	Heteronuclear correlation spectroscopy
HPLC	High-performance liquid chromatography
h	Hour(s)
HR	High resolution
HSQC	Heteronuclear single quantum correlation

Hz	Hertz
IR	Infrared
J	Coupling constant
kV	Kilovolt(s)
m	Multiplet (NMR); medium intensity (IR)
MeOH	Methanol
MHz	Megahertz
mL	Millilitre(s)
mol	Mole(s)
mmol	Millimole(s)
MP	Melting Point
MS	Mass spectrometry
m/z	Mass to charge ratio
n	normal
NMR	Nuclear magnetic resonance
ORTEP	Oak Ridge Thermal Ellipsoid Plot
o	ortho
p	Para
Pet. Ether	Petroleum ether
Ph	Phenyl
ppm	Parts per million
q	Quartet
rt	Room temperature
s	Singlet (NMR); strong intensity (IR)
SD	Standard deviation
SHOP	Shell higher olefin process
syngas	Synthesis gas
t	Triplet
TOF	Turnover frequency
TRIS	Tris-2-(aminoethyl)amine
vs	Versus
w	Weak intensity (IR)
XRD	X-ray diffraction

Table of Contents

CHAPTER 1

Introduction and literature review

1.1 Catalysis

The use of catalyzed processes invoking transition metals form an integral part of both synthetic chemical and industrial processes as an efficient pathway for transformation of low-value feedstocks into higher-value. These compounds with applications in pharmaceutical, petrochemical and polymer industries.[1] Industrially, catalytic processes are ubiquitous and the need for designing and development of improved catalysts and catalytic processes for reducing the environmental impact is an important consideration for large-scale 'greener' chemistry.[2] The Green Chemistry philosophy (Figure 1.1, *vida infra*) is becoming more prominent and the demand for new and more efficient methods of synthesis in academia and industry synthetic chemistry is increasing. In this regard, catalysis ties into several other green chemistry principles, namely, atom economy, energy efficiency and reduction in undesirable by-products.[3,4]

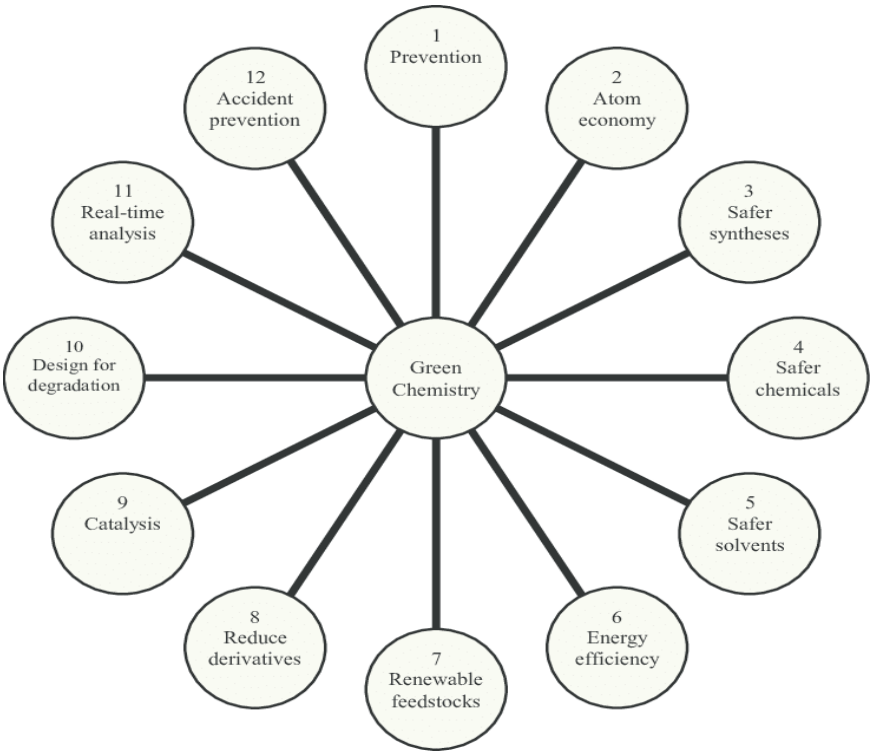

Figure 1.1*: Illustration of the twelve principles of green chemistry*

Due to the wide scope of applications and advantages of catalytic processes, more sustainable synthetic methods in large scale processes through the reduction or elimination of harmful by-products and waste in various chemical processes, compared to more conventional synthetic methods.[5,6]

Catalytic processes offer a range of benefits such as increases in selectivity, lower energy requirements, minimising waste and the use of catalytic amounts of expensive/toxic materials.[4] Catalysis is divided into two classes, namely, heterogeneous and homogeneous systems.

1.1.1 Heterogeneous catalysis

Heterogeneous catalysis makes use of a catalytic species which is in a different phase to the reaction medium allowing for relatively facile separation processes such as direct filtration. This is advantageous in the industrial sector where recovery of expensive and possibly toxic transition-metal catalysts is desirable. A disadvantage in this class of catalysis is that reactions take place at the interphase between different media, impacting the selectivity and reactivity negatively through limited interaction between the substrate- and catalyst containing phases.

1.1.2 Homogeneous catalysis

Homogeneous catalytic systems contain a reaction medium with the catalysts and substrate in the same phase. The primary advantages of homogeneous systems are high selectivity and reactivity since the catalyst-substrate interaction is maximised throughout the reaction medium as well as the ability to modify key aspects such as the chemoselectivity, regioselectivity and enantioselectivity of the catalyst.[7-9] Examples of catalysts modified for enantioselectivity are widely used in organic synthesis such as in Sharpless epoxidation[10], where the accessibility of incoming substrates are hindered by chiral ligands which induce chirality to the metal complex. While characteristics of homogeneous systems are widely considered to be advantageous, a major disadvantage in the form of separation of the desired product from the expensive or toxic transition-metal catalytic species is encountered. This is usually accomplished by energy intensive processes such as distillation.[9.10] Additionally, separation of products in homogeneous systems carried out through distillation may cause catalyst degradation if high temperatures are required.[11] Furthermore, catalyst degradation may occur through the breaking

and reforming of metal-ligand bonds throughout the catalytic cycle, hence, optimal binding of the ligand remains an important factor to consider when designing highly efficient catalysts.[1]

1.2 Hydroformylation

Hydroformylation is the transition-metal catalysed addition of carbon monoxide and hydrogen to olefins resulting the formation of C-C bonds and ultimately, formation of aldehydes (Scheme 1.1, *vida infra*). The process was first discovered by Otto Roelen in 1938 using a carbonyl based cobalt active catalyst species, $HCo(CO)_4$, obtained *in situ* from the catalytic precursor $Co_2(CO)_8$ in the presence of high pressure molecular hydrogen.[12] Although aldehydes are the major product, hydrogenation of the alkene substrate to form alkanes and alcohols can also occur.[9,13] Catalytic methods of functionalizing alkene feedstocks is one of the largest important industrial processes, converting low-value substrates from the petroleum and chemical industries into higher value aldehyde precursors with many synthetic applications.[13,14] Aldehyde products obtained from the hydroformylation of suitable feedstocks can be used to produce compounds such as acrolein, alcohols, carboxylic acids, acetals, amines and pyrans through more conventional stoichiometric means.

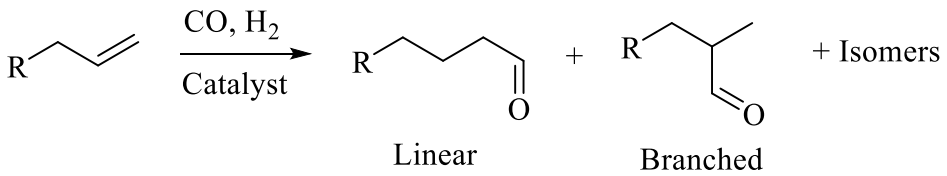

R = alkyl, aryl

Scheme 1.1*: Outline of products formed in the hydroformylation reaction*

Catalysts studied in hydroformylation reactions mostly make use of metals such as ruthenium, platinum, iridium, cobalt and rhodium, with the latter being subject to intensive study.[15,16] Thus far, at least theoretically, it seems reasonable to assume that any transition metal atom capable of forming a carbonyl-hydride complex with suitable activity under the right reaction conditions could be viable as a catalyst species.

Investigations into the hydroformylation activity of transition metals such as osmium, ruthenium, iridium, platinum, palladium, iron and nickel have been carried out.[16,17] Intensive study into catalyst precursors containing rhodium, cobalt, ruthenium and platinum centred

transition metal complexes have been undertaken, with ruthenium and platinum studied mostly for academic interest.[16,17]

Historically, rhodium and cobalt are the transition metals of choice for the design of catalysts for hydroformylation in industrial application for first- and second-generation processes in modified and unmodified forms.[7,8,19] First generation hydroformylation processes made use of cobalt-based carbonyl (CO) containing catalysts almost exclusively in industry, initially providing adequate reaction rates and target products.[20] Primary disadvantages of the unmodified cobalt catalyst systems are the harsh reaction conditions necessary, requiring high temperatures and pressures, as well as low selectivity and the formation of by-products such as alcohols. In addition, catalyst deactivation leads to the formation of metallic cobalt requiring a prior 'de-cobaltation' step before separation by distillation.[21] The use of ligands such as phosphines affording cobalt-phosphine based second-generation catalysts were attempted to address factors in the optimisation of the process and are mostly utilized in the Shell Process.[22]

Rhodium-based catalysts typically requiring milder reaction conditions than the cobalt counterparts, in addition to a decrease in the formation of hydrogenated products and increases in the activity and selectivity.[7,23,24] The regioselectivity (linear vs branched) as well as chemoselectivity (aldehydes vs alcohols or iso-octenes) aspects can be altered through the use of modified ligands, whereby increases in steric interactions and manipulation of the electronic character on the metal centre result in favouring the formation of desired products.[25]

Second generation rhodium-based catalysts utilize modified phosphine ligands, initiated by Wilkinson *et al.* in the 1960s, with chloridotris(triphenylphosphino)rhodium(I) and hydridotris(triphenylphosphino)rhodium(I) being classic examples.[25] Exchanging carbonyl for triphenylphosphine ligands to afford second generation rhodium-centred catalytic precursors show increased selectivity towards linear aldehydes as well as minimisation of isomerisation of the substrate.[26] Wilkinson described two plausible catalytic cycles (Scheme 1.2, *vida infra*) for rhodium based catalysts whereby both dissociative (D) and associative (A) mechanistic pathways are described, starting at the activated catalyst species.[25]

Major differences between the associative and dissociative mechanisms is the initial loss of a carbonyl ligand, although key reaction steps occur in either case. By way of example, the associative mechanism proceeds *via* the formation of a rhodium hydride 5-coordinate species (a), followed by coordination of the alkene substrate forming a coordinatively saturated octahedral complex (b). A hydride migration step forms the rhodium alkyl intermediate (c),

before migratory insertion of a carbonyl ligand occurs to form the rhodium-acyl species (d). The oxidative addition step where the addition of molecular hydrogen forms an octahedral acyl-dihydride complex (e) is formed before reductive elimination occurs, releasing the aldehyde product and reforming the active catalyst species.

Experimental evidence shows that the lowering of CO partial pressure and higher ligand concentration favours the production of linear aldehydes, thus supporting the premise that the increased crowding around the metal centre plays a major role in the formation of specific products in the hydroformylation reaction for these systems.[27]

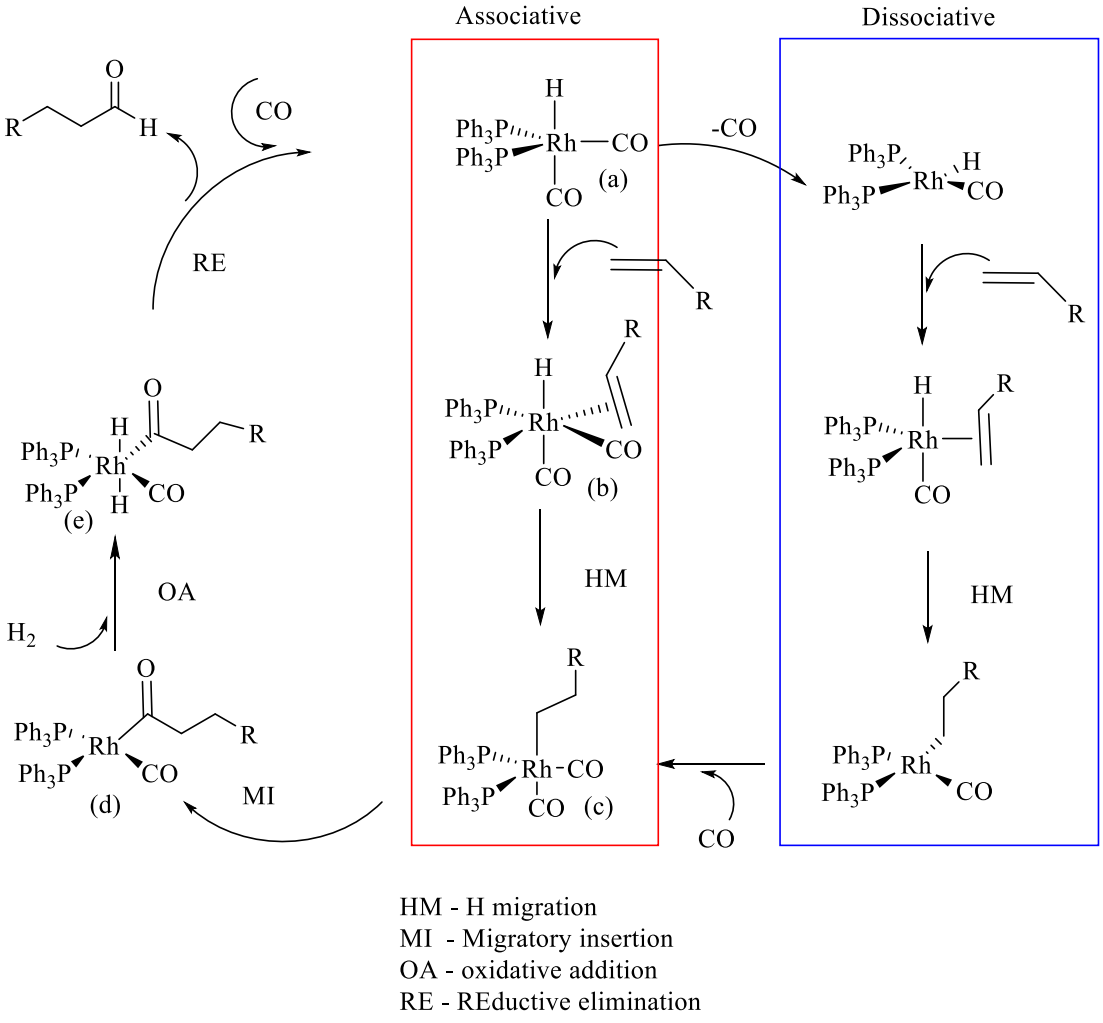

***Scheme 1.2**: Rhodium catalytic cycle depicting associative and dissociative mechanisms*[27]

Variation of the reaction conditions for hydroformylation such as temperature, pressure, catalyst concentration and ligand concentration can be used to affect the regioselectivity, chemoselectivity and activity for catalytic systems. Therefore, careful considerations into the

appropriate reaction conditions are required for the formation of desired products in terms of intermediate reaction kinetics.

The electronic environment around the metal centre is an important factor to consider with the use of ligands having different σ-donor and π-acceptor characteristics being attractive areas of investigation. Based on a multistep the catalytic cycle, influencing the stability of intermediates in the cycle and the ability of the metal centre to undergo reductive elimination or oxidative addition influences the comparable rates of these steps and, in turn, the product distribution. Tucci *et al.* reported that the effects of increasing the basicity of coordinating atoms have a major effect on hydroformylation rates, the trend being the lower the Lewis basicity, the lower the binding affinity and the higher the observed rate of linear product formation when using ligands bearing group 15 coordinating atoms (phosphorous, arsenic and antimony), more specifically, PPh_3, $AsPh_3$ and $SbPh_3$.[28]

The consequence of using these ligands as modifications in cobalt, rhodium, and ruthenium catalyst systems resulted in comparable activities between the phosphorous and arsenic ligands with the obvious trend being a marginal difference in the *n:iso* ratios, 1.0 and 0.8 respectively, due to the expected higher π-acidity of the arsenic bearing ligand which promoted Markovnikov addition in the catalytic cycle. The $SbPh_3$ bearing catalyst showed lower selectivity towards aldehydes with a higher *n:iso* ratio of 2.0 and a twenty percent conversion to hydrogenation products being observed.

In this regard, ligands containing nitrogen atoms should have the highest binding affinity affording a slower hydroformylation rate when directly compared to analogous phosphines. Catalyst precursors with ligands containing oxygen, phosphine and nitrogen atoms are well documented.[16,29,30]

More recently it has been shown that multinuclear complexes exhibit hydroformylation activities greater or equal to their mononuclear counterparts.[31] In this regard, dirhodium complexes are of interest and studies involving the activity of both mono- and bimetallic compounds are common, having shown valuable activities in other catalytic reactions such as allylic oxidation, carbonylation and hydrogenation.[31,32] Govender *et al.* reported and enhancement in the activity in the hydroformylation of 1-octene using mixed valent bimetallic Rh(I)/Rh(III) complexes.[33] Studies on effects of ligand modification to bimetallic catalytic species and improvements with respect to the activity of such complexes by other methods is an attractive area for investigation.

1.3 Dirhodium(II,II) paddlewheel complexes

The effects of binuclearity may be further investigated through complexes containing a bimetallic core as opposed to those containing two discrete metal centres tethered through a bidentate linker ligand. Paddlewheel complexes containing a variety of metal atoms such as vanadium, niobium, chromium, tungsten, molybdenum, rhenium, ruthenium, iron, cobalt, iridium and rhodium have been reported (Figure 1.2), with varying bond orders between metal atoms located in the core.[34]

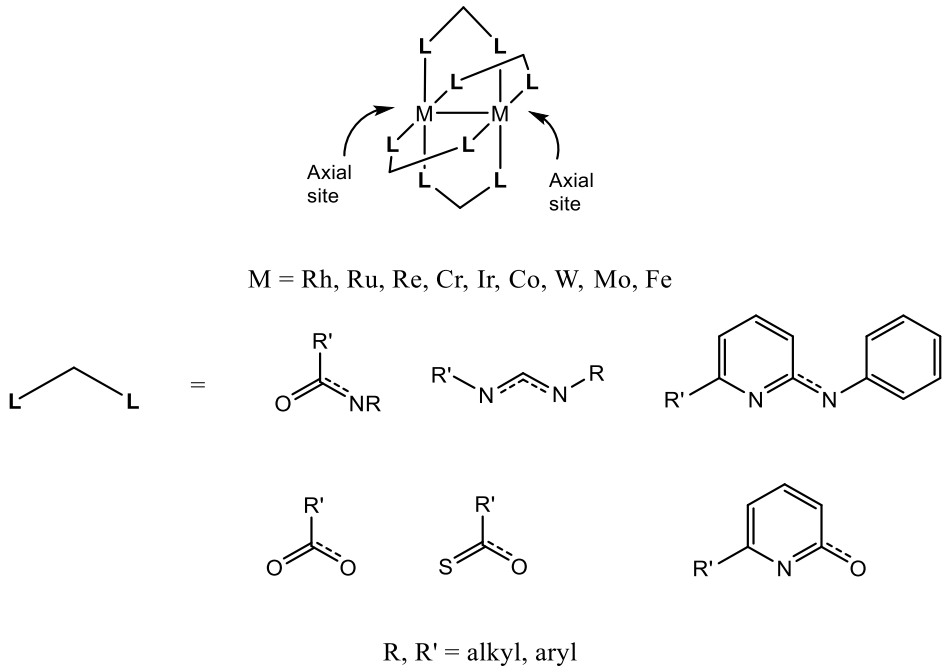

***Figure 1.2**: Bimetallic paddlewheel structure with examples of bridging ligands*

Dirhodium(II,II) paddlewheel complexes having structural nuances such as a metal-metal bond, D_{4h} symmetry and vacant axial sites available for coordination have been studied for their interesting spectroscopic and electrochemical properties.[35] The bridging ligands may be modified to tune the electronic character of the metal centres, allowing for stabilization of higher or lower oxidation states of the bimetallic core.[36]

Early dirhodium complexes were afforded by reacting hexachlorido rhodate species in formic acid to obtain the dirhodium(II,II) tertraformate complex.[37] More recently, dirhodium(II,II) tetraacetate is efficiently obtained through a reaction of $RhCl_3 \cdot 3H_2O$ in a mixture of sodium acetate, ethanol and acetic acid.[38] Further dirhodium(II,II) compounds are afforded through ligand metathesis reactions by reacting suitable ligands derived from carboxylic acids, formamidines, benzamidines, and oxopyridines (Figure 1.2, *vida supra*).[39-42]

The availability of uncoordinated axial sites may be occupied by solvent molecules containing electron donor atoms, additional pre-formed ligands or modified bridging ligands containing a suitable tether.[43] Coordination to the vacant axial sites of the complex result in changes in the electronic character of the complex. Thus, for reactions such as hydroformylation, the catalytic cycle relies on the ability of the metal to undergo changes in oxidation state (Scheme 1.2, *Section 1.2*).

Comparatively, the intermediary oxidation state of 2+ in dirhodium paddlewheel complexes, in relation to the 1+ oxidation state in more conventional rhodium centred hydroformylation catalytic precursors, may allow for more facile oscillation between Rh(I) and Rh(III) oxidation states required in the catalytic cycle. Additionally, the bond between the rhodium atoms may allow for delocalization of charge in the core combined with the electronic effects of the bridging ligands. This could further allow for better accessibility to higher and/or lower oxidation states as required.[44]

1.4 Methods of catalyst immobilization

Homogeneous and heterogeneous catalysis are widely used in industry, however, increasing the ease of separability of catalysts from homogeneous systems would have major benefits to the recyclability of the catalyst species in decreasing factors such as the cost, degradation and possible ecological hazards. The immobilization of catalysts onto various inorganic and organic supports has been attempted to achieve these goals.[7] Several types of immobilization techniques have been introduced to homogeneous catalysis, each can be identified or defined by the types of support used and the catalyst-support interaction, including covalent interaction, electrostatics, adsorbtion, encapsulation.[45-47] Covalent bonding is a popular type of method for the anchoring of catalysts (Figure 1.3), being robust enough to withstand the harsh conditions in reactions such as hydrofomylation.[7, 49]

The process of heterogenizing catalysts which would otherwise fall into the class of homogeneous catalysis uses suitably functionalized ligands which are attached to solid materials, usually inorganic oxides or polymers to form insoluble supports. These then allow for separation by direct filtration.[7] An observable trend with the use of polymeric supports as a means of catalyst immobilization results in a notable decrease in catalytic activity or selectivity, due to poor substrate to catalyst contact is observed in heterogeneous catalytic systems.[14]

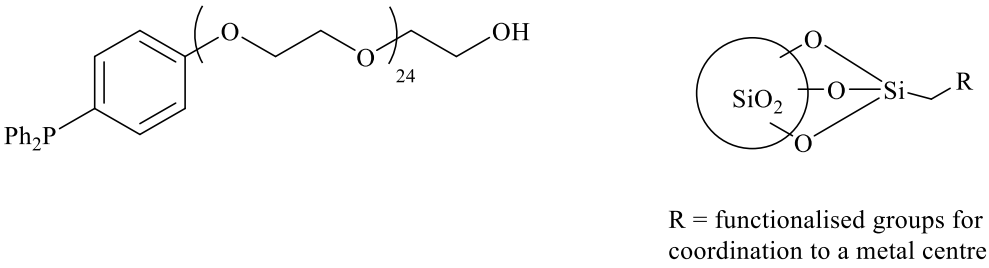

***Figure 1.3**: Examples of modified polyethylene glycol and silica supports*[7]

1.4.1 Metallodendrimers

A variation on the polymer support approach is to use a suitable dendrimer than can be removed from the solution easily *via* precipitation, membrane filtration or a combination of these two methods.[14] Dendrimers are three-dimensional molecules characterized by a central core which expands into a periphery which becomes denser with increasing generation number, *n* (Figure 1.4).[54] These types of macromolecules possess features and physical properties such as precise control of molecular weight, monodispersity and 100% branching degree, and as such have become increasingly popular in chemistry, biology and material and nanotechnololgy.[50]

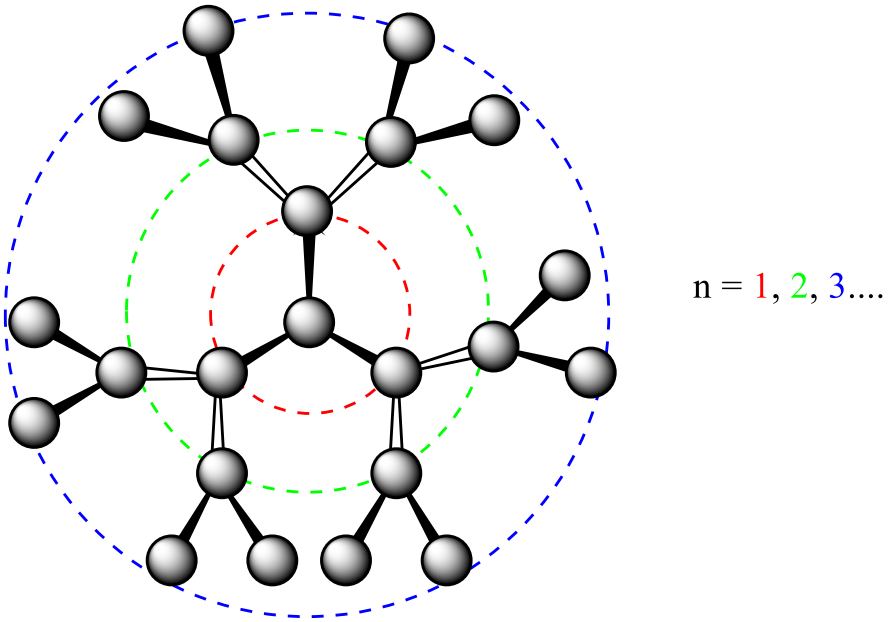

***Figure 1.4**: Graphic representation of a general dendritic structure*

By way of example, the synthesis of dendritic scaffolds based on a diaminobutane core is obtained through a Michael addition of acrylonitrile to diamino butane, forming a branched nitrile species, followed by a Raney-Cobalt reduction of the terminal nitrile groups to afford the branched amine species.[48,51]

The applications of dendrimers include drug delivery agents, adhesives, high performance polymers, biosensors, chemotherapeutic agents, diagnostic imaging and catalysis.[52,53] Common dendrimers make use of functionalities such as polypropyleneimine, poly(amidoamine) and poly(benzylether) moieties.[54,55] An example of a widely used dendritic scaffold from the polypropyleneimine family makes use of diaminobutane (DAB) as a base or core, branching into 4*n* propylamine chains, depending on the generation number *n*. In theory, these terminal amine groups can then be functionalized to incorporate ligands such as phosphines, imines and oxides capable of binding to metal complexes, thereby forming metallodendrimers. Low-valent scaffolds may be obtained through a similar synthetic modifications to suitable molecules such as tris(2-aminoethyl)amine.[56] Molecular structures of simple polyamine scaffolds are shown in Figure 1.5 below.

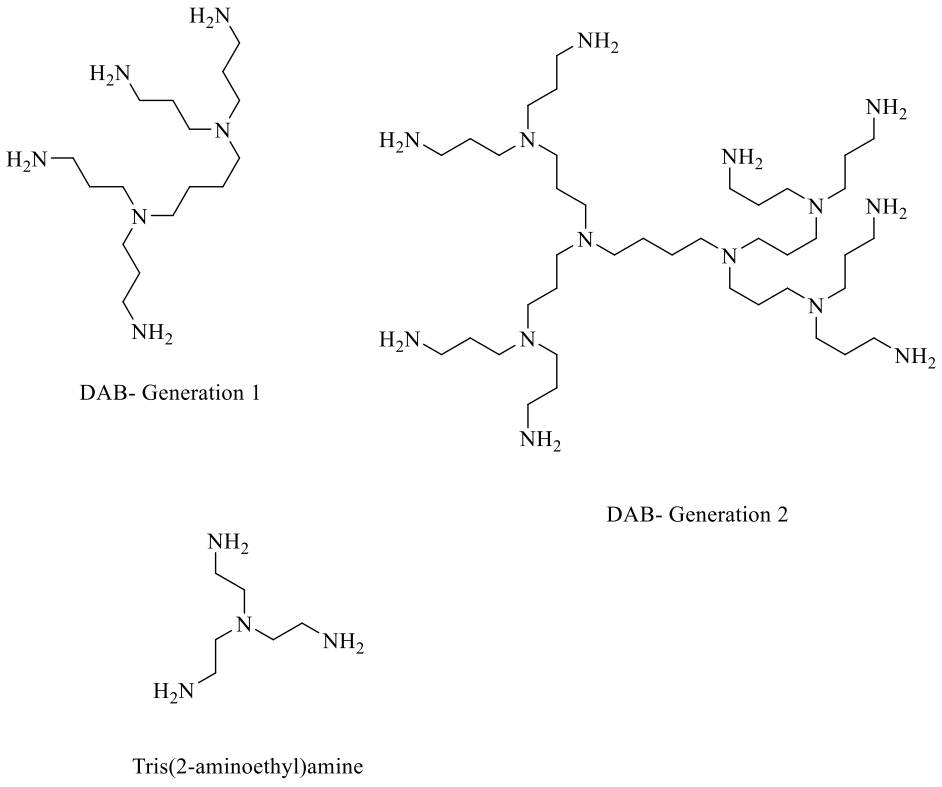

Figure 1.5*: Tris(2-aminoethyl)amine and first-and second-generation DAB-based dendrimers*

Metallodendrimers, like their dendrimer conjugates, are branched monodisperse macromolecules which contain metal atoms at the core, interspersed throughout the molecular

framework or at the periphery (Figure 1.6, *vida infra*).[23,29] The integration of transition metals into dendritic frameworks to form metallodendrimers was initiated by Newkome *et al.* in the 1990s who reported the use and modification of functional groups capable of binding to metallic complexes located on the periphery of dendrimer scaffolds.[57]

The application of these techniques to afford catalytic species in the form of metallodendrimers may be used as a method of catalyst immobilization *via* covalent interactions as previously described.[53] This allows for an increase in the concentration of metal complexes at defined sites in the macromolecule which can, in turn, influence factors such as reactivity, selectivity and separability, which have become a recurring motif in the area of catalysis.

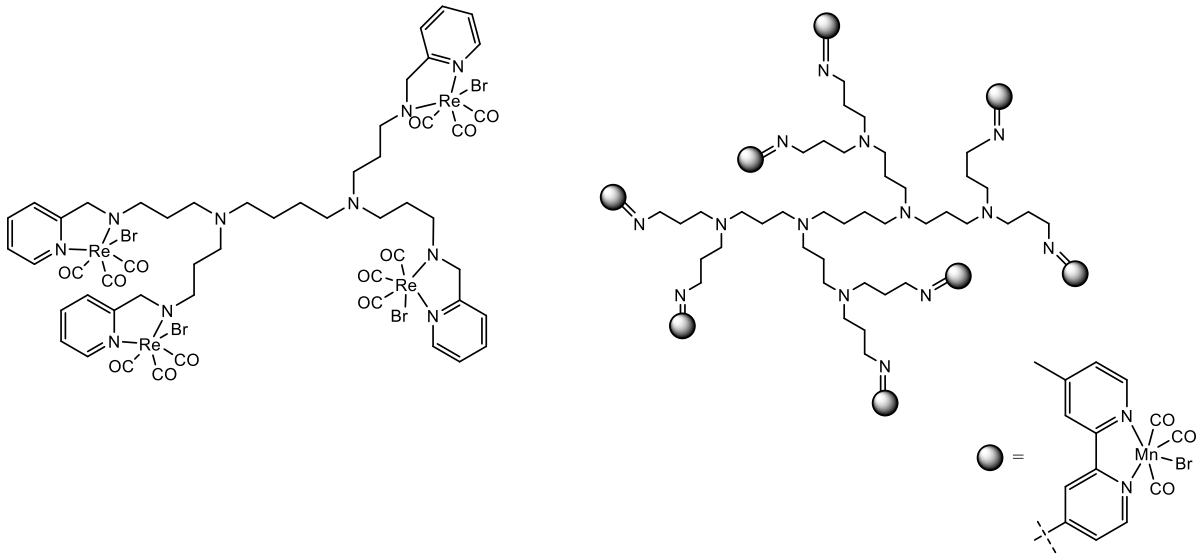

***Figure 1.6**: Examples of first- and second-generation DAB- based metallodendrimers with metal centres located at the periphery*[23,29]

The separability aspect of metallodendrimers is usually achieved through ultrafiltration, of catalysts from the reaction medium and products formed.[3] Dendritic frameworks may contribute to the stabilization of metal complexes through functional groups throughout the molecular structure.[58]

Careful design or selection of a dendritic support for specific catalytic applications may be used in order to combine the best properties of both heterogeneous and homogeneous systems for industrial applications.

1.5 Aims and objectives

1.5.1 General aims

The application of dirhodium(II,II) complexes in catalytic reactions is widely reported due to the ability of complexes in this class to access high and low oxidation states with the use of appropriate ligands. Reports of dendritic structures having these bimetallic complexes are less prominent. The use of dirhodium(II,II) catalytic precursors based on acetate and formamidinate ligands, as well as coordination of these complexes to dendritic scaffolds is an attractive area for further investigation. In this regard, the aims of this project were:

- To synthesize and characterize a series of *ortho*- and *para*-substituted diphenylformamidine ligands bearing electron withdrawing and electron releasing groups.
- To synthesize and characterize fully substituted dirhodium(II,II) complexes with carboxylate and diphenylformamidinate bridging ligands.
- To synthesize and characterize a series of low-valent metallodendrimers bearing dirhodium(II,II) complexes on the periphery.
- To evaluate all synthesized complexes in the hydroformylation of 1-octene

1.5.2 Specific objectives

1. The synthesis of diphenylformamidine ligands bearing fluoro- and methyl substituents at either the *ortho*- or *para*- positions (Scheme 1.3).

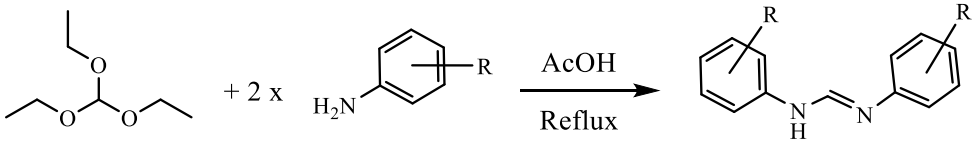

R = 4-Methyl, 2-Methyl, 4-Fluoro, 2-Fluoro

Scheme 1.3*: Outline for the synthesis of diphenylformamidine ligands*

2. Fully substituted dirhodium(II,II) paddlewheel complexes containing bridging carboxylate and diphenylformamidinate ligands were synthesized and characterized (Scheme 1.4).

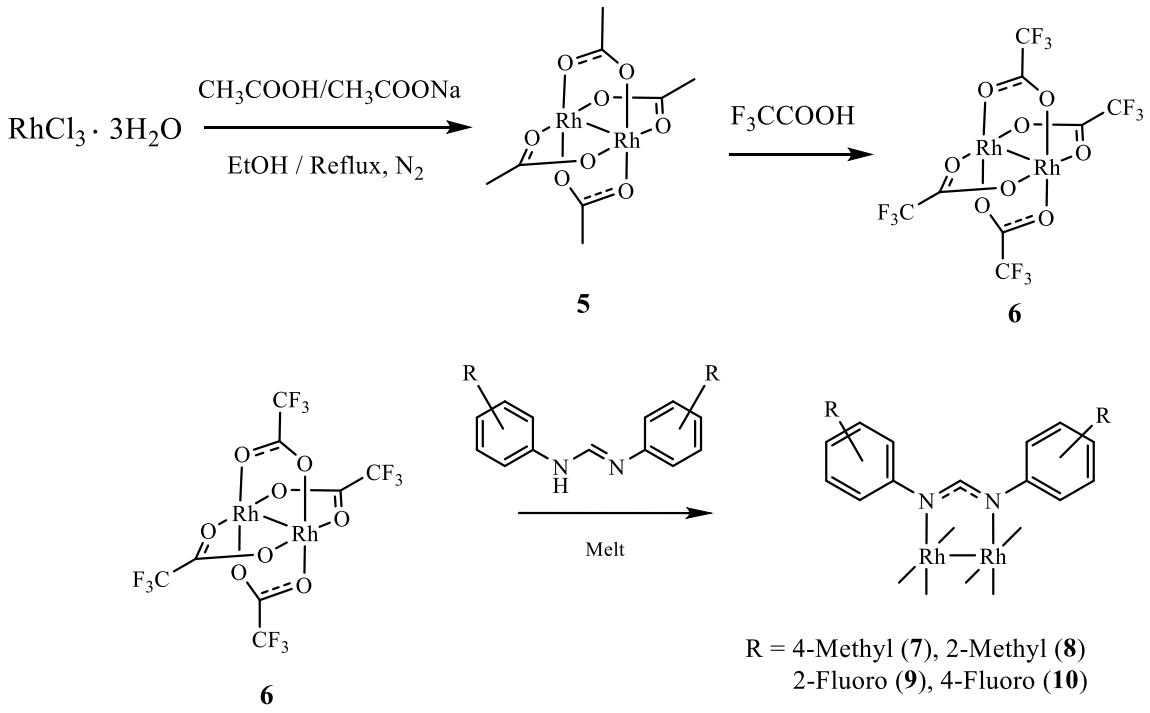

Scheme 1.4*: Outline for the synthesis of dirhodium(II,II)complexes*

3. A tris(2-aminoethyl)amine based scaffold bearing pyridyl groups on the periphery was synthesized and characterized (Scheme 1.5).

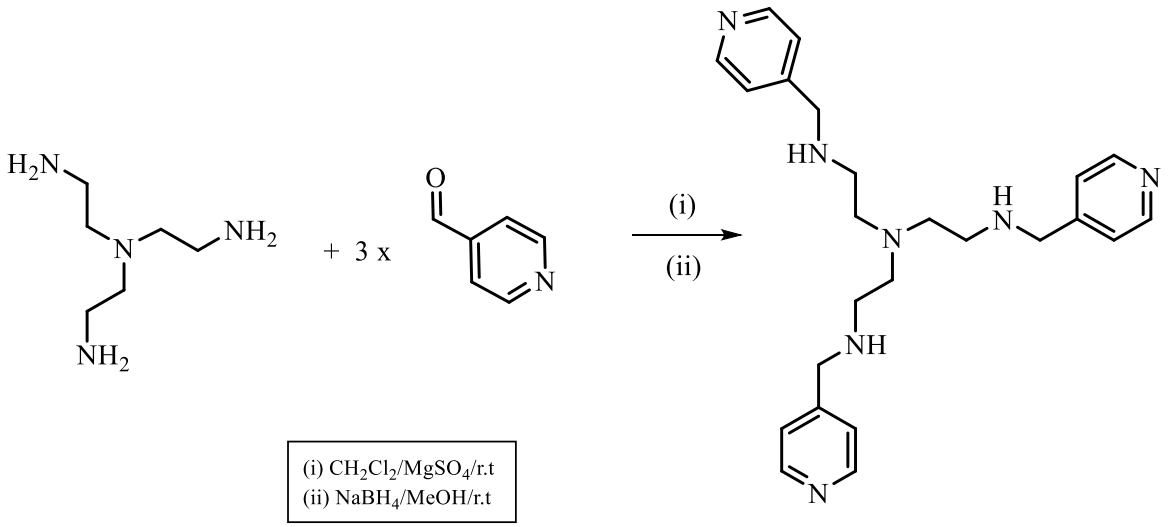

Scheme 1.5*: Outline for the synthesis of low-valent dendritic scaffold*

4. The conjugation of synthesized dirhodium(II,II) complexes to model and dendritic scaffold moieties *via* coordination of the pyridyl moiety to an axial site (Scheme 1.6).

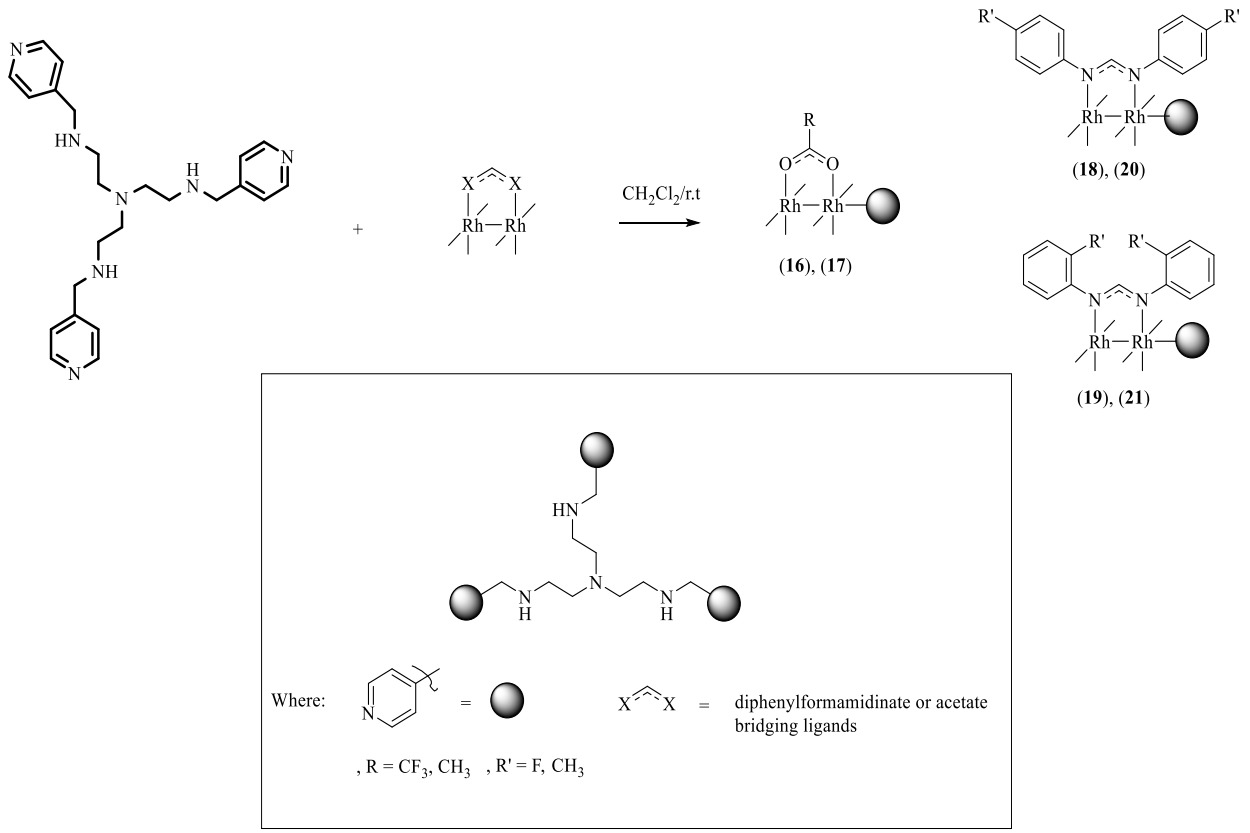

***Scheme 1.6**: Outline for the synthesis of low-valent metallodendrimers with dirhodium(II,II) complexes on the periphery*

5. All compounds were characterized using standard spectroscopic and analytical techniques, including Nuclear Magnetic Resonance spectroscopy (NMR), Fourier-Transform Infrared spectroscopy (FT-IR), and Electron Impact (EI) or Electro-Spray Ionization (ESI) spectrometry. Single Crystal X-ray Diffraction (XRD) analysis was used in the cases where single crystals were obtained to verify molecular structures.

6. The synthesized complexes and low-valent metallodendrimers were evaluated as catalytic precursors in the hydroformylation of 1-octene to determine optimum conditions to produce aldehydes and whether conjugation to a scaffold favours product selectivity and activity. The hydroformylation products were quantified using GC-FID.

1.6 References

1. R. J. Detz, S. A. Heras, R. de Gelder, P. W. N. M. van Leeuwen, H. Hiemstra, J. N. H. Reek and J. H. van Maarseveen, *Org. Lett.*, 2006, **8**, 3227-3230.
2. E. de Jesus and J. C. Flores, *Ind. Eng. Chem. Res.*, 2008, **47**, 7968-7981.
3. P. T. Anastas, L. B. Bartlett, M. M. Kirchhoff and T. C. Williamson, *Catal. Today*, 2000, **55**, 11-22.
4. P. T. Anastas, M. M. Kirchhoff and T. C. Williamson, *Appl. Catal., A*, 2001, **221**, 3-13.
5. P. J. Baricelli, M. Rodriguez, L. G. Melean, M. M. Alonso, M. Borusiak, M. Rosales, B. Gonzalez, K. C. B. De Oliveira, E. V. Gusevskaya and E. N. Dos Santos, *Appl. Catal. A.* **2015**.
6. G. Centi, P. Ciambelli, S. Perathoner and P. Russo, *Catal. Today*, 2002, **75**, 3-15.
7. D. J. Cole-Hamilton, *Science*, 2003, **299**, 1702-1706.
8. N. Karodia, S. Guise, C. Newlands and J. A. Andersen *Chem. Commun.*, 1998, 2341.
9. R. Franke, D. Selent and A. Börner, Chemical Reviews, 2012.
10. K. Tsutomo and K. Barry Sharpless, *J. Am. Chem. Soc.* 1980, **102,** 5974.
11. P. Arya, N. V. Rao, J. Singkhonrat, H. Alper, S. C. Bourque and L. E. Manzer, *J. Org. Chem.*, 2000, **65**, 1881-1885.
12. O. Roelen, DE Patent DE 849 548 C (1938).
13. P. J. Baricelli, M. Rodriguez, L. G. Melean, M. Modrono Alonso, M. Borusiak, M. Rosales, B. Gonzalez, K. C. B. de Oliveira, E. V. Gusevskaya and E. N. dos Santos, *Appl. Catal., A*, 2015, **490**, 163-169.
14. S. C. Bourque, F. Maltais, W. J. Xiao, O. Tardif, H. Alper, P. Arya and L. E. Manzer, *J. Am. Chem. Soc.*, 1999, **121**, 3035.
15. B. Cornils, and J. Falbe, *New Syntheses with Carbon Monoxide*, Springer, Berlin, 1980, Chapter 1.
16. W. Alsalahi, R. Grzybek and A. M. Trzeciak, *Catal. Sci. Technol.*, 2017, **7**, 3097-3103.
17. S. Pandey, K.V. Raj, D. R. Shinde, K. Vanka, V. Kashyap, S. Kurungot, C. P. Vinod and S. H. Chikkali, *J. Am. Chem. Soc.*, 2018, **140**, 4430-4439.
18. J. Wencel-Delord, T. Dröge, F. Liu and F. Glorius, *Chem. Soc. Rev.*, 2011, **40**, 4740.
19. F. P. Pruchnik, *Organometallic Chemistry of Transition Metals*, 1990, 691.
20. A. Chalk and J. Harrod, *Adv. Organomet. Chem.*, 1968, **6**, 119-170.
21. S. L. Desset, PhD thesis, University of St. Andrews, 2009.
22. W. Keim, *Chem. Ing. Tech.*, 1984, **56**, 850.

23. T. Mizugaki, M. Ooe, K. Ebitani and K. Kaneda, *J. Mol. Catal. Chem.* 1999, **145**, 329.
24. J. Pospech, I. Fleischer, R. Franke, S. Buchholz and M. Beller, *Angew. Chem. Int. Ed*., 2013, **52**, 2852-2872.
25. D. Evans, J. A. Osborn and G. Wilkinson, *J. Am. Chem. Soc*., 1968, **90**, 3133-3142.
26. M. Schreuder-Goedheijt, P. C. J. Kamer and P. W. N. M van Leeuwen, *J. Mol.Catal.*, 1998, **134**, 243.
27. R. L. Pruett, *Adv. Organomet. Chem*., 1979, **17**, 1.
28. E. R. Tucci, *Ind. Eng. Chem., Prod. Res. Dev*., 1971, **9**, 516.
29. N. C. Antonels, J. R. Moss and G. S. Smith, *J. Organomet. Chem.*, 2001, **696**, 2003.
30. M. T. Reetz, G. Lohmer, R. Schwickardi, *Angew. Chem. Int. Ed. Engl*., 1997, 36 (13), 1526-1529.
31. S. Siangwata, N. C. C. Breckwoldt, N. J. Goosen and G. S. Smith, *Appl. Catal. A.*, 2019, **585**, 117179.
32. H. K. Kisan and R. B. Sunoj, *J. Org. Chem.*, 2015, **80,** 2192.
33. P. Govender, S. Ngubane, B. Therrien and G. S. Smith, *J. Organomet. Chem.*, 2017, **848**, 281-287.
34. F. A Cotton, C. Murillo and R. Walton, *Multiple bonds between metal atoms*, Springer, Boston, MA, 2005, 3rd edition, Chapter 12, 465-589.
35. J. L. Bear, B. Han, Y. Li, S. Ngubane, E. Van Caemelbecke and K. M. Kadish, *Polyhedron*, 2009, **28** (8), 1551–1555.
36. J. L. Bear, E. Van Caemelbecke, S. Ngubane, V. Da-Riz, and K. M. Kadish, *Dalton Trans.*, 2011, **40** (11), 2486–2490.
37. T. A. Stephenson, S. M. Morehouse, A. R. Powell, J. P. Heffer and G. Wilkinson, *J. Chem. Soc.*, 1965, 3632.
38. G. A. Rempel, P. Legzdins, H. Smith and G. Wilkinson, *Inorg. Synth.*, 1972, **13**, 90.
39. F. A. Cotton, E. V. Dikarev and S. E. Stiriba, *Inorg. Chem.*, 1999, **38**, 4877-4881.
40. T. Ren, C. Lin, E. J. Valente and J. D. Zubkowski, *Inorg. Chim. Acta.*, 2000, **297**, 283.
41. L. P. He, C. L. Yao, M. Naris, J. C. Lee, J. D. Korp and J. L. Bear, *Inorg. Chem.*, 1992, **31**, 620.
42. F. A. Cotton and T. R. Felthouse, *Inorg. Chem.*, 1981, **20**, 584.
43. B. G. Anderson, D. Cressy, J. J. Patel, C. F. Harris, G. P. A. Yap, J. F. Berry and A. Darko, *Inorg. Chem.*, 2019, **58** (3), 1728-1732.
44. A. Cassimiro, MSc Thesis, University of Cape Town, 2018.

45. P. McMorn, and G. J. Hutchings, *Chem. Soc. Rev.*, 2004, **33**, 108.
46. S. Malaza, P. Govender, M. Schutte-Smith, H. G. Visser and G. S. Smith, *Eur. J. Inorg. Chem.* 2017, 3919.
47. Y. Guoyu, S. Ailing, Z. Wenfeng, Z. Hailin and J. Denggao, *Catal. Lett.*, 2007, **118**, 275-279.
48. U. Boas, J. B. Christensen and P. M. H. Heegaard, *J. Mater. Chem.*, 2006, **16**, 3785.
49. X. S. Zhao, X. Y. Bao, W. Guo and F. Y. Lee, *Materials Today*, 2006, 9, **3**, 32.
50. J. Y. Chen, M. Smet, J. C. Zhang, W. K. Shao, X. Li, K. Zhang, Y. Fu, Y. H. Jiao, T. Sun, W. Dehaen, F. C. Liu and E. H. Han, *Polym. Chem.* 2014, **5**, 2401.
51. A. W. Bosman, H. M. Janssen and E. W. Meijer, *Chem. Rev.*, 1999, **99**, 1665-1688.
52. S. Malaza, P. Govender, M. Schutte-Smith, H. G. Visser and G.S. Smith, *Eur. J. Inorg. Chem.* 2017, 3919.
53. R. Malgas, S. F. Mapolie, S. O. Ojwach, G. S. Smith and J. Darkwa, *Cat. Comm*., 2008, **9,** 1612.
54. D. A. Tomalia, A. M. Naylor and W. A. Goddard, *Angew. Chem., Int. Ed.*, 1990, **29**, 138-175.
55. J. W. Lee, B. K. Kim, S. C. Han and J. H. Kim, *Bull. Korean Chem. Soc.*, 2009, **30**, 157-162.
56. D. Giffard, E. Fischer-Fodor, C. Vlad, P. Achimas-Cadariu and G. S. Smith, Eur. J. Med. Chem., 2018, **157**, 773-781.
57. G. R. Newkome, C. N. Moorefield, G. R. Baker, A. L. Johnson and R. K. Bahera, *Angew. Chem. Int. Ed. Eng*, 1991, **30**, 1689.
58. C. Williams, M. Ferreira, E. Monflier, S. F. Mapolie and G. S. Smith, *Dalton Trans.*, 2018, **47**, 9418.

CHAPTER 2

Synthesis of *N,N'*-diphenyl formamidine ligands and dirhodium(II,II) paddlewheel complexes bearing acetate and formamidinate bridging ligands

2.1 Introduction

Since the first report of bimetallic lantern/paddlewheel complexes in the 1960's[1], extensive investigations into their redox, structural and chemical properties have been undertaken. Interesting features and observations made for this type of complex includes the presence of a metal-metal bond and a lantern or paddlewheel-like structure. This structure arises from the equatorial ligands binding across the metal-metal core through donor atoms in a bridging fashion (Scheme 2.1). Since the 1970's, ligands have been synthesized with chemically distinct bridging moieties bearing electron withdrawing and releasing groups in order to alter the electronic environment.[1,2]

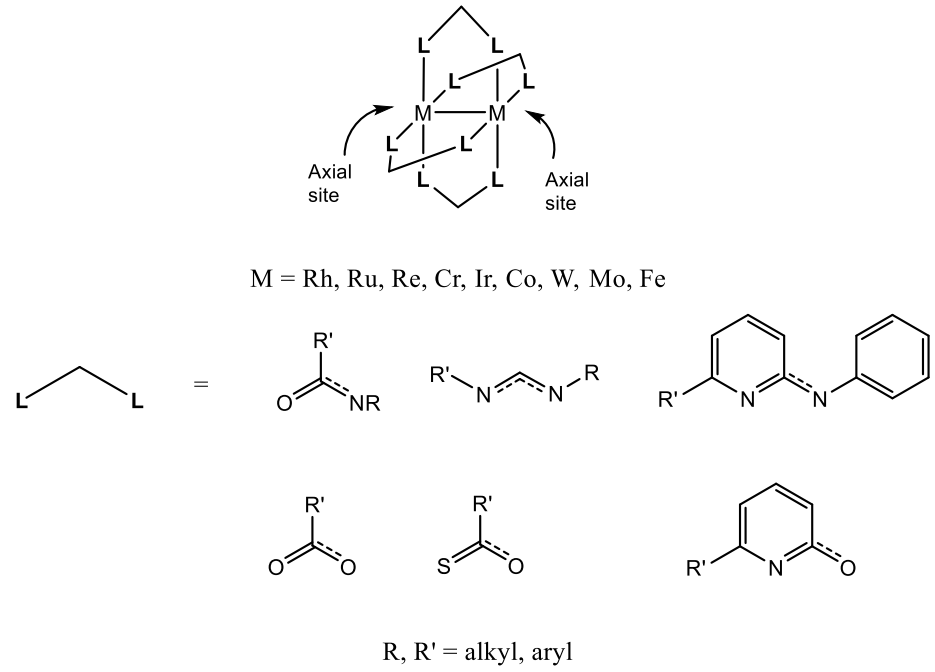

Scheme 2.1*: Paddlewheel structural motif and examples of bridging ligands*

Complexes of the paddlewheel family may contain a variety of metal atoms, with reports of bimetallic complexes containing chromium, tungsten, molybdenum, rhenium, ruthenium, iron, cobalt, iridium and rhodium atoms in the core.[2]

The synthesis of the dirhodium complexes were initially obtained by refluxing a hexachlorido rhodate species $[RhCl_6]^{3-}$ in formic acid, although poor yields were obtained due to the formation of rhodium metal during the course of the reaction.[3,4] The most efficient method for preparing the dirhodium tetraacetato complex is achieved by refluxing $RhCl_3 \cdot 3H_2O$ in a mixture of sodium acetate, ethanol and acetic acid, although deposition of rhodium metal occurs after refluxing for extended periods of time.[5]

The ability for complexes of this type to undergo ligand exchange allows for substitution of the acetate ligands with other functional groups. As a result, the dirhodium tetraacetato complex is widely used as a precursor for the synthesis of dirhodium complexes containing a variety of bridging ligands such as carboxamidates, phosphates, thiocarboxylates, oxopyridinates, aminopyridinates and formamidinates.[6] This affords the dirhodium paddlewheel complex with an oxidation state of 4+ in the core, denoted Rh_2^{4+}.

Additionally, ligands binding to one or both axial sites of dirhodium tetraacetate complexes have been reported to facilitate colour changes through influence on the energy of the LUMO σ^* orbital.[7,8,9] Interactions with molecules capable of coordination as well as their effect on the dirhodium core electronics, catalytic activity and complex structure have previously been investigated.[10,11]

Dirhodium complexes containing binucleating ligands of the diphenyl formamidinate type have been shown to stabilize oxidation states of the core ranging from Rh_2^{3+} to Rh_2^{6+} by increasing the available electron density at the dirhodium core through better σ-donation.[12,13] In addition, electron donating substituents of the phenyl moieties have been demonstrated to produce lower oxidation potentials than complexes containing analogous ligands with electron withdrawing groups.[14]

The tuneability of diphenyl formamidinate type ligands favouring accessibility of the Rh_2^{5+} oxidation or reduction to Rh_2^{3+} could lead to an increase in the catalytic activity of these complexes towards formation of desired products in the hydroformylation reaction. This is discussed later in Chapter 4.

This chapter describes the synthesis and characterization of four *N,N'*-diphenylformamidine ligands bearing mono- substituted phenyl moieties, two dirhodium tetraacetate complexes and four dirhodium tertrakis(diphenylformamidinate) complexes. Characterization was carried out using spectroscopic and analytical techniques such as ^{1}H, $^{13}C\{^{1}H\}$, ^{19}F, ^{103}Rh, two-dimensional (2-D) heteronuclear single quantum coherence (HSQC) and heteronuclear multiple quantum

coherence (HMQC) nuclear magnetic resonance (NMR), infrared (IR) spectroscopy as well as high resolution mass spectrometry (HR-MS).

2.2 Synthesis and characterization of diphenyl formamidine ligands

Synthesis of the formamidine ligands was carried out using literature methods[15,16] with modifications made to the recrystallization step to obtain high purity, albeit ultimately at the expense of higher yields. The ultrasound mediated synthesis of diphenylformamidines from triethyl orthoformate and substituted anilines reported by Dar *et al.*[16] was attempted as a 'greener' alternative to the more classical acid-catalysed procedure. Although ultimately comparable yields were obtained from either method, the greener method was adopted due to the reduction in reaction time (1-2 hours) in comparison to the acid catalysed method (18 hours).

By way of example, the mechanism for the acid catalysed reaction of the aniline with triethyl orthoformate (Scheme 2.2). Protonation of an ethoxy group on triethylorthofomate by the acetic acid results in an ethyloxonium ion, a good leaving group, and allows for the nucleophilic nitrogen atom of the substituted aniline to attack the formyl carbon *via* an S_N2 mechanism with liberation of ethanol (EtOH).

Another, more probable mechanism, may proceed through an oxocarbenium stabilized S_N1 type reaction, however, detailed mechanistic studies were omitted since formation of the ethyloxonium leaving group and the formamidine product is the result in either case. A similar substitution type mechanism should be applicable to the ultrasound method in the absence of the acid catalyst, driven instead by high energy collisions between the molecules as micro-voids in the solution collapse during the process of sonication.

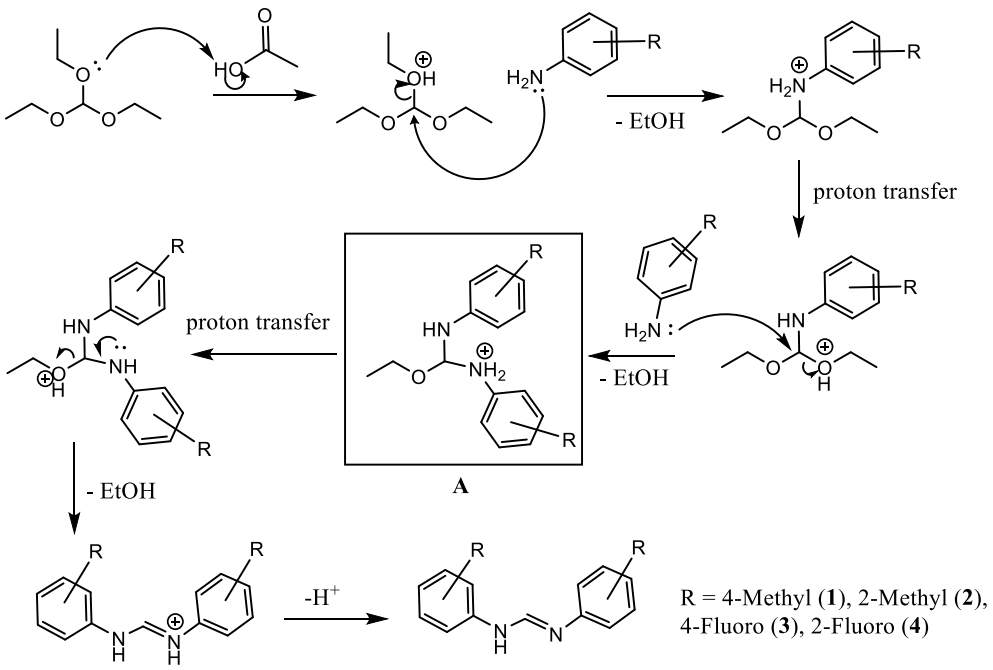

***Scheme 2.2**: Proposed S_N2 mechanism for formamidine synthesis using acetic acid as a catalyst*

Procedures toward the synthesis formamidine ligands were carried out under similar conditions and compared for reactivity. The higher yield for compounds containing substituents in the ortho- position of each phenyl ring was obtained for compound **2**. This may be due to the increased steric bulk of the methyl group of **4**, slowing the rate of the substitution reaction through the bulky intermediate **A** highlighted in Scheme 2.1.

Similarly, when comparing formamidine ligands with substituents in the para position, lower yields were obtained for **3** compared to the **1**. This may be attributed to the lowering of the nucleophilicity of the amine group in 4-fluoroaniline reagent (**4FA**), driven by the strong, inductive electron- withdrawing effect of the fluorine atom dominating the electron donating mesomeric effects.

The subtleties observed in the characterization of methyl (**1**, **2**) and fluoro (**3**, **4**) substituted ligands are outlined separately below.

*2.2.1 Synthesis of methyl substituted N,N'-diphenylformamidine ligands (**1**, **2**)*

Under the reported conditions,[15] synthesis of known compounds **1** and **2** was carried out by reacting two equivalents of either 2-methyl aniline or 4-methyl aniline with one equivalent of triethyl orthoformate in the presence of an acetic acid catalyst under reflux for 18 hours. Ligand **1** was isolated as a light-yellow solid in 59% yield, while ligand **2** was isolated as a white

crystalline solid in 61% yield. Both **1** and **2** were found to be air stable and soluble in dichloromethane, acetone, chloroform, methanol, ethanol and dimethyl sulfoxide.

2.2.1.1 ^{1}H- and ^{13}C{^{1}H}-NMR spectroscopy

The methyl substituted ligands **1** and **2** were characterized by ^{1}H- and ^{13}C{^{1}H}-NMR spectroscopy with full spectroscopic details reported in Chapter 6. Indications of successful synthesis of the ligands is suggested by the appearance of a $(CH)_{formamidine}$ proton signal in the ^{1}H-NMR spectrum (Figure 2.2) at 8.11 ppm (H_1) and 8.04 ppm (H_{1a}) for ligands **1** and **2** respectively.

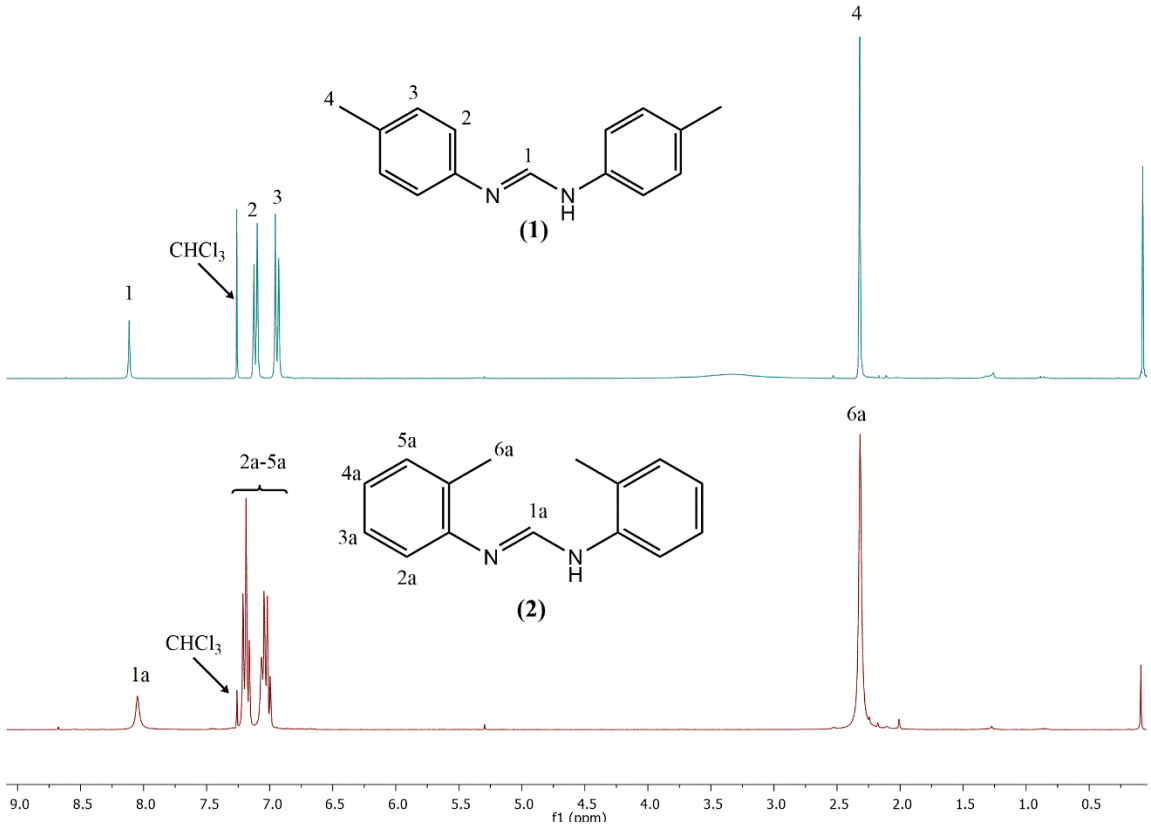

***Figure 2.2**: ^{1}H NMR spectra obtained for **1** and **2** in $CDCl_3$*

Additionally, corresponding downfield shifts observable in the aromatic and methyl proton regions when compared to the respective aniline starting materials can be attributed to the introduction of the N-C=N bond system.

As an example, the spectra obtained for 4-methyl aniline (**4MA**) and compound **1** is shown in Figure 2.3, with the aromatic and methyl regions highlighted in red and blue respectively. Spectroscopic findings are in line with reported data from the literature.[15,16]

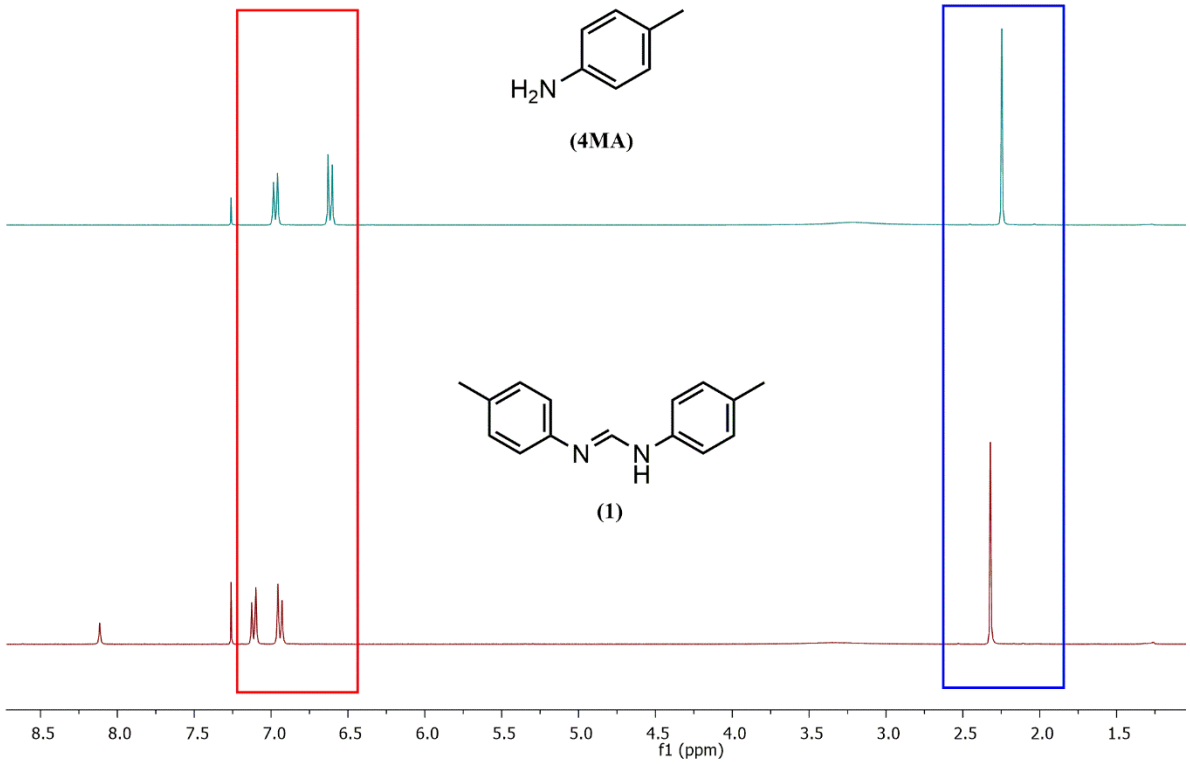

***Figure 2.3**: [1]H-NMR spectra obtained for **1** and **2** in $CDCl_3$*

The $^{13}C\{^1H\}$-NMR spectral analysis of ligands **1** and **2** shows six and eight distinct signals respectively (Figure 2.4). The signals observed at 20.7 and 17.9 ppm were assigned to the methyl substituent on each of the phenyl rings for **1** and **2** respectively. The aromatic carbons were observed in the 117 -145 ppm region and was assigned with the aid of HSQC-NMR analysis, with the characteristic formamidine carbon signal appearing in the 147-149 ppm region. By way of an example, the HSQC spectrum obtained for compound **1** is shown in Figure 2.5.

Although non-equivalent signals were initially expected due do the differences between the imine and amine functionalities in the formamidine system, the nature of the observed NMR signals suggests a symmetrical species present in each case. This is an indication of possible prototropic tautomerism occurring between the imine and amine motifs within the formamidine functionality.

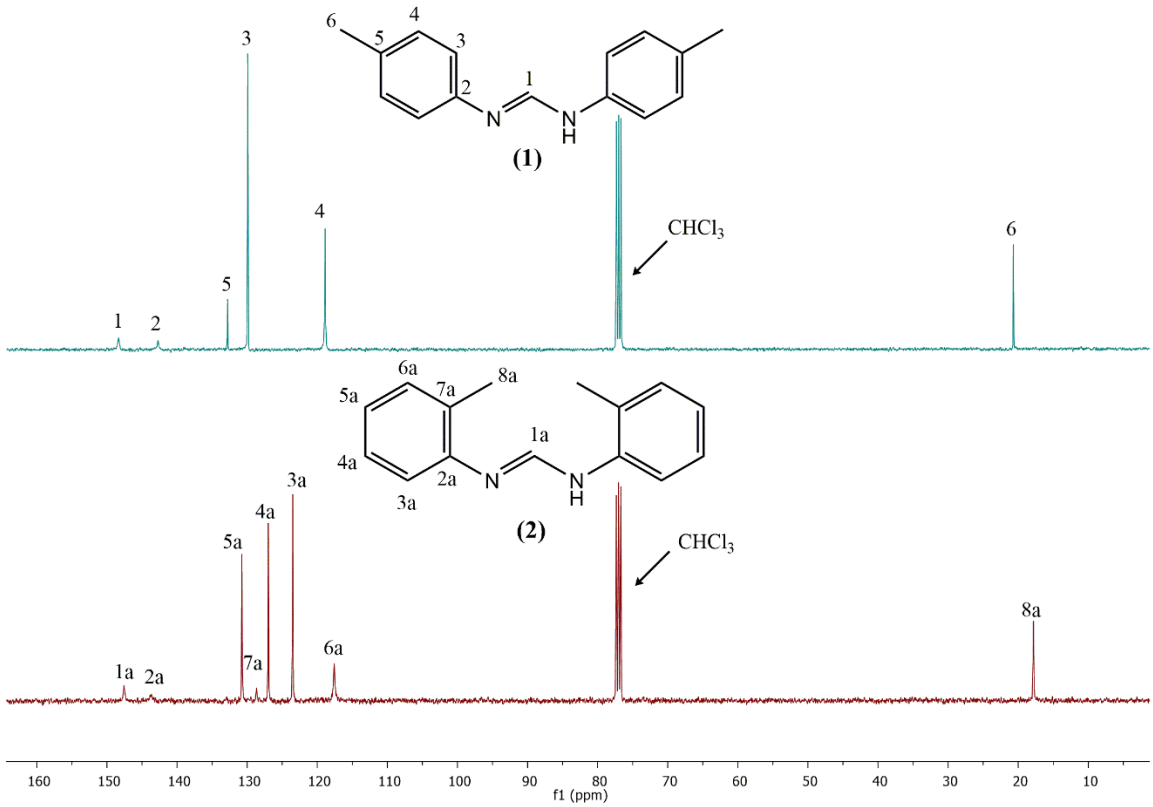

***Figure 2.4**: $^{13}C\{^{1}H\}$-NMR spectra **1** and **2** in $CDCl_3$*

The fluxionality and tautomerism of substituted phenyl formamidines have previously been reported.[17] Possible inversion of the *p*-orbital on secondary amine results is a pseudo-transition state in which the amine lone pair lies in a periplanar arrangement alongside the formamidine *pi*-system, allowing proton exchange and delocalisation of the imine-amine electron system (Figure 2.6).

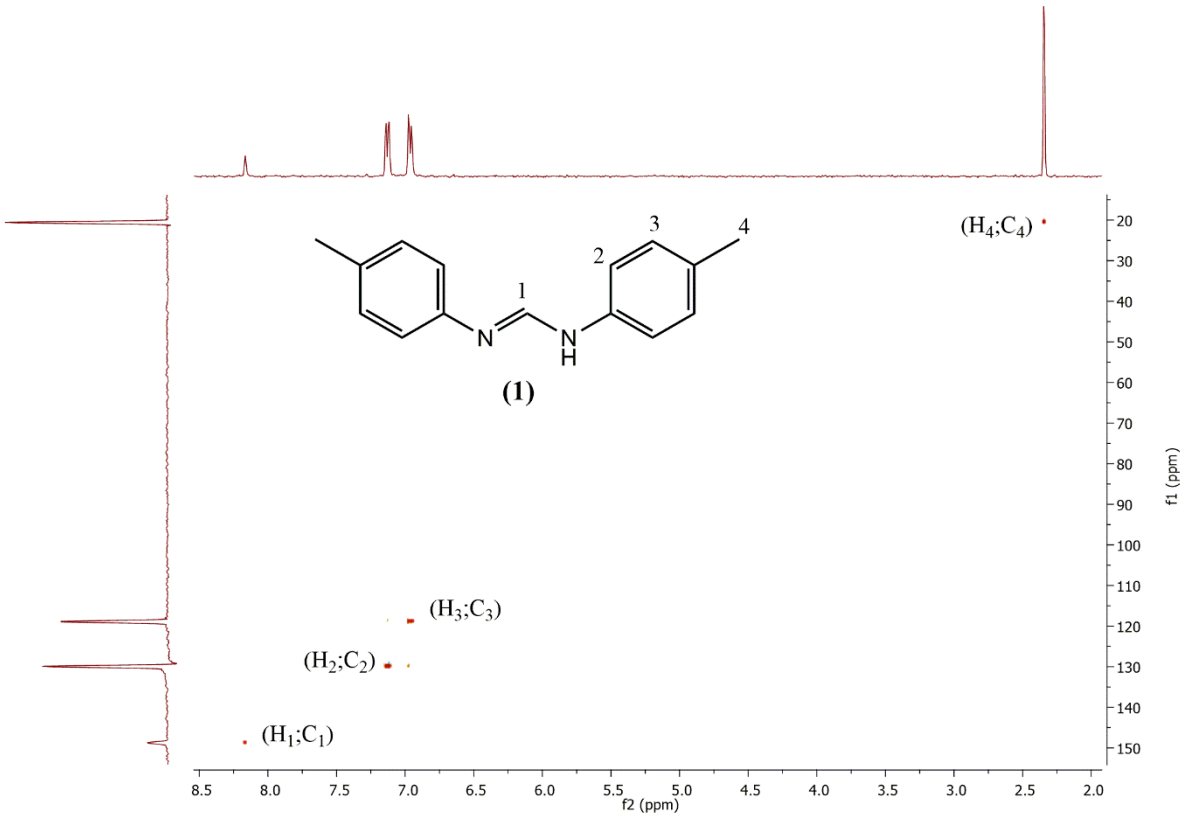

***Figure 2.5**: HSQC-NMR spectra obtained for **1** in $CDCl_3$*

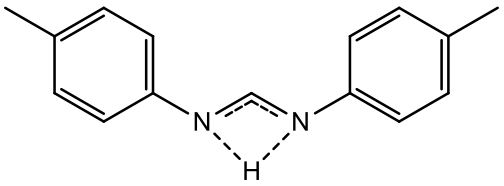

***Figure 2.6**: Depiction of proposed delocalisation of the amine-imine electron system*

2.2.1.2 Infrared (IR) spectroscopy

Infrared spectroscopy was used as a diagnostic tool for confirming successful synthesis. The obtained spectrum of formamidine systems shows characteristic absorption bands for the ν(C=N) vibration mode at 1670 and 1664 cm^{-1} for **1** and **2** respectively, in addition to a broad absorption band observable in the 3000 – 2800 cm^{-1} region, assigned to ν(N-H), the secondary amine functionality in each case.

2.2.1.3 Mass spectrometry

The data obtained from ESI-MS analysis supports the ^{1}H-, ^{13}C{^{1}H}-NMR and IR spectral data, in which a molecular ion peak corresponding to an $[M+H]^{+}$ fragment is observed in the spectra of **1** and **2** at *m/z* 225.1391 and *m/z* 225.1392 respectively.

2.2.1.4 Single Crystal X-Ray Diffraction

Single crystal X-ray diffraction is a useful means of determining the structure of molecules in the solid state. Crystals were grown by slow diffusion of hexane into a concentrated solution of **2** in dichloromethane. The molecular structure obtained (Figure 2.7) and selected bond lengths and angles (Table 2.1) is represented below.

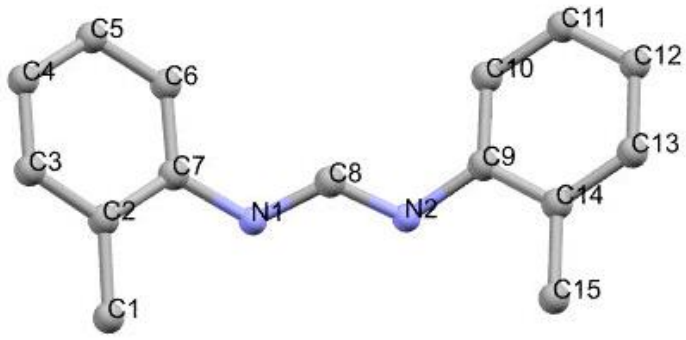

Figure 2.7*: ORTEP diagram of compound **2**, hydrogen atoms omitted for clarity*

Compound **2** crystallizes in the triclinic space group *P-1* with 2 molecules occupying the unit cell. Selected bond lengths, angles and torsion angles obtained for compound **2** is given in table 2.1. The torsion angles of 178.56 (C7-N1-C8-N2) and 176.12 (C9-N2-C8-N1) degrees with bond lengths of 1.32 and 1.30 Å between the N1-C8 and N2-C8 atoms respectively. A bond angle of 123.96 degrees was found for the N1-C8-N2 formamidine system, indicating a trigonal arrangement about the C8 atom.

Similarly, bond angles of 117.39 and 119.23 degrees were calculated for the C8-N2-C9 and C7-N1-C8 systems respectively. The combination of the torsion angles, bond lengths and bond angles strongly suggest a planar arrangement of the atoms across the formamidine system. Hydrogen bonding between H1 and N2 atoms was observed with a bond distance of 2.00 Å.

The observed bond lengths across the formamidine system were found to be considerably shorter than the expected range for a secondary amine (*ca.* 1.45 Å) and longer than expected for the imine portion of the molecule. This data supports the previously speculated delocalised nature of the formamidine system. The methyl substituents on each phenyl ring are observed in the *syn*- conformation.

Table 2.1*: Selected bond lengths, angles and torsion angles for compound **2***

Selected bond lengths	**Interatomic distances (Å)**
N1-C8	1.4219(17)
$N2_{imine}$-C8	1.3235(18)
N1-H1----$N2_{imine}$	2.00(2)

Selected bond angles	**Angle (degrees)**
N1-C8-N2	123.96
C8-N2-C9	117.39
C7-N1-C8	119.23

Selected torsion angles	**Angle (degrees)**
C7-N1-C8-N2	178.56
C9-N2-C8-N1	176.12

*2.2.2.1 Synthesis of fluoro substituted N,N'-diphenylformamidine ligands (**3**, **4**)*

The synthesis of known compounds **3** and **4** was carried out by reacting 2 equivalents of either 4-fluoroaniline or 2-fluoroaniline with one equivalent of triethyl orthoformate in the same manner as described for **1** and **2**. Compound **3** was isolated as an opaque brown solid in 52% yield, while compound **4** was isolated as a white crystalline solid in 75% yield. Both **3** and **4** were found to be air stable and soluble in the same laboratory solvents described for **1** and **2**.

2.2.2.2 ^{1}H-, ^{13}C{^{1}H}-, ^{1}H{^{19}F}- and ^{19}F-NMR spectroscopy

Ligands **3** and **4** were characterized with ^{1}H-, ^{13}C{^{1}H}- and ^{19}F-NMR spectroscopy using deuterated chloroform as a solvent, with full details and associated coupling constants available

in Chapter 6. Successful synthesis is suggested by the $(CH)_{formamidine}$ proton signal observed in the ^{1}H-NMR spectrum (Figure 2.8) at 8.02 and 8.21 ppm for H_1(**3**) and H_{1a} (**4**) respectively.

The expected aromatic signals were observed in ligand **4** however, the spectrum obtained for **3** shows an unexpected doublet signal in the aromatic region integrating for the required number of protons (8H).

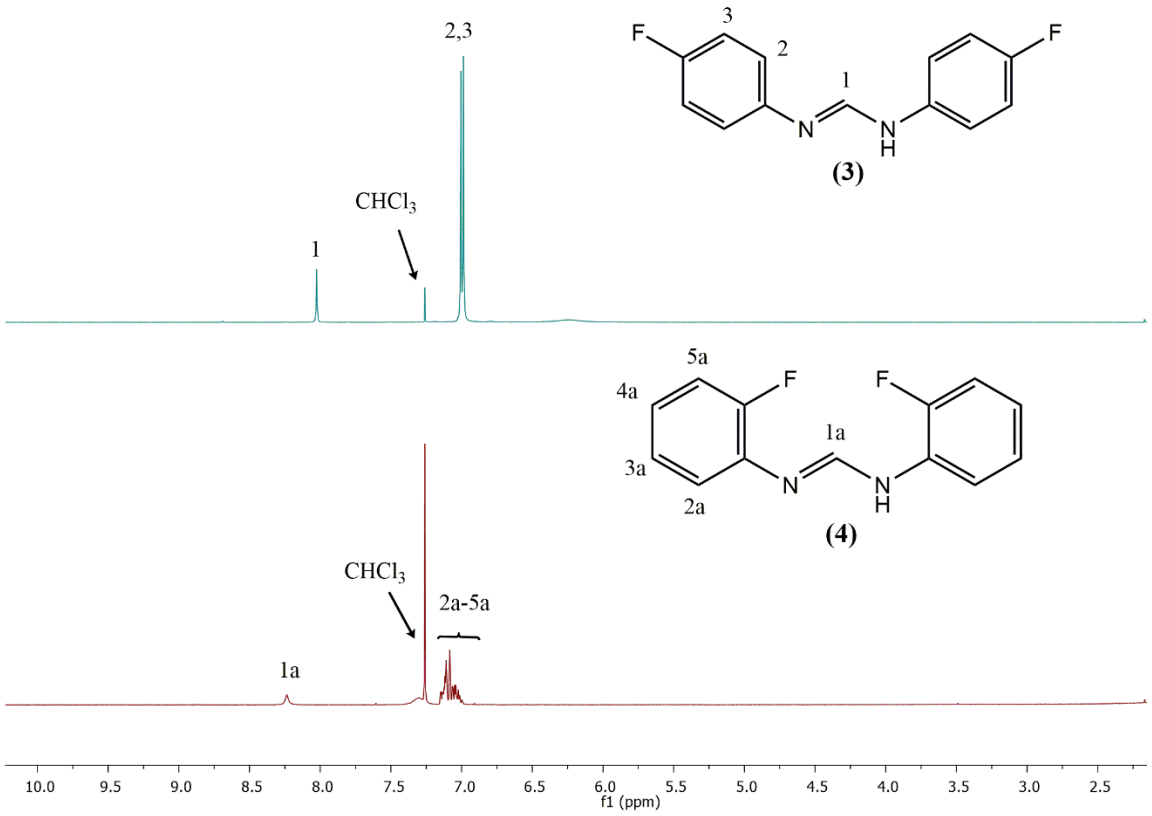

***Figure 2.8**: ^{1}H-NMR spectra obtained for **3** and **4** in $CDCl_3$*

The secondary amine (NH) signals are observed at 6.20 and 7.32 ppm for **3** and **4** respectively, but interestingly the expected triplet and doublet of doublet multiplicity reported for aromatic protons to the fluorine substituent in a 1,4-disubstituted aromatic system was not observed in the case of **3**.

The ^{1}H-NMR spectrum was obtained for 4-fluoro aniline (**4FA**) (Figure 2.9) and compared to the spectrum obtained for **3**. The expected splitting was observed in the starting material with the primary amine signal of **4FA** observed at 3.48 ppm.

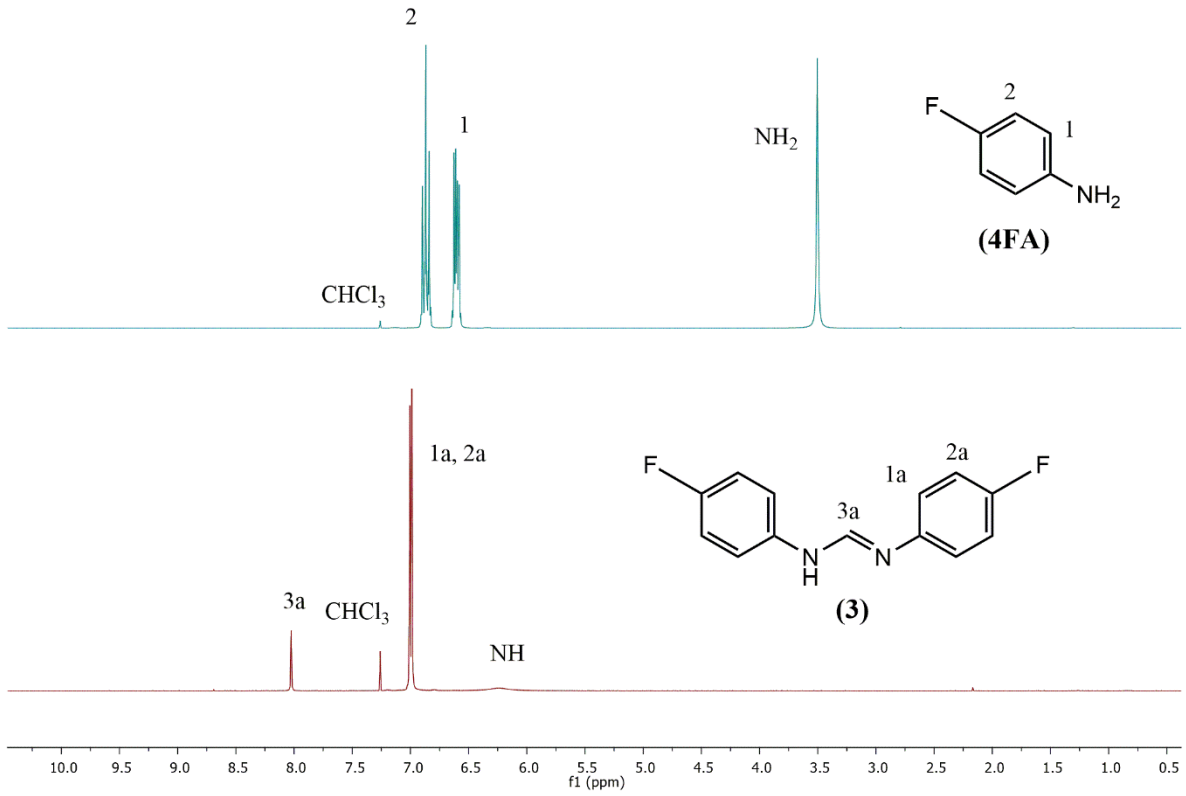

***Figure 2.9**: ^{1}H-NMR spectra obtained for **4FA** (top) and **3**(bottom) in $CDCl_3$*

Further investigation into this observation was carried out using $^{1}H\{^{19}F\}$-NMR spectroscopy. A broadened signal is now observed instead of the doublet previously seen for **3** (Figure 2.10).

Both the assumed doublet (H_2, H_3) and broadened signal (H_{2a}, H_{3a}) observed in either spectrum corroborates the likelihood of a highly symmetrical species present through rapid proton exchange relative to the NMR timescale, possibly due to the imine-amine delocalization previously illustrated in Figure 2.3. Introduction of the fluorine substituent at the para- position seemingly allows further de-shielding of the formamidine N_1-C-N_2 system through electron-withdrawing inductive effects. The results observed in the collected spectra can be rationalized by comparable electronic effects between the delocalized formamidine system opposing that of the fluoro substituent, culminating in the appearance of the broadened singlet single in the $^{1}H\{^{19}F\}$-NMR spectrum suggesting similar proton environments for protons 1_a and 2_a.

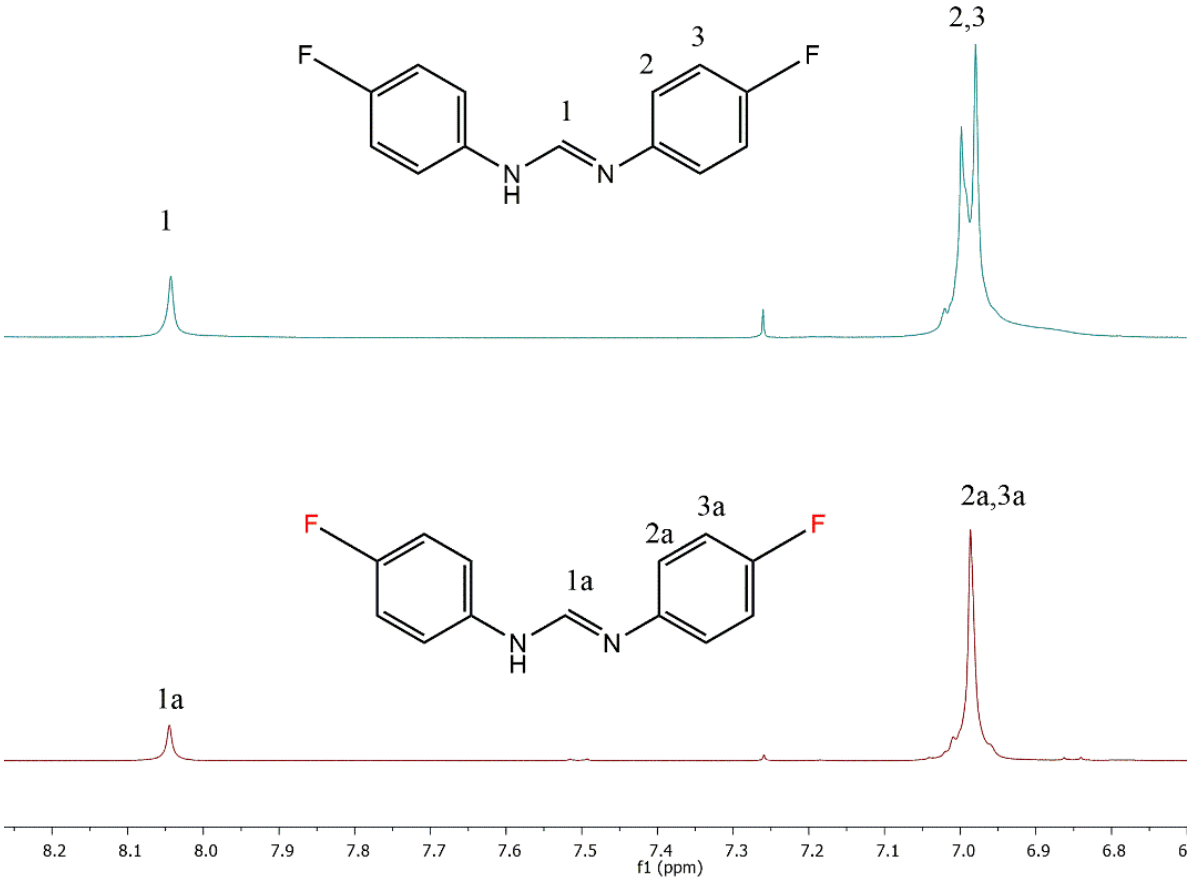

***Figure 2.10**: ^{1}H-(top) and $^{1}H\{^{19}F\}$- NMR (bottom) spectra obtained for **3** in $CDCl_3$*

Analysis of the $^{13}C\{^{1}H\}$-NMR spectra obtained for **3** and **4** (Figure 2.11) shows several doublet signals observed in the aromatic regions. The $^{13}C\{^{1}H\}$-NMR spectrum obtained for **3** shows six signals where five were initially expected. Upon further investigation, a series of doublet signals were observed at 160, 120 and 116.0 ppm. These doublets are due to the coupling of the fluorine atom to the carbon atoms on the aromatic ring. Coupling constants for these signals were obtained as 242, 22 and 6 Hz and were assigned to aromatic carbon atoms C_5, C_3 and C_4 respectively with comparable trends reported for fluorine substituted aromatic systems.[18,19]

Similarly, doublets in the spectrum of **4** were observed at 153.9, 116.0 ,123.9 and 124.7 ppm with corresponding coupling constants 243, 19, 7, and 3 Hz were assigned to aromatic carbon atoms C_{7a}, C_{6a}, C_{5a} and C_{4a} respectively. The quaternary carbons adjacent to the formamidine system were assigned in the 130 – 135 ppm region and assignments were verified by two-dimensional HSQC NMR spectral analysis as before.

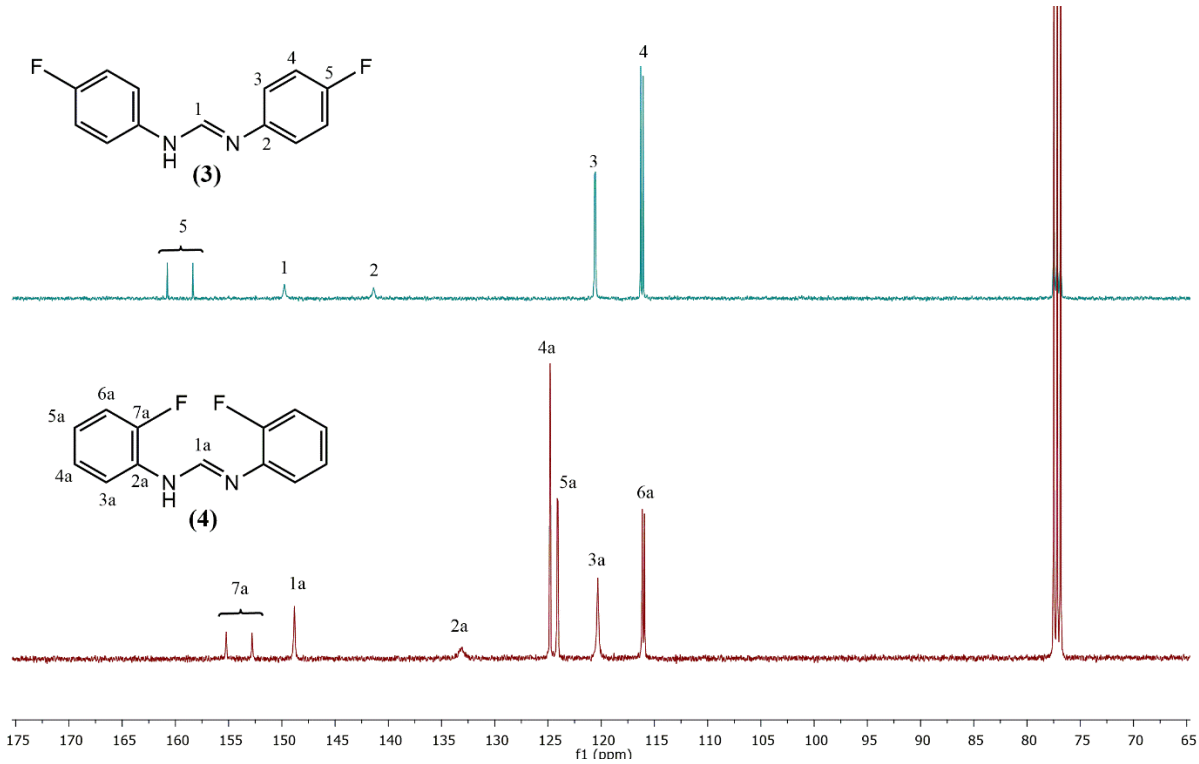

***Figure 2.11**: [13]C-NMR spectra obtained for **3** and **4** in $CDCl_3$*

The [19]F-NMR spectra obtained for compounds **3** and **4**, reveals a singlet observed at -120.0 and -130.0 ppm respectively.

2.2.2.3 Infrared (IR) spectroscopy

Infrared spectroscopy was used as a diagnostic tool for the characterization of compounds **3** and **4**. The characteristic absorption bands for the ν(C=N) formamidine vibration mode were observed at 1669 and 1668 cm^{-1} for **3** and **4** respectively with a broad absorption band observable in the 3000 - 2900cm^{-1} region assigned to the secondary amine as before. In addition, a strong absorption band is observed in the 1200 – 1100 cm^{-1} region corresponding to the aromatic ν(C-F) vibration mode of the fluoro substituent.

2.2.2.4 Mass spectrometry

As for compounds **1** and **2**, the data obtained from ESI-MS analysis supports the ^{1}H-, ^{13}C{^{1}H}-NMR and IR spectral data. A molecular ion peak, assigned to an $[M+H]^+$ fragment is observed in the spectra obtained for **3** and **4** at *m/z* 232.0902 and *m/z* 232.0893 respectively.

2.3 Dirhodium(II,II) aceto complexes

The synthesis of the tetrakis-μ-acetato dirhodium(II,II) (**5**) and tetrakis-μ-trifluoroacetato dirhodium(II,II) (**6**) complexes was carried out using modified literature procedures.[5] The synthesis of compound **5** was achieved by reacting rhodium(III) trichloride trihydrate with sodium acetate in a 1:1 acetic acid/ethanol mixture under reflux. compound **5** was isolated as an emerald-green powder was in a 67% yield. The synthesis of **6** was carried out by a ligand metathesis substitution reaction between **5** with excess trifluoroacetic acid (Scheme 2.2). Near quantitative yields (92%) were obtained for compound **6**, isolated as a bright green flaky solid. Although the synthetic procedure carried out for **5** may be used to synthesize **6** by using sodium trifluoroacetate as described above, lower yields are obtained due to the lowering of the nucleophilicity of the carboxylate through the strong inductive withdrawing effects of the trifluoromethyl moiety.[20]

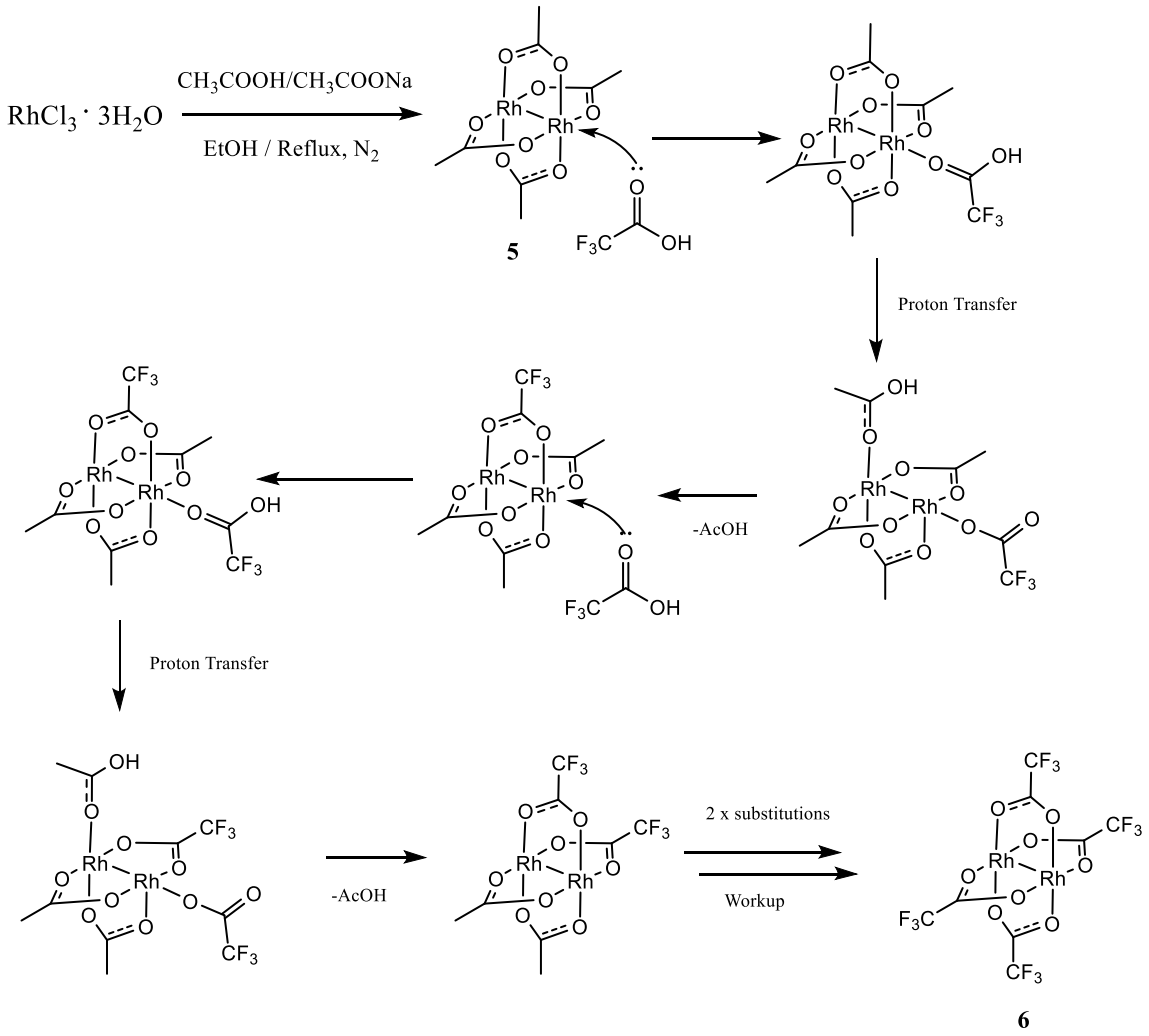

***Scheme 2.2**: Metathesis ligand exchange mechanism for fully substituted complexes*

2.3.1 ^{1}H-, $^{13}C\{^{1}H\}$- and ^{19}F-NMR spectroscopy

Successful synthesis of compound **5** is suggested by the observance of a singlet in the ^{1}H-NMR spectrum at 1.81ppm and corresponds to the acetyl protons (H_1) of the equatorial ligands. Although no proton signals were expected for compound **6**, the ^{1}H-NMR spectrum was obtained to determine whether the fully substituted complex was formed. The ^{1}H-NMR spectra obtained for **5** and **6** is shown in Figure 2.12 below.

Unexpectedly, a singlet is observed in the spectrum obtained for **6**, resonating at 2.08 ppm. Initially, this was thought to be attributed the incomplete substitution of the acetate ligands for the trifluoroacetate, giving a mixed ligand species with both acetate and trifluoroacetate ligands or the coordination of acetate ligands in a monodentate mode to the axial sites of the complex. This is probable since the trifluoroacetate ligand is assumed to be more labile than the acetate ligand due to the electron withdrawing tri-fluoro group offering increased stability of the carboxylate through inductive electron withdrawing effects.

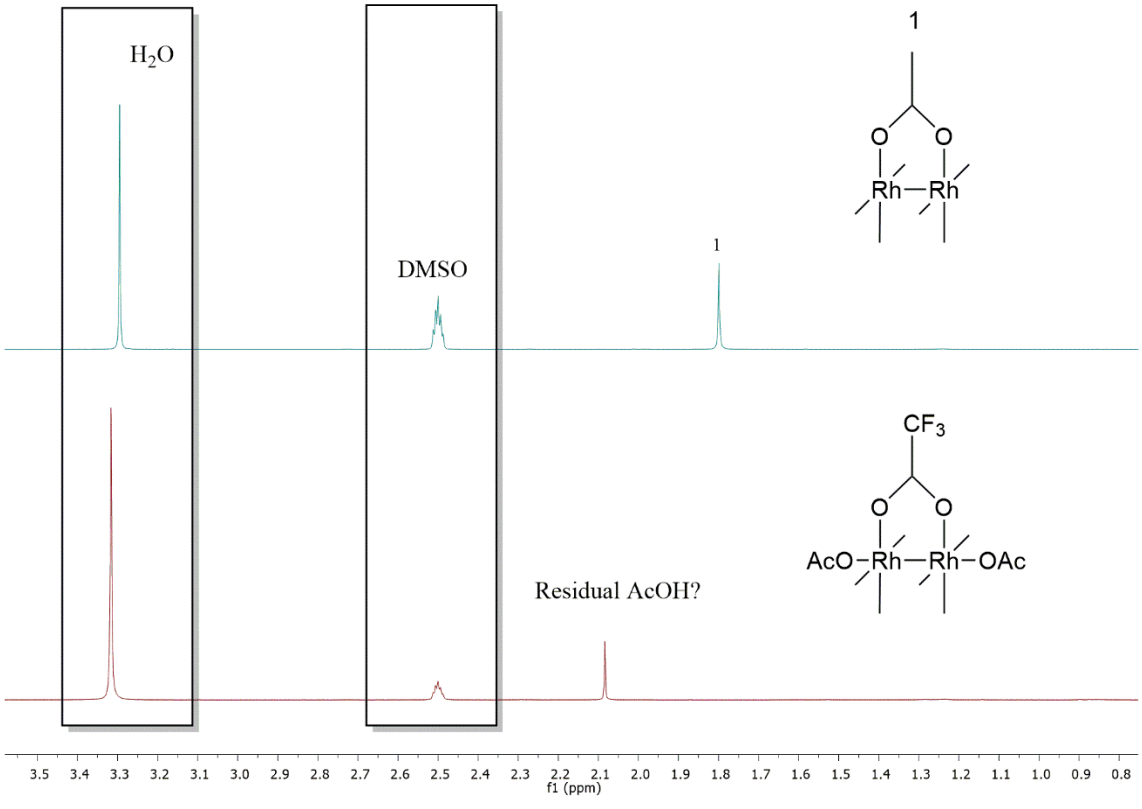

***Figure 2.12**: Comparison of ^{1}H-NMR spectra of **5** and **6** in DMSO-d6*

To further investigate the structure of **6**, NMR samples were prepared and doped with either acetic acid or acetone and the ^{1}H-NMR spectrum of each was collected and compared (Figure 2.13). This experiment was carried out to determine whether the signal observed at 2.10 ppm

was a result of incomplete ligand substitution, axially coordinated acetic acid or axially coordinated acetone.

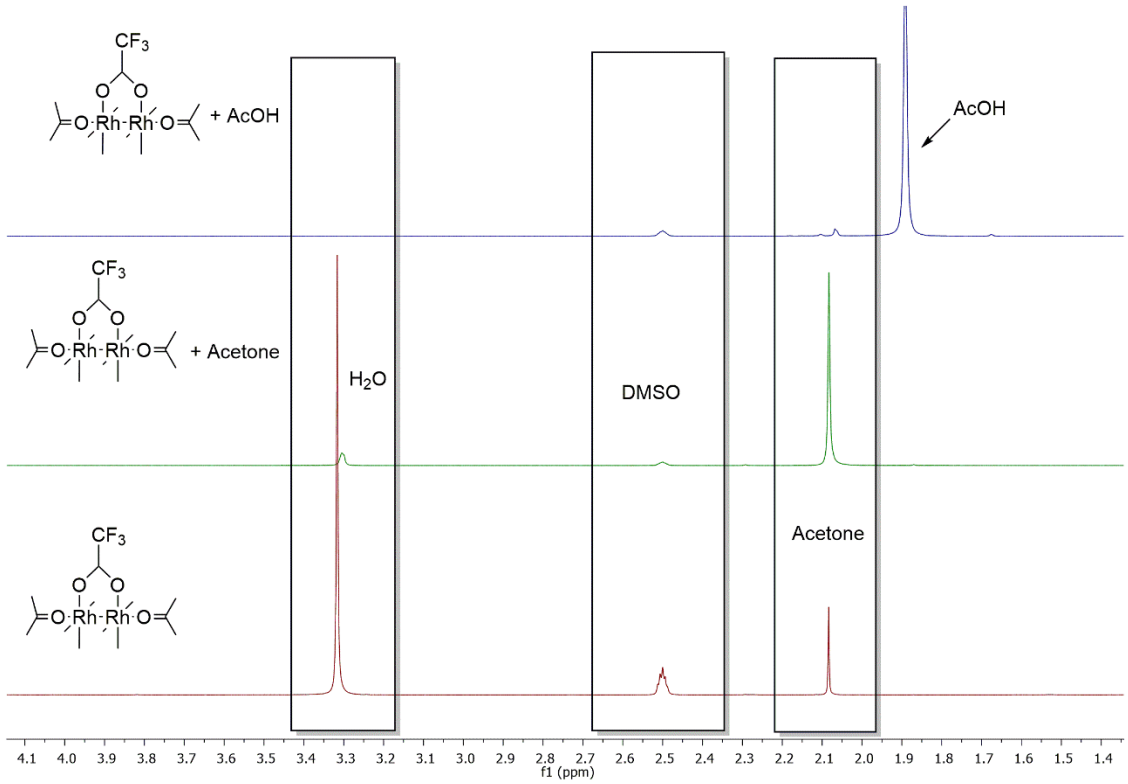

***Figure 2.13**: Comparison of ^{1}H-NMR spectra of compound **6**(bottom) doped with acetic acid(top) and acetone(middle) in DMSO-d6*

The results seen in Figure 2.13 confirms acetone coordination to the axial positions is likely which was subsequently confirmed by mass spectrometry.

The $^{13}C\{^{1}H\}$-NMR spectrum obtained for compound **5** shows two signals at 23.53 and 190.6 ppm assigned to the methyl (**C**H_3) and carbonyl (**C**O) carbons respectively. Similarly, carbon signals obtained for compound **6** were observed at 30.12 and 199.5 ppm assigned to the trifluoromethyl (**C**F_3) and carbonyl (**C**O) carbons. Analysis of ^{19}F-NMR spectrum of **6** shows a multiplet signal centred at -73.8 ppm. This is likely due to the different magnetic environments imposed on the fluorine nuclei by the axial coordination of acetone ligands, depending on the energy requirements of the preferred conformational arrangement.

2.3.2 Infrared (IR) spectroscopy

The IR spectra obtained for **5** and **6** (Figure 2.13) shows the expected absorption bands for both complexes are observed with the characteristic ν(C=O) and ν(C-O) absorption bands for compound **5** (blue) at 1572 and 1408 cm^{-1} respectively. The absorption band of the ν(C=O) absorption band of the carboxyl group was initially expected to lie between 1750 and 1650 cm^{-1}. However, the shift to a lower than expected wavenumber for the C=O and the higher than expected C-O absorption band suggests a greater extent of delocalisation in the carboxylate group.

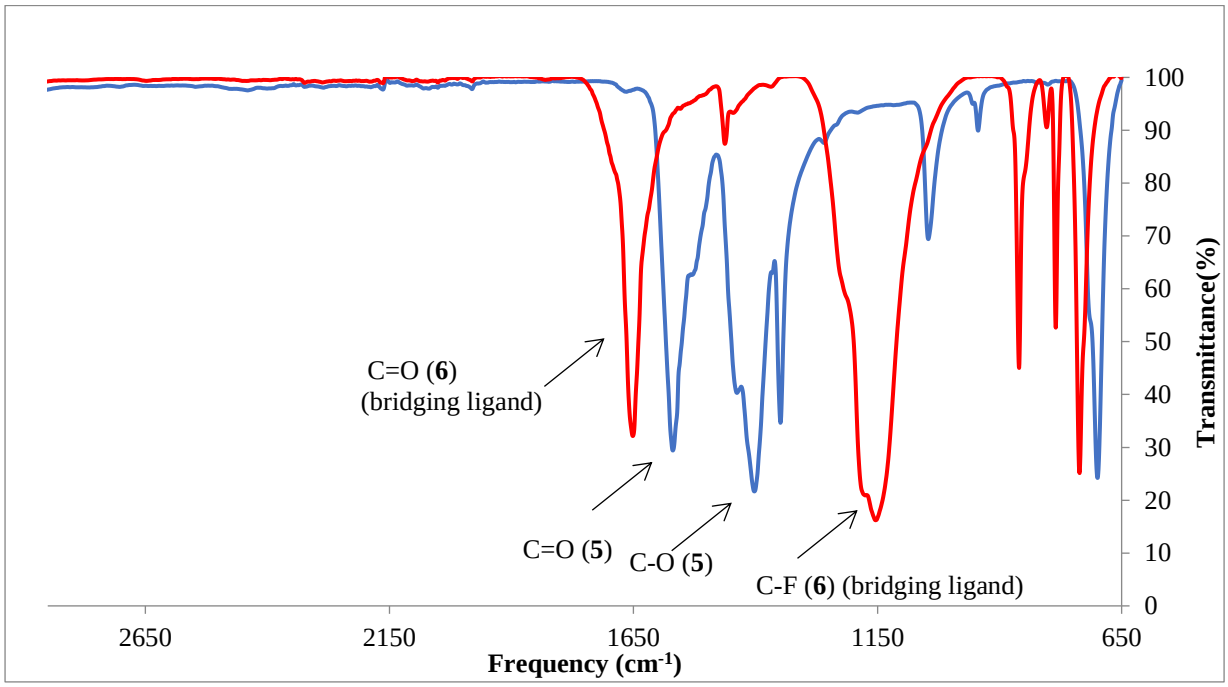

***Figure 2.13**: IR Spectra collected for compounds **5** (blue) and **6** (red)*

Characteristic absorption bands in the IR spectrum obtained for compound **6** (red) are a strong ν(C-F) stretch is observed at 1160 cm^{-1} in addition to a ν(C=O) band observed at 1655 cm^{-1}.

Upon exposure to light and air, a colour change is observed for **6,** from bright green to light blue. For the purpose of determining if this compound decomposes under ambient conditions, the apparent sensitivity to moisture/air and light of complex **6** was investigated by adding 10 mg of green complex to two vials, the first vial was purged with N_2 and the other not. Both vials were then exposed to light over the course of 12 hours. The IR-(Figure 2.14) and ^{1}H-NMR spectra were recorded for both samples.

The spectrum obtained from both IR traces shows a small shift in the C=O absorption band, negligible difference in the C-F band, indicating that no significant decomposition had occurred.

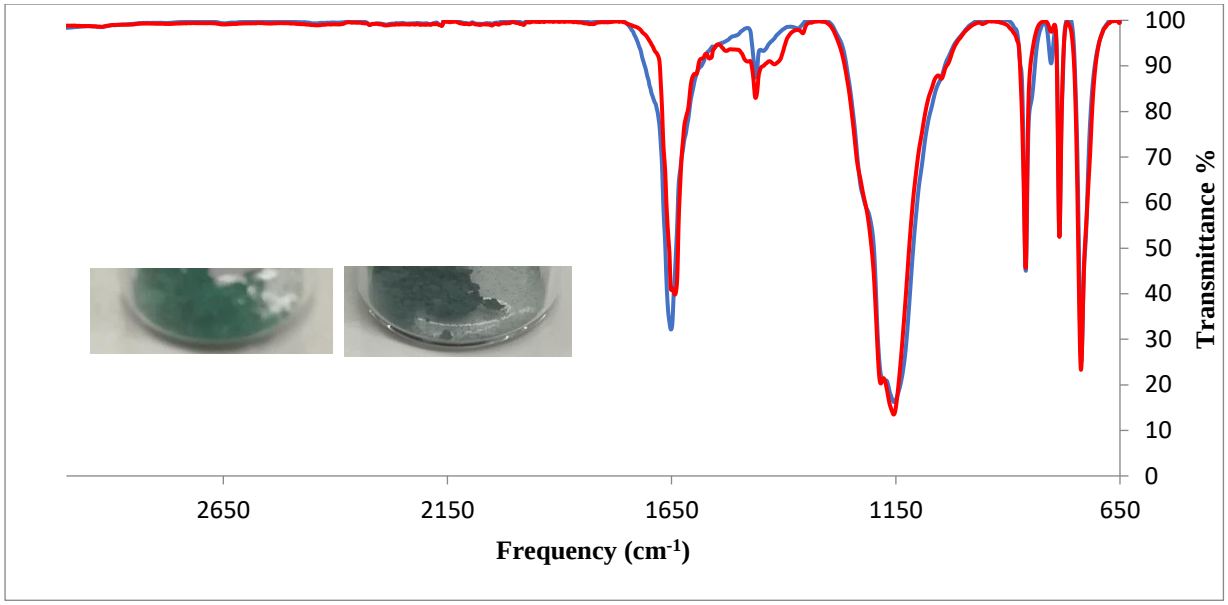

***Figure 2.14**: IR spectra of **6** before(red) and after(blue) light and air exposure*

The complex was dissolved in hot acetone and filtered. The filtrate was collected and dried in *vacuo* while heating at 100˚C, resulting in the reappearance of the flaky green solid as before, the nature of which was confirmed by NMR and IR spectroscopy with identical signals obtained in either case. These results confirm that the complex had not decomposed under the above conditions as previously speculated.

2.3.3 Mass spectrometry

Mass spectrometry was used as a tool for supporting the successful synthesis for both compounds **5** and **6** (Table 2.2). A molecular ion peak for compound **5** was observed at *m/z* 460.8655 for **5**, assigned to $[M+H_2O]^+$, the *mono*- aqua adduct. The molecular ion peak assigned to an $[M+(C_3H_6O)_2+H]^+$ fragment at *m/z* 777.7986, corresponding to the proposed structure for **6**, with the presence of two coordinated acetone molecules. The coordination of axial ligands including water forming *mono*- and *bis*- adducts on the axial sites of complexes of this type have been previously reported.[3,21-24]

Table 2.2**: Mass spectrometry results obtained for compounds **5** and **6

Compound	*m/z* calculated	*m/z* found
5 + H_2O	459.8748	460.8655 $[M+H_2O+H]^+$
6 + 2x(C_3H_6O)	776.7778	777.7986 $[M+2x(C_3H_6O)+H]^+$

2.4 Dirhodium(II,II) formamidinato complexes

The synthesis of the formamidinato complexes (**7 - 10**) was carried out using metathesis ligand substitution reactions of complex **6** with the appropriate ligands (**1 - 4**).[25] Theoretically, this reaction is possible using compound **5** as a precursor however the trifluoroacetate bridging ligands in compound **6** is a better leaving group due to the stabilization of the carboxylate through the electron withdrawing effects of the fluorine atoms.[26] The overall reaction outline is given in Scheme 2.4 below, which proceeds *via* a similar mechanism as previously outlined in Scheme 2.3.

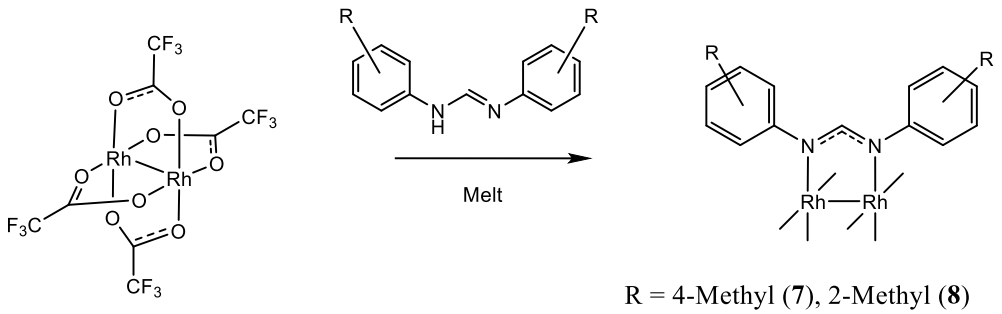

6

Scheme 2.4**: Outline of the synthesis of compounds **7 - 10** from precursor **6

*2.4.1 Synthesis of methyl-substituted formamidinato complexes (**7** and **8**)*

The synthetic procedure used to synthesize compounds **7** and **8** involves a ligand melt with addition of **6** in a 30:1 mol equivalent of ligand to **6**, a wasteful process according to the 12 principles of green chemistry.[27] Taking this into consideration, the synthetic procedure was optimised such that a 10:1 mol ratio was used in the melt carried out under vacuum to facilitate removal of trifluoroacetic acid from the reaction medium. Compound **7** was isolated as a dark green solid in a good yield of 82%, while compound **8** was isolated as a light brown powder in

a moderate yield of 34%. Both **7** and **8** were found to be soluble in chloroform, dichloromethane, benzene, acetonitrile and dimethyl sulfoxide.

2.4.1.1 ^{1}H-, $^{13}C\{^{1}H\}$-NMR and HMQC spectroscopy

Successful synthesis of known compound **7** and novel compound **8** is initially suggested by the change in chemical shift of the $(CH)_{formamidinate}$ proton signal relative to the signal obtained in the ligand from which the complex was synthesized. The change in chemical shift of the imine signal for ligands and corresponding complexes are given in Table 2.3.

Table 2.3*: Comparison of formamidine/formamidinate proton signals of ligands and complexes*

Ligand formamidine signal (ppm)	Complex formamidinate signal (ppm)
1 (8.11)	**7** (7.69)
2 (8.02)	**8** (7.73)

Analysis of the ^{1}H-NMR spectra (Figure 2.15) results in an upfield shift of the aromatic signals upon formation of the complex in addition to the shift previously described for the formamidine protons H_1 and H_{1a} for complexes **7** and **8** respectively. The aromatic region in each spectrum show the expected signal splitting as observed in each of the corresponding ligands **1** and **2**.

The chemical shift differences in proton signals of the methyl substituents for **7** and **8** can be rationalized through electron withdrawing effects of the formamidinate, de-shielding the *para*-position (H_4) to a larger degree than the ortho- position (H_{6a}).

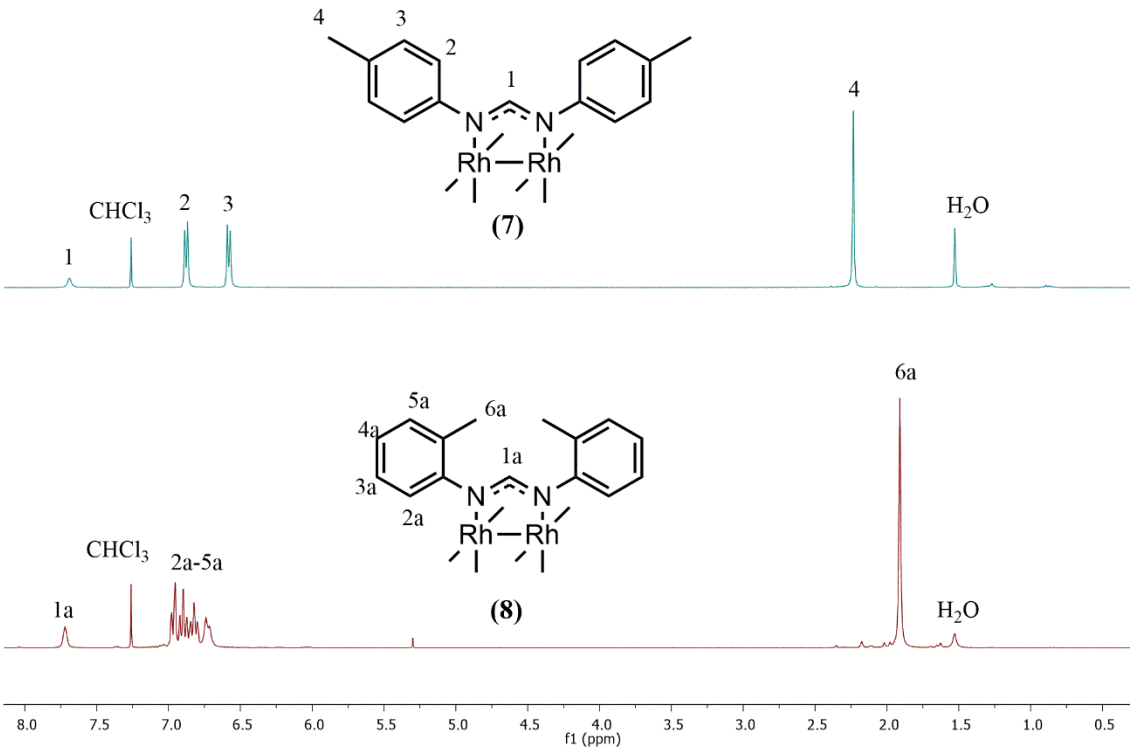

***Figure 2.15**: [1]H-NMR spectra comparison of **7** and **8** in $CDCl_3$*

To investigate possible contributing factors towards the broadening observed for this signal and to mitigate possible effects caused by polar deuterated solvents such as $CDCl_3$, the ^1H NMR spectra of **7** and **8** was obtained in deuterated benzene. The spectrum obtained for compound **7** (Figure 2.16) illustrates the result. Indeed, analysis of the signal corresponding to the formamidine proton at 7.80 ppm is seen as a triplet resonating at 3.1 Hz (shown in the expansion).

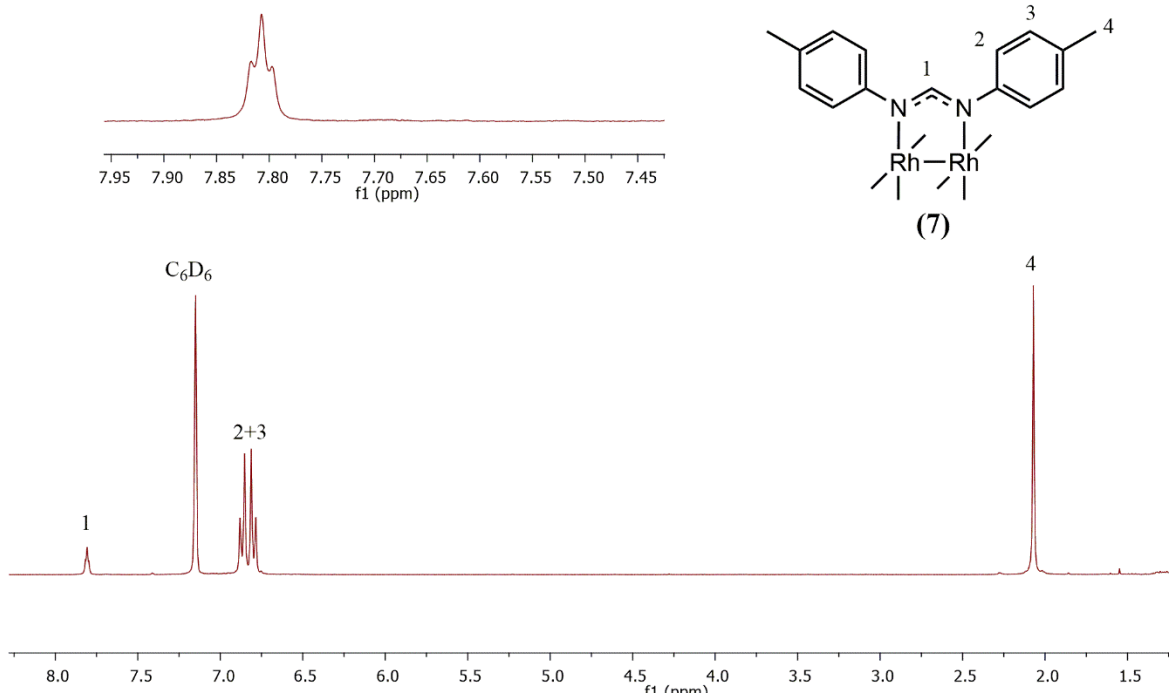

***Figure 2.16**: [1]H-NMR spectra of **7** obtained in C_6D_6*

Additional NMR analysis using HMQC ^{1}H-^{103}Rh spectroscopy shows a cross-peak at (7.70; 5130) ppm, a result of the signals obtained for proton (H_1) and the rhodium atoms in the core of the complex. The combined spectroscopic data confirms the coupling of this proton with the NMR-active rhodium nuclei.

The ^{13}C{^{1}H}-NMR spectrum obtained for **7** and **8** (Figure 2.17) and was assigned with aid of the HSQC analysis. Six signals are observed for compound **7** with seven signals observed for compound **8**. The downfield shift in the (**C**H)$_{formamidinate}$ carbon signal further corroborates the successful synthesis of complexes, observed at 162.3 (C_1) and 168.4 (C_{1a}) ppm for compounds **7** and **8** respectively shifting from 148.6 and 147.3 ppm observed for the corresponding carbons in the ligands. Downfield shifts are also observed for carbons at the *ortho*- and *para*- positions (C_2 and C_4) relative to the formamidinate system, but to a lesser extent (2-5ppm).

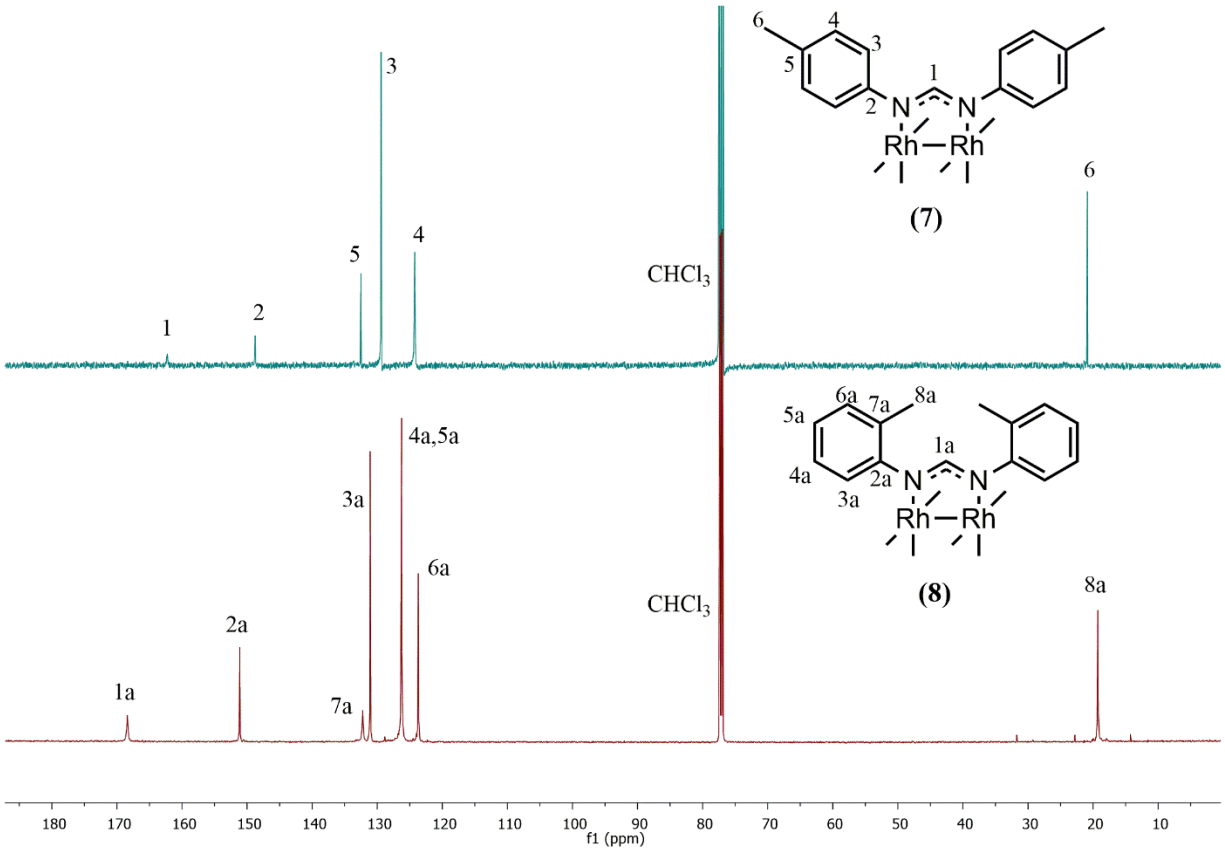

***Figure 2.17**: $^{13}C\{^{1}H\}$-NMR spectrum of **7** and **8** in $CDCl_3$*

2.4.1.2 Infrared (IR) spectroscopy

The IR spectral analysis of **7** and **8** was carried out and compared to the IR spectra obtained for the ligands **1** and **4**. The overlaid spectra of compounds **1** and **7** (Figure 2.18) shows characteristic features observable upon formation of the complex. These features include the shift in the absorption bands for the ν(C=N) formamidine moiety from the 1670 - 1660 cm^{-1} range to a lower region (1595 - 1585 cm^{-1}).

In addition, the absence of absorption bands corresponding to the secondary amine ν(N-H) stretch at around 3000 cm^{-1} and the characteristic ν(C-F) stretch observed for precursor **6** further support successful synthesis. The absorption bands for the aromatic ν(C-H) stretch around 2900 cm^{-1} are more easily observed here, because of the absence of the secondary amine band.

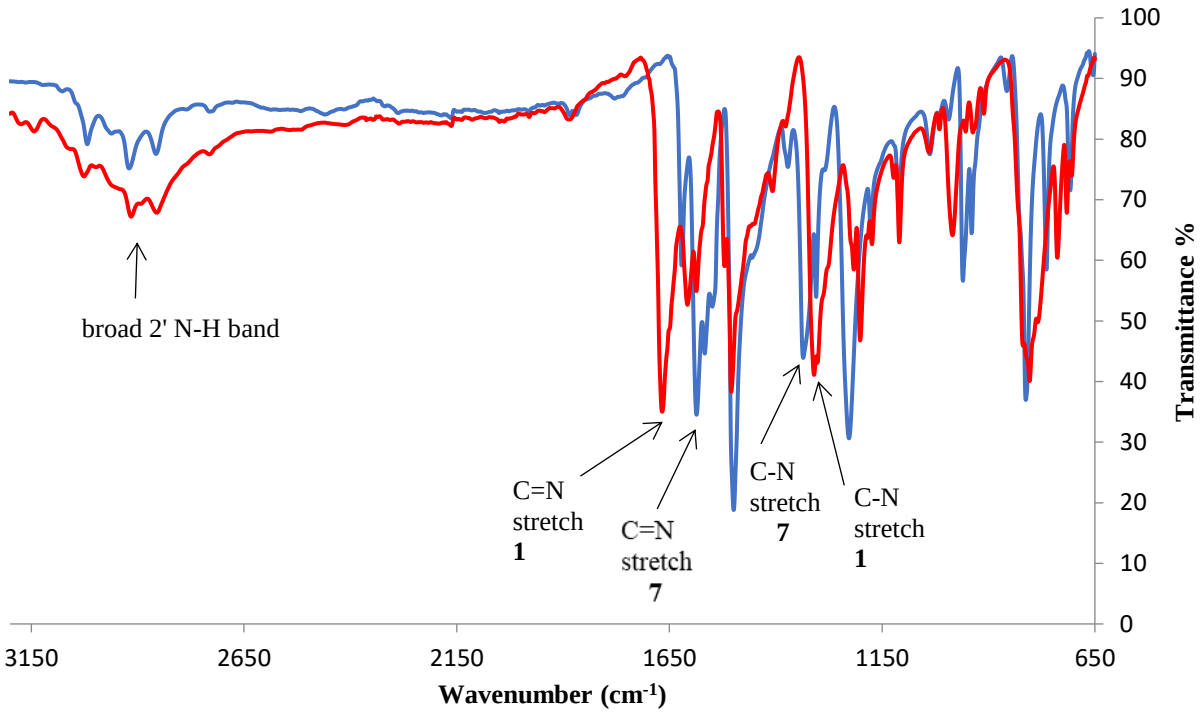

Figure 2.18**: IR spectral comparison of compounds **1** and corresponding complex **7

This shift in the absorption band of the formamidine C=N to the lower wavenumber can be attributed to the synergistic effect and the delocalisation of the formamidine system through metal ligand π-back-bonding. A shift in the C-N absorption band to a higher wavenumber further suggests a delocalised formamidine system across the N_1-CH-N_2 system.

2.4.1.3 Mass spectrometry

The data obtained from ESI-MS analysis supports the ^{1}H-, ^{13}C{^{1}H}-NMR and IR spectral data obtained, where a molecular ion peak in the spectra of **7** and **8** was observed at *m/z* 1098.3007 and *m/z* 1098.3041 respectively. The observed peaks were assigned as $[M]^+$ species for both compounds **7** and **8**.

2.4.1.4 Single Crystal X-Ray Diffraction

Single crystals were grown by slow diffusion of hexane into a concentrated solution of **7** in dichloromethane. with the obtained molecular structure is represented in Figure 2.19 shows an ORTEP representation of compound **7** crystalizing in the tetragonal space group *I-4* with 2 molecules occupying the unit cell. The Rh-Rh bond length was calculated to be 2.45 Å, in line

with similar compounds reported in the literature.[21] The torsion angle across the N1-Rh1-Rh1a-N2 system was calculated to be 4.1˚ indicating a pseudo-planar arrangement of these atoms. Selected bond lengths and angles are given in Table 2.4.

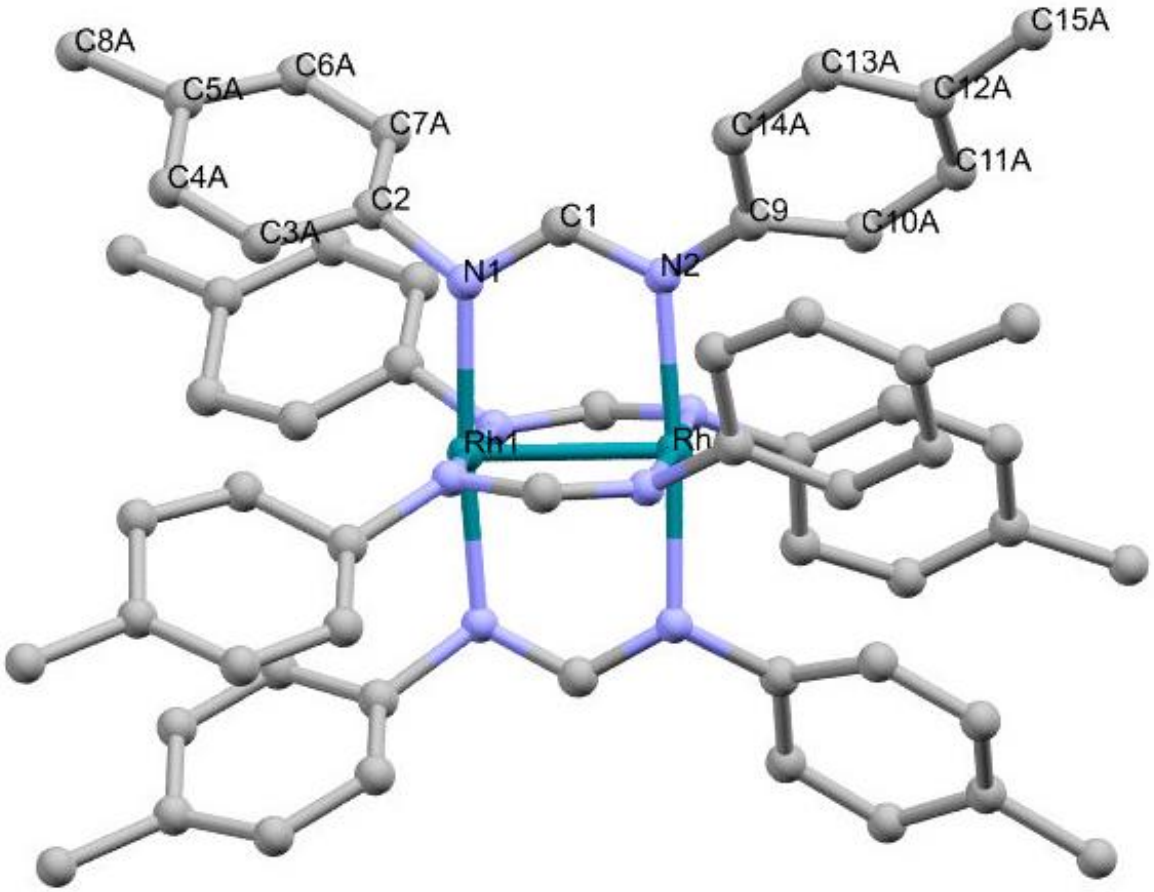

Figure 2.19*: ORTEP representation of compound* ***7****, hydrogen atoms omitted for clarity*

Table 2.4*: Selected bond lengths, angles and torsion angles for compound* ***7***

Selected bond lengths	**Interatomic distances (Å)**
Rh-Rh1	2.4509(4)
N1-C1	1.31(2)
N2-C1	1.32(2)

Selected bond angles	**Angle (degrees)**
N1-C1-N2	123.3(7)
C1-N1-C2	113.4(6)
C1-N2-C9	114.1(7)
Rh1-N1-C2	117.4(8)
N1-Rh1-N2a	94.0(3)
N1-Rh1-Rh	87.8(5)

Selected torsion angles	**Angle (degrees)**
N1-Rh1-Rh-N2	4.1(3)
Rh1-N1-C1-N2	2.3(9)

The bond angles obtained N1-Rh1-N2a and N1-Rh1-Rh1a were calculated to be 94˚ and 87.8˚ respectively. Calculated bond lengths of 1.31 and 1.32 Å between the N1-C1 and N2-C1 atoms were obtained indicating a more delocalised system upon formation of the complex.

The torsion angles, bond lengths and bond angles support the geometry of a paddlewheel structure although the phenyl moieties of each bridging formamidinate ligand is observed in the *anti*- conformation in relation to the Rh-N2-C1 plane. Additionally, disorder observed in the phenyl moieties indicates that arrangement in the solid state occurs as a result of more than one conformer, likely due to steric bulk and interactions between the phenyl groups.

2.4.2 Synthesis of fluoro-substituted formamidinato complexes (9 and 10)

The synthesis of the dirhodium formamidinato complexes bearing fluoro substituents was carried out as described for the methyl bearing formamidinate complexes. Compounds **9** and **10** were found to be soluble in chloroform, dichloromethane, benzene, acetonitrile and dimethyl sulfoxide as for compounds **7** and **8**. Compound **9** was isolated as a brown powder in a yield of 70 %, with **10** being obtained as a dark green solid in 91% yield.

2.4.2.1 ^{1}H-,^{13}C{^{1}H}-, ^{19}F-, ^{1}H{^{19}F}-NMR and HMQC spectroscopy

Compound **9** was isolated as a brown powder in a yield of 70%, with **10** being obtained as a dark green solid in 91% yield. Successful synthesis is initially suggested by a shift in the $(CH)_{formamidinate}$ proton signal, not unlike those observed for **7** and **8**. The observed proton signals of **9** and **10** are compared to respective ligands **2** and **3**, given in Table 2.5 below.

Table 2.5*: comparison of fluoro-substituted formamidine proton signals in $CDCl_3$*

Ligand formamidine signal (ppm)	Complex formamidine signal (ppm)
4 (8.21)	**9** (7.89)
3 (8.02)	**10** (7.70)

The ^{1}H-NMR spectral analysis of complex **10** resulted in the observation of splitting for the $(CH)_{formamidinate}$ proton signal in $CDCl_3$. The broadened singlet observed in the cases for **7** and **8** was not observed in the spectrum obtained for **10** where a triplet (H_{1a}) is observed in $CDCl_3$ (Figure 2.20). The coupling constants obtained were found to be in the 3.1 Hz region as for compounds **7** and **8**.

Interestingly, this splitting is not observed for the equivalent proton (H_1) in the spectrum obtained for compound **9**, however at this point it seemed clear that the electronic environment of the dirhodium core plays a crucial role in whether the coupling of this proton to the rhodium atoms in the core is immediately observable.

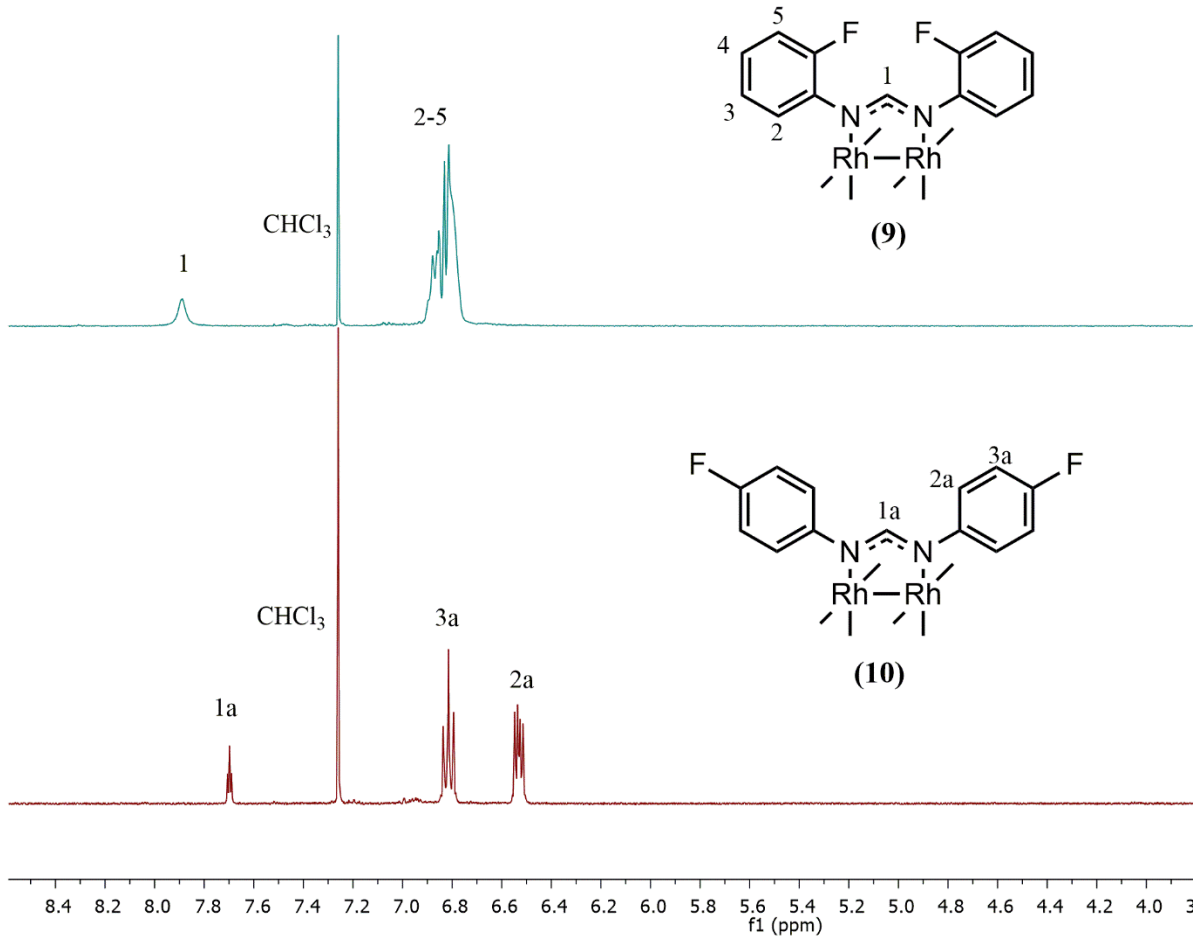

Figure 2.20: *^{1}H-NMR spectra comparison of **9** and **10** in $CDCl_3$*

The position of the fluorine substituent and its electronic effects seem to affect the appearance of this signal more readily than in the analogous methyl substituted complexes **7** and **8**.

Additional analysis using HETCOR $^{1}H\{^{19}F\}$-NMR was carried out on compound **9**, resulting in the $(CH)_{formamidinate}$ proton signal now appearing as a triplet once the decoupled spectrum was obtained and analysed. The triplet multiplicity is still observed in the $^{1}H\{^{19}F\}$-NMR spectrum of **10** (Figure 2.21) with the appearance of the characteristic doublet signals observed for aromatic protons in 1,4-disubstituted aromatic systems.

^{1}H-^{103}Rh HMQC spectroscopy analysis revealed a cross-peak at (7.90; 5109) ppm observed for **9** and a cross-peak at (7.72; 5102) ppm as in the spectrum obtained for compound **10** (Figure 2.22), occurring with a complex splitting pattern. This data, along with the findings from compounds **7** and **8** confirms the formamidine proton coupling to the rhodium atoms in the core of the formamidinato complexes.

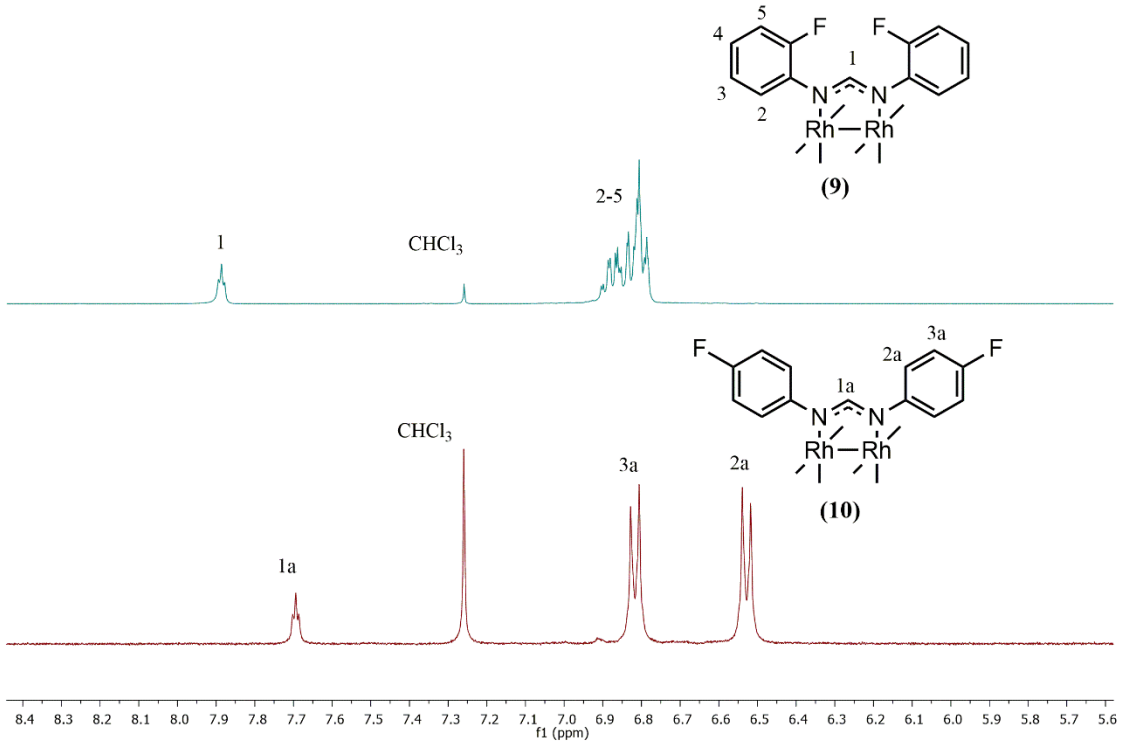

Figure 2.21: *$^{1}H\{^{19}F\}$-NMR spectra comparison of **9** and **10** in $CDCl_3$*

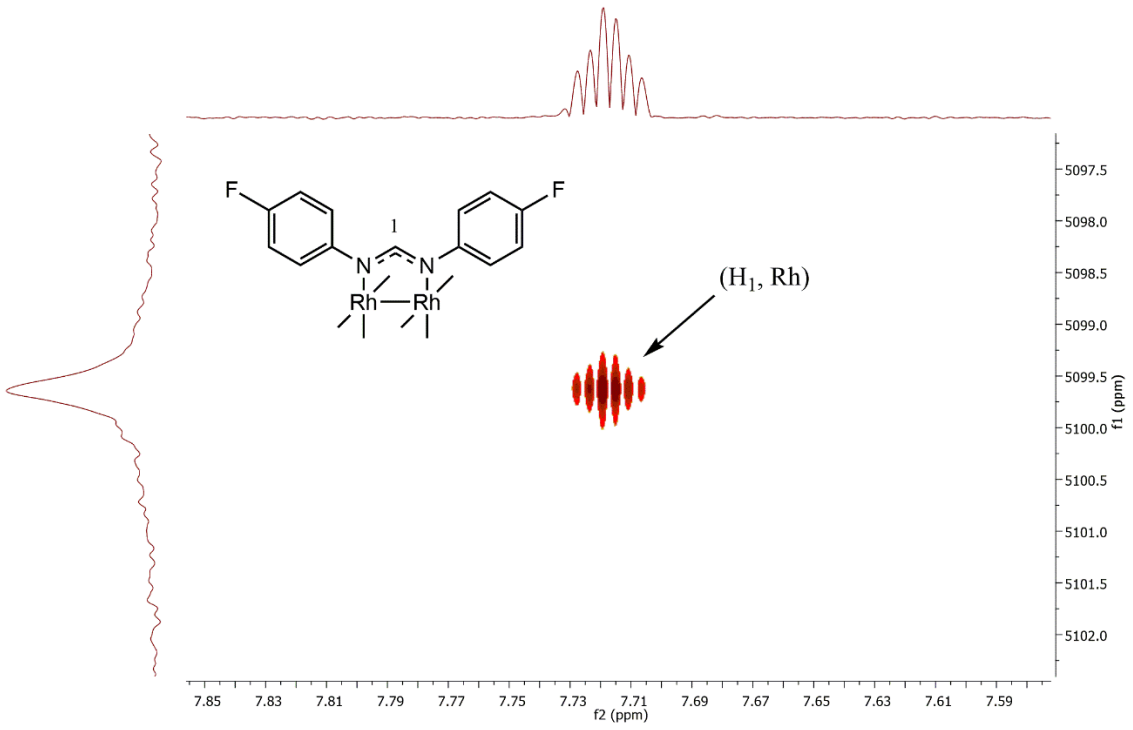

Figure 2.22: *^{1}H-^{103}Rh HMQC NMR spectrum of compound **10** obtained in $CDCl_3$*

The $^{13}C\{^{1}H\}$-NMR spectral analysis of compound **9** shows signals with downfield shifts observable for C_1, C_2, C_3, C_4 and C_7 and an upfield shift in the signal corresponding to C_6 upon coordination. Similar shifts were observed in the case of complex **10**, with distinctive downfield shifts observed for C_{1a}, C_{2a} and C_{3a} (Figure 2.23) upon complexation. In addition, the doublet signals with associated coupling constants are observed for the aromatic carbons atoms for each complex as seen in the $^{13}C\{^{1}H\}$-NMR spectra obtained for associated ligands **3** and **4**, further supporting the successful synthesis.

Analysis of the ^{19}F-NMR spectrum for the complexes **9** and **10** shows a singlet at 128.9 and -119.8 ppm for each compound respectively, shifting upon coordination from -130 and -120.8 observed in the ^{19}F-NMR spectra obtained for the analogous ligands **3** and **4**.

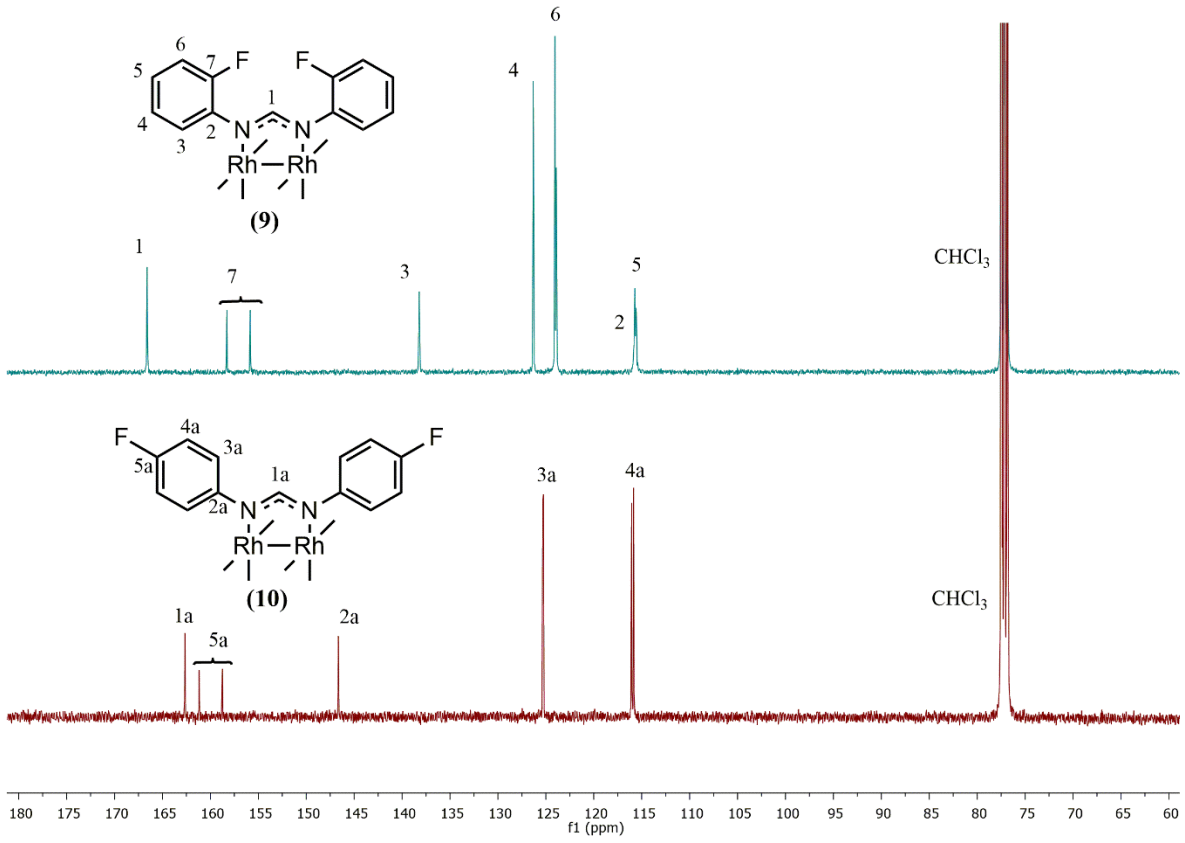

***Figure 2.23**: Comparison of $^{13}C\{^{1}H\}$ spectra obtained for **9** and **10** in $CDCl_3$*

2.4.2.2 Infrared (IR) spectroscopy

The IR spectrum analysis of **9** and **10** was compared to the IR spectra obtained for the corresponding ligands **2** and **3**. As an example, the overlaid spectra obtained for **3** and **10** is shown in Figure 2.24 for comparison.

Characteristic absorption bands were observed as in the case for methyl bearing formamidinato complexes (**7** and **8**), namely the shift in the absorption bands for the formamidine moiety from the 1670 - 1660 cm^{-1} range to a lower region (1584 - 1581 cm^{-1}), absence of bands for the secondary amine absorption bands at around 3000 cm^{-1}. The presence of the aromatic ν(C-F) absorption band observed in the respective ligands is still present in the 1100-1200 cm^{-1} region.

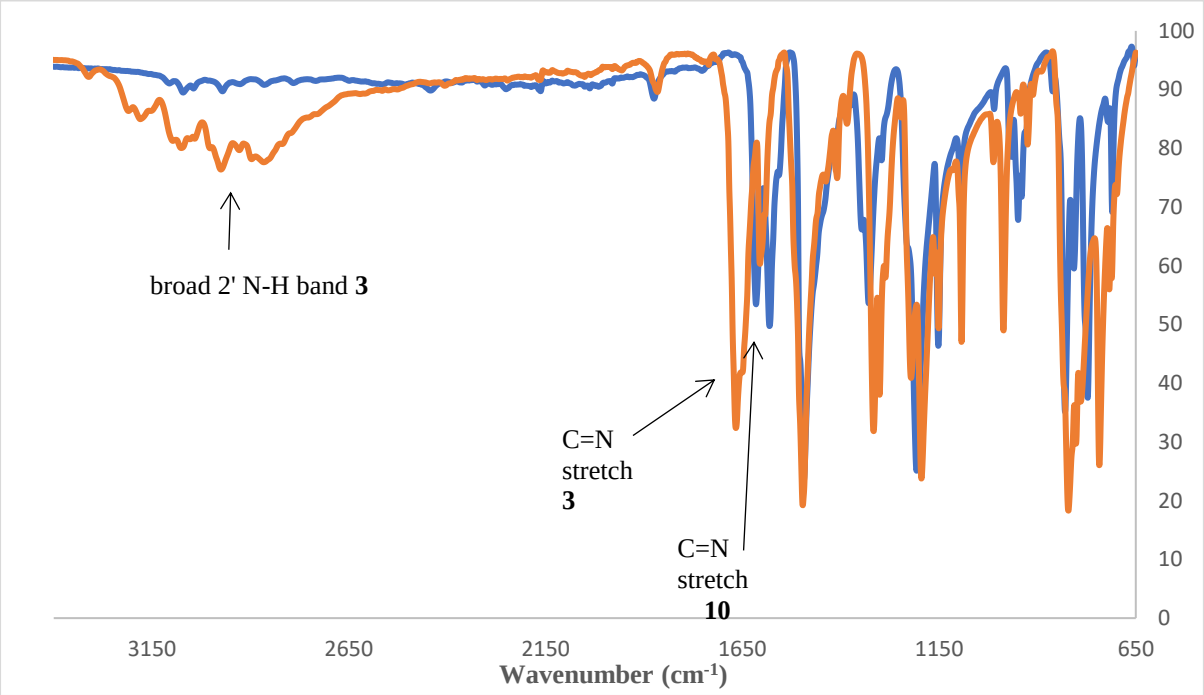

Figure 2.24**: comparison of Infrared spectra obtained for **3** and **10

2.4.2.3 Mass spectrometry

The data obtained from ESI-MS analysis supports the ^{1}H-, $^{13}C\{^{1}H\}$-NMR and IR spectral data obtained, where a molecular ion peak in the spectra of **9** and **10** is observed at *m/z* 1131.1124 and *m/z* 1131.1107 respectively. Both peaks were assigned as $[M+H]^{+}$ protonated species.

2.5 Overall Summary

A series of four diphenyl formamidine ligands (**1- 4**) were synthesized and isolated in moderate to good yields (52-75%). Fluoro- substituted compounds **3** and **4** show interesting signals and observed multiplicities in the ^{1}H- and ^{13}C{^{1}H}-NMR spectra. In addition, two dirhodium tetraacetato (**5**,**6**) and four dirhodium tetrakis(diphenyl formamdinato) complexes (**7**-**10**) were synthesized and isolated in moderate to excellent yields (34-92%). Methods for synthesis of compounds **7**-**10** were modified to enhance atom economy and reduce waste in line with Green Chemistry principles. Spectroscopic analysis of compounds **7** to **10** revealed an interesting triplet multiplicity of the formamidinate proton in the obtained ^{1}H-NMR spectra. This proton was shown to be coupling to NMR active rhodium nuclei in the bimetallic core of the diphenyl formamidinato complexes (**7**-**10**), confirmed by ^{1}H{^{19}F}- and ^{1}H- ^{103}Rh HMQC spectroscopy, not previously reported for complexes of this type. Single crystal X-ray diffraction was used to elucidate the structures of compounds **2** and **7**, confirming the molecular structures of each as well as more subtle details of conformational arrangements. Structural features include the partial delocalisation of electrons and pseudo planar geometry of the formamidine N-C-N system in compound **2** and confirmation of the paddlewheel geometry around the dirhodium core of compound **7**.

2.6 References

1. F. A. Cotton and C. B. Harris, *Inorg. Chem.* 1965, **4**, 330.
2. F. A Cotton, C. Murillo and R. Walton, *Multiple bonds between metal atoms*, Springer, Boston, MA, 2005, 3rd edition.
3. I. I. Chernyaev, E. V. Shenderetskaya, A. G. Maiorova and A. A. Koryagina, *Russ. J. Inorg. Chem.* 1965, **10**, 290.
4. T. A. Stephenson, S. M. Morehouse, A. R. Powell, J. P. Heffer and G. Wilkinson, *J. Chem. Soc.* 1965, 3632.
5. G. A. Rempel, P. Legzdins, H. Smith and G. Wilkinson, *Inorg. Synth.* 1972, **13**, 90.
6. E. B. Boyar and S. D. Robinson, *Coord. Chem. Rev.* 1983, **50**, 109.
7. J. W. Trexler, Jr., A. F. Scheiner and F. A. Cotton, *Inorg. Chem*. 1988, **27**, 3265.
8. F. A. Cotton, E. A. Hillard and C. A. Murillo, *J. Am. Chem. Soc.* 2002, **124**, 5658.
9. S. A. Johnson, H. R. Hunt and H. M. Neumann, *Inorg. Chem.* 1963, **2**, 960.
10. B. G. Anderson, D. Cressy, J. J. Patel, C. F. Harris, G. P. A. Yap, J. F. Berry, and A. Darko, *Inorg. Chem.*, 2019, **58** (3), 1728-1732.
11. F. A. Cotton, E. V. Dikarev and S. E. Stiriba, *Inorg. Chem.* 1999, **38**, 4877-4881.
12. J. L. Bear, B. Han, Y. Li, S. Ngubane, E. Van Caemelbecke and K. M. Kadish, *Polyhedron*, 2009, **28** (8), 1551–1555.
13. J. L. Bear, E. Van Caemelbecke, S. Ngubane, V. Da-Riz, and K. M. Kadish, *Dalton Trans.* 2011, **40** (11), 2486–2490.
14. K. Das, K. M. Kadish, and J. L. Bear, *Inorg. Chem.* 1978, **17** (4), 930–934.
15. K. M. Kuhn and R. H. Grubbs, *Org. Lett.* 2008, **10** (10), 2075–2077.
16. B. A. Dar, S. N. Ahmad, M. A. Wagay, A. Hussain, N. Ahmad, K. A. Bhat, M. A. Khuroo, M. Sharma, and B. Singh; *Tet. Lett.* 2013, **54**, 4880–4884.
17. D. M. Grove, G. van Koten, H. J. C. Ubbels, K. Vrieze, L. C. Niemann and C. H. Stam, *Dalton Trans.* 1986, **4**, 717-724.
18. T. Schaefer, K. Marat, J. Peeling and R. P. Veregin, *Can. J. Chem.* 1983 ,**6** ,2779.
19. I. Ingeborg, M. Schuster, *J. Magn. Reson*, 1969, **17** (1), 104-111.
20. G. Winkhaus and P. Ziegler, *Z. anorg. allg. Chem.* 1967, **350**, 51.
21. G. G. Christoph, J. Halpern, G. P. Khare, Y. B. Koh and C. Romanowski, *Inorg. Chem.* 1981, **20**, 3029.
22. J. F. Gallagher, G. Ferguson and A. J. McAlees, *Acta Crystallogr.*, 1997, **53**, 576.
23. R. H. Clark, D. J. West and R. Withnall, *Inorg. Chem*., 1992, **31**, 456.

24. J. Telser and R. S. Drago, *Inorg. Chem.*, 1984, **23**, 2599.
25. T. P. Zhu, M. Q. Ahsan, T. Malinski, K. M. Kadish and J. L. Bear, *Inorg. Chem.*, 1984, **23** (1), 2–3.
26. J. L. Bear, C. Yao, R. S. Lifsey, J. D. Korp and K. M. Kadish, *Inorg. Chem.* 1991, **30** (2), 336–340.
27. P. T. Anastas, L. B. Bartlett, M. M. Kirchhoff and T. C. Williamson, *Catalysis Today*, 2000, 11.

CHAPTER 3

Conjugation of dirhodium(II,II) paddlewheel complexes to a polypyridyl trisamine scaffold

3.1 Introduction

The immobilization of transition metal catalysts onto inorganic and organic supports has been reported to yield greater selectivity and a higher concentration of active sites/catalysts per unit volume.[1] Several types of immobilization can be introduced to homogeneous catalysis and biological applications, each identified or defined by the types of support used. Means of immobilization or conjugation of active molecules onto supports include covalent interaction,[2] electrostatics,[3] adsorption,[4] encapsulation.[3,5,6] Covalent bonding as a means of conjugation is a popular method for anchoring due to the bonding being robust enough to withstand the harsh conditions of reactions like hydroformylation, discussed later in Chapter 4.[1,7] Some examples are shown below in Figure 3.1.

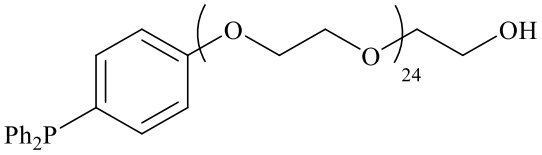

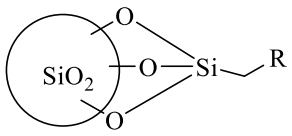

R = functionalised group for coordination to a metal centre

Figure 3.1*: Examples of inorganic and organic polymeric supports*[1]

A variation on the polymer-type support is the use of dendrimers. These macromolecular structures are three-dimensional and characterized by a central core which expands into a periphery which becomes denser with increasing generation number.[8] As such, a higher molecular density is expected with extension to higher generation dendrimers. Dendrimers possess features and physical properties such as precise control of molecular weight, mono-dispersity and 100% branching degree. Dendrimers have therefore become increasingly popular areas of study in chemistry,[5] biology[9] and material science and nanotechnology.[10] The use of suitably functionalized dendritic scaffolds may add to the recyclability of catalysts which can be removed from the solution easily *via* low temperature precipitation or nanofiltration.[11]

Homogeneous catalysts are traditionally separated from substrate and product mixtures through distillation, an energy intensive process. This is a drawback considering the energy efficiency concept of the twelve principles of Green Chemistry.[12] In addition to the excessive energy requirements in homogeneously catalysed reactions, degradation of the catalyst may occur at elevated temperatures. Additionally, poisoning from impurities in feedstocks, side reaction product formation and reduction of active metal complexes resulting in the formation of inactive metallic particles.[13]

Metallodendrimers like their dendrimer conjugates are branched monodisperse macromolecules which contain metals at the core, interspersed throughout the molecular framework or at the periphery.[14,15] The integration of transition metals into dendritic frameworks to form metallodendrimers was initiated by Newkome *et al.* in the 1990s, where the use and modification of functional groups on the periphery of dendrimer scaffolds is reported. Introduction of these functional groups would then be capable of binding to metal complexes, generating macromolecular structures.[16] In line with the metallic complexes discussed in Chapter 2, Takeda *et al.* reported the immobilization of chiral dirhodium(II,II) paddlewheel complexes to polymeric structures using copolymerization for asymmetric catalysis in 2010.[17]

Common dendritic frameworks make use of networks based on polypropyleneimine,[8] poly(amidoamine)[18] and poly(benzylether) scaffolds.[19] An example of a widely used dendritic scaffold from the polypropyleneimine family makes use of diaminobutane (DAB) as a base or core, branching into 4*n* propylamine chains, depending on the generation number *n*. Another core structural motif used is the tris(2-aminoethyl)amine whereby the terminal amine groups can then be functionalized to incorporate ligands such as phosphines, imines and oxides. This modification, binding to metal complexes is achieved thereby forming metallodendrimers.[20] Examples of a first-generation DAB and the addition of an amino-pyridyl moiety for coordination to a metal complex are shown in Figure 3.2.[5]

The aforementioned modifications have led to improved efficiency in the scope of applications for dendrimers and metallodendrimers including catalysis,[16,21,22] photoactivated carbon monoxide releasing molecules (photo-CORMs),[23] high performance polymers, [24,25] chemotherapeutic agents [26,27,8] and diagnostic imaging in nuclear medicine.[2,28]

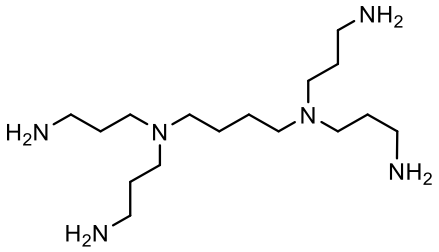

Diaminobutane (DAB) Generation 1

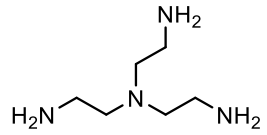

Tris(2-aminoethyl)amine

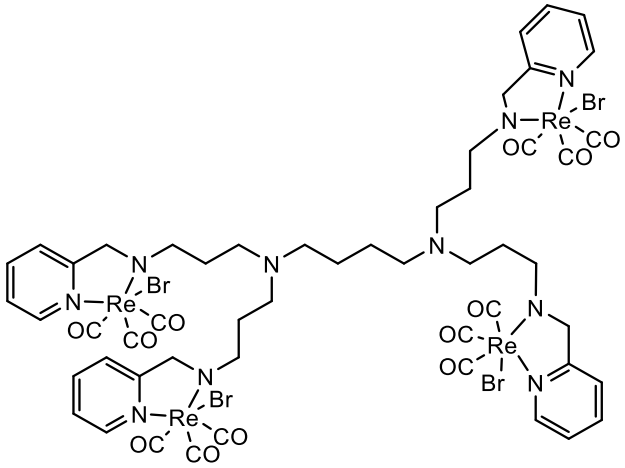

Diaminobutane (DAB)-Generation 1 based Metallodendrimer

***Figure 3.2**: Examples of first-generation DAB and trisamine dendritic core, and functionalized DAB based metallodendrimer*[2]

To the best of our knowledge, the synthesis and application of dendritic structures containing dirhodium complexes having a paddlewheel structural motif bound to the dendritic framework *via* an axial coordination site has not yet been established for use in the catalysis. Herein we report the synthesis of mono- and tris- polypyridyl based metallodendrimers bearing both acetate and formamidinate bridging ligands over a rhodium-rhodium core (Figure 3.3).

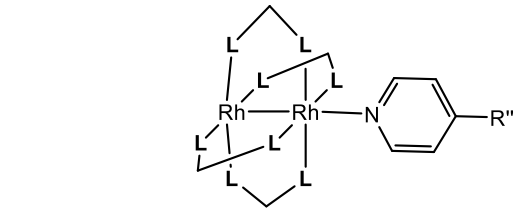

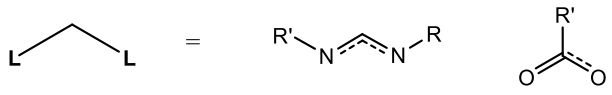

R, R', R'' = alkyl, aryl

***Figure 3.3**: Outline for proposed conjugation to synthesized dirhodium(II,II) complexes*

3.2 Synthesis of monomeric scaffold and model metallodendrimers

*3.2.1 Synthesis and characterization of monomeric pyridyl ligand (**11**)*

The synthesis of known compound **11** (Scheme 3.1) was carried out by a Schiff-base condensation reaction, by reacting amounts of 4-pyridinecarboxaldehyde and n-propylamine in the presence of anhydrous $MgSO_4$.[2,8,20]

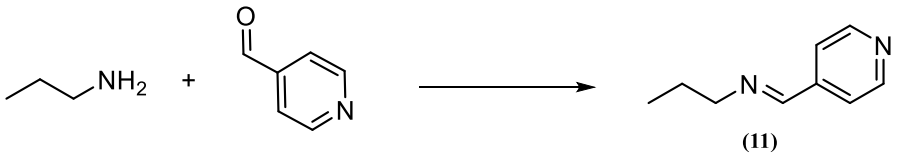

***Scheme 3.1**: Synthetic outline for synthesis of compound **11**[8,20]*

The mechanism (Scheme 3.2) proceeds through protonation of the carbonyl oxygen facilitating the nucleophilic attack by the amine. A proton transfer to the hydroxyl portion of the intermediate forms a hydronium cation which is eliminated as H_2O during imine formation. A subsequent proton transfer from the resulting iminium to the liberated H_2O yields the desired product. The resulting hydronium catalyzes the subsequent condensation reaction by protonating the carbonyl of the aldehyde in the first step of the mechanism.

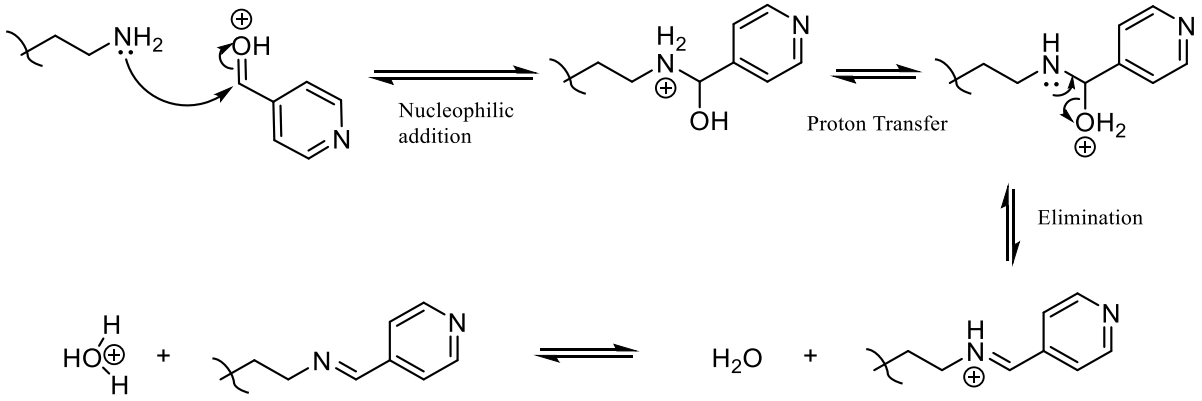

***Scheme 3.2**: General mechanism for Schiff-base condensation reactions*

Since the formation of the imine relies on an equilibrium throughout several steps in the mechanism, by Le Chatelier's principle, the removal of water from the reaction medium is essential in favouring the formation of the desired product.

TLC analysis shows the disappearance of n-propylamine over the course of the reaction, visualized by a previously prepared ninhydrin stain. The product spot is observed at a similar R_f to the 4-pyridinecarboxaldehyde (0.35 v 0.37) in a 50:50 mixture of CH_2Cl_2:petroleum ether.

Known compound **11** was isolated as a yellow oil in a yield of 84% and was found to be soluble in methanol, dichloromethane, chloroform and dimethylsulfoxide.

3.2.1.1 ^{1}H- and $^{13}C\{^{1}H\}$-NMR spectroscopy

Successful formation of compound **11** is suggested through analysis of the ^{1}H-NMR spectrum (Figure 3.4). The appearance of a singlet at 8.23 ppm corresponding to the $(CH)_{imine}$ proton (H_3), with correct integration (1H:2H) relative to aromatic proton signal (H_1). The absence of an aldehyde proton signal at *ca.*10.5ppm and the correct multiplicities and integration is observed for the proton signals of the propyl portion of the molecule (H_4-H_6) and further suggests the formation of compound **11**. This data is consistent with values reported in the literature.[29]

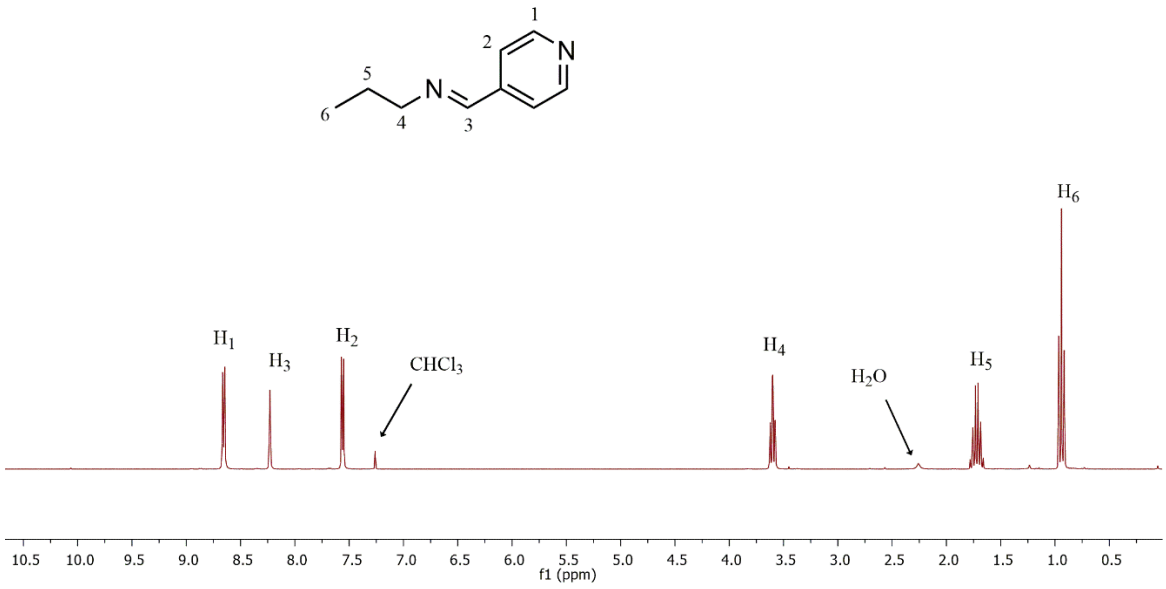

***Figure 3.4**: ^{1}H-NMR spectra for **11** in $CDCl_3$*

The $^{13}C\{^{1}H\}$-NMR spectrum for compound **11** shows 7 distinct signals. The characteristic imine carbon signal (C_4) resonates at 159.5 ppm, with the pyridyl carbon signals resonating at 150.3, 143.2 and 129.9 ppm assigned to carbons C_1, C_3 and C_2 respectively. The assignments are corroborated by values reported in literature.[29]

3.2.1.2 Infrared (IR) spectroscopy

Infrared spectroscopy was used as a diagnostic tool to confirm the successful formation of the imine functionality. A strong absorption band is observed in the spectrum at 1647 cm^{-1} assigned to the $\nu(C{=}N)_{imine}$ and a band at 1595 cm^{-1} corresponding to the $\nu(C{=}N)_{pyridyl}$ stretching modes. The data obtained was further corroborated by previously reported data.[29]

*3.2.2 Synthesis and characterization of mono-adduct model complexes (**12-14**)*

A model reaction to form the *mono*-adduct with compound **5** was attempted to determine the conditions necessary for selective binding to one axial site of the dirhodium acetate complex (**5**) and exclusive formation of the desired product. Theoretically, the overall challenge to overcome is electronic symmetry and identical Lewis acidity of the vacant axial sites on the paddlewheel complexes. The coordination of a pyridyl functionalized ligand with suitable σ-donating and possible π- donating electronic effects was chosen as a means of conjugating the previously synthesized dirhodium complexes to model dendritic scaffold **11**.

Conjugation studies were carried out by reacting the previously synthesized dirhodium tetraacetato complex (**5**) with compound **11** in a 1:1 molar ratio in CH_2Cl_2 at 21˚C over six hours according to the method based on the reported work by Malaza *et al.*[5] Over the course of the reaction, a colour change from green to red was observed in the reaction medium. New compound **12** was isolated as a pink solid in a low yield of 34 % and found to be soluble in chloroform, dichloromethane, dimethylsulfoxide and acetonitrile.

3.2.2.1 ^{1}H- and $^{13}C\{^{1}H\}$-NMR spectroscopy

The ^{1}H-NMR spectrum of compound **12** was recorded and compared to the spectrum obtained for compound **11** (Figure 3.5) with the largest downfield signal shift observed for the pyridyl proton signal which is observed from 8.67 (H_{1a}) to 9.42 (H_1) ppm. This de-shielding effect is due to the pyridyl nitrogen atom becomes electron deficient once bound to the rhodium atom in the complex. Additionally, a less significant shift of the $(CH)_{imine}$ proton signal is observed from 8.23 (H_{3a}) to 8.45 (H_3) ppm, likely caused by the delocalisation of the entire imine-pyridyl π-electron system.

The obtained data suggests that although coordination through the imine or pyridyl nitrogen atoms is possible, coordination of dendron (**11**) to an axial site of compound **5** occurs preferentially through the pyridyl nitrogen. The possibility of coordination through both functionalities was ruled out since the appearance of two distinct sets of aromatic doublet signals was not observed.

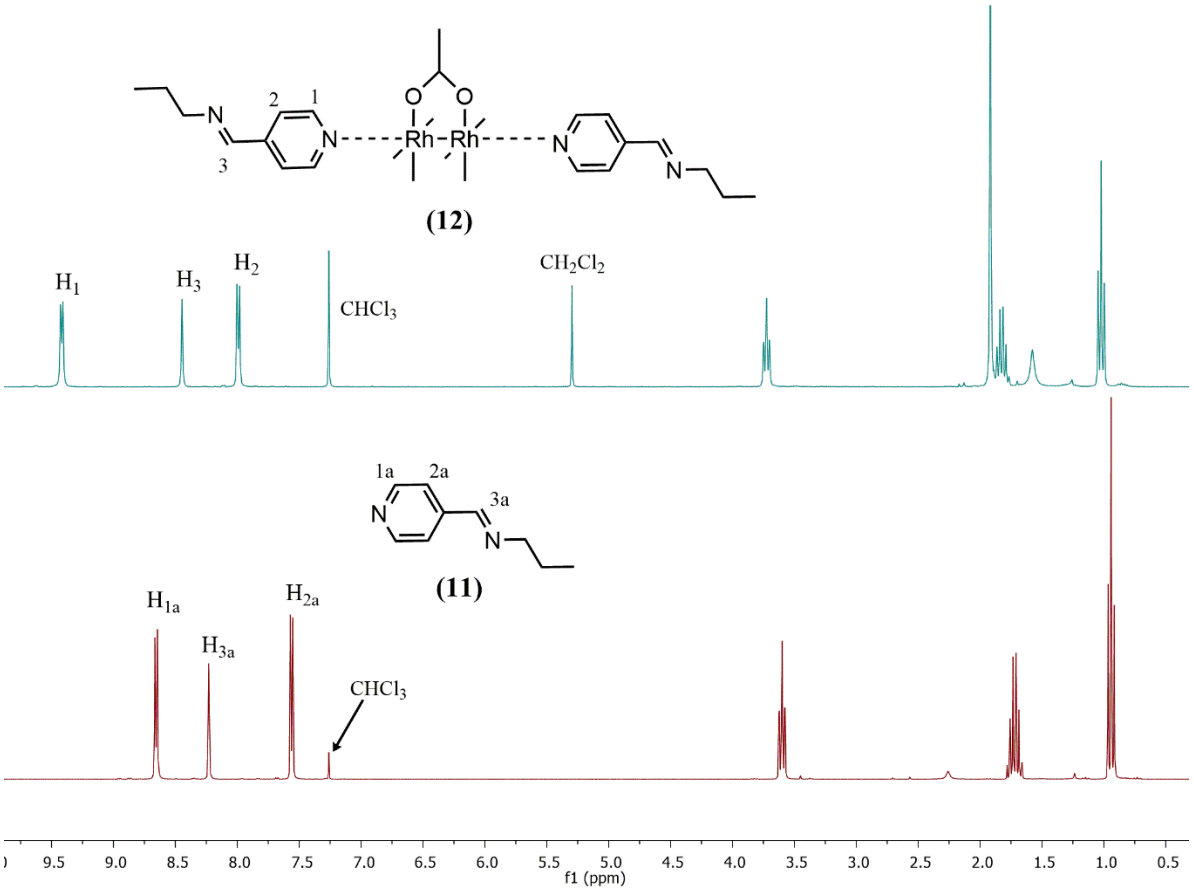

***Figure 3.5**: [1]H-NMR spectral comparison between compounds **11** (below) and **12** (above) in $CDCl_3$*

Comparison of the integration obtained for pyridyl (H_1) and acetyl (H_5) proton signals for **12** (Figure 3.6) suggests that binding at both axial sites had occurred. The expected integration ratio between proton signals H_1 and H_5 for the mono-adduct is 2H:12H, with the ratio found to be 4H:12H. Additionally, the aliphatic signals H_4, H_5 and H_6 were found to have double the expected integration thereby strongly supporting the formation of the *bis*-adduct.

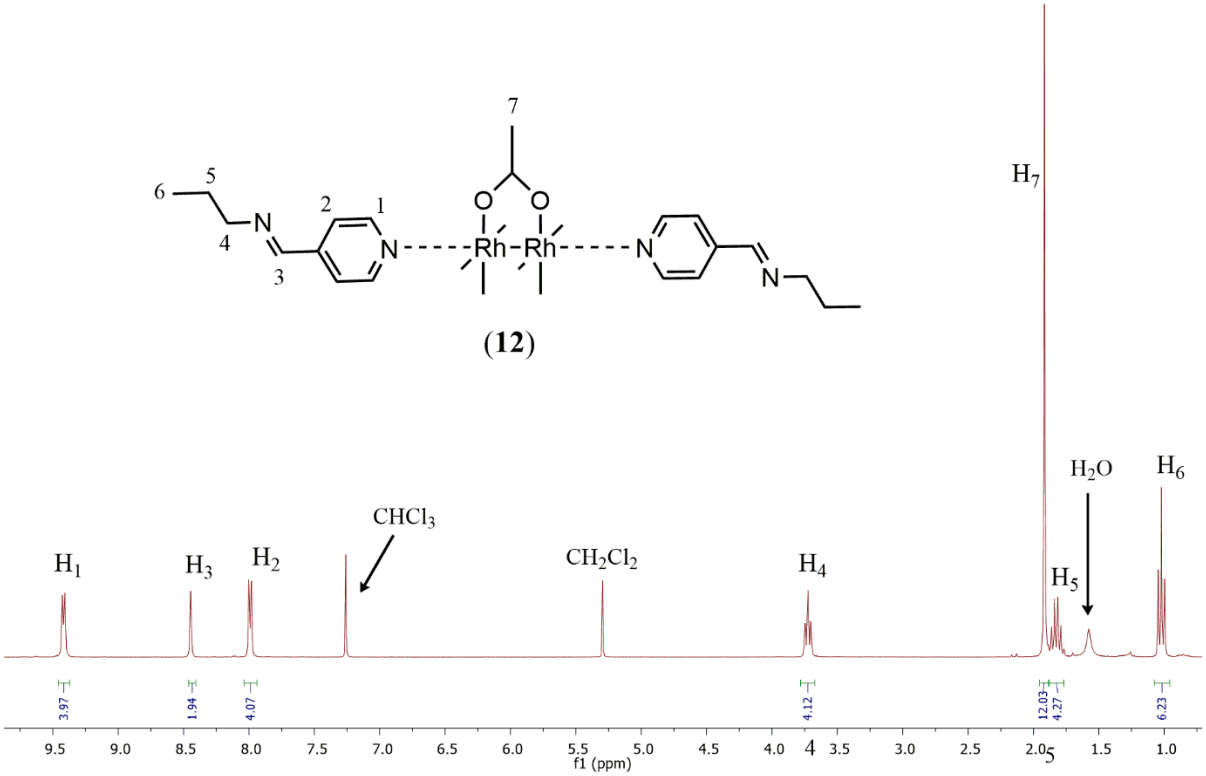

***Figure 3.6**: [1]H-NMR spectrum obtained for **12** in $CDCl_3$*

Although the reaction was carried out using a 1:1 molar ratio of compounds **5** and **11**, further modification to the reaction conditions was applied to synthesize the required *mono*-adduct. The data obtained from the recorded ^{1}H-NMR spectrum indicates that running the reaction at a lower temperature results in the same product formation, eliminating the possibility of kinetic factors playing a role in the formation of the *mono*- over the *bis*- adduct.

Variation of the molar ratio of compounds **5**:**11** from 1:1 to 1.1:1 for the reaction was attempted with the addition of a dilute solution (3.00 mL) of **11** added to the reaction mixture dropwise over a period of 10 minutes. Similar colour changes in the reaction medium were observed, however, new compound **13** was isolated as a light pink solid in a low yield of 28%. The low yield obtained was due to the similarities in the solubility of compounds **5** and **11** in the recrystallization step during purification.

To our delight, successful formation of compound **13** is suggested from the integration of proton signals H_1 and H_7 (Figure 3.7) with relative integration ratios of 2H:12H. The deshielding effect observed in the pyridyl proton signal (H_1) of **12** at 9.42 ppm is less pronounced in the spectrum of **13** with the signal corresponding to H_1 observed at 9.21 ppm.

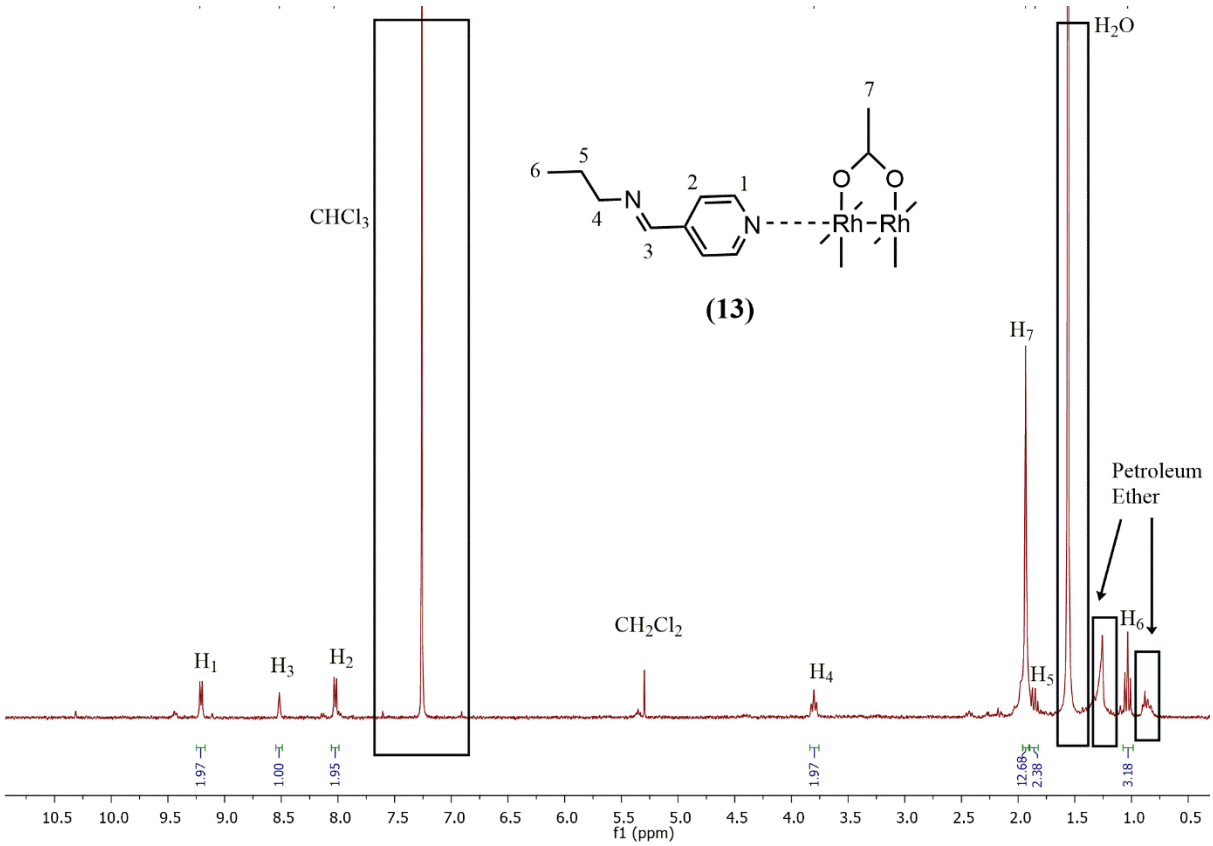

***Figure 3.7**: [1]H-NMR spectrum obtained for **13** in $CDCl_3$*

The appearance of an aldehyde signal at *ca*. 10.3 ppm, accompanied by doublets at 9.45 and 8.15 ppm may be caused by a degradation of the compound **11** during the reaction or hydrolysis of the imine from externally introduced moisture. Alternatively, coordination to the dimer may also occur, however, this is less likely. Speculation into the stability of **13** prompted a solution stability study ^{1}H-NMR spectroscopy whereby the compound was stored in the NMR tube overnight before recording the ^{1}H-NMR spectrum (Figure 3.8).

The spectrum shows a substantial increase in the relative intensity of the $(CH)_{aldehyde}$ proton signal in relation to the $(CH)_{imine}$ proton signal, with the appearance of multiple doublet signals in the expected pyridyl aromatic region.

Additionally, the prepared NMR sample solution is dark red in colour, but over 12 hours the formation of a green precipitate was observed with a loss of intensity of the colour of the solution. This colour change is accompanied by the appearance of the aldehyde proton signal and multiple aromatic doublet signals (Figure 3.8).

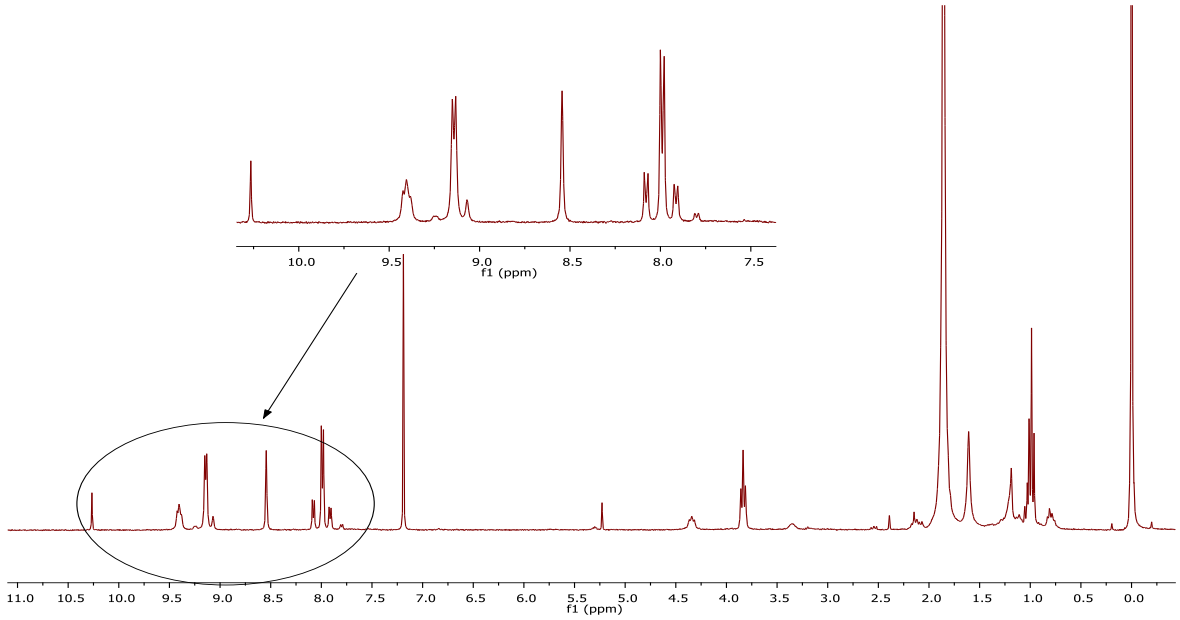

***Figure 3.8**: ^{1}H-NMR spectrum obtained for **13** in $CDCl_3$ after 12 hours*

After an additional 12 hours in solution the amount of green precipitate had significantly increased. Figure 3.9 below shows a comparison between a freshly prepared NMR solution (right) and the solution after 24 hours (left), with the precipitate highlighted in red.

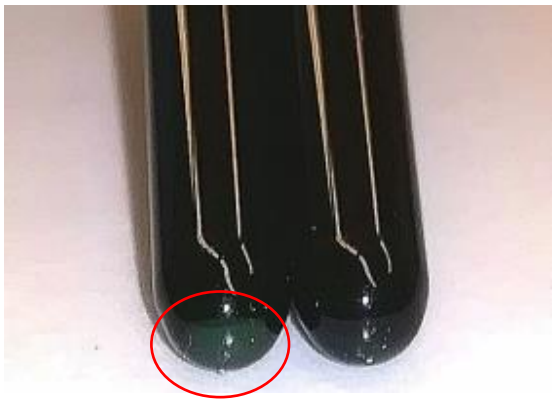

***Figure 3.9**: Pictorial representation of precipitate formation over 24 hours*

This is speculated due to the availability of the vacant axial site to coordinate with the lone pair of the imine to other bimetallic complex molecules in solution. The effect here should, in theory, create a more electrophilic imine carbon which would then be prone to hydrolysis in the presence of any H_2O.

Another model reaction was attempted with 4-picoline (4-methylpyridine) to determine whether the inductive electron-donating effects of the methyl substituent would negatively influence binding to the axial site. The rationale behind this is that once the imine functionality

is reduced, the resulting benzylic CH_2 and secondary amine would have lower electron withdrawing effects than the imine, possibly enhancing the binding strength of the pyridyl nitrogen to the dirhodium core. Under the same conditions as carried out for the formation of compound **13**, novel compound **14** was isolated as a red solid in a 72% yield**.**

The successful formation of **14** is primarily suggested from ^{1}H-NMR spectroscopy. The ^{1}H-NMR spectrum (Figure 3.10) shows the relative integration of the acetyl protons of the equatorial acetate ligands (H_4) and pyridyl proton signal (H_1) in the ratio of 12H:2H, not unlike the ratio seen in the spectrum of compound **13**. In addition, the pyridyl protons (H_1) are observed at 9.21 ppm as previously observed for compound **13** (Figure 3.6) upon coordination to the dirhodium core.

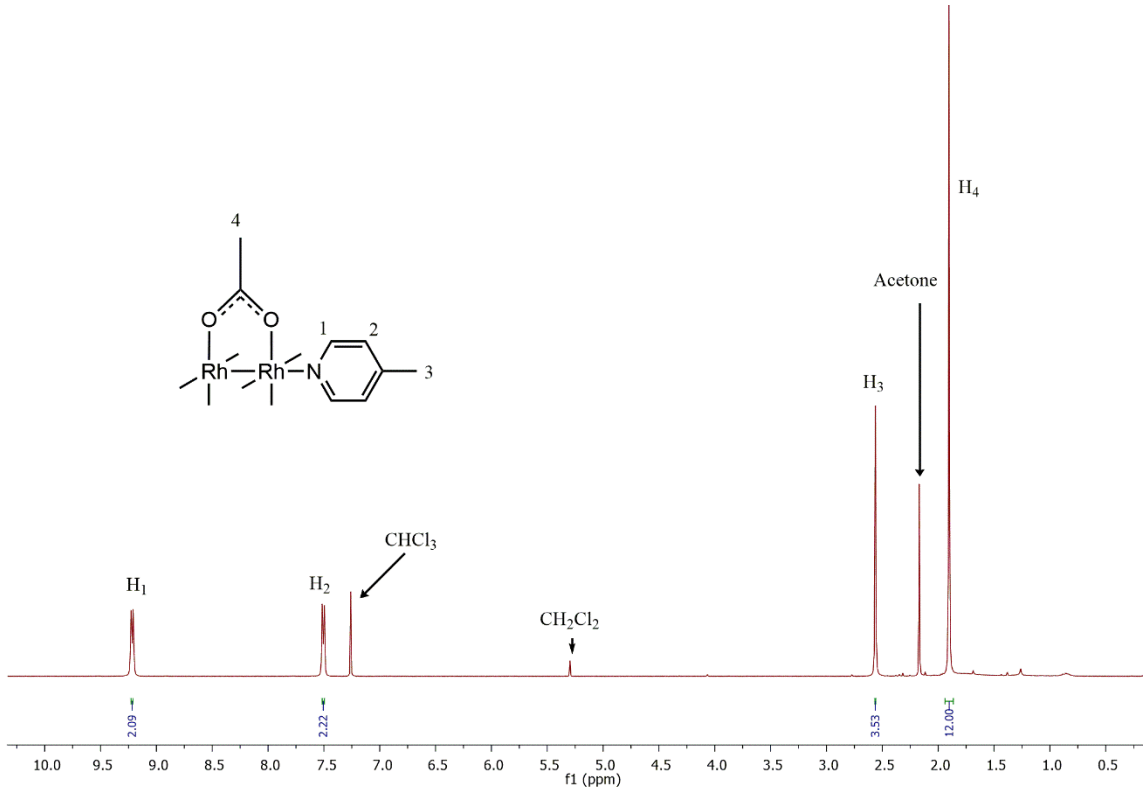

***Figure 3.10**: ^{1}H-NMR spectrum of compound **14** in CDCl3*

The ^{13}C{^{1}H}-NMR spectrum obtained for compound **14** (Figure 3.11) shows six signals, where the bridging acetate carbons signals C_1 and C_2 are observed, resonating at 191.8 and 23.9 ppm respectively. The four remaining signals arise from the picolyl ligand with aromatic carbon atoms C_3, C_5 and C_4 resonating at 150.9, 148.7 and 125.9 ppm respectively. Additionally, the methyl carbon atom (C_6) is observed resonating at 21.4 ppm.

Since the formation of the *mono*-adduct was successful, reduction of the imine moiety to a secondary amine would be favourable to avoid hydrolysis of the imine as seen for compound **12**.

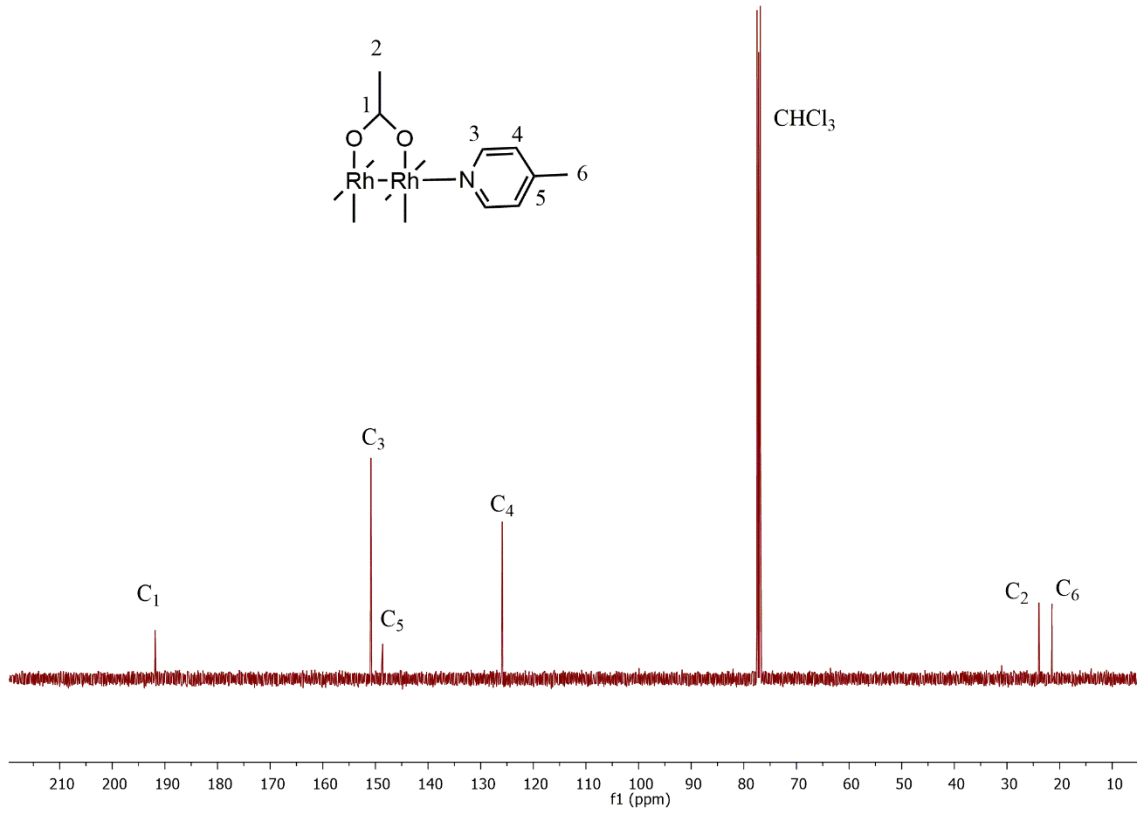

***Figure 3.11**: $^{13}C\{^{1}H\}$-NMR spectrum of compound **14** in $CDCl_3$*

3.2.2.2 Infrared (IR) spectroscopy

Infrared spectroscopy was used as a means of confirming the successful coordination of the pyridyl entity to the axial site of compound **5**. The obtained spectrum (Figure 3.12) shows an absorption band corresponding to the $\nu(C{=}N)_{pyridyl}$ stretching mode observed at 1587 cm^{-1} shifting from the expected 1605 cm^{-1} region. This corresponds to a reduction in the electron density in the bonding orbitals of the pyridyl aromatic system, supporting the deshielding effects seen in the ^{1}H-NMR spectrum for compound **14**. A strong absorption band is observed at 1407 cm^{-1} corresponding to the $\nu(C{=}O)$ stretching mode of the equatorial ligand as discussed in Chapter 2 for compound **5**.

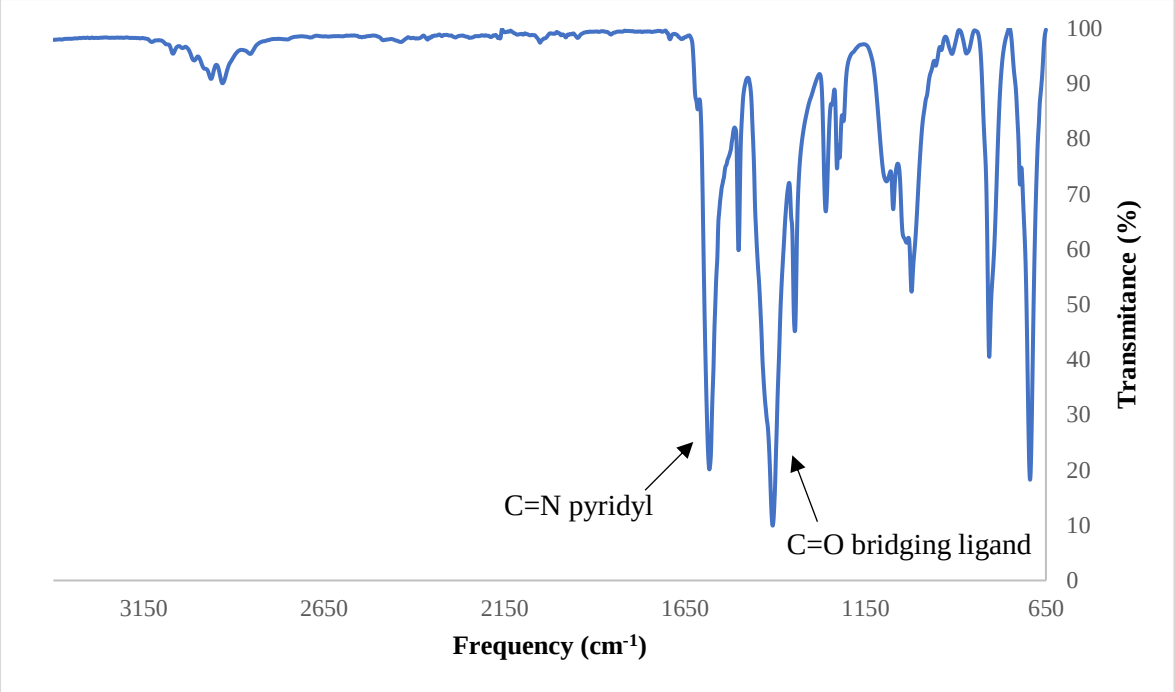

Figure 3.12**: IR spectrum obtained for compound **14

3.2.2.3 Mass spectrometry

The data obtained from ESI-MS analysis supports the ^{1}H-, ^{13}C{^{1}H}-NMR and IR spectral data, whereby a base peak corresponding to an $[M\text{-}CH_3+H]^+$ fragment is observed in the spectrum of **14** at *m/z* 520.8856.

3.3 Synthesis of tris-amine scaffold and associated low-valent metallodendrimers

*3.3.1 Synthesis and characterization of functionalized trisamine dendritic scaffold (**15**)*

Successful synthesis of known compound **15** was achieved through an imine condensation reaction between 3.3 equivalents of 4-pyridinecarboxaldehyde and one equivalent tris(2-aminoethyl)amine in the presence of anhydrous magnesium sulfate as described for compound **13** (Scheme 3.3).[2] The method was modified in such a way that no prior purification of the imine intermediary product (**I1**), whose ^{1}H-NMR is shown in Figure 3.14, was carried out before the reduction step.

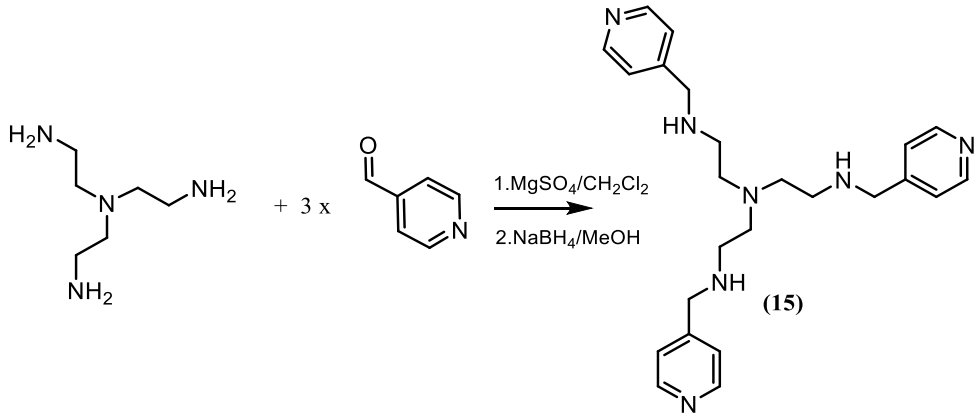

Scheme 3.3: *Synthetic outline for the synthesis of compound **15***

The reduction of the imine was carried out by reacting sodium borohydride with the crude intermediate product (**I1**) in anhydrous methanol to afford the secondary amine product **15**.[20] An excess of 4-pyridinecarboxaldehyde was used since the reduction step would reduce this to the corresponding alcohol or alkoxide, both of which are easily separable from the desired product in an aqueous extraction. The mechanism of this reaction (Scheme 3.4) suggests that the formation of the alcohol is favoured over the alkoxide in the presence of an acid or a protic solvent such as methanol.

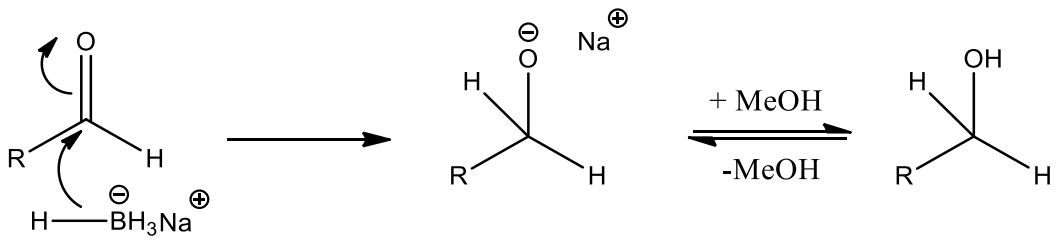

***Scheme 3.4**: proposed mechanism for the reaction of an aldehyde and sodium borohydride.*

Compound **15** was isolated as an air-stable viscous yellow oil in 55% yield and was found to be soluble in chloroform, dichloromethane, dimethylsulfoxide and methanol.

3.3.1.1 ^{1}H- and $^{13}C\{^{1}H\}$-NMR spectroscopy

Compound **15** was characterized by ^{1}H and $^{13}C\{^{1}H\}$-NMR spectroscopy with full spectroscopic details reported in Chapter 6, comparable to previously reported data.[20] Indications of successful synthesis are suggested by the appearance of a singlet signal in the ^{1}H-NMR spectrum (Figure 3.13) resonating at 3.68 ppm integrating for 6H, assigned to the $(CH_2)_{benzylic}$ protons (H_4).

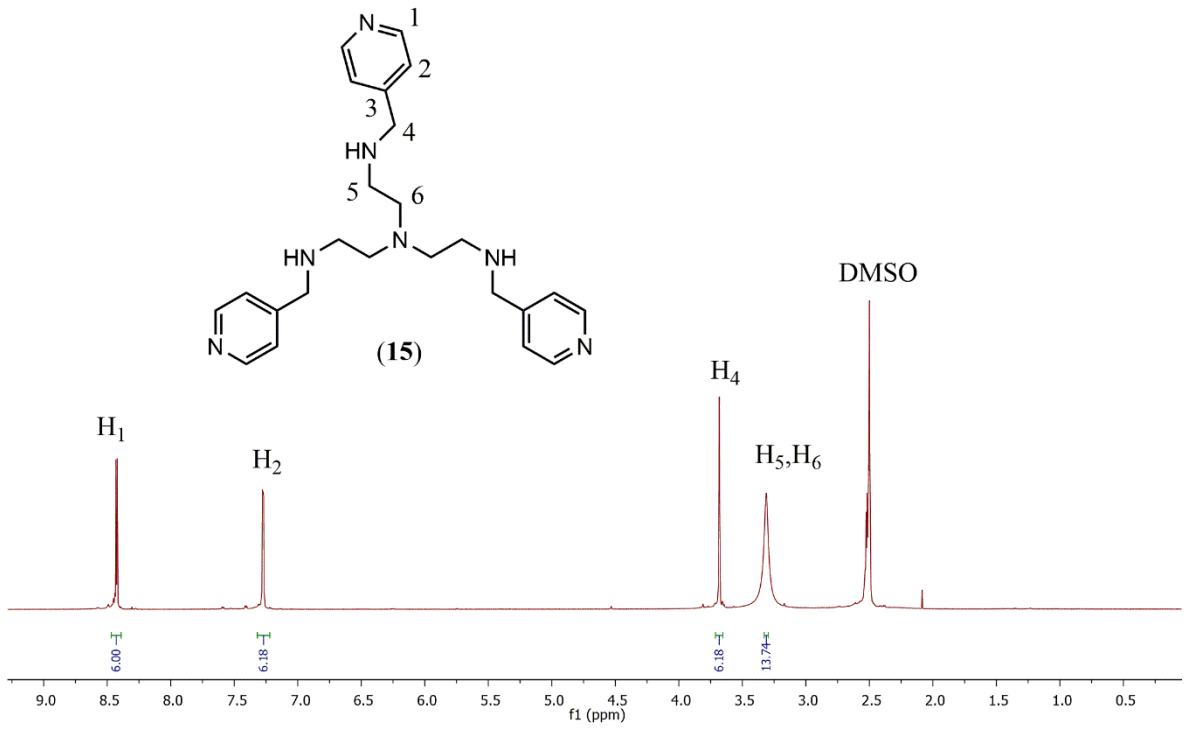

***Figure 3.13**: ^{1}H-NMR spectrum of isolated compound **14** in DMSO-d_6*

Doublet signals for the pyridyl protons are observed resonating at 8.47 and 7.27 ppm, assigned to protons H_1 and H_2 respectively with a broad signal appearing at 3.31 ppm assigned to the methylene protons (H_5,H_6).

Comparison of the ^{1}H-NMR spectra recorded of the isolated imine intermediate (**I1**) and **15** (Figure 3.14) shows an upfield shift in the signals corresponding to pyridyl proton (H_{1a}, H_{2a}),

the absence of the imine proton signal (H_3) at 8.15 ppm and the appearance of the benzylic singlet (H_{3a}) at 3.73 ppm. The triplet signals observed in the spectrum of **I1** resonating at 4.5 and 2.8 ppm were assigned to the methylene protons, assigned to H_4 and H_5 respectively.

The coalition of proton signals (H_{4a},H_{5a}) further support the successful reduction of the imine to the secondary amine, due to magnetic similarity of the secondary and tertiary amine functionalities. In addition, the upfield shift observed for the ethyl protons further corroborates the successful reduction of the imine functionality.

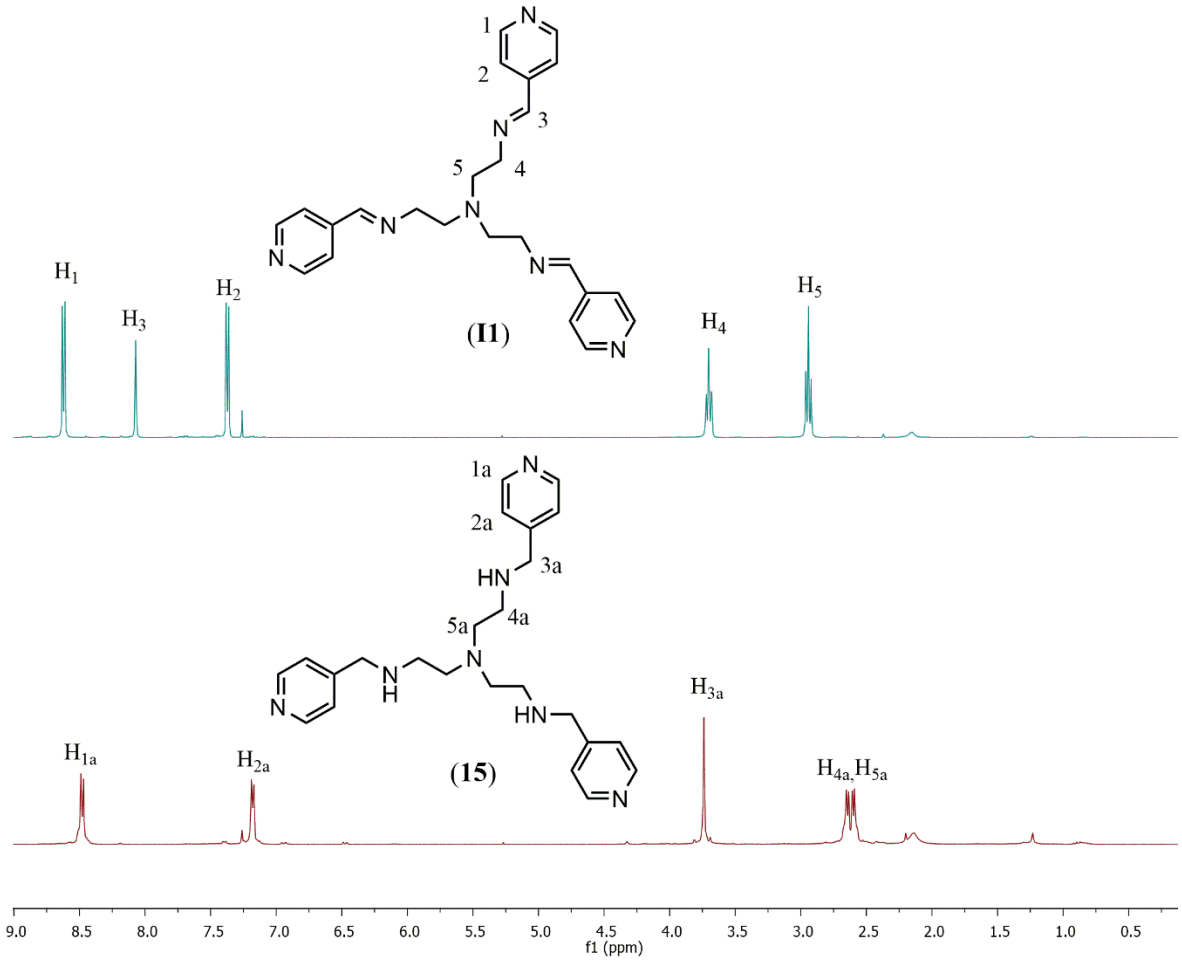

***Figure 3.14**: Comparison of ^{1}H-NMR spectra of **I1** (above) and **15** (below) in $CDCl_3$*

The $^{13}C\{^1H\}$-NMR spectrum of compound **15** (Figure 3.15) shows six signals, with three signals in the aromatic region resonating at 150.1, 149.3 and 122.8 ppm assigned to C_3, C_1 and C_2 respectively. The benzylic carbon signal (C_4) is observed at 54.0 ppm, with the ethyl chain carbon signals resonating at 51.7 and 46.7 ppm assigned to C_5 and C_6 respectively. The obtained spectroscopic data is comparable with previously reported data.[20]

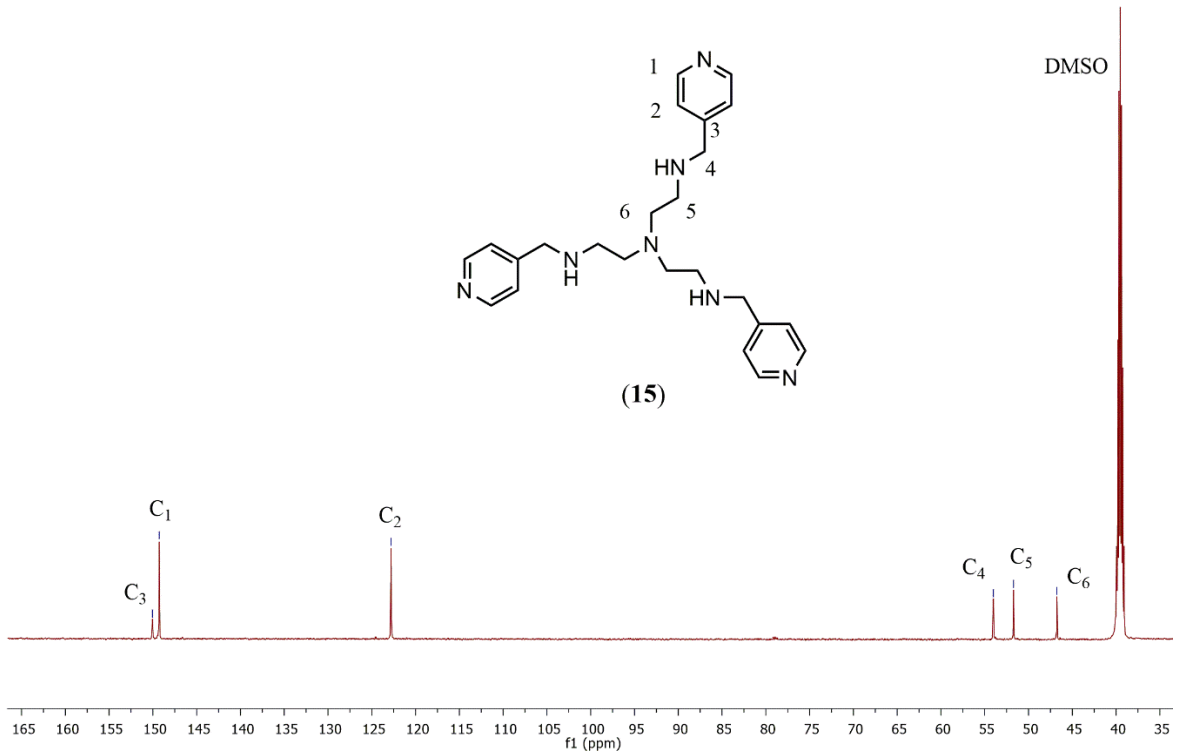

***Figure 3.15**: $^{13}C\{^{1}H\}$-NMR spectrum of compound **15** in DMSO-d_6*

3.3.1.2 Infrared (IR) spectroscopy

Infrared spectroscopy was to determine the presence of characteristic functional groups and successful formation of the compound as for compounds previously synthesized. The obtained infrared spectrum (Figure 3.16) shows the presence of the $\nu(C{=}N)_{pyridyl}$ absorption band at 1610 cm^{-1} and the appearance of a broad secondary amine band at 3334 cm^{-1}. No absorption band in the 1640 cm^{-1} region corresponding to the imine functionality is present in **I1**, further confirming successful synthesis through reduction of the imine entity.

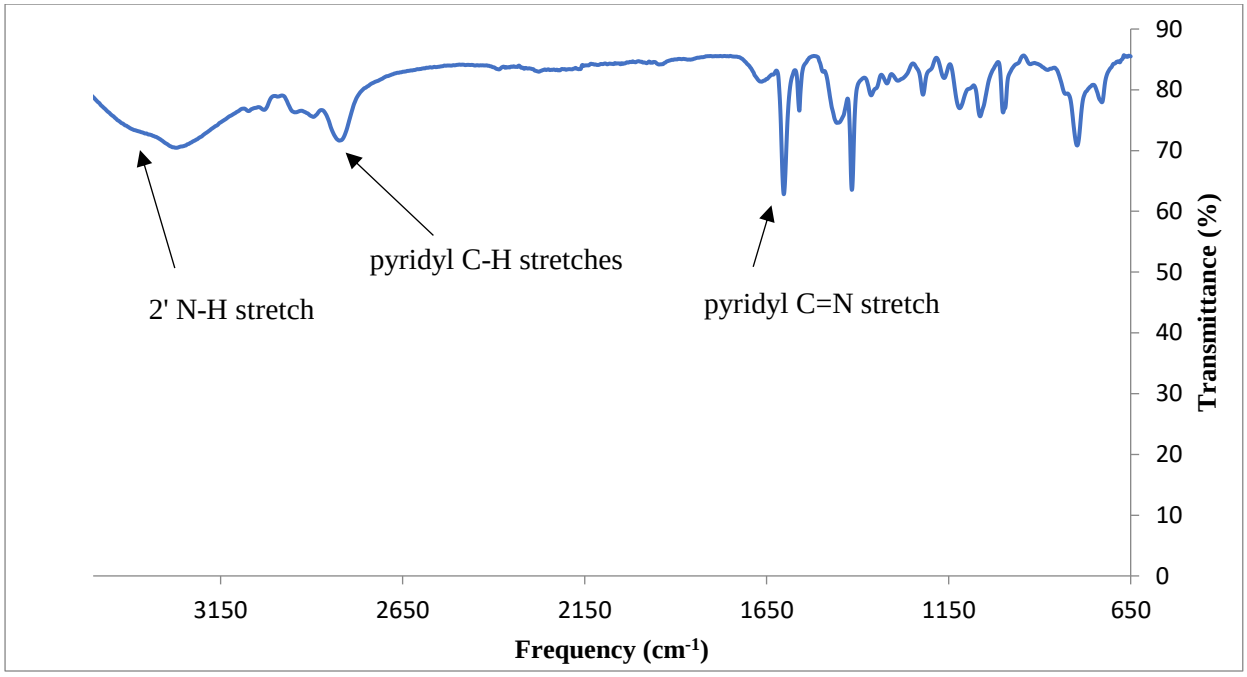

Figure 3.16**: IR spectrum obtained for **15

3.3.1.3 Mass spectrometry and HPLC-MS analysis

The data obtained from HPLC-MS analysis supports the ^{1}H-, ^{13}C{^{1}H}-NMR and IR spectral data, whereby a protonated species corresponding to an $[M+H]^+$ is observed at *m/z* 420.581. The analytical HPLC trace obtained for compound **15** shows a single peak at t_R = 0.12 minutes, with a calculated percentage purity of 99.49%.

*3.3.2 Synthesis and characterization of low-valent metallodendrimers bearing dirhodium acetato paddlewheel complexes on the periphery (**16**,**17**)*

Extension of the modified method for synthesis of the *mono*- adduct **13** was carried out for the synthesis of the *tris*-based metallodendrimers, with exception to the stoichiometry. Dirhodium acetato complexes (**5**, **6**) and compound **15** were reacted in a 3.3:1 molar ratio. Reactions between compound **15** and acetate complexes **5** and **6** proceeded as in the case of **13** resulting in the isolation of new compound **16** as a red crystalline solid in 72 % yield whereas new compound **17** was isolated as a purple powder in an 83 % yield.

Compound **16** was found to be partially soluble in chloroform, dichloromethane, dimethylsulfoxide, toluene and acetone while compound **17** was found to be sparingly soluble in toluene, acetone and dimethylsulfoxide.

3.3.2.1 ^{1}H-NMR spectroscopy

The successful synthesis of compound **16** is confirmed by ^{1}H-NMR spectroscopy, however the low solubility of this complex in deuterated dimethylsulfoxide (DMSO-d_6), chloroform ($CDCl_3$), acetone ($CO(CD_6)_2$), benzene (C_6D_6) and acetonitrile (CD_3CN) was observed. The most discernible spectrum obtained of compound **16** was recorded in DMSO-d_6 charged with a small amount of dichloromethane (20 µL) to enhance solubility. Broad signals are observed in the ^{1}H-NMR spectrum (Figure 3.17) for pyridyl protons (H_1, H_2), $(CH_2)_{benzylic}$ (H_3) resonating at 9.01, 7.75 and 3.89 ppm respectively. The broadening of these signals is due to magnetically similar environments averaging over similar chemical shifts on the NMR timescale. In addition, methylene protons (H_4, H_5) in the interior of the scaffold are observed in the 2.75 ppm range with the acetyl proton signal resonating at 1.76 ppm. Comparison of the integration of the broad signals suggest successful formation with the H_6:H_1 ratio calculated at 6H:36H.

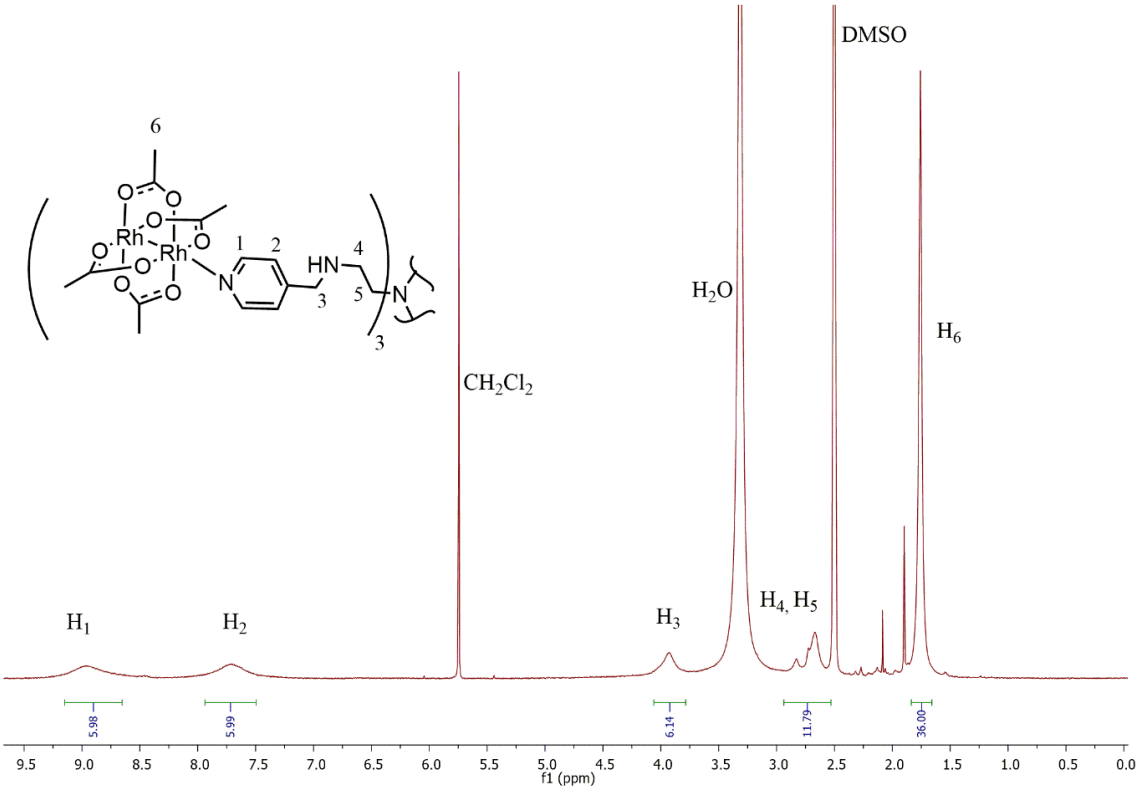

***Figure 3.17**: ^{1}H-NMR spectrum of compound **16** in DMSO-d_6*

The ^{1}H-NMR spectrum could not be recorded for compound **17** due to the sparingly soluble nature in deuterated solvents DMSO-d_6, $CDCl_3$, $CO(CD_6)_2$, C_6D_6 and CD_3CN as tested for compound **16**.

The $^{13}C\{^{1}H\}$-NMR spectra could not be recorded for both compounds **16** and **17** due to the low solubility previously described.

3.3.2.2 Infrared (IR) spectroscopy

Infrared spectroscopy to determine successful coordination of the scaffold to the dirhodium core yielding compound **16**. The recorded spectrum shows a shift of the $\nu(C{=}N)_{pyridyl}$ absorption band from 1610 to 1586 cm^{-1} as for compound **14**, overlapping with the $\nu(C{=}O)$ absorption band from compound **5**. The broad secondary amine absorption band arising from the scaffold (**15**) is observed at around 3300 cm^{-1}. By way of example, Figure 3.18 below shows a comparison of the obtained spectra for compounds **5**, **15**, and **16**, with the pyridyl and carbonyl region highlighted in red.

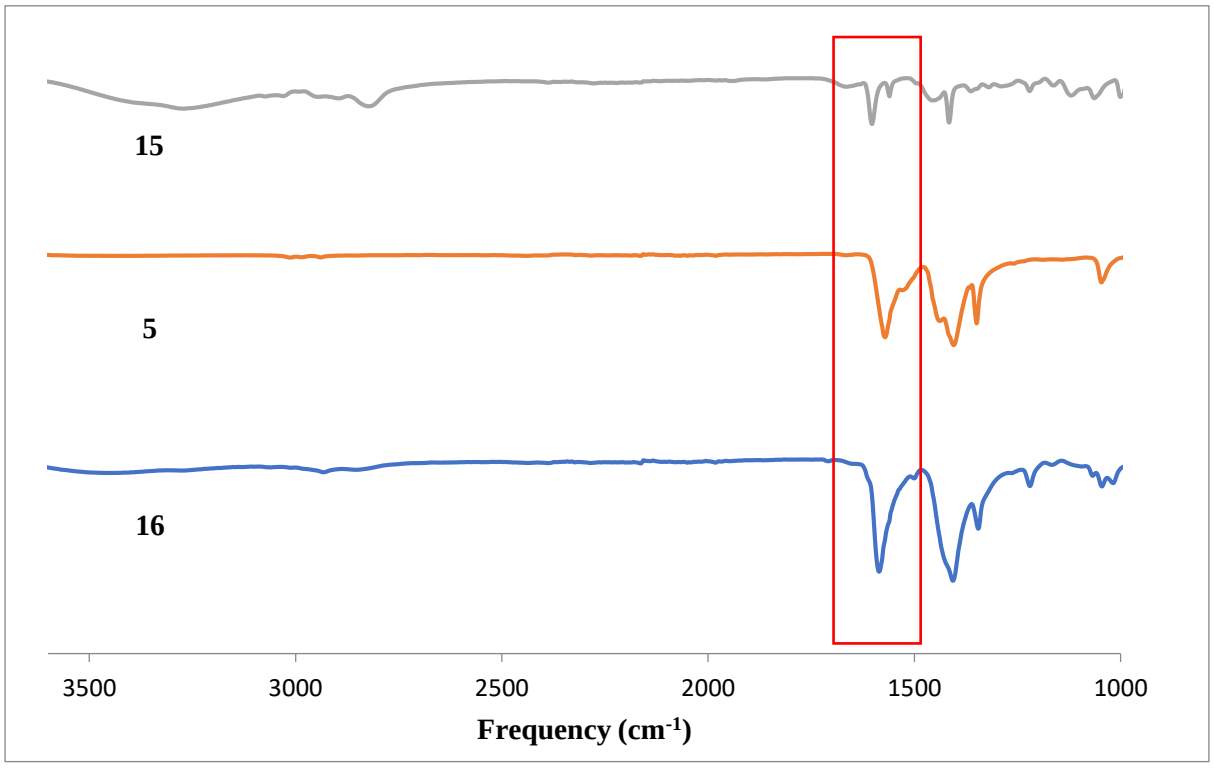

***Figure 3.18**: IR spectral comparison of compounds **15** (top), **5** (middle) and **16** (bottom)*

The IR spectrum (Figure 3.19) obtained for compound **17** shows characteristic absorption bands corresponding to the ν(C-F) at 1225 cm^{-1} in addition to the shifted absorption bands of

the scaffold for the ν(C-O), $\nu(C{=}N)_{pyridyl}$ and a weak ν(N-H) at 1496, 1583 and 3300 cm^{-1} respectively. The shift to higher wavenumber for the C-F absorption band indicates the strong inductive electron-withdrawing effects of the trifluoromethyl group, withdrawing electron density from the pyridyl-Rh_2 core thereby strengthening the C-F bonds.

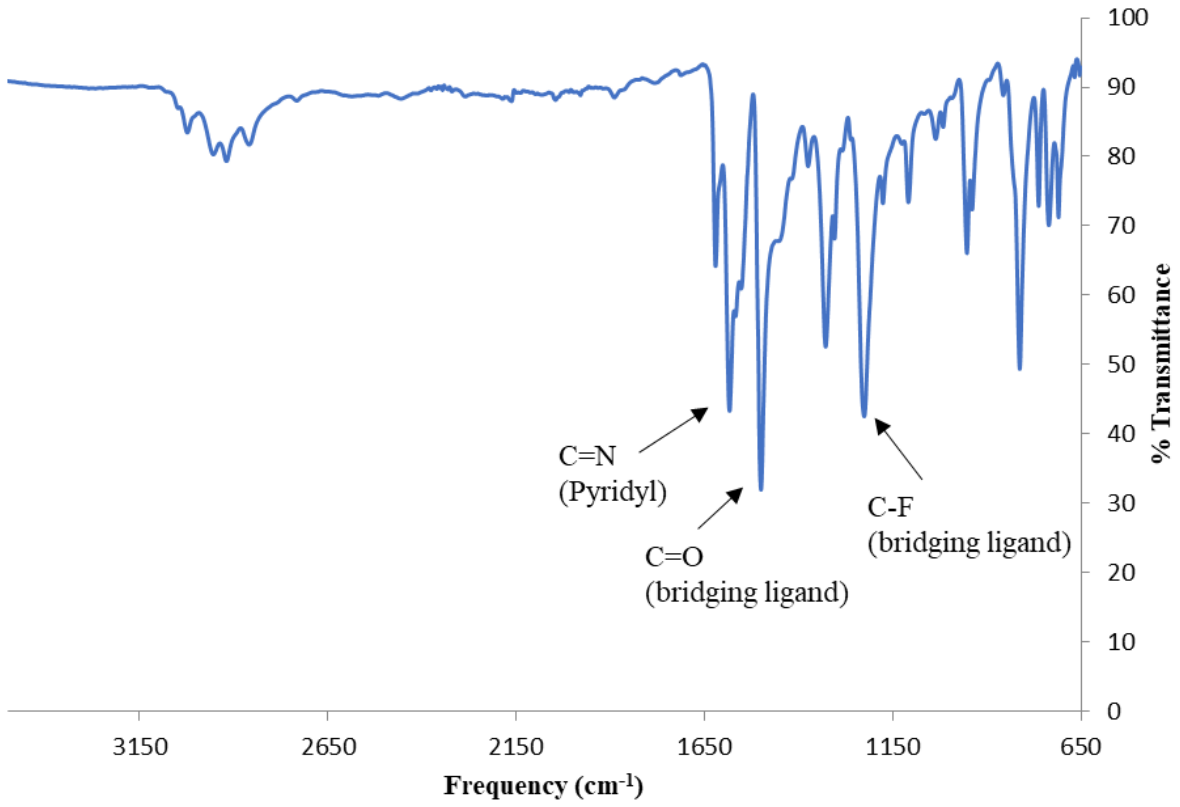

Figure 3.19**: IR spectrum obtained for compound **17

3.3.2.3 Mass spectrometry

The data obtained from ESI-MS analysis supports the ^{1}H-NMR and IR spectral data, in which a base peak corresponding to an $[M+Na]^+$ species is observed in the spectra of compound **16** at *m/z* 1768.4221. The base peak corresponding to an $[M+(NCCH_3)+2K]^{2+}$ species is observed in the spectrum of compound **17** at *m/z* 1350.4651.

*3.3.3 Synthesis and characterization of low-valent metallodendrimers bearing dirhodium formamidinato paddlewheel complexes on the periphery (**18 - 21**)*

The synthetic procedure outlined for the synthesis of compounds **14**, **16** and **17** was then extended to the dirhodium formamidinato complexes to obtain new compounds **18** - **21** in moderate to good yields of 42 - 89 %.

The synthetic procedure was further modified for the successful synthesis of **19**,[2] where an increase in temperature was needed to facilitate coordination. The increased steric influences of the methyl substituent in the 2-position was speculated to reduce the ability of the pyridyl group to bind effectively. The reaction temperature was raised from 20 to 40˚C to increase rotation of the 2-methyl phenyl entities outlined in Scheme 3.5 below, leading to a higher statistical probability of less steric hinderance occurring at the axial sites.

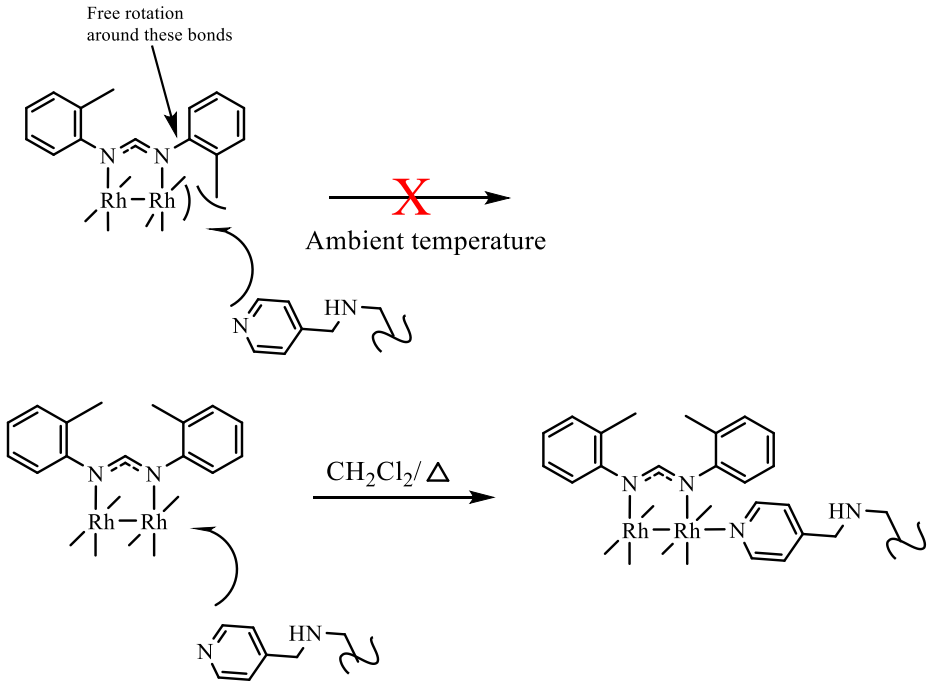

Scheme 3.5**: Illustration of possible steric influence on coordination at axial site of **10

Theoretically, this increase in temperature would also lead to an increase in more successful molecular collisions and a higher probability of the formation of the desired compound. To our delight, the increase in temperature lead to significantly more product formation, increasing the yield from 7% to 42 %.

Compounds **18** and **19** were isolated as a dark green flaky solid and a brown powder with **20** and **21** isolated as a dark blue flaky solid and an orange solid respectively. Compounds **18** - **21**

were found to be air stable and soluble in chloroform, dichloromethane, toluene, benzene and dimethylsulfoxide with precipitation occurring after extended periods of time.

*3.3.3.1 ^{1}H- and ^{13}C{^{1}H}-NMR spectroscopic analysis of compounds **18** and **19***

Methyl substituted compounds **18** and **19** were characterized by ^{1}H- and ^{13}C{^{1}H}-NMR spectroscopy with full spectroscopic details reported in Chapter 6. Successful synthesis is suggested from the relative integration of the $(CH)_{formamidine}$ (H_1, H_{1a}) and the pyridyl proton signals (H_2, H_{2a}) in the ^{1}H-NMR spectra observed in a 12H:6H ratio. The integration calculated for all observed signals further supports successful formation. By way of example, the ^{1}H-NMR spectrum for **18** (Figure 3.20) is shown with integration.

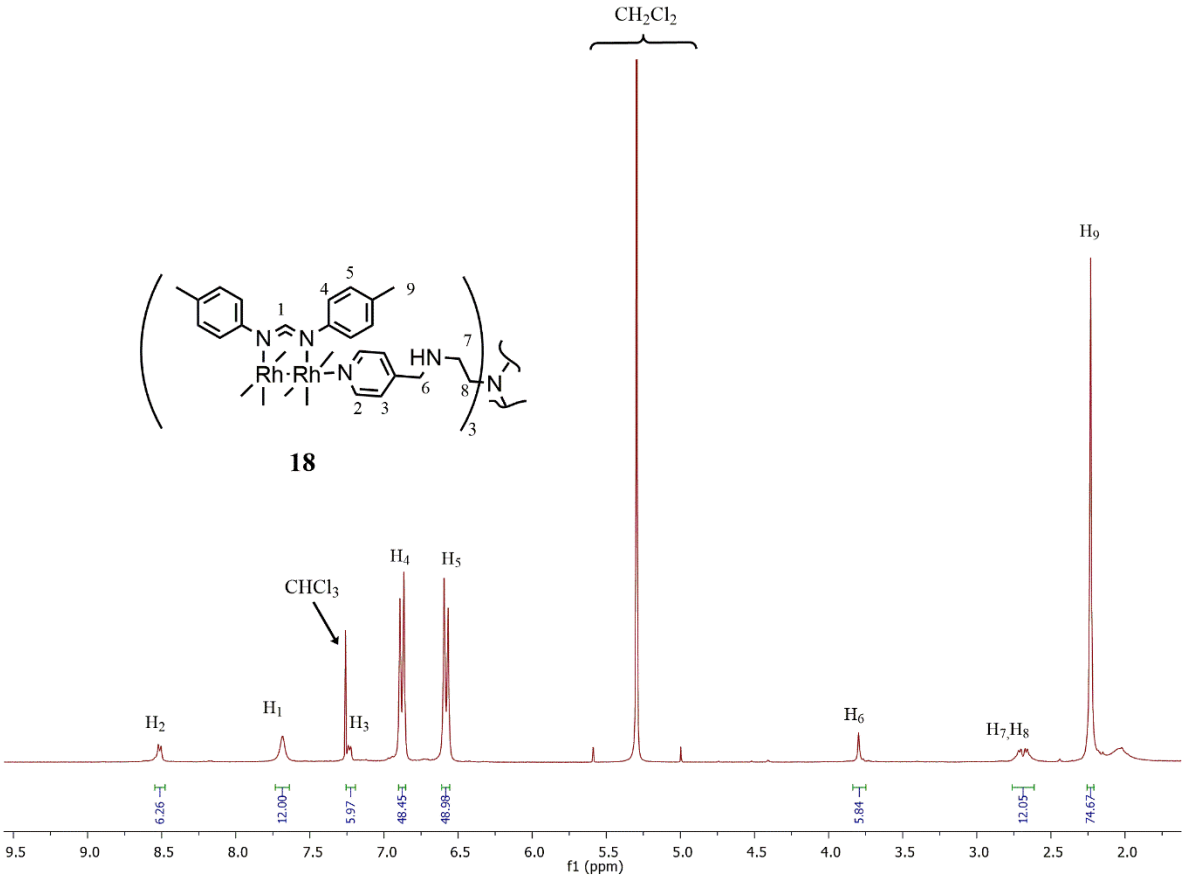

18

***Figure 3.20**: ^{1}H-NMR spectrum of compound **14** in $CDCl_3$*

Additionally, the ^{1}H-NMR spectral comparison between compounds **18** and **19** (Figure 3.21) shows a shift in the $(CH_2)_{benzylic}$ proton signal from 3.73 ppm (observed in compound **15**) to 3.81 ppm (H_6), 3.88 and 3.79 ppm (H_{9a}) respectively. The two signals observed in the case of compound **19** is likely due to the different conformation around the $(C\text{-}N)_{benzylic}$ bond possible

in the dendritic arms in solution. Rotation around this bond would lead to a difference in observed benzylic proton signals and the sum of the integrals obtained for both signals corresponds to the expected 6H. The conformation difference is further suggested by the broadening of the methylene proton signals in the 2.70 ppm region.

Furthermore, the downfield shift of the pyridyl protons is observed with signals resonating at 8.52 (H_2) and 8.53 (H_{2a}) from 8.47 ppm compared to analogous protons in compound **15**. This is a noticeably less significant shift compared to the 9.01 ppm observed in compound **16**. The data obtained here suggests that the formamidinate bridging ligands have similar electronic effects to the pyridyl entity, leading to the magnetically similar environments observed for the pyridyl protons in the spectrum when compared with analogous protons in model compound **13**.

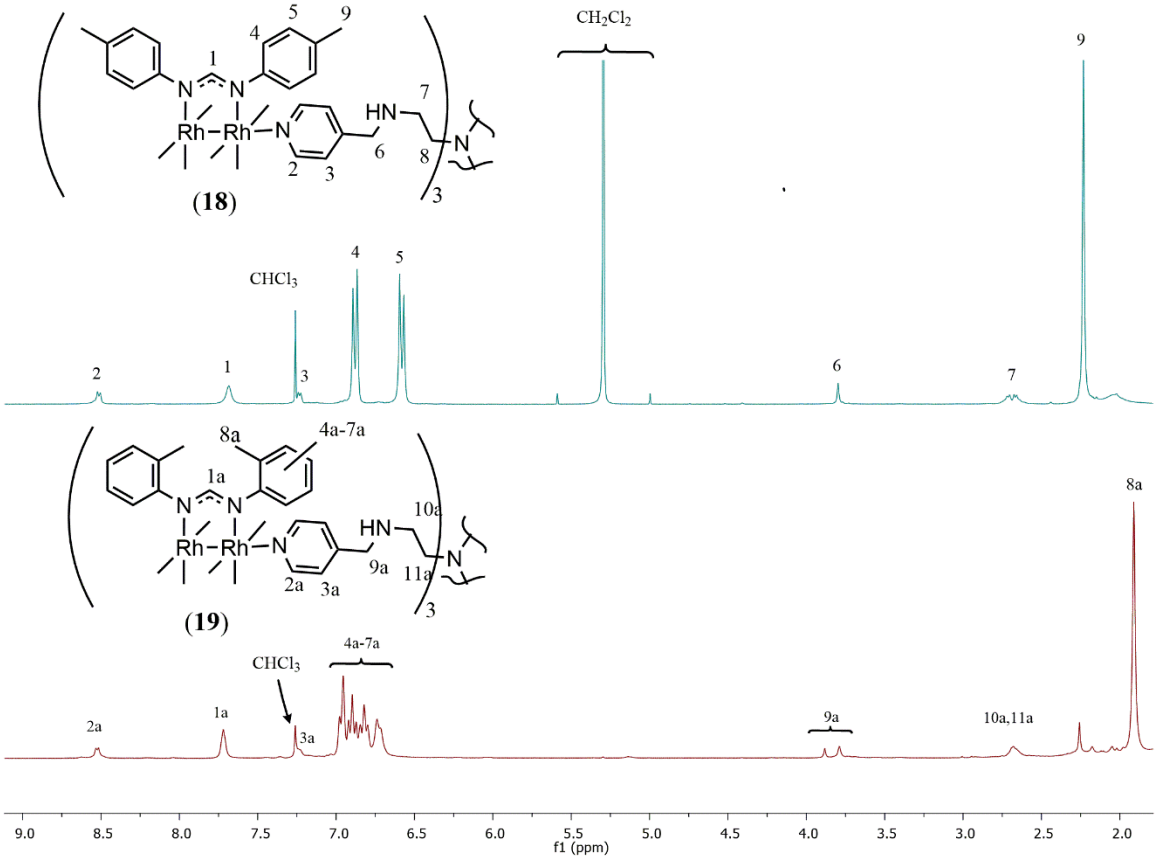

***Figure 3.21**: [1]H-NMR spectra obtained for **18** and **19** in $CDCl_3$*

Variable solubility of compounds **18** and **19** in deuterated solvents was encountered as seen for **16** and **17**, although to a lesser extent. The $^{13}C\{^1H\}$-NMR analysis for compound **19** was attempted in deuterated dimethylsulfoxide (DMSO-d_6), chloroform ($CDCl_3$), acetone

($CO(CD_3)_2$), benzene (C_6D_6) and acetonitrile (CD_3CN) with significant precipitation occurring *in situ* at the lowest required concentration while preparing the NMR sample. As a result, a $^{13}C\{^1H\}$-NMR spectrum could not be recorded for **19**.

The $^{13}C\{^1H\}$-NMR spectrum (Figure 3.22) of **18** was recorded in C_6D_6 and shows signals corresponding to the pyridyl scaffold (**15**) in addition to signals corresponding to precursor **7**, resulting in a combined total of 12 carbon signals. Carbon atoms corresponding to the $(\mathbf{C}H_2)_{ethylene}$, $(\mathbf{C}H_2)_{benzylic}$, and $(\mathbf{C}H_3)_{tolyl}$ are observed in the 20-60 ppm range, assigned to C_8, C_9, C_{10}, and C_{11} resonating at 54.7, 47.8, 31.5 and 21.4 ppm respectively. A signal was observed at 53.46 ppm, corresponding to dichloromethane. Attempts were made to remove the residual dichloromethane, however standard techniques such as gentle heating and removal of solvent *in vacuo* had no significant effect. This was attributed to encapsulation of solvent molecules due to conformational folding of the dendritic branches in metallodendrimers as has previously been reported in literature.[5,6]

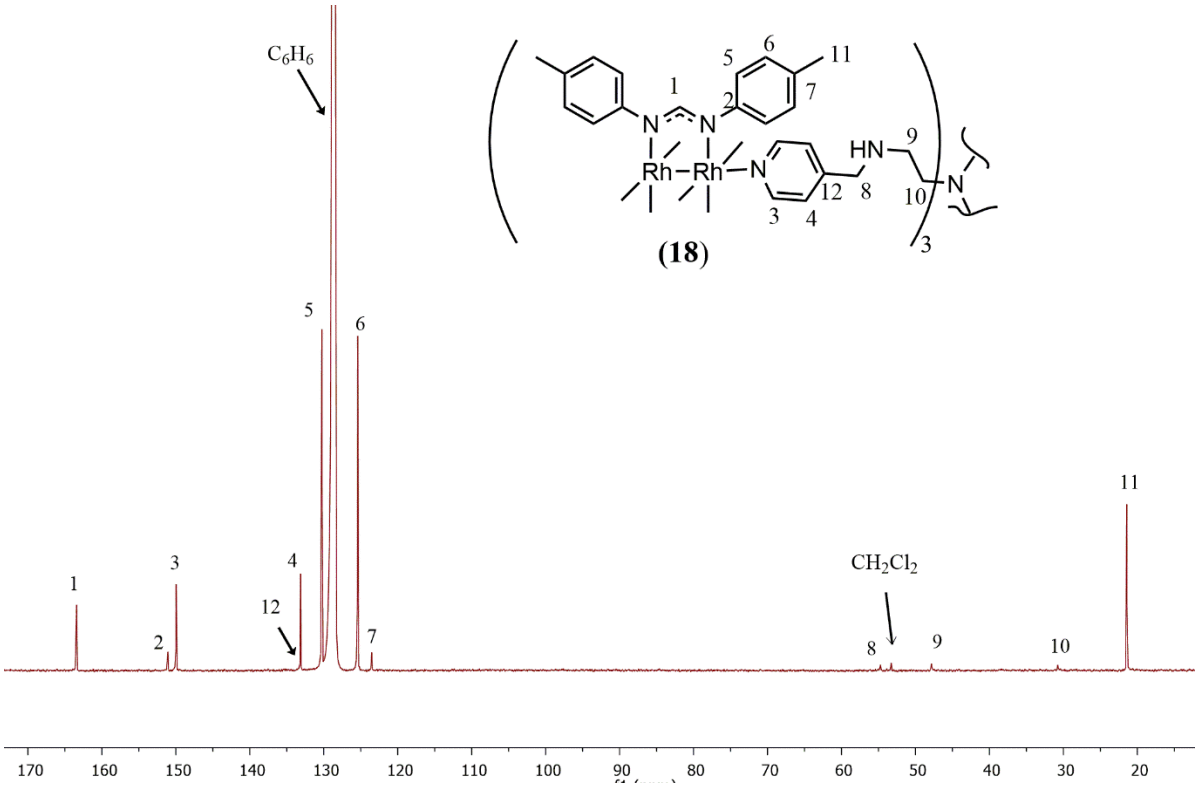

***Figure 3.22**: $^{13}C\{^1H\}$-NMR spectra obtained for **18** in C_6D_6*

Aromatic carbon signals corresponding to the diphenylformamidine entities C_2, C_5, C_6, and C_7 are observed at 151.0, 130.3, 125.4 and 123.5 ppm respectively. Additionally, the relative intensity of aromatic pyridyl carbon signals and aromatic diphenylformamidine signals was calculated to be *ca.* 1:2.

*3.3.3.2 ^{1}H- and ^{13}C{^{1}H}-NMR spectroscopic analysis of compounds **20** and **21***

As for compounds **18** and **19**, fluoro- substituted compounds **20** and **21** were characterized by ^{1}H- and ^{13}C{^{1}H}-NMR with full spectroscopic details reported in Chapter 6. The successful synthesis is initially suggested by signals on the ^{1}H-NMR spectra (Figure 3.23) with the relative integration of $(CH)_{formamidine}$ proton signals H_{1c} (**20**), H_{1d} (**21**) and pyridyl proton signals H_{2c} (**20**), H_{2d} (**21**) observed in a ratio of 12H:6H as seen for compounds **18** and **19**. Upon further analysis of the spectrum recorded for **20**, the introduction of the pyridyl group results in a loss in resolution of the multiplicity of the formamidine proton signal, seen previously as a triplet for precursor compound **10** in Chapter 2.

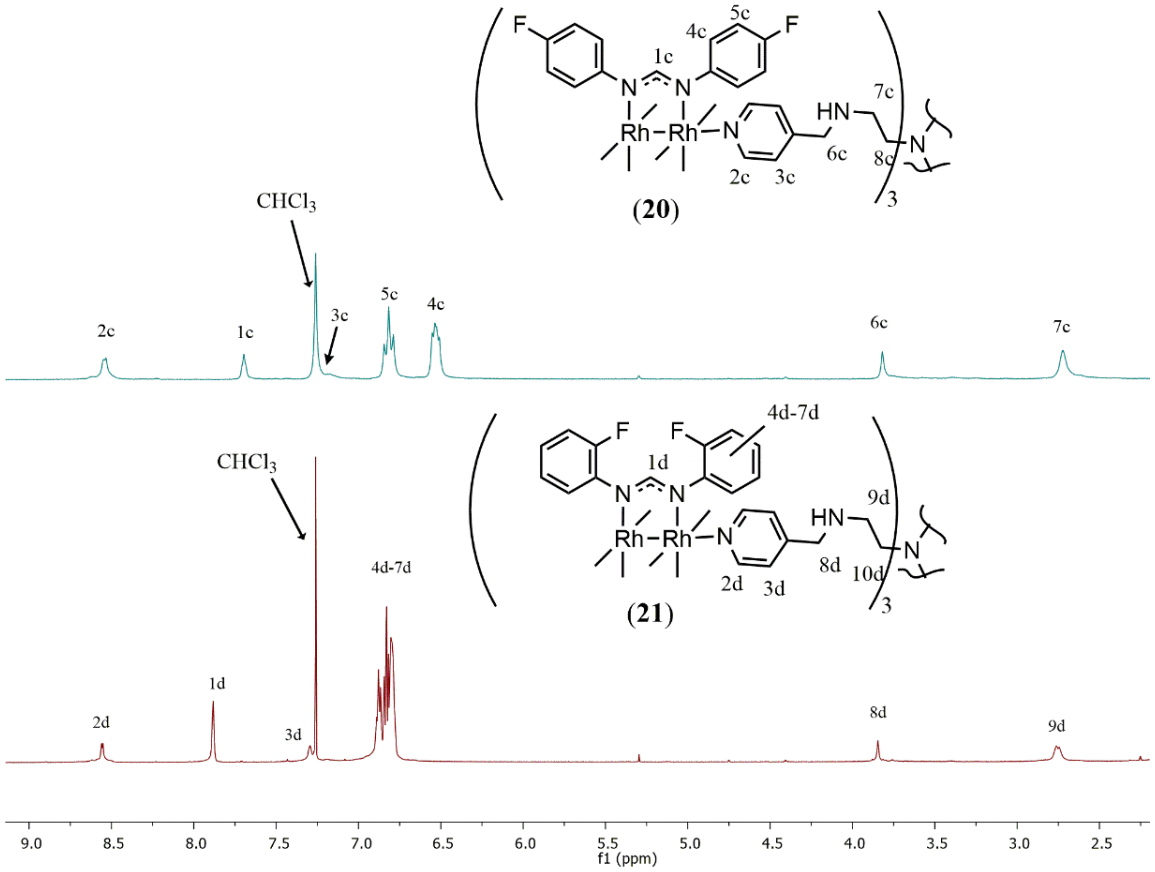

***Figure 3.23**: ^{1}H-NMR spectra obtained for **20** and **21** in $CDCl_3$*

Furthermore, the downfield shift observed in pyridyl proton signals is more pronounced than observed in the ^{1}H spectra compounds **18** and **19**, with observed proton signals H_{2c} and H_{2d} resonating at 8.56 and 8.58 ppm respectively. A similar effect is observed with proton signal H_{3d} in relation to H_{3c}, producing signals resonating at 7.29 and 7.26 ppm respectively. The latter signal was found to coalesce with the chloroform proton signal resulting in significant broadening in the 7.26 ppm region. The larger de-shielding effect due to the fluorine substituent

in the 2-position of the diphenylformamidine group on pyridyl protons (H_{2d}, H_{3d}) is observed, likely due to the placement of the substituent at the 2-position on the phenyl entity.

$^{13}C\{^{1}H\}$-NMR spectral analysis of compounds **20** and **21** was attempted with a sufficiently resolved spectrum collected for **21** only, due to precipitation occurring *in-situ* for compound **20**. The characteristic doublet signals previously observed in fluoro substituted compounds (**9**, **10)** are evident in the spectra obtained for **21**, with twelve signals observed and their expected coupling constants as reported in literature.[30]

The $^{13}C\{^{1}H\}$-NMR spectrum obtained for **21** is shown below in Figure 3.24. Carbon atoms corresponding to the $(\mathbf{C}H_2)_{ethylene}$ and $(\mathbf{C}H_2)_{benzylic}$ are observed in the 30-60 ppm range as for compound **18**, with analogous intensity ratios observed between signals corresponding to precursor compounds **9** and **15.**

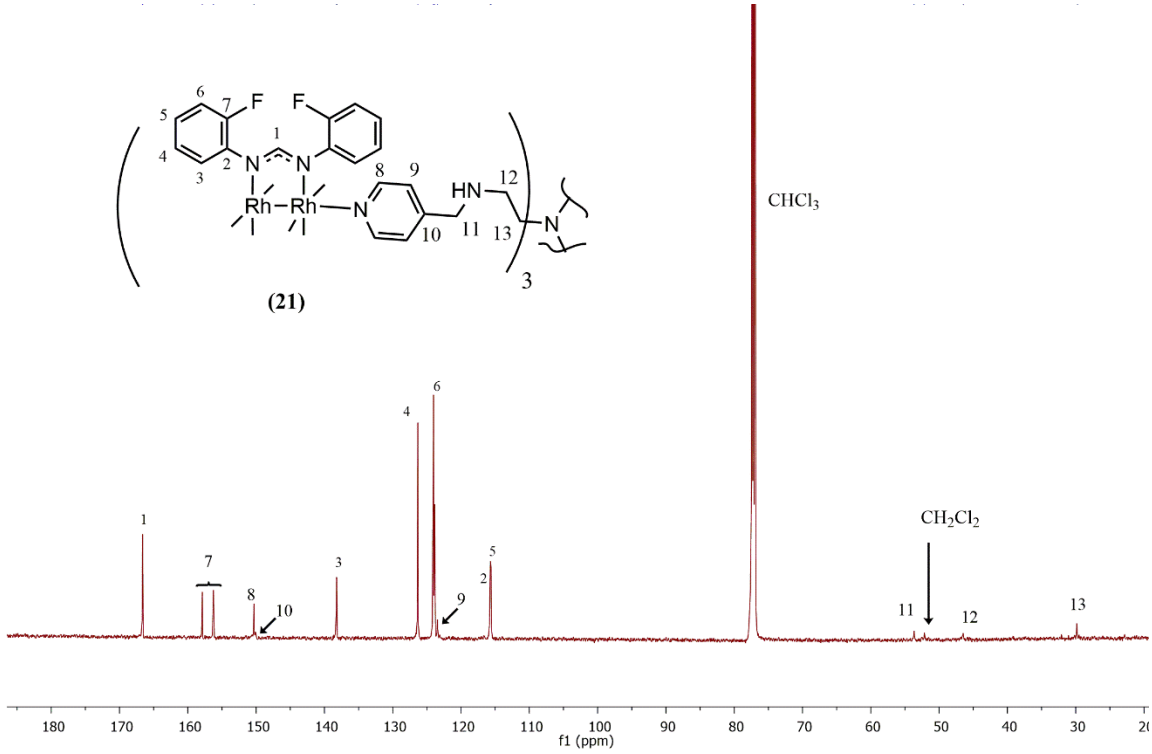

***Figure 3.24**: $^{13}C\{^{1}H\}$-NMR spectra obtained for **21** in $CDCl_3$*

A negligible downfield shift is observed for the $(\mathbf{C}H)_{formamidine}$ carbon signal (C_1) observed resonating at 166.6 ppm. Signals corresponding to C_7, C_3, C_6 and C_5 are observed as doublets centred at 157.0, 138.2, 124.0 and 115.6 ppm with respective coupling constants as reported for precursor complex **9**.

3.3.3.3 Infrared (IR) spectroscopy

Infrared spectroscopy was used to determine whether successful synthesis of compounds **18** – **21** (Figure 3.25) was achieved. Successful coordination is suggested here by absorption bands corresponding to the $\nu(C{=}N)_{pyridyl}$ stretch, shifting from 1610 cm^{-1} to the 1585 cm^{-1} region. This results in an overlap between the $\nu(C{=}N)_{pyridyl}$ and $\nu(C{=}N)_{formamidine}$ absorption bands seen in region (**A**). The presence of a weak absorption band in the 3200 - 3400 cm^{-1} region (**B**) corresponding to the ν(N-H), further suggesting that coordination occurs through the pyridyl nitrogen atom as previously seen in the IR spectra recorded for compounds **16** and **17**.

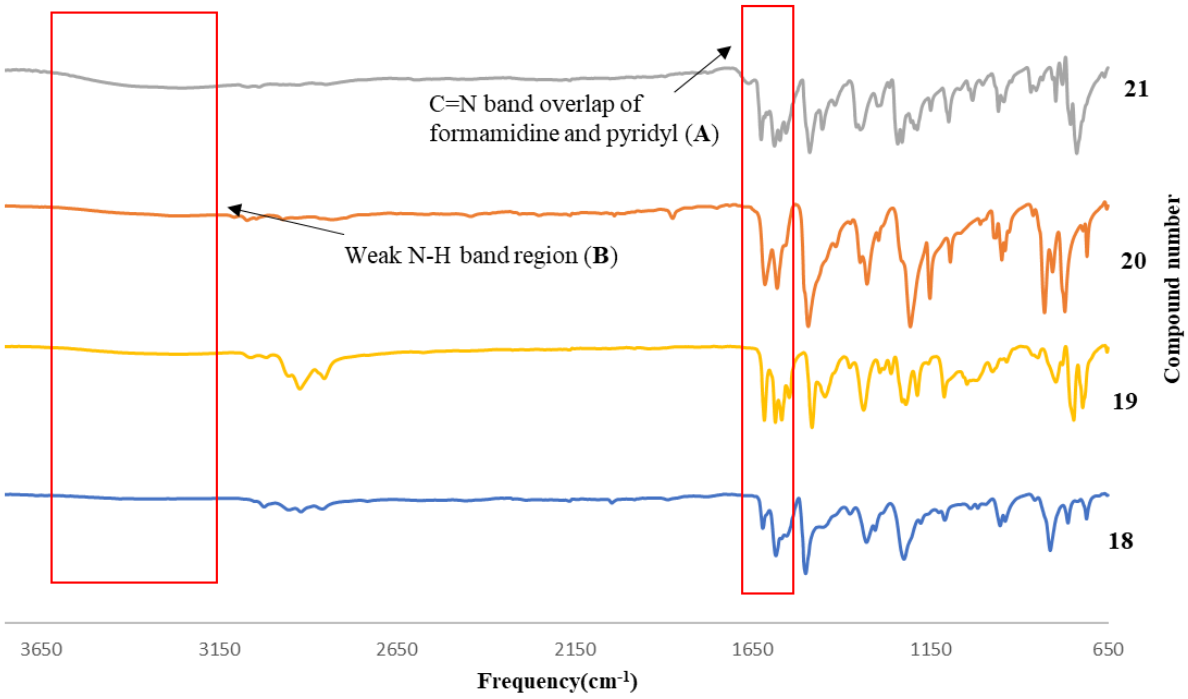

Figure 3.25**: Infrared spectral comparison of compounds **18- 21

3.3.3.4 Mass spectrometry

The data obtained from ESI-MS analysis supports the ^{1}H-, $^{13}C\{^{1}H\}$-NMR and IR spectral data obtained where applicable. Base peaks are observed for compounds **18**, **19** and **20** corresponding to $[M + 4(CH_2Cl_2) + 2K]^{2+}$ at *m/z* 2072.4199, $[M + 3NCCH_3 + 2Na]^{2+}$ at *m/z* 1945.4124 and $[M + 3Na]^{3+}$ at *m/z* 1294.4554 species respectively. The spectrum obtained for compound **21** shows complex fragmentation peaks, which could not accurately be assigned.

3.4 Overall Summary

Known model Schiff base ligand (**11**) and known polypyridyl trisamine scaffold (**15**) were synthesized in yields of 84% and 55 % respectively and characterized by ^{1}H- ^{13}C{^{1}H}-NMR and IR spectroscopy with spectroscopic details comparable to data previously reported. Model reactions for coordinating compounds **5** and **11** were carried out using 1:1 molar ratio resulting in formation of the *bis*-adduct. Reduction in the molar ratios of **11** to **5** in excess results in *mono*-adduct (**13**) formation in a low yield of 28%, with an observable cleavage of the imine functionality over time. A second model reaction with 4-picoline and compound **5** resulted in formation of the mono adduct (**14)** in a good yield of 72%. Characteristic absorption bands were observed in the infrared spectrum, namely a shift of the pyridyl C=N absorption band from 1605 to 1587 cm^{-1} upon coordination. Conjugation of compound **15** with compounds **5** and **6** resulted in the formation of novel metallodendrimers **16** and **17** in moderate to excellent yields of 72 and 83 % respectively, with variable solubility in common laboratory solvents. Similarly, reactions carried out with **15** and compounds **7-10** resulted in the isolation of new compounds **18** – **21** in moderate to good yields (42 – 89%). Low valent metallodendrimers (**16-21**) were characterized using various spectroscopic (^{1}H-, ^{13}C{^{1}H}- Infrared) and mass spectrometry where possible.

3.5 References

1. D. J. Cole-Hamilton, *Science*, 2003, **299**, 1702-1706.
2. S. Malaza, P. Govender, M. Schutte-Smith, H. G. Visser and G. S. Smith, *Eur. J. Inorg. Chem.* 2017, 3919.
3. P. McMorn, and G. J. Hutchings, *Chem. Soc. Rev.*, 2004, **33**, 108.
4. J. Jamis, J. R. Anderson, R. S. Dickson, E. M. Campi and W. R. Jackson, *J. Organomet. Chem.*, 2001, **37**, 627.
5. Y. Guoyu, S. Ailing, Z. Wenfeng, Z. Hailin and J. Denggao, *Catal. Lett.*, 2007, **118**, 275-279.
6. A. Caminade, C. O. Turrin, R. Laurent, A. Ouali and B. Delavaux-Nicot, *Dendrimers - Towards Catalytic, Material and Biomedical Uses*, John Wiley & Sons, Toulouse, France, 2011.
7. X. S. Zhao, X. Y. Bao, W. Guo and F. Y. Lee, *Materials Today*, 2006, **9**(3), 32.
8. P. Govender, N. C. Antonels, J. Mattsson, A. K. Renfrew, P. J. Dyson, J. R. Moss, B. Therrien and G. S. Smith, *J. Organomet. Chem.*, 2009, **694**, 3470-3476.
9. Z. Cheng, D. L. J. Thorek and A. Tsourkas, *Angew. Chem. Int. Ed.*, 2010, **49**, 346-350.
10. J. Y. Chen, M. Smet, J. C. Zhang, W. K. Shao, X. Li, K. Zhang, Y. Fu, Y. H. Jiao, T. Sun, W. Dehaen, F. C. Liu and E. H. Han, *Polym. Chem.* 2014, **5**, 2401.
11. S. C. Bourque, F. Maltais, W. J. Xiao, O. Tardif, H. Alper, P. Arya and L. E. Manzer, *J. Am. Chem. Soc.*, 1999, **121**, 3035.
12. P. T. Anastas, M. M. Kirchhoff and T. C. Williamson, *Appl. Catal.*, 2001, **221**, 3-13.
13. P. W. M. N. van Leewen, *Appl. Catal.*, 2001, **212**, 61-81.
14. T. Mizugaki, M. Ooe, K. Ebitani and K. Kaneda, *J. Mol. Catal. Chem.* 1999, **145**, 329.
15. N. C. Antonels, J. R. Moss and G. S. Smith, *J. Organomet. Chem.*, 2001, **696**, 2003.
16. G.R. Newkome, C.N. Moorefield, G.R. Baker, A.L. Johnson and R. K. Bahera, *Angew. Chem. Int. Ed. Eng*, 1991, **30**, 1689.
17. K. Takeda, T. Oohara, M. Anada, H. Nambu and S. Hashimoto, *Angew. Chem. Int. Ed. Eng*, 2010, **122**, 7133.
18. D. M. Shadrack, E. D. Mubofu and S. S. Nyandoro, *Int. J. Mol. Sci.*, 2015, **16**, 26363-26377.
19. J. W. Lee, B. K. Kim, S. C. Han, U. Y. Lee, J. H. Kim, J. Oh and S. H. Jin, *Mol. Cryst. Liq. Cryst.*, 2008, **491**, 164-172.

20. D. Giffard, E. Fischer-Fodor, C. Vlad, P. Achimas-Cadariu and G. S. Smith, Eur. J. Med. Chem., 2018, **157**, 773-781.
21. M. T. Reetz, G. Lohmer and R. Schwickardi, *Angew. Chem. Int. Ed. Engl.*,1997, **36**, 1526.
22. G. E. Oosterom, J. N. H. Reek, P. C. J. Kamer and P. W. N. M. van Leeuwen, *Angew. Chem. Int. Ed.*, 2001, **40**, 1828.
23. P. Govender, S. Pai, U. Schatzschneider and G. S. Smith, *Inorg. Chem.*, 2013, **52**, 5470-5478.
24. Y. Jin, G. Huang, D. Han, P. Song, W. Tang, J. Bao, R. Li and Y. Liu, *Compos. A. Appl. Sci. Manuf.*, 2016, **86**, 9-18.
25. I. Taniguchi, S. Duan, S. Kazama and Y. Fujioka, *J. Membr. Sci.*, 2008, **322**, 277-280.
26. H. Yang and W. J. Kao, *J. Biomater. Sci. Polymer Edn.*, 2006, **17**, 3.
27. M. Mammen, S.K. Choi and G. M. Whitesides, *Angew. Chem. Int. Ed.*, 1998, **37**, 2755.
28. R. Malgas, S. F. Mapolie, S. O. Ojwach, G. S. Smith and J. Darkwa, *Cat. Comm.*, 2008, **9,** 1612.
29. N. Wilhelms, S. Kulchat and J. Lehn, *Helv. Chim. Acta*, 2012, **95**, 2635-2651.
30. I. Ingeborg, M. Schuster, *J. Magn. Reson,* 1969, **17**(1), 104-111.

CHAPTER 4

The catalytic evaluation of dirhodium(II,II) complexes and associated low-valent metallodendrimers in the hydroformylation of 1-octene

4.1 Introduction

Hydroformylation is the addition of a formyl group to olefins by using a mixture of molecular hydrogen and carbon monoxide (syngas), and a transition metal catalyst. The process was first discovered by Otto Roelen in 1938 while conducting investigations into the Fischer-Tropsch reaction with $HCo(CO)_4$, a carbonyl-based cobalt hydride active catalyst species, obtained *in situ* under high syngas pressure from the $Co_2(CO)_8$ catalyst precursor.[1] Although aldehydes are the major products, hydrogenation of the alkene substrate to form alkanes and alcohols can also occur.[2,3] Scheme 4.1 below illustrates the possible product formation.

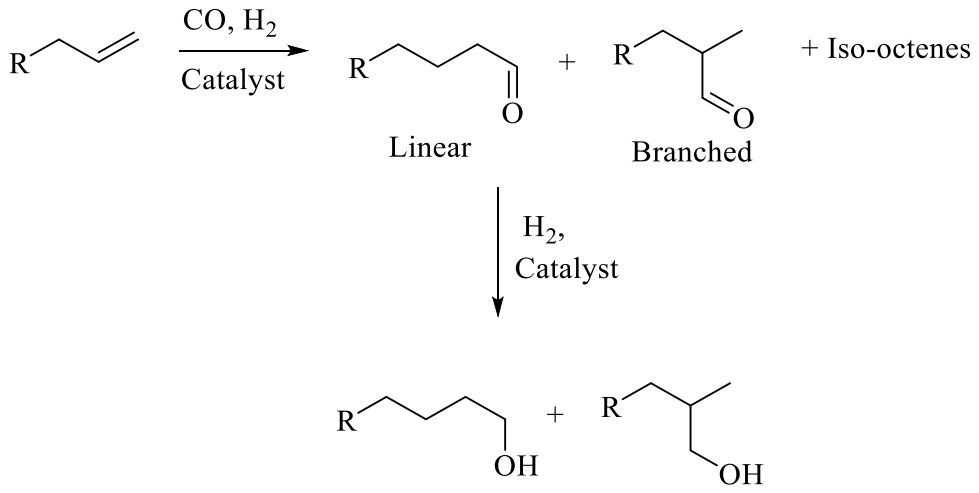

***Scheme 4.1**: Outline of general products obtained from hydroformylation processes*

Catalysts studied in hydroformylation most often make use of metals such as ruthenium, platinum, iridium, cobalt, iron and/or rhodium.[4,5] The latter examples have undergone extensive study with rhodium-based catalysts typically requiring milder reaction conditions than the cobalt counterparts.[6,7,8] The regioselectivity (linear vs. branched aldehydes) as well as chemoselectivity aspects (aldehydes vs alcohols or *iso*-octenes) can be altered through the use of different or modified ligands, resulting in rhodium and cobalt being the ideal transition

metals for use in hydroformylation in industrial applications for first- and second-generation processes in both modified and unmodified forms.[6,7]

First-generation hydroformylation processes made use of cobalt and rhodium based-carbonyl containing catalysts exclusively in industry, initially providing adequate reaction rates and the desired products. The conditions of reactions using first-generation catalysis are generally harsh, requiring high temperatures and pressures, facilitating improvements being made with respect to ligands and transition metals for selectivity and by-product formation.[8,9,10] The use of different or modified ligands to afford complexes like cobalt-phosphine based catalysts attempted to address factors in the optimisation of the process, was mostly utilized by the Shell Higher-Olefin Process.[11]

Second-generation processes used catalysts based on modified phosphine ligands and rhodium as a metal centre discovered by Wilkinson *et al.* in the 1960s,[12] [$RhCl(PPh_3)_3$] being a classic example. Modification made to the ligands of these catalyst precursors demonstrated advantages such as increased selectivity towards linear aldehydes as well as minimal isomerization of the substrate[13], the latter is shown in Scheme 4.2 below.

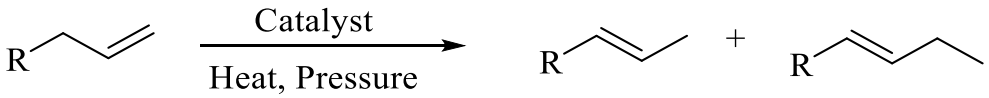

***Scheme 4.2**: Possible isomerization products obtained with terminal alkenes in the presence of catalysts*

More recently, it has been shown that multinuclear complexes show higher activity in hydroformylation reactions.[14] In this regard, dirhodium(II,II) paddlewheel complexes are of interest and investigation into the activity of these bimetallic compounds are common in other catalyzed reactions such as allylic oxidation[15], cyclopropanation,[16] cross coupling[17], hydroformylation[18] and hydrogenation.[19,20]

Some examples of dirhodium complexes studied for catalytic activity are shown in Figure 4.1. Studies on the effects of ligand modification on these complexes, their active catalytic species and investigations with respect to the activity of such complexes with the aid of techniques such as cyclic voltammetry are attractive areas of investigation.

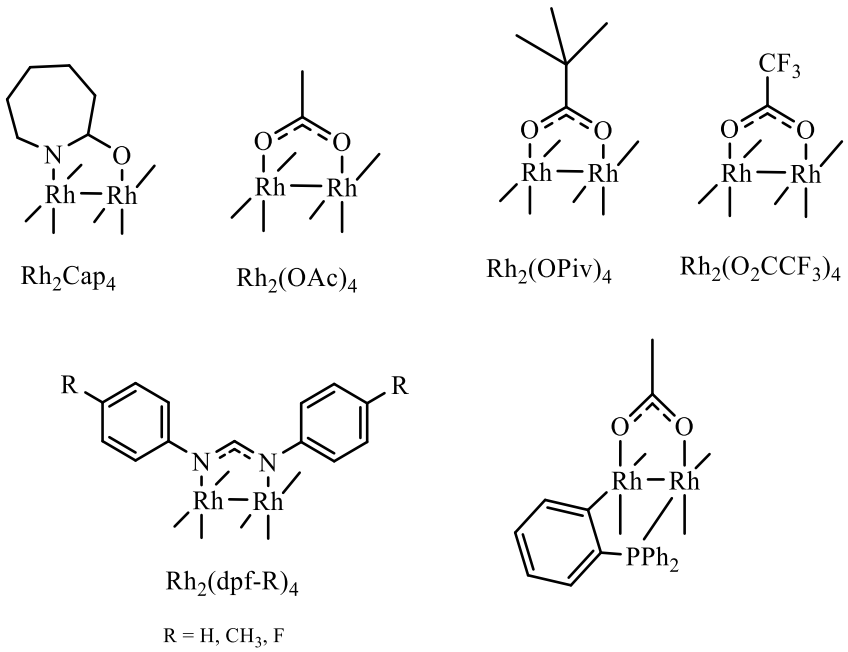

***Figure 4.1**: Dirhodium(II,II) catalyst precursors used in various catalytic reactions*

Herein we report the catalytic optimization and evaluation of previously synthesized dirhodium(II,II) complexes and associated tris metallodendrimers (Figure 4.3) in the hydroformylation reaction with 1-octene as a substrate.

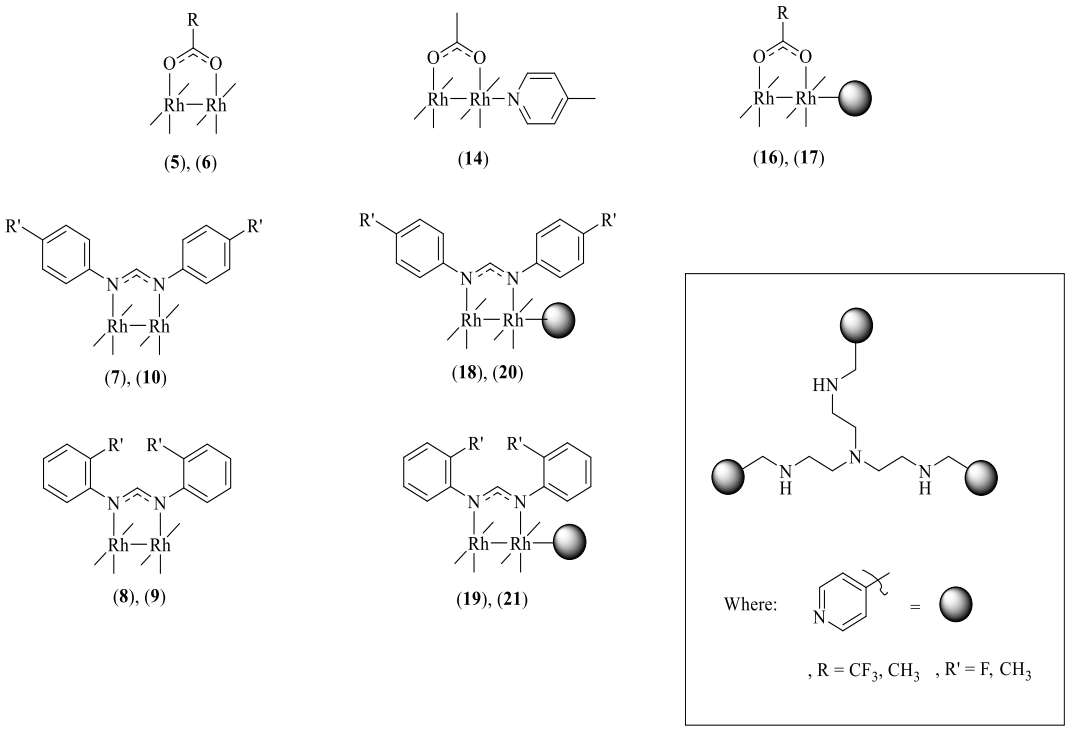

***Figure 4.2**: Dirhodium(II,II) compounds used as catalyst precursors in the hydroformylation of 1-octene*

4.2 Optimization of reaction conditions using dirhodium(II,II) complexes as catalyst precursors

4.2.1 Effects of temperature variation on catalyst performance

Preliminary studies on catalyst performance were carried out using compound **5** as a model catalyst precursor in the hydroformylation reaction with 1-octene as a substrate (Scheme 4.3).

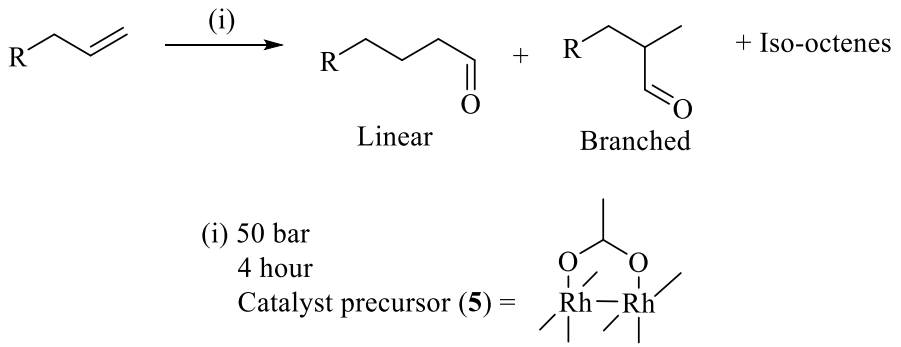

***Scheme 4.3**: Outline of model reaction for optimising hydroformylation reaction conditions*

An initial a pressure of 50 bar was chosen for the temperature-dependent study, with a four-hour reaction time based on analogous experiments carried out in previous work.[14,21,22] The temperature was varied between 75, 85 and 95˚C (Table 4.1). Although the aim of the temperature optimization experiments was to determine which temperature resulting in favouring of either aldehyde or *iso*-octene products is maximised, it is noted that quantitative conversion of substrate is observed for the optimisation reaction run at 95˚C.

Table 4.1**: Hydroformylation data obtained from temperature variation with compound **5

Entry	Temperature (˚C)	Conversion (%)	Total Aldehydes (%)	Total *iso*-octenes (%)	Linear aldehydes (%)	Branched aldehydes (%)	TOF (h^{-1})	*n:iso*
1	75	81.45	72.54	27.46	62.32	37.68	378.1	1.88
2	85	94.74	84.75	15.25	70.98	29.02	506.5	2.45
3	95	99.94	98.24	1.76	43.56	56.44	613.8	0.78

Hydroformylation of 1-octene in toluene (5 mL), 1:1 $CO:H_2$, 50 bar pressure, reaction time of 4 hours and catalyst loading of 2.87 x 10^{-3} mmol. GC conversions were obtained using an internal standard of *n*-decane. Total aldehydes are composed of linear and branched aldehydes in a mixture with percentage sum of 100. TOF = (mmol aldehydes per mmol Rh)/ time. Reactions carried out in triplicate with an average error value of 1.12%

A noticeable increase in the chemoselectivity toward total aldehydes is observed, from 72 - 98% when the temperature is varied across the 75 - 95˚C range with a significant reduction in the *n:iso* ratio over the same range. This suggests that although hydroformylation of 1-octene takes place, the isomerization of substrate occurs in the reaction medium from 75˚C. The largest *n:iso* ratio indicates that the greatest regioselectivity toward linear aldehydes is obtained at 85˚C (Entry 2), showing a balance between the energy requirements for the hydroformylation and isomerization reactions. A proposed mechanism (Scheme 4.4), based on a report by Powers *et al.*, is described below whereby a bimetallic Rh(I) complex forms a metal-metal bonded Rh_2(II,II) species through bimetallic oxidation of H_2.[23]

The reduction in the total number of *iso*-octenes at 95˚C (Entry 3) suggests that at this temperature, there is enough energy to promote the hydroformylation of the isomerized octenes,[24,25] contributing to the increase in branched aldehydes and the reduction in the *n:iso* ratio.

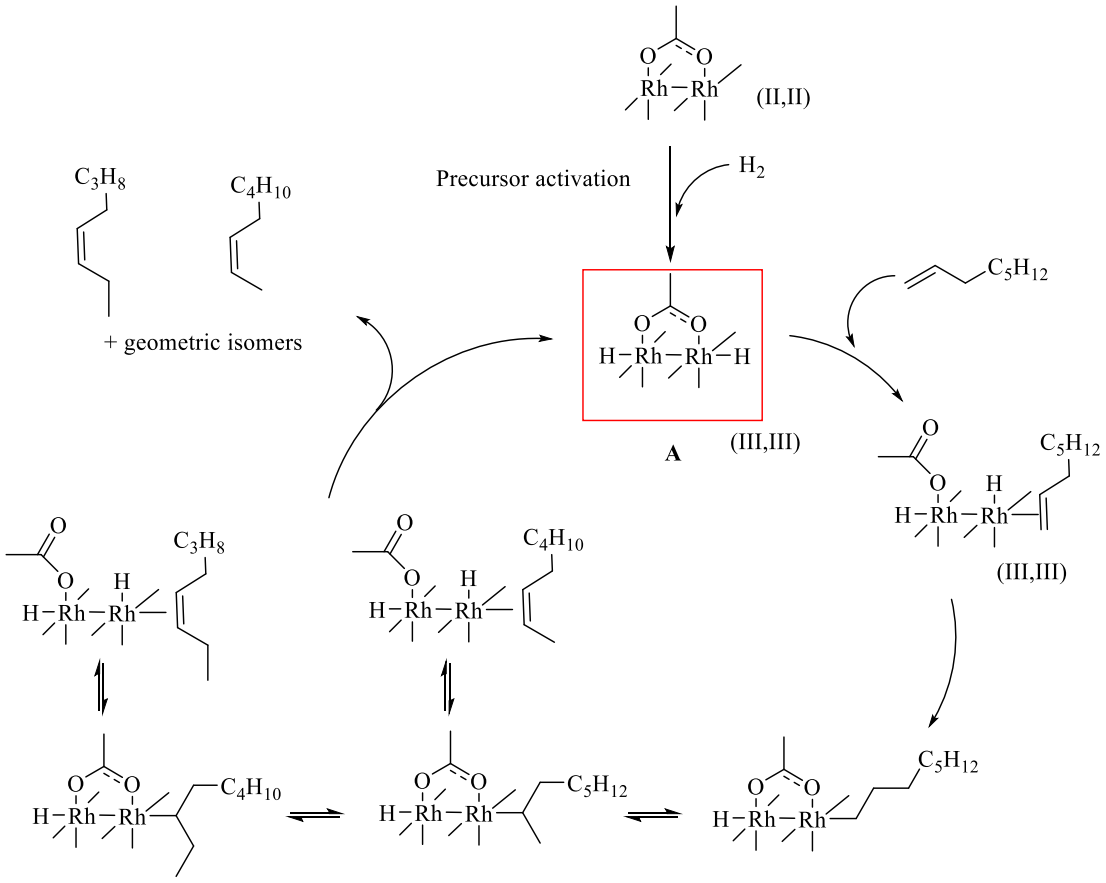

***Scheme 4.4**: Proposed mechanism for the dirhodium catalyzed isomerization of 1-octene*

In a stepwise mechanism, such as proposed above, the rearrangement and partial dissociation of equatorial ligands is necessary to introduce the coordinatively unsaturated species. This

would then allow for coordination of substrate and facilitate known migratory insertion steps based on more classical Rh(I) based catalytic cycles.

4.2.2 Effects of pressure variation on catalyst performance

Experiments were carried out by varying the syngas pressure were carried out to determine the sensitivity of the concentration of carbon monoxide in solution on product formation. The relationship between the syngas pressure applied to the reaction medium and the concentration of carbon monoxide in solution is directly proportional.[26,27]

Experimental data obtained from pressure variation is shown in Table 4.2. A fixed temperature of 95˚C results in total products as a function of syngas pressure in a similar distribution of aldehyde to *iso*-octene formation from 95:5 to 98:2 between 30 and 50 bar syngas pressure. If required, the pressure could be reduced to 30 bar without a significant negative impact on the formation of aldehyde products, and therefore the chemoselectivity over a four-hour period. A more significant increase in the regioselectivity toward linear aldehydes is observed, from 37 to 44% when the syngas pressure is increased from 30 to 50 bar. Theoretically, increasing carbon monoxide concentration should result in a lower rate of isomerization, favouring formation of the linear acyl species over the branched species.[27]

Table 4.2**: Hydroformylation data obtained from syngas pressure variation with compound **5

Entry	**Syngas pressure (bar)**	**Conversion (%)**	**Total Aldehydes (%)**	**Total *iso*-octenes (%)**	**Linear aldehydes (%)**	**Branched aldehydes (%)**	**TOF (h^{-1})**	***n:iso***
1	30	99.93	95.57	4.43	37.21	62.79	598.2	0.60
2	40	99.78	98.74	1.26	40.01	59.99	623.6	0.67
3	50	99.94	98.24	1.76	43.56	56.44	613.8	0.78

Hydroformylation of 1-octene in toluene (5 mL), 1:1 $CO:H_2$ pressure varied, 95˚C, reaction time of 4 hours and catalyst loading of 2.87×10^{-3} mmol. GC conversions were obtained using an internal standard of *n*-decane. Total aldehydes are composed of linear and branched aldehydes in a mixture with percentage sum of 100. TOF = (mmol aldehydes per mmol Rh)/ time. Reactions carried out in triplicate with an average error value of 0.89%

4.2.3 Effects of time variation on catalyst performance

A time dependent study was carried out by varying reaction times between thirty minutes and four hours to determine, if any, differences in chemo- and regioselectivity as a function of time could be observed. The results (Table 4.3) show that at 0.5 hours (Entry 1), conversion of substrate remains relatively low at 2.78. After one hour (Entry 2), the conversion percentage rises sharply to 99.82% with the chemoselectivity toward aldehyde formation showing a less significant increase over that observed at 0.5 hours. This suggests that initial activity in the first 0.5 is hindered by total energy available to the system or the initial activation of the catalyst precursor over an induction period before full activation leads to the formation of an active catalyst species.[28] The conversion percentage remains near quantitative (98.80 to 99.94%) across the time period between one and four hours (Entries 2 to 5) with a sharp rise in the relative amount of aldehydes formed between two and three hours (52.04 to 96.65%), seen in Entries 3 and 4.

Table 4.3**: Hydroformylation data obtained from time variation with compound **5

Entry	**Time (hours)**	**Conversion (%)**	**Total Aldehydes (%)**	**Total *iso*-octenes (%)**	**Linear aldehydes (%)**	**Branched aldehydes (%)**	***n:iso***
1	0.5	2.78	47.60	50.24	66.93	33.07	2.12
2	1	99.82	50.25	49.75	67.78	32.22	2.13
3	2	99.82	52.04	47.96	65.39	34.61	1.98
4	3	99.82	96.65	3.35	43.35	56.65	0.77
5	4	99.94	98.24	1.76	43.56	56.44	0.78

Hydroformylation of 1-octene in toluene (5 mL), 1:1 $CO:H_2$ pressure 50 bar, 95˚C and catalyst loading of 2.87 x 10^{-3} mmol. GC conversions were obtained using an internal standard of *n*-decane. Total aldehydes are composed of linear and branched aldehydes in a mixture with percentage sum of 100. Reactions carried out in triplicate with an average error value of 1.79%

The data obtained in this study suggests that at 95˚C, the tandem isomerization and hydroformylation reactions proceed at similar rates, as seen in comparable amounts of aldehyde formed over the 0.5 to 2-hour range (Entries 1 to 3). Additionally, an *n:iso* ratio of between 2.12 and 1.98 is observed across this time period indicating that until the concentration of 1-

octene falls below to a certain minimum, the hydroformylation of 1-octene occurs over the hydroformylation of *iso*-octenes from the isomerization reaction.

Furthermore, once the 1-octene is consumed, the conversion of *iso*-octenes to branched aldehydes is predominantly observed (Entries 4 and 5) resulting in a reduction of the *n:iso* ratio from *ca.* 2.00 to 0.78 across the two to four-hour period. The substantial decrease in the % of *iso*-octenes from 47.96 to 1.76% between the 2- and 4-hour period (Entries 3 to 5) further supports this observation.

In order to favour the production of aldehyde products based on the data summarized in table 4.1 and 4.2, the optimized reaction conditions chosen for the evaluation of bimetallic complexes as catalyst precursors for further hydroformylation experiments are 95˚C, 50 bar and 4 hours.

4.2.4 Effects on catalyst to substrate ratio

A study on the sensitivity to the amount of feedstock was carried out by increasing the molar catalyst to substrate ratio from 1:2500 to 1:5000. Speculated competition between the binding of CO and 1-octene, thus limiting the migratory insertion steps in the catalytic cycle could lead to a lower activity as the catalyst to substrate ratio is increased. Interestingly, the increase in the amount of substrate shows no significant decrease in the conversion, chemoselectivity and regioselectivity (Table 4.4).

Table 4.4*: Hydroformylation data obtained for catalyst to substrate ratio variation with compound* ***5***

Catalyst: substrate ratio	**Conversion (%)**	**Total Aldehydes (%)**	**Total *iso*-octenes (%)**	**Linear aldehydes (%)**	**Branched aldehydes (%)**	**TOF (h^{-1})**	***n:iso***
1:2500	99.94	98.24	1.76	43.56	56.44	613.6	0.78
1:5000	99.97	99.90	0.10	42.67	57.33	1348.8	0.64

Hydroformylation of 1-octene in toluene (5 mL), 1:1 $CO:H_2$ pressure 50 bar, 95˚C, reaction time of 4 hours and catalyst loading of 2.87 x 10^{-3} mmol. GC conversions were obtained using an internal standard of *n*-decane. Total aldehydes are composed of linear and branched aldehydes in a mixture with percentage sum of 100. TOF = (mmol aldehydes per mmol Rh)/ time. Reactions carried out in triplicate with an average error value of 2.01%.

This is likely due to the nature of the Rh_2^{4+} core, resulting in a higher charge to mass ratio and a better binding affinity for CO than additional substrate molecules. The increase in the rate of the reaction observed in the same time period suggests a strong dependence on the concentration of substrate for these systems. Furthermore, an increase in the concentration of substrate under these conditions marginally affected the chemoselectivity resulting in a reduction in the total *iso*-octene percentage from 1.76 to 0.10%. This suggests that the anticipated increase in the rate of the hydroformylation reaction relative to that of the isomerization reaction occurs at higher substrate concentrations, likely due to CO having a higher affinity for binding to the active site relative to 1-octene for this catalyst type.

4.2.5 Mercury poisoning studies

A mercury poisoning study was used as a means of determining the homogeneity of the hydroformylation reaction when using compound **5** as a catalyst precursor. The rationale is that if rhodium nanoparticles are formed in solution, the mercury present in the reaction vessel would form an amalgam with the aggregated rhodium particles.[29,30] The amalgam deactivates the rhodium nanoparticles in the hydroformylation reaction. Therefore, if a portion of the activity was due to nanoparticle formation, a subsequent reduction in the turn over frequency (TOF) and therefore the catalyst activity would be observed.[14,29] The results obtained (Table 4.5) show comparable conversion and TOF values calculated for reactions carried out with and without the addition of elemental mercury suggesting that the hydroformylation is due to a molecular catalyst species and not rhodium nanoparticles.

Table 4.5*: Hydroformylation data obtained for mercury poisoning with compound* ***5***

Mercury present	**Conversion (%)**	**Total Aldehydes (%)**	**Total *iso*-octenes (%)**	**Linear aldehydes (%)**	**Branched aldehydes (%)**	**TOF (h^{-1})**	***n:iso***
Yes	99.90	99.15	0.85	42.82	57.18	624.0	0.75
No	99.94	98.24	1.76	43.56	56.44	613.6	0.78

Hydroformylation of 1-octene in toluene (5 mL), 1:1 CO:H_2 pressure 50 bar, 95˚C, reaction time varied and catalyst loading of 2.87 x 10^{-3} mmol. GC conversions were obtained using an internal standard of *n*-decane. Total aldehydes are composed of linear and branched aldehydes in a mixture with percentage sum of 100. TOF = (mmol aldehydes per mmol Rh)/ time. Reactions carried out in triplicate with an average error value of 0.59%.

4.3 Comparison of dirhodium(II,II) complexes (5-10) and associated low-valent metallodendrimers (16-21) as catalyst precursors in the Hydroformylation of 1-octene

4.3.1 Effects of substituents and size on the results of acetato-based catalyst precursors

Under the optimized conditions of 95˚C, 50 bar and 4 hours, compounds **5**, **6**, **14**, **16** and **17** were evaluated as catalyst precursors in the hydroformylation of 1 octene (Table 4.6).

Table 4.6*: Hydroformylation data obtained for acetate bearing complexes under optimized conditions*

Catalyst precursor	Conversion (%)	Total aldehydes (%)	Total *iso*-octenes (%)	Linear aldehydes (%)	Branched aldehydes (%)	TOF (h^{-1})	*n:iso*
5 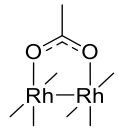	99.94	98.24	1.76	43.56	56.44	613.6	0.78
14 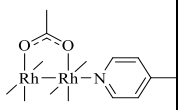	99.45	99.22	0.78	41.53	58.47	619.64	0.71
16 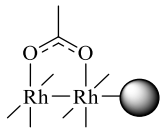	99.91	87.98	12.02	47.51	52.49	549.55	0.91
6 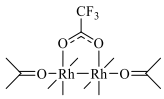	99.81	100	0	39.42	60.58	623.6	0.65
17 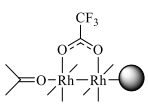	99.77	100	0	42.19	57.81	623.9	0.73

Hydroformylation of 1-octene in toluene (5 mL), 1:1 CO:H_2 pressure 50 bar, 95˚C, reaction time of 4 hours and catalyst loading of 2.87 x 10^{-3} mmol. GC conversions were obtained using an internal standard of *n*-decane. Total aldehydes are composed of linear and branched aldehydes in a mixture with percentage sum of 100. TOF = (mmol aldehydes per mmol Rh)/ time. Reactions carried out in triplicate with an average error value of 3.39%.

The data obtained from each experiment shows comparable results with respect to conversion between compounds **5**, **6**, **14 16** and **17**, however, significant differences in both chemo- and regioselectivity are observed. No hydrogenation products were detected throughout hydroformylation experiments for any compounds used as catalyst precursors. The data obtained for TOF for the above compounds shows a general decrease in activity due to the reduction in the amount of aldehyde formed upon coordination to tris-amine scaffold **15**. The comparable activity of compounds **6** and **17** are the result of total conversion of substrate to aldehydes, with minimal reduction in the conversion of substrate upon coordination.

The results obtained for compound **5** and *mono*-adduct **14** show that introduction of the picolyl moiety to the axial site of the dirhodium core results in a marginal increase in the chemoselectivity toward aldehyde formation when compared to compound **5** (98.24 to 99.22%). Chemoselectively, compound **16** shows a reduction in the percentage of total aldehydes at 87.98% from the 98.24% as seen for compound **5**. This is attributed to the solubility differences between the compounds, with **5** observed to be more soluble in toluene when compared to **16**. A graphical representation (Figure 4.3) depicts the trends in chemoselectivity.

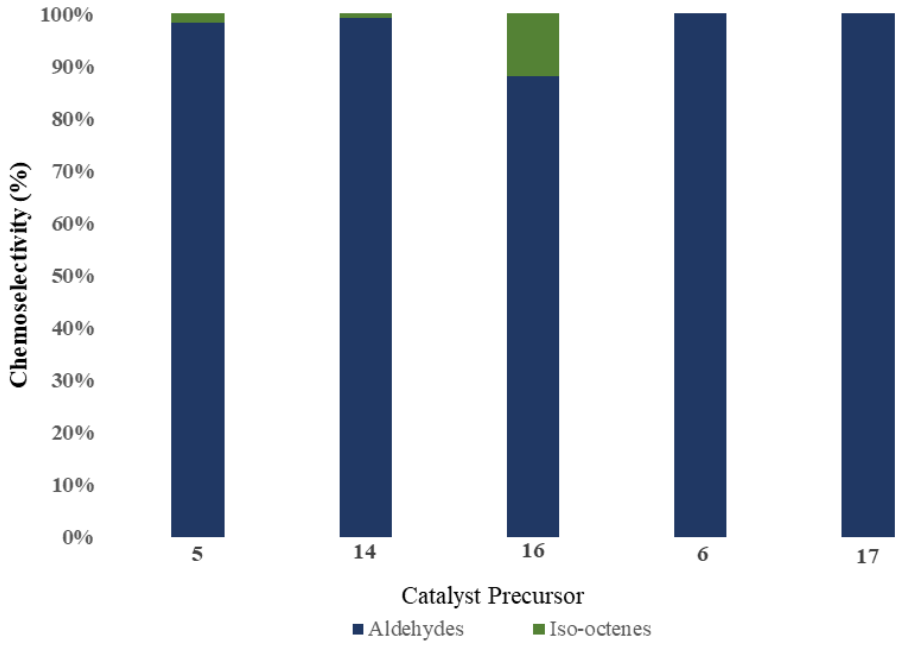

Figure 4.3*: Graphical representation of trends observed chemoselectivity of acetate compounds* **5**, **6**, **14**, **16** and **17**

The results obtained for trifluoroacetate-bearing compound **6** shows near quantitative conversion comparable to that obtained for **5** with full conversion to aldehyde products.

Comparatively, the strong electron-withdrawing effect of the trifluoromethyl substituent is speculated to favour the reductive elimination step of the dirhodium species (Rh_2^{5+} to Rh_2^{3+}) compared to the methyl analogue. Assuming a catalytic cycle like Rh(I) catalytic systems, this results in quantitative conversion of substrate and *iso*-octenes to aldehydes for this complex. The chemoselectivity observed for compound **17** remains quantitative towards the formation of aldehydes.

Additionally, trends in the regioselectivity data (Figure 4.4) are observed with favouring of the formation of branched aldehydes in compound **14** calculated at 58.47%, from 56.44% calculated for compound **5**. This indicates that the electronic effects imposed by the addition of the picolyl entity have no substantial effect on product distribution for acetate bearing compounds under these conditions. Comparison of the regioselectivity data shows that production of the linear aldehyde is favoured for **16**, likely due to steric interference at the migratory insertion step in the catalytic cycle.[31]

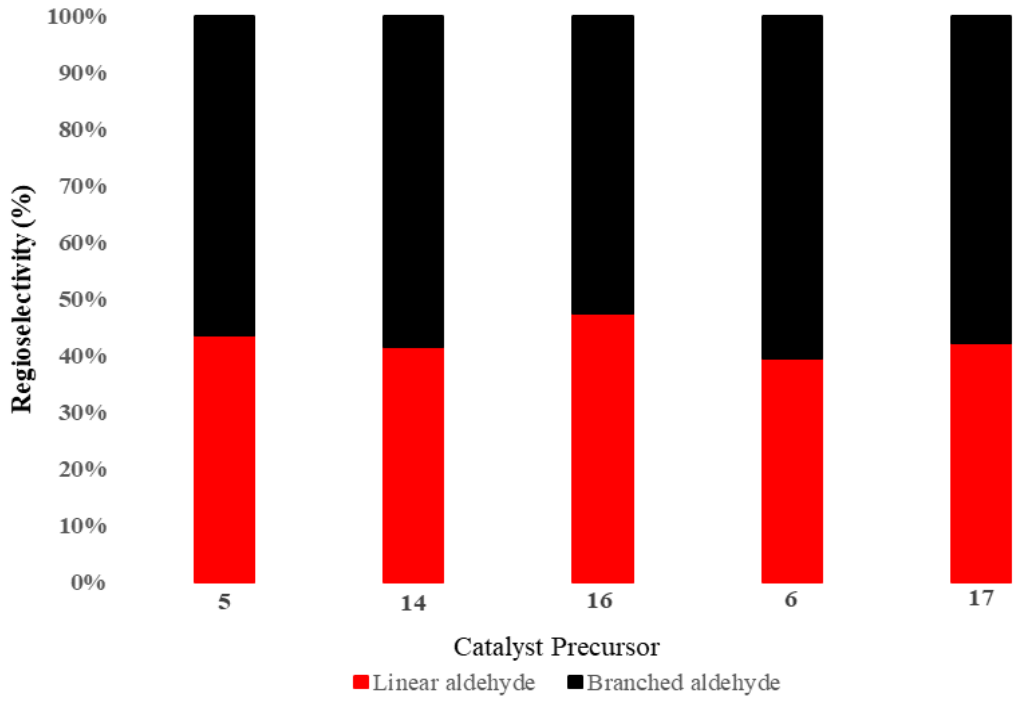

***Figure 4.4**: Graphical representation of trends observed regioselectivity of acetate compounds* **5**, **6**, **14**, **16** and **17**

Additionally, this proposed steric influence would affect the rate of coordination of *iso*-octenes resulting in the higher amount of isomerized octenes present after 4 hours as seen in the data (Table 4.6, *vida supra*). A similar trend is seen in the regioselectivity for compound **17** as previously observed in the data obtained with compound **16**, with an increase in the formation

of linear aldehydes from bimetallic complex **6** (39.42%) to associated metallodendrimer **17** (42.19%).

4.3.2 Effects of substituent and size for formamidinato-based complexes substituted at the para-position

Under the same conditions of 95˚C, 50 bar and 4 hours, *para*-substituted formamidinate bearing compounds **7**, **9**, **18** and **19** were used as catalyst precursors in the hydroformylation of 1-octene. Results obtained (Table 4.7) show conversion percentages for complexes with substituents in the 4-position are observed to be near quantitative, ranging from 98.43% (**18**) to 99.80% (**7**).

A substantial difference in the chemoselectivity is observed with 87.36% aldehyde formation observed for **7** and 60.24% aldehyde formation for compound **10**. This difference in aldehyde formation leads to an increase in the activity (TOF) of the 4-methyl substituted compound (**7**) compared to the 4-fluoro substituted compound (**10**).

Thus, for formamidinato compounds, the introduction of an electron-donating substituent at the *para*-position leads to an increase in chemoselectivity towards aldehyde. Stabilization of higher oxidation states are related to increases in electron-releasing capabilities of equatorial ligands of dirhodium(II,II) complexes.[32] Therefore, by way of the classical catalytic cycle, the elementary oxidative addition step likely occurs faster, initiating the cycle and resulting in the observed favouring of aldehyde products.

Results for compounds **18** and **20** shows a significant reduction in the chemoselectivity toward aldehyde formation, and by extension activity, with total aldehyde percentages of 74.75 and 50.15% respectively, compared to related compounds **7** and **10**.

Table 4.7*: Hydroformylation data obtained for 4-substituted formamidinate bearing compounds under optimized conditions*

Catalyst precursor	Conversion (%)	Total aldehydes (%)	Total *iso*-octenes (%)	Linear aldehydes (%)	Branched aldehydes (%)	TOF (h^{-1})	*n:iso*
7 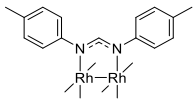	99.80	87.36	12.64	48.30	51.70	545.02	0.94
18 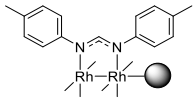	98.43	74.75	25.25	51.08	48.92	464.20	1.09
10 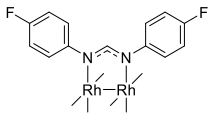	98.77	60.24	39.76	64.61	35.39	374.35	1.92
20 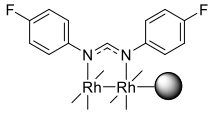	99.26	50.15	49.85	67.63	32.37	311.19	2.09

Hydroformylation of 1-octene in toluene (5 mL), 1:1 $CO:H_2$ pressure 50 bar, 95˚C, reaction time of 4 hours and catalyst loading of 2.87 x 10^{-3} mmol. GC conversions were obtained using an internal standard of *n*-decane. Total aldehydes are composed of linear and branched aldehydes in a mixture with percentage sum of 100. TOF = (mmol aldehydes per mmol Rh)/ time. Reactions carried out in triplicate with an average error value of 2.85%.

Since no observable differences in solubility were observed as was the case for the acetate complexes, factors influencing these results could be due to steric hinderance around the remaining axial site by the diphenyl formamidinate ligands, or electronic factors based on the introduction of the pyridyl moiety through which the compound is tethered to the scaffold.

Formation of the electron-deficient pyridyl nitrogen upon conjugation (rationalized through the Infrared and ^{1}H-NMR spectral data in Chapter 3) would lead to a reduction in the stabilization of the higher oxidation state species during the catalytic cycle, therefore impeding the initial oxidative addition step. A graphical representation of the chemoselectivity is shown in Figure 4.5 (*vida infra*).

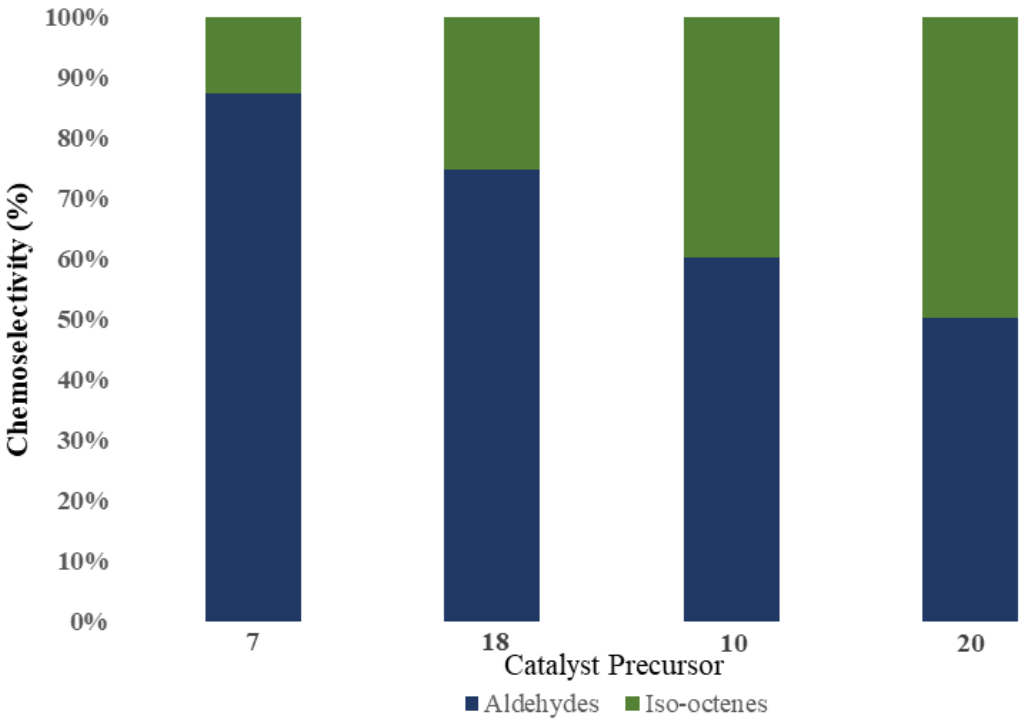

Figure 4.5*: Graphical representation of trends observed in chemoselectivity for formamidinate-based compounds* **7**, **10**, **18**, and **20**

Regioselectively, an opposite trend is observed, with compound **10** significantly favouring the formation of linear aldehydes (64.61%) as compared to **7** (48.30%). The electron-withdrawing effects of the fluoro-substituent should favour the lower oxidation state compared to the methyl substituent and therefore increase the rate the reductive elimination step, thus favouring the linear aldehyde through the faster formed linear acyl intermediate.

Trends in the regioselectivity for compounds **18** and **20** show a higher percentage of linear aldehydes formed at 51.08 and 67.63% respectively. The increase is likely due to a combination of the steric influence after introduction of the scaffold, favouring the formation of the *anti*-Markovnikov acyl species, and the electronic influence of the pyridyl moiety favouring the reductive elimination step. A graphical representation of the regioselectivity is shown in Figure 4.6.

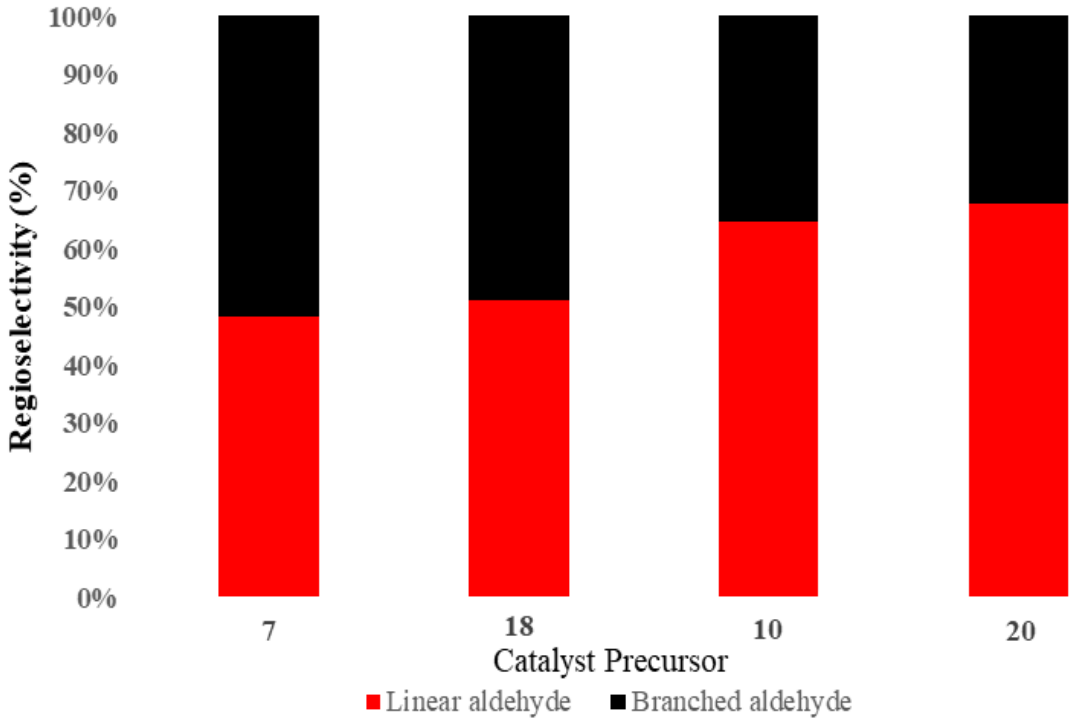

Figure 4.6*: Graphical representation of trends observed in regioselectivity for formamidinate-based compounds* **7**, **10**, **18**, and **20**

4.3.3 Effects of substituent and size for formamidinato complexes substituted at the ortho-position

Hydroformylation reactions were carried out using formamidinato-based catalyst precursors bearing substituents at the *ortho*-position, namely, compounds **8**, **9**, **19** and **21.** The results obtained (Table 4.8) show that in respect of conversion percentages, a 2% margin is obtained for compounds **8** and **9**, calculated at 97.69 and 97.86% respectively, in comparison to previously discussed compounds **7** and **10**.

The differences in chemoselectivity toward the formation of aldehydes between methyl- and fluoro-substituents at the *ortho*-position are observed at 60.27 and 59.49% for compounds **8** and **9** respectively. This suggests that for formamidinate complexes under hydroformylation conditions, varying the nature of the substituent at the *ortho*-position between electron-donating methyl- and the electron-withdrawing fluoro- groups results in negligible differences in chemoselectivity and hence the activity over the 4-hour reaction time period. The observation is likely due to the minimization of the different electronic effects when

substituents are located at the *ortho*- position (compounds **8** and **9**) relative to the *para*-position (compounds **7** and **10**).

***Table 4.8**: Hydroformylation data obtained for ortho-substituted formamidinate bearing compounds under optimized conditions*

Catalyst precursor	Conversion (%)	Total aldehydes (%)	Total *iso*-octenes (%)	Linear aldehydes (%)	Branched aldehydes (%)	TOF (h^{-1})	*n:iso*
8 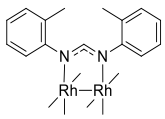	97.86	60.27	39.73	64.36	35.64	368.6	1.84
19 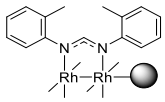	99.39	65.81	34.19	58.20	41.80	409.0	1.39
9 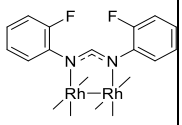	97.69	59.49	40.51	71.36	28.64	362.4	2.51
21 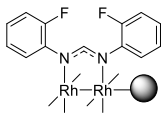	87.31	41.99	58.01	72.96	27.04	228.5	2.71

Hydroformylation of 1-octene in toluene (5 mL), 1:1 CO:H_2 pressure 50 bar, 95˚C, reaction time of 4 hours and catalyst loading of 2.87 x 10^{-3} mmol. GC conversions were obtained using an internal standard of *n*-decane. Total aldehydes are composed of linear and branched aldehydes in a mixture with percentage sum of 100. TOF = (mmol aldehydes per mmol Rh)/ time. Reactions carried out in triplicate with an average error value of 4.05%.

In addition, the chemoselectivity observed for compounds **8** and **9** is comparable to that observed for compound **10** (60.24 %), thereby implying that varying the position of the fluoro-substituent also has minimal effect on the chemoselectivity. A graphic representation of this chemoselectivity is shown in Figure 4.7

A larger decrease in the chemoselectivity toward aldehydes is observed between compounds **9** and **21**, with a reduction in the aldehyde percentage from 59.49 to 41.99% compared to that of compounds **10** and **20** (60.24 to 50.15% respectively). Interestingly, an increase in the percentage formation of aldehydes is observed from 60.27% (**8**) to 65.81% (**19**) suggesting that

although the differences in electronic effects appear lowered for compounds **8** and **9**, conjugation of the pyridyl favours hydroformylation over isomerization for the methyl-substituted compound **8**.

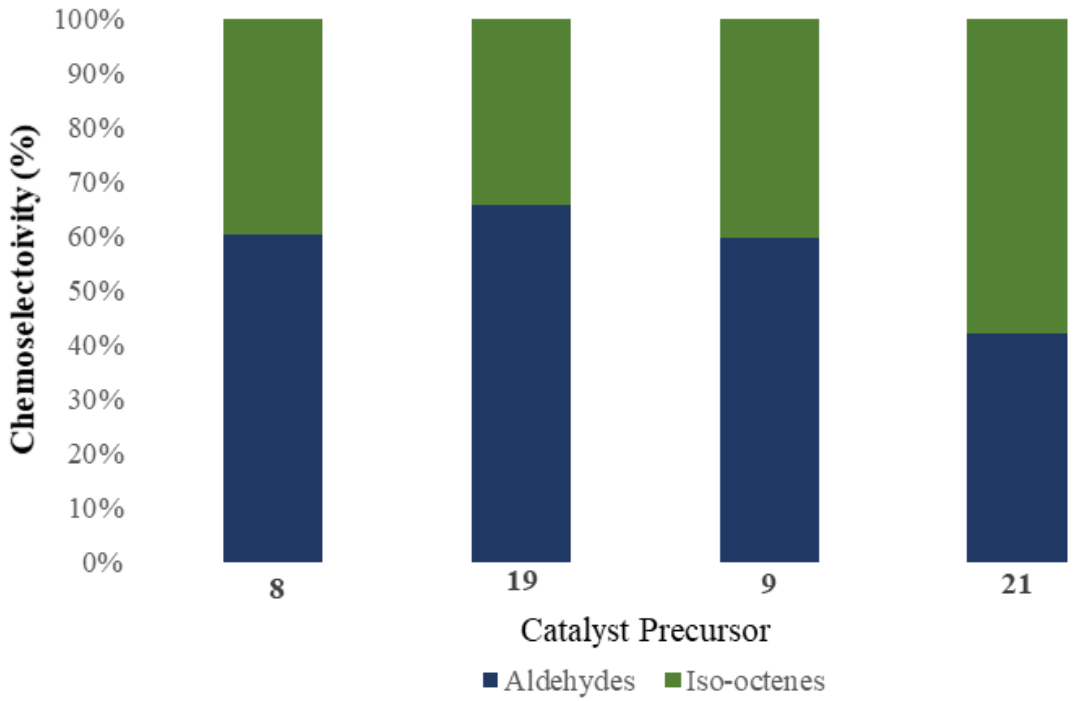

Figure 4.7*: Graphical representation of trends observed in chemoselectivity for formamidinate-based compounds* **8**, **9**, **19**, and **21**

Differences in the regioselectivity show a similar trend as previously discussed (Section 4.3.2), whereby an observed increase in the formation of linear aldehydes for compound **9** (71.36 %) over compound **10** (64.36%). Similarly, comparison of the results between compounds **7** (48.30%) and **8** (64.36%) show a higher percentage of linear aldehydes formed for the same substituent at the 2- position. This data suggests that increases in the steric demand around the core of the complex favours the *anti*-Markovnikov product. Figure 4.8 below illustrates the product distribution trends for compounds **8**, **9**, **19**, and **21**.

Regioselectively, conjugation of formamidinato compounds **9** and **15** resulted in a negligible increase in the favouring linear aldehyde products from 71.36 (**9**) to 72.96% (**21**). This suggests that a possible maximal effect of the steric and electronic factors may be reached in the case of the 2-fluoro substituted complex.

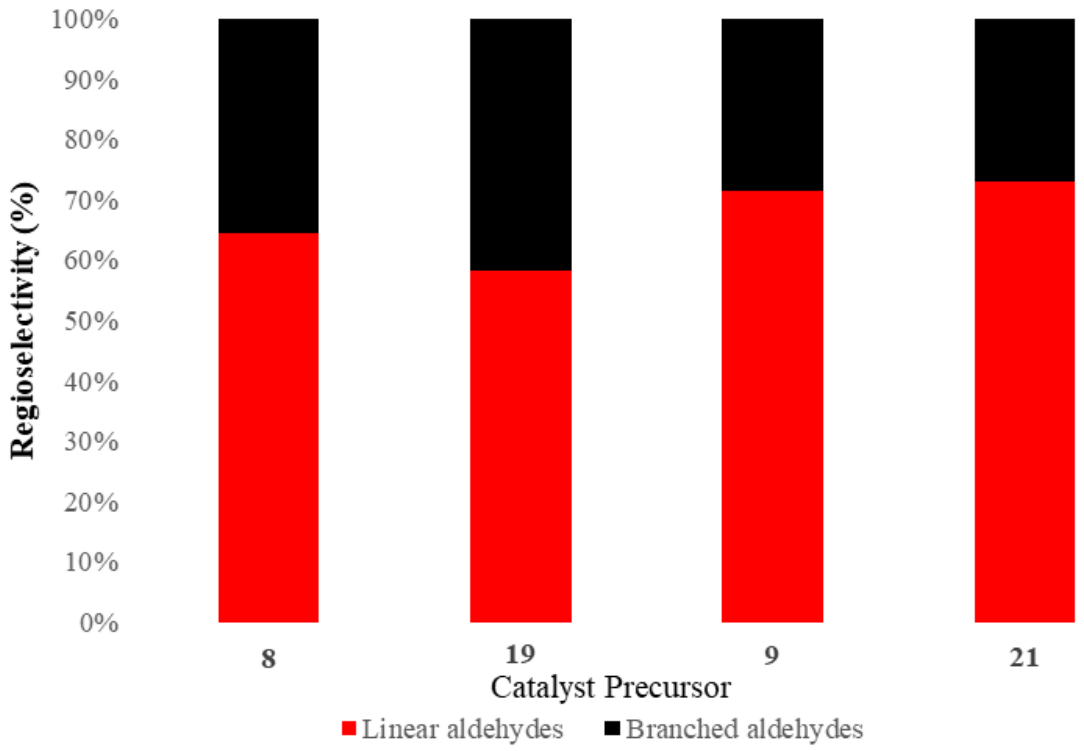

***Figure 4.8**: Graphical representation of trends observed in regioselectivity for formamidinate-based compounds* **8**, **9**, **19**, and **21**

Conjugation of compounds **8** and **9** to compound **15** show an interesting trend, whereby a reduction in the formation of linear aldehyde from 64.36 (**8**) to 58.20% (**19**) is observed. This observation is likely a result of the electronic influence of the pyridyl entity on elementary steps in the catalytic cycle rather than steric factors, the latter of which is expected to increase the percentage of linear relative to branched aldehydes.

*4.3.4 Preliminary cyclic voltammetry analysis of formamidinato complexes (**7 - 10**)*

Cyclic voltammetry studies for the compounds **7 - 10** were carried out at ambient temperature using a solution of 0.1M TBAP in anhydrous dichloromethane with an Ag/AgCl reference electrode, glassy-carbon working electrode and Pt wire auxiliary electrode under inert atmosphere. All measurements were obtained using a scan rate of 100 mV/s to determine comparable effects of electron withdrawing, electron releasing and positional changes on red-ox properties of the dirhodium(II,II) or (Rh_2^{4+}) core. In addition, this allows for some insight into the previously speculated electronic factors of varying both substituent type and position

on the chemo- and regioselectivities observed for dirhodium formamidinate compounds in the hydroformylation data.

As expected, electron donating methyl substituents allow for lower half wave potentials (Table 4.9) for oxidation compared to fluoro substituents in the same position, with reversible Rh_2^{4+} to Rh_2^{5+} oxidation events observed.

Table 4.9*: Calculated half-wave potentials for oxidation and reduction events for compounds* ***7*** *–* ***10*** *measured in 0.1M TBAP/CH_2Cl_2*

Compound	$E^{1/2}$ **(V) vs Ag/Ag^+**		
	$Rh_2^{5+/6+}$	**$Rh_2^{4+/5+}$**	**$Rh_2^{3+/4+}$**
7	1.06	0.259	-1.34
8	1.23	0.311	-1.63
9	1.32	0.391	-1.51
10	1.20	0.264	-1.18

Stacked voltammograms of the oxidation potentials (Figure 4.9) obtained show the differences in the effects of electron donating, withdrawing and position of substituent. In this regard, altering the position of a substituent seems to have larger influences the oxidation potential. Compounds with substituents in the 4-position are observed to stabilize the oxidation events compared to those in the 2- position, with fluoro substituents generally generating higher half wave potentials. This indicates that electron donating methyl substituents stabilize higher oxidation states compared to analogous fluoro- substituted compounds.

Results obtained with respect to reduction events (Figure 4.10) show reversible Rh_2^{4+} to Rh_2^{3+} reduction potentials for compounds **7** and **10**. The half wave potential for compound **10** (-1.18 V) is notably lower than that of compound **7** (-1.34 V) supporting the initial speculation of the reductive elimination step being favoured for **10**, leading to the increase in linear aldehyde formation previously discussed.

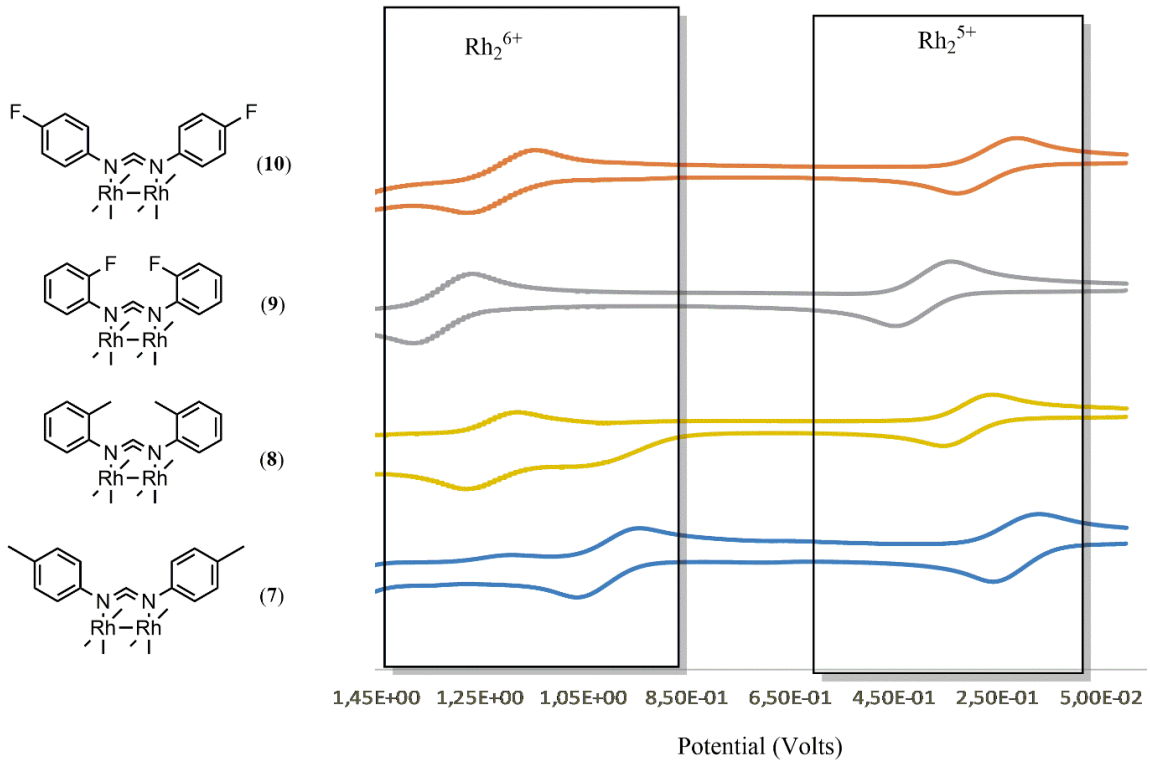

Figure 4.9**: Stacked voltammograms depicting oxidation events from Rh_2^{4+} to $Rh_2^{5+}$and $Rh_2^{6+}$for compounds **7 - 10

The reduction events obtained for compounds **8** and **9** show quasi-reversible reductions occurring at -1.63 V and -1.51 V respectively. In addition to the relative increase in reduction potential of **8** and **9**, the irreversibility of the reduction event is a likely contributor to the amount of linear aldehyde product formed for these compounds.

Assuming the localization of charge on rhodium atoms in the core and elements of the classical catalytic cycle requiring an oxidation state change between Rh^{1+} and Rh^{3+}, the corresponding species in the case of dirhodium compounds would be Rh_2^{3+} and Rh_2^{5+}. The relative energy differences between these oxidation states may be inferred by the differences in the potential required oxidize or reduce the neutral Rh_2^{4+} catalyst precursor.

The absolute differences in oxidation and reduction potentials $\left|E^{1/2}(ox)- E^{1/2}(red)\right|$ were calculated (Table 4.10) and compared to the chemoselectivity obtained in the hydroformylation reaction for compounds **7 - 10**. This elementary calculation gives an indication of the HOMO-LUMO energy difference in the dirhodium compounds, possibly providing insight into the observed product distributions.

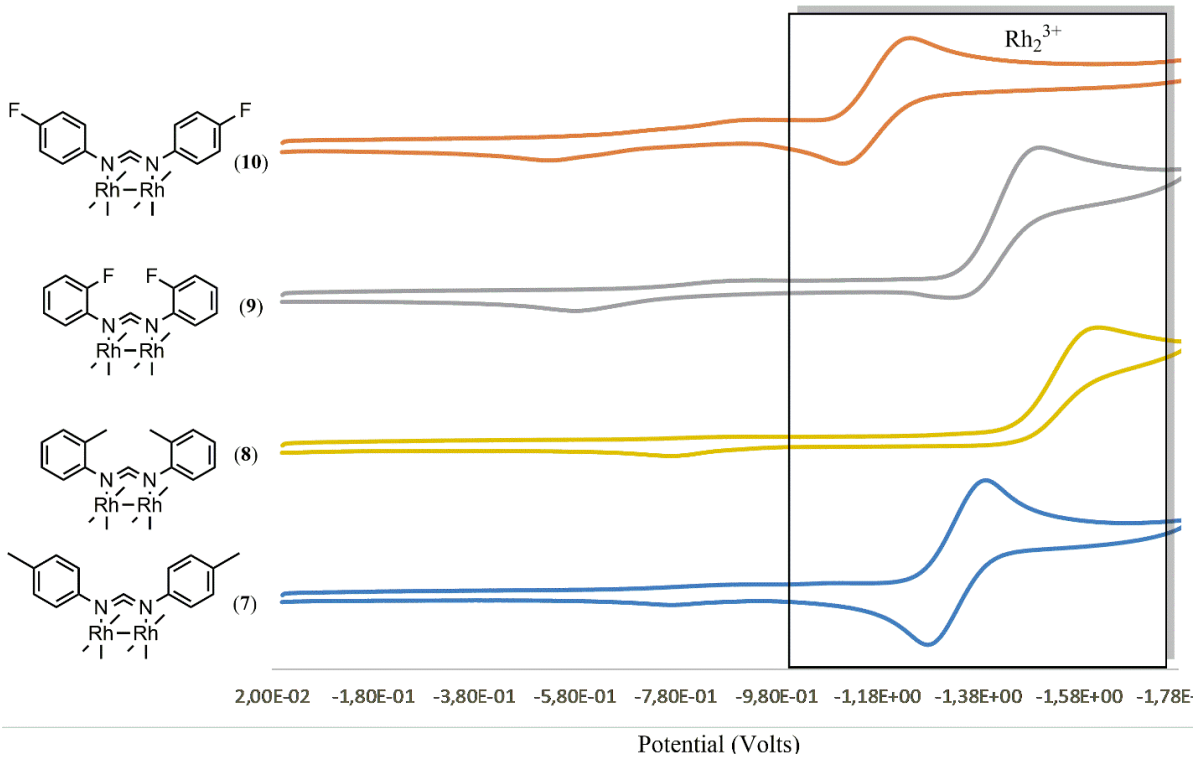

Figure 4.10**: Stacked voltammograms depicting reduction events from Rh_2^{4+} to Rh_2^{3+} for compounds **7** - **10

Table 4.10**: Comparison of aldehyde formation and absolute differences between oxidation and reduction potentials of compounds **7** - **10

Compound	$E^{1/2}$ (V) vs Ag/Ag^+		$\lvert E^{1/2}(ox)-E^{1/2}(red) \rvert$ (V)	Aldehyde (%)
	$Rh_2^{4+/5+}$	$Rh_2^{3+/4+}$		
7	0.259	-1.34	1.59	87.36
8	0.311	-1.63	1.94	60.27
9	0.391	-1.51	1.90	59.49
10	0.264	-1.18	1.44	60.24

The data shows that the higher chemoselectivity observed in hydroformylation occurred with the highest absolute difference in oxidation and reduction potential for compounds **7** (1.59 V) and **10** (1.44 V), when both reduction and oxidation events occur reversibly. Similarly, when reduction events are quasi-reversible (**8**, **9**), a comparable % of aldehyde formation is observed when the absolute differences in oxidation reduction potentials are comparable.

4.4 Overall Summary

Compounds **5** - **10** and **16** – **21** were evaluated as catalyst precursors in the hydroformylation of 1-octene. Compound **5** was used in optimization reactions, arriving at optimal conditions of 95˚C, 50 bar syngas pressure and 4-hour reaction time. All synthesized compounds display excellent conversion capabilities (87 -99%). No detectable hydrogenation products were observed for any synthesized compounds under the above conditions. Compounds **5** and **6** show excellent chemoselectivity toward aldehyde formation (98 -100 %) whereas compounds **7** – **10** display moderate to good chemoselectivity (59 – 87 %). Compounds **7** – **10** show higher regioselectivity toward linear aldehyde (48 – 71%) compared to compounds **5** and **6** (39 – 43 %).

Conjugation of a pyridyl entity to an axial site of each compound results in lower activity for compound **14**, but comparable results are observed between bimetallic (**5**, **6**) and hexa-metallic (**16**, **17**) acetate-bearing compounds. A marginal increase in the regioselectivity is observed upon conjugation for acetate-bearing complexes.

Conjugation of the pyridyl scaffold to formamidinate complexes results in a significant reduction in activity (*ca*. 10%) observed in all but one case (**19**). Significant increases in regioselectivity is observed for 4-substituted compounds upon conjugation (**18**, **20**), with little to no effect observed for **21** and a decrease observed for **19**.

Results from mercury poisoning experiments show no significant loss in activity, suggesting that the reaction is exclusively homogeneous.

Preliminary results observed in the cyclic voltammetry data obtained suggest a combination of the accessibility of the oxidized Rh_2^{5+} and the reduced Rh_2^{3+} species, resulting in a comparative estimation of the HOMO-LUMO energy gap. Additionally, favouring of oxidized or reduced forms of the active catalyst results in the speculated favouring of intermediary steps in the hydroformylation catalytic cycle influencing regio- and chemoselectivity.

4.5 References

1. O. Roelen, DE Patent DE 849 548 C (1938).
2. R. Franke, D. Selent and A. Börner, Chemical Reviews, 2012.
3. S. C. Bourque, F. Maltais, W. J. Xiao, O. Tardif, H. Alper, P. Arya and L. E. Manzer, *J. Am. Chem. Soc.*, 1999, **121**, 3035.
4. J. Pospech, I. Fleischer, R. Franke, S. Buchholz and M. Beller, *Angew. Chem. Int. Ed*. 2013.
5. S. Pandey, K. V. Raj, D. R. Shinde, K. Vanka, V. Kashyap, S. Kurungot, C. P. Vinod and S. H. Chikkali, *J. Am. Chem. Soc*. 2018, **140**, 4430−4439.
6. D. J. Cole-Hamilton, *Science*, 2003, **299**, 1702-1706.
7. T. Mizugaki, M. Ooe, K. Ebitani and K. Kaneda, *J. Mol. Catal. Chem.* 1999, **145**, 329.
8. C. D. Frohling and C. W. Kohlpaintner, in *Applied Homogeneous Catalysis with Organometallic Compounds*, eds. B. Cornils and W. A. Herrmann,VCH, Weinheim, Germany, 1996, vol. 1, pp 27-104.
9. A. Chalk and J. Harrod, *Adv. Organomet. Chem.*, 1968, **6**, 119-170.
10. P. J. Baricelli, M. Rodriguez, L. G. Melean, M. Modrono Alonso, M. Borusiak, M. Rosales, B. Gonzalez, K. C. B. de Oliveira, E. V. Gusevskaya and E. N. dos Santos, *Appl. Catal., A*, 2015, **490**, 163-169.
11. W. Keim, *Chem. Ing. Tech*., 1984, **56**, 850.
12. D. Evans, J. A. Osborn and G. Wilkinson, *J. Chem. Soc*. *(A)*, 1968, 3133.
13. M. Schreuder-Goedheijt, P. C. J. Kamer and P. W. N. M van Leeuwen, *J. Mol.Catal.*, 1998, **134**, 243.
14. C. Williams, M. Ferreira, E. Monflier, S. F. Mapolie and G. S. Smith, Dalton Trans, 2018, **47**, 9418-9429.
15. A. J. Catino, R. E. Forslund and M. P. Doyle, *J. Am. Chem. Soc*. 2004, **126**, 13622-13623.
16. H. M. L. Davies, A. M. Walji and T. Nagashima, *J. Am. Chem. Soc.*, 2004, **126**, 4271-4280.
17. P. M. P. Gois, A. F. Trindade, L. F. Veiros, V. Andr, M. T. Duarte, C. A. M. Afonso, S. Caddick, and F. G. N. Cloke, *Angew. Chem. Int. Ed.* 2007, **46**, 5750 –5753.
18. M. Nowotny, T. Maschmeyer, B. F. G. Johnson, P. Lahuerta, J. M. Thomas and J. E. Davies, *Angew. Chem. Int. Ed.* 2001, **40,** 955-958.

19. J. Wencel-Delord, T. Dröge, F. Liu and F. Glorius, *Chem. Soc. Rev.*, 2011, **40**, 4740.
20. H. K. Kisan and R. B. Sunoj, *J. Org. Chem.*, 2015, **80,** 2192.
21. S. Siangwata, N. C. C. Breckwoldt, N. J. Goosen and G. S. Smith, *Appl. Catal*., *A*, 2019, **585**, 117179.
22. J. M. Andersen, N. Karodia, D. J. Miller, D. Stones and D. Gani, *Tetrahedron Lett., 1998*, **39**, 7815-7818.
23. I. G. Powers and C. Uyeda, *ACS Catal.*, 2017, **7**, 936−958.
24. M. Haumann, H. Yildiz, H. Koch and R. Schomäcker, *Appl. Catal., A*, 2002, **236**, 173-178.
25. M. Haumann, H. Koch and R. Schomäcker, *Catal. Today*, 2003, **79-80**, 43-49.
26. J. Hjortkjaer, *J. Mol. Catal.*, 1979, **5**, 377-384.
27. P. W. Van Leeuwen and C. Claver, *Rhodium catalyzed hydroformylation*, Kluwer Academic Publishers, New York, 2002.
28. B. C. E. Makhubela, A. Jardine and G. S. Smith, *Green Chem.*, 2012, **14**, 338-347.
29. S. Siangwata, S. Chulu, C. L. Oliver and G. S. Smith, *Appl. Organomet. Chem.*, 2017, **31**, 3593.
30. A. Behr, Y. Brunsch and A. Lux, *Tetrahedron Lett.*, 2012, **53**, 2680-2683.
31. A. van Rooy, E. N. Orij, P. C. Kamer and P. W. van Leeuwen, *Organometallics*, 1995, **14**, 34-43.
32. K. M. Kadish, T. D. Phan, L. Giribabu, E. Van Caemelbecke and J. L. Bear, *Inorg. Chem.*, 2003, **42**, 8663−8673.

CHAPTER 5

Experimental Procedures

5.1 General Details

All reagents were purchased from Sigma-Aldrich / Merck and used without further purification unless otherwise stated. Rhodium(III) trichloride trihydrate was purchased from Heraeus SA. Solvents used were of analytical grade or freshly distilled and stored over molecular sieves when required. All reactions were carried out under inert (N_2/Ar) atmosphere using standard Schlenk line techniques unless otherwise stated. Reaction progress was monitored using thin-layer chromatography (TLC) on pre-coated silica-gel F254 plates in a suitable solvent system and visualized by ninhydrin, 2.5% solution of *p*-anisaldehyde in a mixture of sulfuric acid and ethanol (1:10 v/v), iodine vapour or under an ultraviolet light at 254 nm. Column chromatography was conducted using 60 Å silica gel (70 – 230 mesh ASTM). Solvents were removed at 40 ºC under reduced pressure using a Büchi Rotavapor.

Nuclear magnetic resonance (NMR) spectra were recorded on either a Bruker X400 (^{1}H: 400.22 MHz; ^{13}C{^{1}H}: 100.65 MHz , ^{19}F: 377 MHz) or a Varian Mercury 300 (^{1}H: 300.08 MHz, ^{13}C{^{1}H}:75.46 MHz) spectrometer. Chemical shifts for ^{1}H and ^{13}C{H} NMR were reported using tetramethylsilane (TMS) as the internal standard. Coupling constants are reported in Hz and chemical shifts are reported in ppm. Infrared (IR) absorptions were measured on a Perkin-Elmer Spectrum 100 FT-IR spectrometer using Attenuated Total Reflectance Infrared spectroscopy (ATR-IR).

Purity was determined using an analytical Agilant HPLC 1260 equipped with an Agilent infinity diode array detector (DAD) 1260 UV-Vis detector, with an absorption wavelength range of 210 – 640 nm. The compounds were eluted using a mixture of solvent A (10 mM NH4OAc/H2O) and solvent B (10 mM NH4OAc/MeOH) at a flow rate of 0.9 mL min−1. The gradient elution conditions were as follows: 10% solvent B from 0 - 1 min, 10 – 95% solvent B from 1 - 3 min, 95% solvent B from 3 - 5 min. Mass spectrometry was carried out using Electron Impact (EI) on a JEOL GCmatell instrument or using a Waters Synapt G2 equipped with an ESI probe with data recorded in positive mode. Melting Points were determined using a Büchi melting point apparatus B-540 and are uncorrected.

5.2 Synthesis of diphenylformamidine ligands

The general method for synthesis of formamidine compounds was obtained from literature and modified as needed to afford compounds **1** - **4**.[1,2] Both methods result in similar yields for compounds **1** - **4**, however, the sonication method was used as a means of scale up as needed.[2]

Sonication method: A round bottomed flask was charged with triethyl orthoformate (1.00 eq.) and the appropriate aniline (2.00 eq.). The reaction flask was transferred to an ultrasound bath and sonicated for 2 hours. The residual ethanol was removed under reduced pressure and the crude solid was recrystallized from hot dichloromethane (15 mL), resulting in the formation of a white solid. The solid was filtered under vacuum and washed with petroleum ether (3 x 10 mL) before drying under vacuum to afford white to opaque solids (**1-4**).

*5.2.1 (E)-N,N'-di(p-tolyl)formamidine (**1**)*

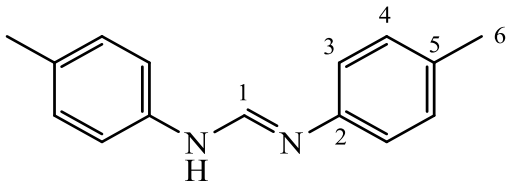

A round bottomed flask equipped with a magnetic stirrer bar was charged with triethyl orthoformate (1.55 mL, 9.32 mmol) and *p*-toluidine (2.02 g, 18.7 mmol) under N_2 atmosphere. Glacial acetic acid (28.0 μL, 0.430 mmol, 0.05 eq.) was then added while stirring. The mixture was heated under reflux at 140 °C for 16 hours. The reaction mixture was cooled to room temperature and the resulting brown solid was filtered under vacuum and washed with hexane (3 x 10 mL). The crude solid was recrystallized from hot dichloromethane (15 mL), resulting in the formation of a white solid. The solid was filtered under vacuum and washed with petroleum ether (3 x 10 mL) before drying under vacuum to afford a white crystalline solid (**1**).

Yield: 1.24 g, 59%. **Melting point**: 138.5 – 139.2°C. **IR (ATR, cm^{-1})**: ν = 2975 (broad, weak, N-H). 1670 (sharp, strong, C=N). **^{1}H NMR (300MHz, $CDCl_3$)** δ_{ppm} = 8.11 (s, 1H, **H_1**), 7.13 (d, ^3J = 8.2Hz, 4H, **H_3**), 6.96 (d, ^3J = 8.2Hz, 4H, **H_4**), 3.32 (br s, 1H, **NH**), 2.32 (s, 6H, **H_6**). **^{13}C{^{1}H} NMR (101 MHz, $CDCl_3$)** δ_{ppm} = 148.1 (s, **C_1**); 142.7 (s, **C_2**); 132.8 (s, **C_5**); 129.9 (s, **C_3**), 118.9 (s, **C_4**); 20.7 (s, **C_6**). **ESI-MS** (*m/z)*: 225.1391 (100%, $[M+H]^+$, requires 225.1386).

*5.2.2 (E)-N,N'-di(o-tolyl)formamidine (**2**)*

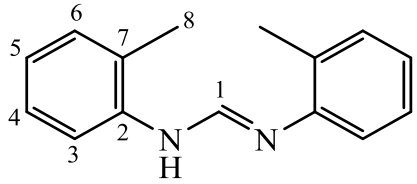

A round bottomed flask equipped with a magnetic stirrer bar was charged with triethyl orthoformate (1.55 mL, 9.32 mmol) and *p*-toluidine (2.02 g, 18.68 mmol) under inert atmosphere. Glacial acetic acid (28.0 µL, 0.43 mmol, 0.05 eq.) was then added while stirring. The mixture was heated under reflux at 140 °C for 16 hours. The reaction mixture was cooled to room temperature and the resulting brown solid was filtered under vacuum and washed with hexane (3 x 10 mL). The crude solid was recrystallized from hot dichloromethane (15 mL), resulting in the formation of a clear crystalline solid. The solid was filtered under vacuum and washed with petroleum ether (3 x 10 mL) before drying under vacuum to afford a clear crystalline solid (**2**).

Yield: 1.67 g, 79%. **Melting point**: 145.2 – 146.7°C. **IR (ATR, cm^{-1})**: ν = 3022 (broad, weak, N-H), 1664 (sharp, strong, C=N). **^{1}H NMR (300 MHz, CDCl$_3$)** δ_{ppm} = 8.04 (s, 1H, **H$_1$**), 7.19 – 7.12 (m, 4H, **H$_3$**, **H$_4$**), 7.02 – 6.98 (m, 4H, **H$_5$**, **H$_6$**), 2.32 (s, 6H, **H$_8$**), **^{13}C{^{1}H} NMR (101 MHz, CDCl$_3$)** δ_{ppm} = 147.8 (s, **C$_1$**); 143.4 (s, **C$_2$**) 130.8 (s, **C$_3$**); 128.7; (s, **C$_6$**) 127.0 (s, **C$_7$**), 123.4 (s, **C$_4$**); 117.5 (s, **C$_5$**), 17.7 (s, **C$_8$**). **ESI-MS** (*m/z)*: 225.1392 (100%, $[M]^+$, requires 225.1386).

*5.2.3 (E)-N,N'-bis(4-fluorophenyl)formamidine (**3**)*

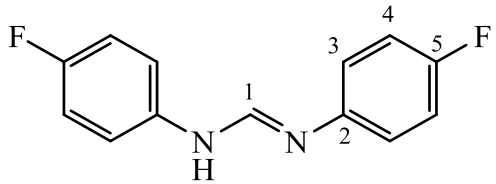

A round bottomed flask equipped with a magnetic stirrer bar was charged with triethyl orthoformate (3.74 mL, 22.6 mmol, 1.00 eq.) and glacial acetic acid (60 µL, 0.562 mmol, 0.05 eq.) under N_2 atmosphere. While stirring, 4-fluoroaniline (4.26 mL, 45.0 mmol, 1.99 eq.) was added to the reaction vessel dropwise. The mixture was heated under reflux at 150 °C for 15 hours. The reaction mixture was cooled to room temperature observing the formation of a grey solid which was filtered under vacuum and washed with hexane (3 x 10 mL). The crude solid was recrystallized from hot dichloromethane (20 mL), resulting in the formation of a white

flaky solid. The solid was filtered under vacuum and washed with petroleum ether (3 x 10 mL) before drying under vacuum to afford an opaque solid (**3**).

Yield: 2.71 g, 52%. **Melting point**: 147.1 – 148.2 °C (Literature). **IR (ATR, cm^{-1})**: ν = 2996 (broad, weak, N-H), 1666 (sharp, strong, C=N). **^{1}H NMR (300 MHz, CDCl$_3$)** δ_{ppm} = 8.02 (s, 1H, **H$_1$**), 7.02 (d, ^{3}J = 7.4Hz 8H, **H$_3$, H$_4$**), 6.22 (br s, 1H, **NH**). **^{13}C{^{1}H} NMR (100 MHz, CDCl$_3$)** δ_{ppm} = 160.1 (d, ^{1}J = 242.5 Hz, **C$_5$**), 149.3 (s, **C$_1$**), 141.3 (s, **C$_2$**), 120.6 (d, ^{3}J = 7.9 Hz, **C$_3$**), 116.3 (d, ^{2}J = 22.4 Hz, **C$_4$**) **^{19}F NMR (377 MHz, CDCl$_3$)** δ_{ppm} = -120. **ESI-MS** (*m/z)*: 233.0902 (100%, $[M+H]^+$, requires 233.0820).

*5.2.4 (E)-N,N'-bis(2-fluorophenyl)formamidine (**4**)*

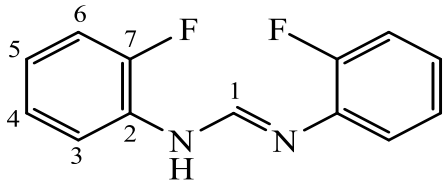

A round bottomed flask equipped with a magnetic stirrer bar was charged with triethyl orthoformate (2.15 mL, 12.9 mmol, 1.00 eq.) and Glacial acetic acid (28.0 μL, 0.43 mmol, 0.05 eq.) under N_2 atmosphere. While stirring, 2-fluoroaniline (2.49 mL, 25.9 mmol, 2.01 eq.) was added to the reaction vessel dropwise. The mixture was heated under reflux at 155 °C for 18 hours. The reaction mixture was cooled to room temperature observing the formation of a yellow solid which was filtered under vacuum and washed with hexane (3 x 10 mL). The crude solid was recrystallized from hot dichloromethane (20 mL), resulting in the formation of a yellow emulsion. The solid was filtered under vacuum and washed with petroleum ether (3 x 10 mL) before drying under vacuum to afford a white solid (**4**).

Yield: 2.27 g, 76%. **Melting point**: 153.7 – 154.3 °C. **IR (ATR, cm^{-1})**: ν = 2997 (broad, weak, N-H), 1668 (sharp, strong, C=N), 1170 (sharp, strong, C-F). **^{1}H NMR (300 MHz, CDCl$_3$)** δ_{ppm} = 8.21 (s, 1H, **H$_1$**), 7.30 (br s, 1H, **NH**), 7.07 (m, 8H, **H$_3$-H$_6$**). **^{13}C{^{1}H} NMR (100 MHz, CDCl$_3$)** δ_{ppm} = 153.1 (d, ^{1}J = 243.5 Hz, **C$_7$**), 148.5 (s, **C$_1$**), 132.9 (s, **C$_2$**), 124.7 (d, ^{4}J =3.4 Hz, **C$_4$**), 123.9 (d, ^{3}J = 7.1 Hz, **C$_5$**), 120.2 (s, **C$_3$**), 116.0 (d, ^{2}J = 21.7 Hz, **C$_6$**). **^{19}F NMR (377 MHz, CDCl$_3$)** δ_{ppm} = -117. **ESI-MS** (*m/z)*: 233.0893 (100%, $[M+H]^+$, requires 233.0822).

5.3 Synthesis of dirhodium(II,II) complexes

Methods for synthesis of compounds **5 - 10** were obtained from the literature and modified as required.[3,4]

*5.3.1 Dirhodium(II,II) tetraacetate (**5**)*

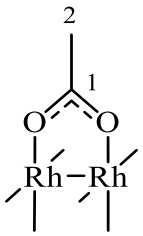

A Schlenk flask equipped with a magnetic stirrer bar was charged with $RhCl_3 \cdot 3H_2O$ (0.504 g, 1.92 mmol, 1.00 eq.) and $NaOAc \cdot 3H_2O$ (0.787 g, 5.78 mmol, 3.01 eq.). The flask was then evacuated under vacuum and filled with N_2 three times. Absolute ethanol (15 mL) and glacial acetic acid (15 mL) were added under N_2 atmosphere. The reaction mixture was heated under reflux at 100°C for 3 hours. A colour change from brown-red to blue-green in the reaction mixture was observed. The reaction mixture was then allowed to cool to ambient temperature, observing the formation of a blue precipitate. The mixture was filtered under vacuum and washed with methanol (3 x 5 mL). The solid was collected and dissolved in hot methanol and filtered quickly. The filtrate was collected, and volume was reduced to approximately half the initial volume before cooling overnight at -20 °C. The resulting precipitate was filtered under vacuum and washed with methanol (5 x 10 mL), before drying at 65°C under vacuum for 24 hours to afford a green powder (**5**).

Yield: 0.289 g, 67%. **Melting point**: 310 – 316 °C (decomposition without melting). **IR(ATR, cm^{-1})**: ν = 1572 (sharp, strong, C=O), 1409 (sharp, medium, C-O). **^{1}H NMR (400 MHz, DMSO-*d*$_6$)** δ_{ppm} = 1.80 (s, 12H, **H**$_2$). **^{13}C{^{1}H} NMR (101 MHz, DMSO-*d*$_6$)** δ_{ppm} = 190.6(**C**$_1$), 23.5 (**C**$_2$). **MS ESI**(HR) **ESI-MS** (*m/z*): 460.8655 (100%, $[M+H_2O+H]^+$, requires 460.8452).

*5.3.2 Dirhodium(II,II) tetrakis(trifluoromethylacetate) diacetone (**6**)*

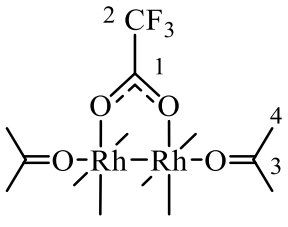

A round-bottomed flask equipped with a magnetic stirrer bar was charged with **5** (0.107g, 0.231 mmol, 1.00 eq.) and trifluoroacetic acid (35 mL, 457 mmol, 1978 eq.) and the mixture was stirred until full dissolution of the solid. The excess trifluoroacetic acid was gently evaporated over a steam bath at 60 °C with continuous stirring for 24 hours. The blue residue was collected and dried under vacuum at 100 °C for 2 hours. The solid was collected and dissolved in acetone (30 mL) and the mixture was filtered under reduced pressure. The filtrate was collected, and the solvent reduced under vacuum forming a blue emulsion. The resulting emulsion was dried under reduced pressure in the absence of light affording a green flaky solid (**6**).

Yield: 0.138 g, 92%. **Melting point**: 330 – 334 °C (decomposition without melting). **IR (ATR, cm^{-1})**: ν = 1655 (sharp, strong, C=O), 1226 (sharp, medium, C-O), 1160 (sharp, strong, C-F). **^{1}H NMR (400 MHz, DMSO-*d*$_6$)** δ_{ppm} = 2.08 (s, 12H, **H$_4$**). **^{13}C{^{1}H} NMR (101 MHz, DMSO-*d*$_6$)** δ_{ppm} = 199.5 (s, **C$_1$**), 30.12 (s, **C$_2$**). **^{19}F NMR (377 MHz, DMSO-*d*$_6$)** δ_{ppm} = -73.8 (m). **ESI-MS**(*m/z*): 777.7986 (100%, $[M+H]^+$, requires 777.7792).

*5.3.3 Dirhodium(II,II) tetrakis(di-p-tolylformamidinate) (**7**)*

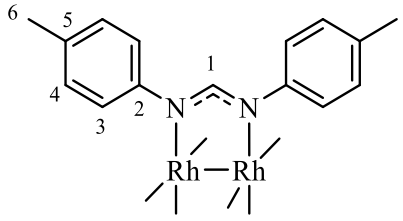

A Schlenk tube equipped with a magnetic stirrer bar was charged with **1** (0.340 g,1.52 mmol) where after the tube was evacuated and filled with N_2 in 3 cycles to create an inert atmosphere. The ligand was heated to melting at 150 °C. To the melt was added $Rh_2(O_2CCF_3)_4$ (0.100 g, 0.152 mmol) and the reaction mixture was stirred at 150 °C for 18 hours under N_2 atmosphere. The reaction mixture was cooled to ambient temperature, observing the formation of a dark brown solid. Methanol (30 mL) was added, forming a dark green suspension. The solid was filtered under vacuum and washed with cold methanol (2 x 20 mL) The crude solid was recrystallized from hot methanol (30 mL). The resulting precipitate was filtered under vacuum and washed with cold methanol (2 x 10 mL) dried under vacuum to afford a green powder (**7**).

Yield: 0.137 g, 82 %. **Melting point**: 376.7 – 379.2 °C (decomposition without melting). **IR (ATR, cm^{-1})**: ν = 1587 (sharp, strong, C=N). **^{1}H NMR (300 MHz, CDCl$_3$)** δ_{ppm} = 7.69 (s, 4H, **H$_1$**), 6.87 (d, ^{3}J = 8.2Hz, 16H, **H$_3$**), 6.59 (d, ^{3}J = 8.2Hz, 16H, **H$_4$**), 2.23 (s, 24H, **H$_6$**). **^{13}C{^{1}H}**

NMR (100 MHz, $CDCl_3$) δ_{ppm} = 162.2 (s, **C1**), 148.7 (s, **C2**), 132.5 (s, **C5**), 129.4 (s, **C3**), 124.5 (s, **C4**), 20.9 (s, **C6**). **ESI-MS** (*m/z*): 1098.3077 (100%, $[M]^+$, requires 1098.3051).

*5.3.4 Dirhodium(II,II) tetrakis(di-o-tolylformamidinate) (**8**)*

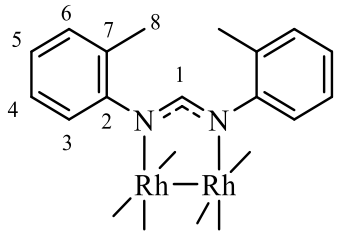

A Schlenk tube equipped with magnetic stirrer bar was charged with **2** (1.68 g, 7.48 mmol, 24.9 eq.) where after the tube was evacuated and filled with N_2 in 3 cycles to create an inert atmosphere. The ligand was heated to melting at 150 °C. To the melt was added $Rh_2(O_2CCF_3)_4$ (0.200 g, 0.304 mmol, 1.00 eq.) and the reaction mixture was stirred at 150 °C for 2 hours. The reaction was placed under vacuum and stirred for an additional 18 hours. The reaction mixture was cooled to ambient temperature, observing the formation of a black solid. Methanol (30 mL) was added, forming a red suspension which was subsequently heated to 70 °C. The mixture was filtered under vacuum and washed with pentane (2 x 10 mL) followed by cold methanol (2 x 20 mL). The crude solid was recrystallized from hot acetone (20 mL). The resulting precipitate was filtered under vacuum and washed with methanol (2 x 10 mL). The solid was dried under vacuum at 100 °C for 6 hours to afford a brown powder (**8**).

Yield: 0.0971 g, 34%. **Melting point**: 364.9 – 367.1 °C (decomposition without melting). **IR (ATR, cm^{-1})**: ν = 1586 (sharp, strong, C=N). **^{1}H NMR (600 MHz, $CDCl_3$)** δ_{ppm} = 7.73 (s, 4H, **H1**), 6.97 (d, 8H, ^3J = 7.3Hz, **H3**), 6.90 (t, 8H, ^3J = 7.6Hz, **H4**), 6.82 (t, 8H, ^3J = 7.3Hz, **H5**), 6.74 (br s, 8H, **H6**), 1.92 (s, 24H, **H8**). **^{13}C{^{1}H} NMR (100 MHz, $CDCl_3$)** δ_{ppm} = 168.4 (s, **C1**), 151.1 (s, **C2**), 132.2 (s, **C7**), 131.0 (s, **C3**), 126.3 (br s, **C4, C5**), 123.7 (s, **C6**), 19.27 (s, **C8**). **ESI-MS** (*m/z*): 1098.3041 (96%, $[M]^+$, requires 1098.3051).

*5.3.5 Dirhodium(II,II) tetrakis(bis-(2-fluorophenyl)formamidinate) (**9**)*

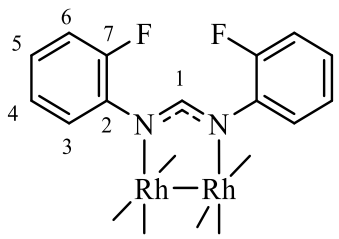

A Schlenk tube equipped with magnetic stirrer bar equipped with stirrer bar was charged with **4** (0.353 g, 1.57 mmol, 10.3 eq.) where after the tube was evacuated and filled with N_2 in 3 cycles to create an inert atmosphere. The ligand was heated to melting at 160 °C. To the melt was added $Rh_2(O_2CCF_3)_4$ (0.100 g, 0.152 mmol, 1.00 eq.) and the reaction mixture was stirred at 160 °C for 16 hours. The reaction mixture was cooled to ambient temperature, observing the formation of a brown solid. Methanol (30 mL) was added, forming a red suspension. The mixture was filtered under vacuum and washed with pentane (2 x 10 mL) followed by cold methanol (2 x 20 mL). The crude solid was recrystallized from hot methanol (20 mL). The resulting precipitate was filtered under vacuum and washed with cold methanol (2 x 10 mL). The solid was dried under vacuum at 100 °C for 6 hours to afford a red powder (**9**).

Yield: 0.125 g, 70%. **Melting point**: 324.1 – 343.8 °C. **IR (ATR, cm^{-1})**: ν = 1588 (sharp, strong, C=N), 1241 (sharp, medium, C-F). **^{1}H NMR (300 MHz, $CDCl_3$)** δ_{ppm} = 7.89 (s, 4H, **H_1**), 6.89-6.78 (m, 32H, **H_3**, **H_4**, **H_5**, **H_6**). **^{13}C{^{1}H} NMR (101 MHz, $CDCl_3$)** δ_{ppm} = 166.4 (s, **C_1**), 156.9 (d, ^1J = 246.1 Hz, **C_7**), 138.5 (d, ^4J = 4.7 Hz, **C_3**), 126.20 (s, **C_4**), 123.9 (d, ^2J = 13.8 Hz, **C_6**), 115.6 (d, ^3J = 6.4 Hz **C_5**), 115.5 (s, **C_2**). **^{19}F NMR (377 MHz, $CDCl_3$)** δ_{ppm} = -128.9 (s). **ESI-MS** (*m/z*):1131.1107(100%, $[M+H]^+$, requires 1131.1125).

*5.3.6 Dirhodium(II,II) tetrakis(bis-(4-fluorophenyl)formamidinate) (**10**)*

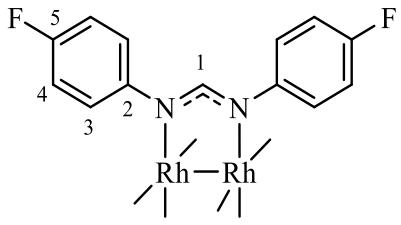

A Schlenk tube equipped with magnetic stirrer bar was charged with **3** (0.351 g, 1.56 mmol, 10.3 eq.) where after the tube was evacuated and filled with N_2 in 3 cycles to create an inert atmosphere. The ligand was heated to melting at 160 °C. To the melt was added $Rh_2(O_2CCF_3)_4$ (0.100 g, 0.152 mmol, 1.00 eq.) and the reaction mixture was stirred at 160 °C for 16 hours. The reaction mixture was cooled to ambient temperature, observing the formation of a black solid. Methanol (30 mL) was added, forming a green suspension. The mixture was filtered under vacuum and washed with pentane (2 x 10 mL) followed by cold methanol (2 x 20 mL). The crude solid was recrystallized from hot methanol (30 mL). The resulting precipitate was filtered under vacuum and washed with cold methanol (2 x 10 mL). The solid was dried under vacuum at 100 °C for 4 hours to afford a green solid (**10**).

Yield: 0.157 g, 91%. **Melting point**: 381.1 – 384.9 °C (decomposition without melting). **IR (ATR, cm^{-1})**: ν = 1583 (sharp, strong, C=N), 1209 (sharp, medium, C-F). **^{1}H NMR (400 MHz, $CDCl_3$)** δ_{ppm} = 7.70 (t, ^{3}J = 3.3Hz, 4H, **H_1**), 6.81 (t, ^{3}J = 8.2Hz, 16H, **H_4**), 6.59-6.49 (m, 16H, **H_3**). **^{13}C{^{1}H} NMR (101 MHz, $CDCl_3$)** δ_{ppm} = 162.6 (s, **C_1**), 160.3 (d, ^{1}J = 243.5 Hz, **C_5**), 146.8 (d, ^{4}J = 2.5 Hz, **C_2**), 125.5 (d, ^{3}J = 7.9 Hz, **C_3**), 116.0 (d, ^{2}J = 22.3 Hz **C_4**). **^{19}F NMR (377 MHz, $CDCl_3$)** δ_{ppm} = - 119.3 (s). **ESI-MS**(*m/z*): 1131.1124 (100%, $[M+H]^+$, requires 1131.1125).

5.4 Synthesis of scaffolds containing pyridyl moieties

The general method for coordination of pyridyl functionalized supports was obtained from literature and modified as needed to afford compounds **11** and **15**.[5,6]

*5.4.1 (E)-N-propyl-1-(pyridin-4-yl)methanimine (**11**)*

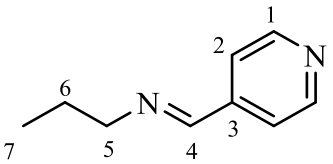

A round bottomed flask equipped with stirrer bar was charged with dry dichloromethane (5 mL) and 4-pyridinecarboxaldehyde (0.102 mL, 1.10 mmol, 1.00 eq.) and anhydrous magnesium sulfate (0.207 g). A solution of n-propylamine (0.0810 mL, 1 mmol, 0.91 eq) in dry dichloromethane (1 mL) was added dropwise to the reaction vessel under inert atmosphere. The reaction was stirred at ambient temperature for 24 hours. The reaction mixture was filtered by gravity and the filtrate was diluted with dichloromethane (15 mL) and washed copiously with deionised water (5 x 10 mL). The organic layer was collected and dried over anhydrous magnesium sulfate before filtration by gravity and removal of solvent under reduced pressure. The resulting residue was dried under vacuum to afford a yellow oil (**11**).

Yield: 0.125 g, 84%. **IR (ATR, cm^{-1})**: ν = 1647 (sharp, strong, $C=N_{imine}$), 1605 (sharp, strong, $C=N_{pyridyl}$). **^{1}H NMR (300 MHz, $CDCl_3$)** δ_{ppm} = 8.67 (d, ^{3}J = 4.4Hz, 2H, **H_1**), 8.23 (s, 1H, **H_4**), 7.57 (d, ^{3}J = 4.4Hz, 2H, **H_2**), 3.60 (t, *J* = 6.8Hz, 2H, **H_5**), 1.71 (m, 2H, **H_6**), 0.94 (t, *J* = 6.8Hz, 3H, **H_7**). **^{13}C{^{1}H} NMR (101 MHz, $CDCl_3$)** δ_{ppm} = 159.5 (**C_4**), 150.3(**C_1**), 121.9 (**C_2**), 143.2 (**C_3**), 60.1(**C_5**), 55.3 (**C_6**), 21.3 (**C_7**).

*5.4.2 N^1-(pyridin-4-ylmethyl)-N^2,N^2-bis(2-((pyridin-4-ylmethyl)amino)ethyl)ethane-1,2-diamine (**15**)*

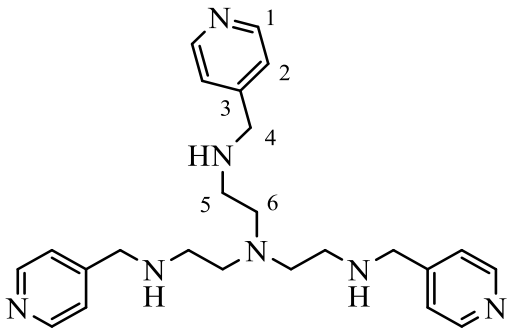

A round bottomed flask equipped with magnetic stirrer bar was charged with a solution of 4 -pyridinecarboxaldehyde (1.25 mL, 13.3 mmol, 3.32 eq.) in dry dichloromethane (10 mL) and anhydrous magnesium sulfate (2.10 g). A solution of tris(2-aminoethyl)amine (0.598 mL, 4.01 mmol, 1.00 eq.) in dry dichloromethane (5 mL) was added dropwise while to the mixture while stirring. The reaction mixture was stirred at ambient temperature for 16 hours. The reaction mixture was filtered by gravity and the solid washed with dichloromethane (3 x 10 mL). The solvent was removed under reduced pressure and the residue was dried under vacuum for 1 hour. The flask was then purged with vacuum and filled with N_2 in three cycles. Dry methanol (15 mL) was added to the flask under inert atmosphere. The reaction vessel was submerged in an ice bath before sodium borohydride solution (0.746 g, 20.1 mmol, 5.01 eq.) in dry methanol (5 mL) was added dropwise. The reaction mixture was stirred for 12 hours. The reaction was quenched with cold deionised H_2O (30 mL). The resulting mixture was extracted using dichloromethane (50 mL) before washing the organic layer with deionised water (3 x 30 mL). The organic fraction was collected and dried over anhydrous magnesium sulfate. The mixture was filtered, and the filtrate volume was reduced under vacuum. The resulting residue was dried under vacuum to afford a viscous yellow oil (**15**).

Yield: 0.925 g, 55%. **IR (ATR, cm^{-1})**: ν = 3334 (broad, weak, N-H), 1608 (sharp, strong, C=$N_{pyridyl}$).**^{1}H NMR (600 MHz, DMSO-*d*$_6$)** δ_{ppm} = 8.73 (d, ^3J = 6.0Hz, 6H, **H$_1$**), 7.27 (d, ^3J = 5.9Hz, 6H, **H$_2$**), 3.68 (s, 6H, **H$_4$**), 2.51 (br s, 12H, **H$_5$**, **H$_6$**). **^{13}C{^{1}H} NMR (101 MHz, DMSO-*d*$_6$)** δ_{ppm} = 160.0 (**C$_3$**), 159.2 (**C$_1$**), 132.8 (**C$_2$**), 64.0 (**C$_4$**), 61.7 (**C$_5$**), 56.7 (**C$_6$**). **ESI-MS**(*m/z*): 420.592 (100%, $[M+H]^+$, requires 420.591).

5.5 Synthesis of model- and low-valent metallodendrimers

The general method for coordination of pyridyl functionalized supports was obtained from literature and modified as needed to afford compounds **12-14** and **16-21**.[5,7]

*5.5.1 Synthesis of bis-dirhodium(II,II) tetraacetate complex (**12**)*

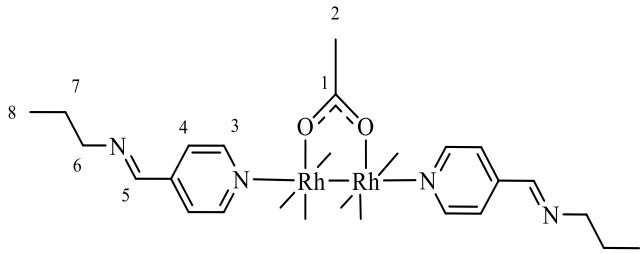

A round bottomed flask equipped with magnetic stirrer bar was charged with a solution of compound **5** (0.0240 g, 0.0358 mmol, 1.00 eq.) in dry dichloromethane (10 mL) under inert atmosphere. A solution of compound **11** (0.00740 g, 0.0501 mmol, 1.00 eq) in dry dichloromethane (5 mL) was added dropwise and the reaction was stirred at ambient temperature for 6 hours. The reaction mixture was concentrated to *ca.* 5 mL under reduced pressure. Petroleum ether (10 mL) was added to the reaction mixture with subsequent formation of a red precipitate. The resulting solid was filtered under vacuum and washed with petroleum ether (5 x 10 mL). Product was dried under vacuum affording a red solid (**12**).

Yield: 0.0720 g, 28%. **Melting point**: 364.7 – 369.6 °C (decomposition without melting). **IR (ATR, cm^{-1})**: ν = 3334 (broad, weak, N-H), 1595 (sharp, strong, C=$N_{pyridyl}$), 1564 (sharp, strong, C=O), 1434 (sharp, medium, C-O).**^{1}H NMR (300 MHz, $CDCl_3$)** δ_{ppm} = 9.42 (d, ^3J = 4.4Hz, 4H, **H_3**), 8.44 (s, 2H, **H_5**), 7.99 (d, ^3J = 4.4Hz, 4H, **H_4**), 3.72 (t, ^3J = 6.8Hz, 4H, **H_6**), 1.81 (m, 4H, **H_7**), 1.90 (s , 12H, **H_2**), 1.02 (t, J = 6.8, 6H, **H_8**).

*5.5.2 mono-dirhodium(II,II) tetraacetate complex (**13**)*

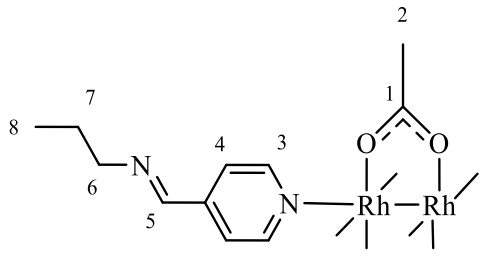

A round bottomed flask equipped with magnetic stirrer bar was charged with a solution of compound **5** (0.0501 g, 0.110 mmol, 1.00 eq.) in dry dichloromethane (10 mL) under inert

atmosphere. A solution of compound **11** (0.0140 g, 0.100 mmol, 0.91 eq) in dry dichloromethane (5 mL) was added dropwise and the reaction was stirred at ambient temperature for 6 hours. The reaction mixture was concentrated to *ca.* 5 mL under reduced pressure. Petroleum ether (10 mL) was added to the reaction mixture with subsequent formation of a red precipitate. The resulting solid was filtered under vacuum and washed with petroleum ether (5 x 10 mL). Product was dried under vacuum affording a red solid (**13**).

Yield: 0.0721 g, 28%. **Melting point**: 352.4 – 357.2 °C (decomposition without melting). **IR (ATR, cm^{-1})**: ν = 1587 (sharp, strong, C=$N_{pyridyl}$), 1564 (sharp, strong, C=O), 1434 (sharp, medium, C-O).**^{1}H NMR (300 MHz, $CDCl_3$)** δ_{ppm} = 9.42 (d, ^{3}J = 4.4Hz, 4H, **H_3**), 8.44 (s, 2H, **H_5**), 7.99 (d, ^{3}J = 4.4Hz, 4H, **H_4**), 3.72 (t, ^{3}J = 6.8Hz, 4H, **H_6**), 1.81 (m, 4H, **H_7**), 1.90 (s , 12H, **H_2**), 1.02 (t, *J* = 6.8, 6H, **H_8**). **^{13}C{^{1}H} NMR:** Not collected due to degradation in solution.

*5.5.3 mono-picolyl-dirhodium(II,II) tetraacetate complex (**14**)*

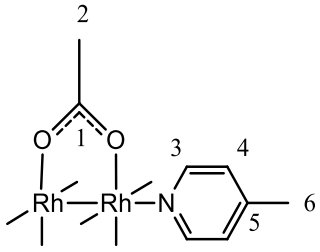

A round bottomed flask equipped with magnetic stirrer bar was charged with a solution of compound **5** (0.0501 g, 0.110 mmol, 1.00 eq.) in dry dichloromethane (10 mL) under inert atmosphere. A solution of 4-picoline (0.0962 g, 0.100 mmol, 0.91 eq) in dry dichloromethane (5 mL) was added dropwise and the reaction was stirred at ambient temperature for 6 hours. The reaction mixture was concentrated to *ca.* 5 mL under reduced pressure. Petroleum ether (10 mL) was added to the reaction mixture with subsequent formation of a red precipitate. The resulting solid was filtered under vacuum and washed with petroleum ether (5 x 10 mL). Product was dried under vacuum affording a red powder (**14**).

Yield: 0.0442 g, 72%. **IR (ATR, cm^{-1})**: ν = 1586 (sharp, strong, C=$N_{pyridyl}$), 1564 (sharp, strong, C=O), 1434 (sharp, medium, C-O). **Melting point**: 352.4 – 357.2 °C (decomposition without melting).**^{1}H NMR (300 MHz, $CDCl_3$)** δ_{ppm} = 9.03 (d, ^{3}J = 4.6Hz, 2H, **H_3**), 7.27 (d, ^{3}J = 4.4Hz, 2H, **H_4**), 2.59 (s, 3H, **H_6**), 1.93 (s, 12H, **H_2**). **^{13}C{^{1}H} NMR (101 MHz, $CDCl_3$)** δ_{ppm} = 191.8 (s, **C_1**), 150.9 (s, **C_3**), 148.7 (s, **C_5**), 125.9 (s, **C_4**), 23.9 (s, **C_2**), 21.4 (s, **C_6**). **ESI-MS** (*m/z*): 520.8856 (100%, $[M\text{-}CH_3+H]^+$, requires 520.8861).

*5.5.4 tris-(dirhodium(II,II) tetraacetate) metallodendrimer (**16**)*

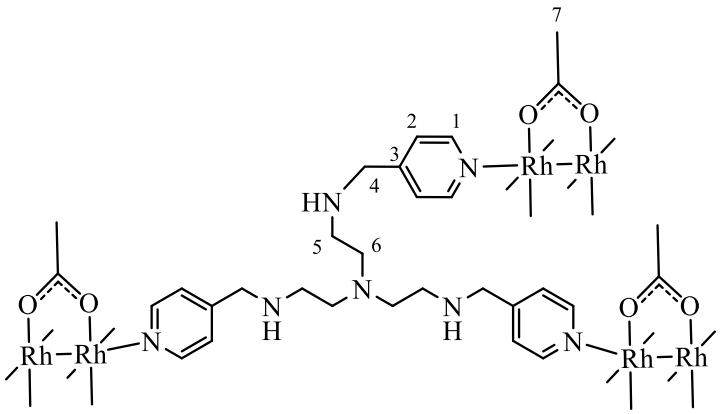

A round bottomed flask equipped with magnetic stirrer bar was charged with a solution of compound **5** (0.0501 g, 0.110 mmol, 3.29 eq.) in dry dichloromethane (10 mL) under inert atmosphere. A solution of **15** (0.0148 g, 0.340 mmol, 1.00 eq) in dry dichloromethane (5 mL) was added dropwise and the reaction was stirred at ambient temperature for 6 hours. The reaction mixture was concentrated to *ca.* 5 mL under reduced pressure. Petroleum ether (10 mL) was added to the reaction mixture with subsequent formation of a red precipitate. The solid was filtered under vacuum and washed with petroleum ether (5 x 10 mL). Product was dried under vacuum affording a red crystalline solid (**16**).

Yield: 0.0522 g, 80%. **Melting point**: 352.4 – 357.2 °C (decomposition without melting). **IR(ATR, cm^{-1})**: υ = 3425 (broad, weak, N-H), 1586 $(C=N)_{pyr}$, 1545 (sharp, strong, C=O), 1440 (sharp, medium, C-O). **^{1}H NMR (300 MHz, DMSO-*d*$_6$)** δ_{ppm} = 8.95 (br d, 6H, **H$_3$**), 7.72 (br d, 6H, **H$_4$**), 3.89 (br s, 6H, **H$_5$**), 2.85 (m, 12H, **H$_6$**, **H$_7$**), 1.76 (s, 36H, **H$_2$**).**^{13}C{^{1}H} NMR:** Not collected due to low solubility. **ESI-MS** (*m/z*): 1768.4221 (100%,$[M+Na]^+$, requires 1768.8586).

*5.5.5 tris-(dirhodium(II,II) tetrakis(trifluoromethylacetate)) metallodendrimer (**17**)*

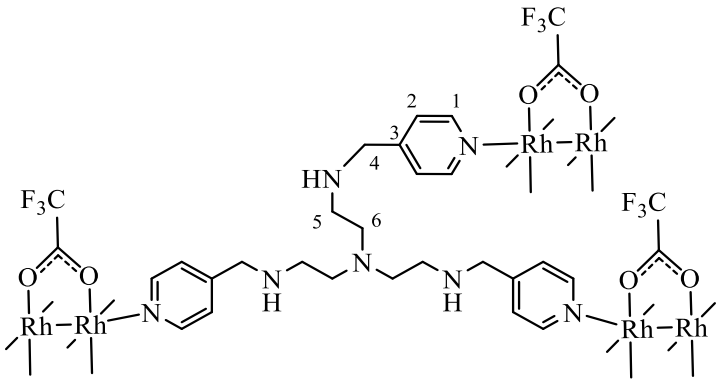

A round bottomed flask equipped with magnetic stirrer bar was charged with a solution of compound **6** (0.0500 g, 0.0763 mmol, 3.05 eq.) in dry dichloromethane (10 mL) under inert atmosphere. A solution of **15** (0.0110 g, 0.254 mmol, 1.00 eq) in dry dichloromethane (5 mL) was added dropwise and the reaction was stirred at ambient temperature for 6 hours. The reaction mixture was concentrated to *ca.* 5 mL under reduced pressure. Petroleum ether (10 mL) was added to the reaction mixture with subsequent formation of a red precipitate. The resulting solid was filtered under vacuum and washed with petroleum ether (5 x 10 mL). Product was dried under vacuum affording a purple solid (**17**).

Yield: 0.051 g, 84%. **Melting point**: 352.4 – 357.2 °C (decomposition without melting). **IR(ATR, cm^{-1})**: ν = 3352 (broad, weak, N-H), 1583 $(C=N)_{pyr}$, 1225 (sharp, strong, C-F). **^{1}H-** and **^{13}C{^{1}H} NMR:** Not collected due to poor solubility. **ESI-MS** (*m/z*): 1350.4651 (100%,$[M+NNCH_3+2K]^{2+}$, requires 1350.4894).

*5.5.6 tris-(dirhodium(II,II) tetrakis(di-p-tolylformamidinate)) metallodendrimer(**18**)*

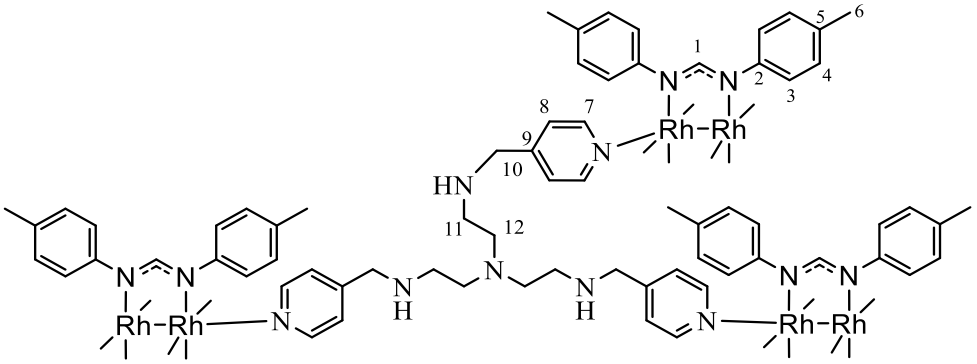

A round bottomed flask was charged with a solution of compound **7** (0.0400 g, 0.0364 mmol, 3.05 eq.) in dry dichloromethane (10 mL) under inert atmosphere. A solution of **15** (0.00460 g, 0.0110 mmol, 1.00 eq) in dry dichloromethane (5 mL) was added dropwise and the reaction was stirred at ambient temperature for 6 hours. The reaction mixture was concentrated to *ca.* 5 mL under reduced pressure. Petroleum ether (10 mL) was added to the reaction mixture with subsequent formation of a green precipitate. The resulting solid was filtered under vacuum and washed with petroleum ether (5 x 10 mL). Product was dried under vacuum affording a green solid (**18**).

Yield: 0.051 g, 76%. **Melting point**: > 400 °C. **IR(ATR, cm^{-1})**: ν = 3425 (broad, weak, N-H), 1592 $(C=N)_{pyr}$. **^{1}H NMR (300 MHz, Benzene-*d*$_6$)** δ_{ppm} = 8.55 (d, ^{3}J = 5.9 Hz, 6H, **H$_7$**), 7.81 (t, ^{3}J = 3.3 Hz, 12H, **H$_1$**), 6.91 (d, ^{3}J = 5.9 Hz, 6H, **H$_8$**), 6.83 (dd, ^{3}J = 20.8, 8.3 Hz, 96H, **H$_3$**, **H$_4$**), 3.35 (s, 6H, **H$_{10}$**), 2.30 (m, 12H, **H$_{11}$**, **H$_{12}$**), 2.07 (s, 72H, **H$_6$**). **^{13}C{^{1}H} NMR (151 MHz,**

Benzene-*d*$_6$) δ_{ppm} = 163.4 (s, **C$_1$**), 151.1 (s, **C$_2$**), 149.9 (s, **C$_7$**), 133.3 (s, **C$_7$**), 133.1 (s, **C$_8$**), 130.3 (s, **C$_3$**), 125.4 (s, **C$_4$**), 125.18 (s, **C$_9$**), 123.51 (s, **C$_7$**), 54.8 (s, **C$_{10}$**), 53.3 (s, **C$_{11}$**), 47.8 (s, **C$_{12}$**), 21.4 (s, **C$_6$**). **ESI-MS** (*m/z*): 2072.4119, (100%, $[M+4(CH_2Cl_2)+2K]^{2+}$, requires 2072.4528).

*5.5.7 tris-(dirhodium(II,II)tetrakis(di-o-tolylformamidinate)) metallodendrimer (**19**)*

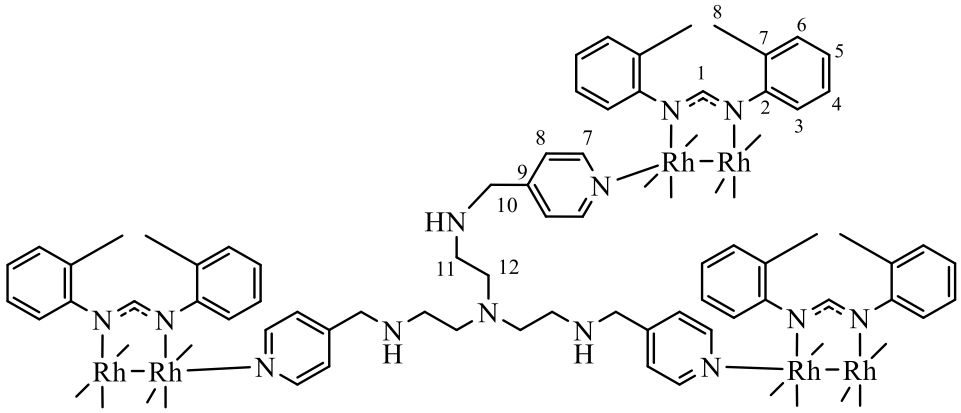

A round bottomed flask was charged with a solution of compound **8** (0.0410 g, 0.0370 mmol, 3.03 eq.) in dry dichloromethane (10 mL) under inert atmosphere. A solution of **15** (0.00480 g, 0.0120 mmol, 1.00 eq) in dry dichloromethane (5 mL) was added dropwise and the reaction was stirred under reflux at 40 ˚C for 6 hours. The reaction mixture was concentrated to *ca.* 5 mL under reduced pressure. Petroleum ether (10 mL) was added to the reaction mixture with subsequent formation of an orange precipitate. The resulting solid was filtered under vacuum and washed with petroleum ether (5 x 10 mL). Product was dried under vacuum affording a brown powder (**19**).

Yield: 0.027 g, 60%. **Melting point**: 376.1- 379.5°C (decomposition without melting). **IR(ATR, cm^{-1})**: ν = 3425 (broad, weak, N-H), 1588 $(C=N)_{pyr}$.**^{1}H NMR (400 MHz, CDCl$_3$)** δ_{ppm} = 8.52 (d, 6H, ^3J = 7.4Hz, **H$_7$**), 7.72 (br s, H, **H$_1$**), 7.22 (d, 6H, ^3J = 7.4Hz, **H$_8$**), 6.97 - 6.74 (m, 96H, **H$_3$ - H$_6$**), 3.88 (s, 2H, **H$_{10}$**), 3.79 (s, 4H, **H$_{10}$**), 2.69 (br s, 12H, **H$_{11}$-H$_{12}$**), 1.91 (s, 72H, **H$_8$**). **^{13}C{^{1}H} NMR:** Not collected to due poor solubility. **ESI-MS**(*m/z*): 1945.4124 (100%, $[M+3(NCCH_3)+2Na\ ]^{2+}$, requires 1945.4523).

5.5.8 *tris-(dirhodium(II,II)tetrakis(bis-(4fluorophenyl)formamidinate)) metallodendrimer (**20**)*

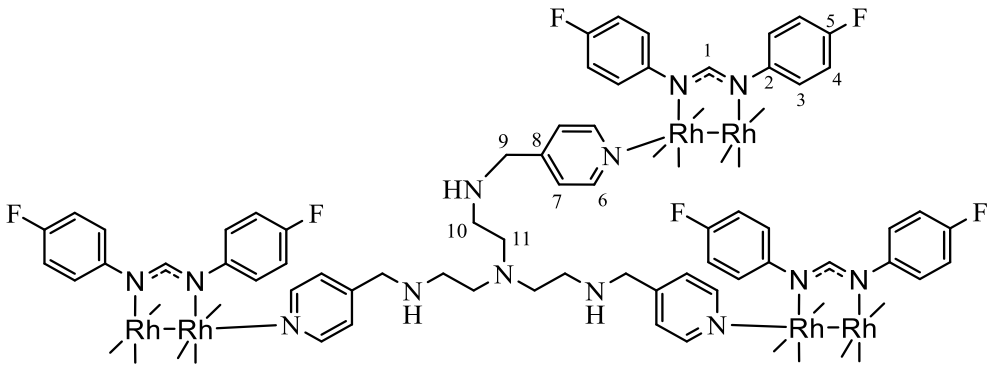

A round bottomed flask was charged with a solution of compound **10** (0.0500 g, 0.0440 mmol, 3.38 eq.) in dry dichloromethane (10 mL) under inert atmosphere. A solution of **15** (0.00550 g, 0.0131 mmol, 1.00 eq) in dry dichloromethane (5 mL) was added dropwise and the reaction was stirred at ambient temperature for 6 hours. The reaction mixture was concentrated to *ca.* 5 mL under reduced pressure. Petroleum ether (10 mL) was added to the reaction mixture with subsequent formation of a dark green precipitate. The resulting solid was filtered under vacuum and washed with petroleum ether (5 x 10 mL). Product was dried under vacuum affording a dark green solid (**20**).

Yield: 0.046 g, 83%. **Melting point**: 397.7 – 398.5°C. **IR (ATR, cm^{-1})**: ν = 3267 (broad, weak, N-H), 1592 (sharp, strong, C=N), 1195 (sharp, strong, C-F). **^{1}H NMR (300 MHz, DMSO-*d*$_6$)** δ_{ppm} = 8.52 (d, ^{3}J = 5.9 Hz, 6H, **H$_6$**), 7.68 (t, ^{3}J = 2.8 Hz, 12H, **H$_1$**), 7.24 (d, ^{3}J = 5.8 Hz, 6H, **H$_7$**), 6.82 (t, ^{3}J = 6.9 Hz, 48H, **H$_4$**),), 6.55 (dd, ^{3}J = 6.9 Hz, 3.7 Hz, 48H, **H$_3$**), 3.69 (s, 6H, **H$_9$**), 2.68 (br s, 12H, **H$_{10}$**, **H$_{11}$**). **^{13}C{^{1}H} NMR:** Not collected to due poor solubility. **ESI-MS**(*m/z*): 1294.4554 (100%, $[M+3Na]^{3+}$, requires 1294.4862).

5.5.9 *tris-(dirhodium(II,II)tetrakis(bis(2-fluorophenyl)formamidinate)) metallodendrimer (**21**)*

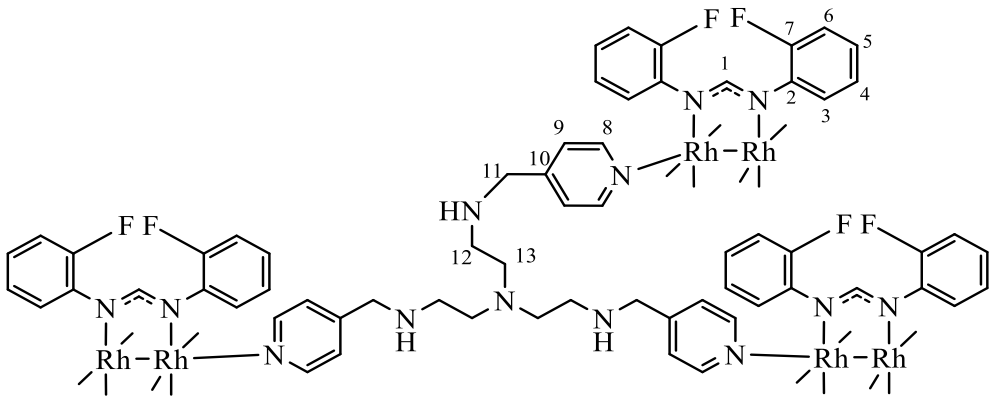

A round bottomed flask was charged with a solution of compound **10** (0.0405 g, 0.0366 mmol, 3.27 eq.) in dry dichloromethane (10 mL) under inert atmosphere. A solution of **15** (0.00450 g, 0.0110 mmol, 1.00 eq) in dry dichloromethane (5 mL) was added dropwise and the reaction was stirred at ambient temperature for 6 hours. The reaction mixture was concentrated to *ca.* 5 mL under reduced pressure. Petroleum ether (10 mL) was added to the reaction mixture with subsequent formation of a brown precipitate. The resulting solid was filtered under vacuum and washed with petroleum ether (5 x 10 mL). Product was dried under vacuum affording a yellow solid (**21**).

Yield: 0.027 g, 67%. **Melting point**: 389.3 – 390.1°C. **IR (ATR, cm^{-1})**: ν = 3357 (broad, weak, N-H), 1590 (sharp, strong, C=N_{pyr}), 1170 (sharp, strong, C-F). **^{1}H NMR (400 MHz, $CDCl_3$)** δ_{ppm} = 8.48 (d, ^{3}J = 5.9 Hz, 6H, **H_7**), 7.78 (br s, 12H, **H_1**), 7.24 (d, ^{3}J = 5.8 Hz, 6H, **H_8**), 6.74 (m, 96H, **H_3-H_6**),), 3.77 (s, 6H, **H_{10}**), 2.71 (s, 12H, **H_{11},H_{12}**). **^{13}C{^{1}H} NMR (151 MHz, $CDCl_3$)** δ_{ppm} = 166.6 (s, **C_1**); 157.1 (d, ^{1}J = 246.1 Hz, **C_7**), 150.3 (s, **C_8**), 150.1 (s, **C_{10}**), 138.2 (d, ^{4}J = 5.4 Hz, **C_3**), 126.3 (s, **C_4**), 123.9 (d, ^{2}J = 20.7 Hz, **C_6**),123.5 (s, **C_9**), 115.7 (s, **C_2**) 115.3 (d, ^{1}J = 14.8 Hz, **C_5**), 53.7 (**C_{11}**), 46.7 (**C_{12}**), 32.1 (**C_{13}**).

5.6 Single Crystal X-ray Diffraction

Single-crystal X-ray diffraction data (compounds **2** and **7**) were collected using a Bruker Kappa APEX II DUO diffractometer equipped with a graphite-monochromated Mo-Kα radiation (λ = 0.71073 Å). The temperature was controlled by an Oxford Cryostream cooling system (Oxford Cryostat). Cell refinement and data reduction were achieved using the program SAINT.[8] The data were scaled, and absorption correction was accomplished using SADABS.[2] The structure was solved by direct methods by using SHELXS-97[9] and refined by full-matrix least-squares methods based on F^2 using SHELXL-2018[9].

Refinement of non-hydrogen atoms were carried out anisotropically. All hydrogen atoms, except amino hydrogen H1(**2**) were placed in idealised positions and refined in riding models with Uiso assigned 1.2 or 1.5 times Ueq of their parent atoms and the bond distances were constrained from 0.95 to 0.99 Å. The hydrogen atom H1 on nitrogen atom N1 was located in the difference electron density maps and refined independently. The methyl-phenyl moieties were disordered over two positions and site occupancies were refined to 0.47(2) vs. 0.53(2), 0.45(2) vs. 0.55(2) respectively. The programs X-Seed, Mercury and POV-Ray were used to produce ORTEP images of compounds **2** and **7**.[10,11] Selected crystal data and structure refinement properties are reported in Table 6.1.

*Table 5.1 Crystal structure data and refinement parameters for compounds **2** and **7***

	Compound **2**	Compound **7**
Empirical Formula	$C_{15}H_{16}N_2$	$C_{60}H_{60}N_8Rh_2$
Formula weight ($g.mol^{-1}$)	224.30	1098.98
Crystal system	triclinic	tetragonal
Space group	*P-1*	*I-4*
Crystal colour and shape	Colourless plate	Green block
Crystal dimensions / mm	0.10 x 0.31 x 0.49	0.08 x 0.22 x 0.25
a / Å	7.3864(12)	14.4463(8)
b / Å	8.4299(13)	14.4463(8)
c / Å	10.4871(17)	14.0305(9)
α / °	74.780(3)	-
β / °	83.623(3)	-
γ / °	80.460(3)	-
V / $Å^3$	619.81	2928.1
Z	2	2
Temperature / K	173	173
ρ / $g.cm^{-1}$	1.202	1.247
μ / mm^{-1}	0.072	0.605
Reflections used	2919	3647
R_{int}	12776, 2919, 0.033	38451, 3647, 0.068
Final R indices [I>2s(I)]	2145	3278
R indices (all data)	0.0451	0.0384
Goodness-of-fit	1.04	1.14
Max, Min Δρ/e $Å^{-3}$	-0.17, 0.27	-0.40, 0.77
F(000)	240	1132

5.7 General methods for Hydroformylation reactions

Hydroformylation reactions were carried out in a 90 mL stainless steel pipe reactor equipped with a Teflon-coated magnetic stirrer bar. The reactor was charged with toluene (5 mL), substrate [1-octene (7.175 mmol)], internal standard *n*-decane (1.26 mmol) and catalyst loading (2.87 x 10^{-3} mmol). The pipe reactor was flushed with nitrogen three times, followed by flushing with syngas (1:1, CO: H_2) three times. The reactor was pressurised to the desired pressure and consequently heated to the desired temperature. Samples were collected at the beginning and end of each reaction. All reactions were performed in triplicate and are recorded as an average of three identical experiments.

5.7.1 Product analysis by GC-FID for 1-octene

Analysis of the hydroformylation samples of reactions with 1-octene were analysed on a Perkin Elmer Clarus 580 GC equipped with a flame-ionisation detector (FID). The products were confirmed in relation to authentic standards for the hydroformylation products of 1-octene (internal-octenes and isomers of nonanal).

5.7.2 Mercury poisoning studies

The hydroformylation reactions were carried out in a 90 mL stainless steel pipe reactor equipped with a Teflon-coated magnetic stirrer bar. The reactor was charged with toluene (5 mL), 1-octene (7.175 mmol), internal standard *n*-decane (1.26 mmol), a drop of mercury and compound **5** (2.87 x 10^{-3} mmol). The pipe reactor was flushed with nitrogen three times, followed by purging with syngas (1:1, CO: H_2) three times. The reactor was pressurised to 50 bar and heated to 95 °C for 4 hours.

5.8 References

1. K. M. Kuhn and R. H. Grubbs, *Org. Lett.* 2008, **10**, 2075–2077.
2. B. A. Dar, S. N. Ahmad, M. A. Wagay, A. Hussain, N. Ahmad, K. A. Bhat, M. A. Khuroo, M. Sharma, and B. Singh; *Tet. Lett.* 2013, **54**, 4880–4884.
3. G. A. Rempel, P. Legzdins, H. Smith and G. Wilkinson, *Inorg. Synth.* 1972, **103**, 90–91.
4. M. Cooke, The Synthesis and Characterization of Rh2(II,II) Templated Photoactive Assemblies, Université de Montréal, 2007.
5. S. Malaza, P. Govender, M. Schutte-Smith, H. G. Visser and G. S. Smith, *Eur. J. Inorg. Chem.* 2017, 3919.
6. D. Giffard, E. Fischer-Fodor, C. Vlad, P. Achimas-Cadariu and G. S. Smith, *Eur. J. Med. Chem*., 2018, **157**, 773-781.
7. P. Govender, N. C. Antonels, J. Mattsson, A. K. Renfrew, P. J. Dyson, J. R. Moss, B. Therrien and G. S. Smith, *J. Organomet. Chem.*, 2009, **694**, 3470-3476.
8. SAINT version 7.60a, Bruker AXS Inc., Madison, WI, USA, 2006.
9. G. M. Sheldrick, SHELXS-97, SHELXL-2018/3, SADABS version 2.05, University of Göttingen, Germany, 1997.
10. L. J. Barbour, *J. Supramol. Chem.*, 2001, ***1***, 189-191
11. J. L. Atwood and L. J. Barbour, *Cryst. Growth Des*., 2003, **3**, 3.

CHAPTER 6

Summary and Future Outlook

6.1 Summary

The objective of this project was to synthesize and characterize a series of diphenylformamidine ligands, dirhodium(II,II) complexes, low-valent tris based metallodendrimers and to characterize these compounds by spectroscopic and analytical techniques such as NMR spectroscopy (^{1}H-, ^{13}C{^{1}H}-, ^{19}F-, HSQC, HMQC), IR spectroscopy and mass spectrometry (HR-ESI, EI). The metal-containing compounds were evaluated as catalyst precursors in the hydroformylation of 1-octene. To the best of our knowledge, metallodendrimers bearing dirhodium(II,II) complexes at the periphery, bound through an axial- pyridyl interaction have not been reported for use in the hydroformylation reaction.

A series of substituted diphenylformamidine ligands (**1**-**4**) were synthesized by known procedures, isolated as pure crystalline solids and characterized using appropriate techniques as described above.[1,2] The dirhodium(II.II) complexes (**5**-**10**) were synthesized according to modified literature methods, obtained in moderate to high yields and characterized accordingly.[3,4] X-ray crystal structures were obtained for compounds **2** and **7**, confirming the molecular structure of the diphenylformamidine type ligand and dirhodium(II,II) paddlewheel structure.

A known model dendron (**11**) was synthesized in good yields through a Schiff-base condensation of propylamine and 4-pyridinecarboxaldehyde.[5] The synthetic method for obtaining *mono*- adducts of dirhodium(II,II) complexes with imino-pyridyl based dendron resulted in initial formation of the *bis*- adduct (**12**) using modified literature methods.[6] Formation of the new *mono*- adduct (**13**) resulted in cleavage of the imine moiety in solution. A *mono*- adduct using 4-picoline (**14**) resulted in the successfully synthesized and characterised accordingly. A known tri-pyridyl functionalized tris(2-aminoethyl)amine based low-valent dendrimer (**15**) was synthesized and appropriately characterized.

Low-valent metallodendrimers were obtained *via* modified literature methods, resulting in the formation on six new compounds (**16**-**21**) obtained in moderate to high yields.[6] Spectroscopic and analytical techniques were used in the characterization, where applicable, in each case.

Spectroscopic subtleties were observed in the NMR and IR spectra the for acetate- and formamidinate-bearing compounds indicating successful formation.

Compounds **5** - **10** and **16** - **21** were evaluated as catalyst precursors in the hydroformylation of 1-octene. Compound **5** was used in optimization reactions, arriving at optimal conditions of 95˚C, 50 bar syngas pressure and 4-hour reaction time. The molar substrate to catalyst ratio was varied from 2500:1 to 5000:1 yielding similar results. All synthesized compounds display excellent conversion capabilities (87 - 99%). Acetate bearing complexes show excellent chemoselectivity toward aldehyde formation (98 - 100%) whereas formamidinate compounds display moderate to good chemoselectivity (59 - 87%) and higher regioselectivity toward linear aldehyde (48 - 71%).

Conjugation of a pyridyl entity to an axial site of each compound results in lower activity for compound **14**, but comparable results are observed between bimetallic and hexametallic acetate-bearing compounds. A marginal increase in the regioselectivity is observed upon conjugation for acetate-bearing complexes. Similarly, conjugation of the pyridyl scaffold to formamidinate complexes results in a significant reduction in activity (*ca.* 10%) observed in all but one case. Significant increases in regioselectivity is observed for *para*-substituted compounds upon conjugation. Mercury poisoning experiments show no significant loss in activity, suggesting that the reaction takes place homogeneously.

Preliminary results observed in the cyclic voltammetry data obtained suggest a combination of the accessibility of the oxidized Rh_2^{5+} and the reduced Rh_2^{3+} species. Additionally, favouring of oxidized or reduced forms of the active catalyst results in the speculated favouring of intermediary steps in the hydroformylation catalytic cycle resulting in the regio- and chemoselectivity through kinetic influence.

6.2 Future Outlook

This study has investigated the synthetic, and some spectroscopic intricacies of dirhodium(II,II) complexes. Although these compounds show appreciable activity in the hydroformylation reaction, quantifying and increasing the recyclability of the catalyst species would greatly benefit their use in larger scale reactions. Conjugation of these compounds to solid supports may allow for increased activity by availing both metal centres for catalytic activation through conjugation of an equatorial moiety.[7]

The tandem isomerization and hydroformylation reactions and the observed conversion capabilities of internal octenes may allow for use in the hydroformylation of large internal olefins for use in the production of Guerbet-type surfactants and suitable substrates for hydroaminomethylation (HAM) for the formation of polymers.[8,9,10]

6.3 References

1. K. M. Kuhn and R. H. Grubbs, *Org. Lett.* 2008, **10** (10), 2075–2077.
2. B. A. Dar, S. N. Ahmad, M. A. Wagay, A. Hussain, N. Ahmad, K. A. Bhat, M. A. Khuroo, M. Sharma, and B. Singh; *Tet. Lett.* 2013, **54**, 4880–4884.
3. G. A. Rempel, P. Legzdins, H. Smith and G. Wilkinson, *Inorg. Synth.* 1972, **13**, 90.
4. T. P. Zhu, M. Q. Ahsan, T. Malinski, K. M. Kadish and J. L. Bear, *Inorg. Chem.*, 1984, **23** (1), 2–3.
5. D. Giffard, E. Fischer-Fodor, C. Vlad, P. Achimas-Cadariu and G. S. Smith, Eur. J. Med. Chem., 2018, **157**, 773-781.
6. S. Malaza, P. Govender, M. Schutte-Smith, H. G. Visser and G. S. Smith, *Eur. J. Inorg. Chem.* 2017, 3919.
7. M. Nowotny, T. Maschmeyer, B. F. G. Johnson, P. Lahuerta, J. M. Thomas and J. E. Davies, *Angew. Chem. Int. Ed.* 2001, **40,** 955-958.
8. Li. Yan, Y. Li, Z. Cui, Bing. Song, X. Pei and J. Jiang, *Energy Fuels*, 2017, **31** (9), 9319-9327.
9. T. Vanbesien, E. Monflier and F. Hapiot, *Green Chem.*, 2017, **19**, 1940-1948.
10. A. Behr, T. Seidensticker and A. J. Vorholt, *Eur. J. Lipid Sci. Technol.*, 2014, **116**, 477-485.